

NMR Study of Peptide Derivatives in Cryoprotective Media and Dimethyl Sulfoxide

by

Robert Marius Bieganski

B.S., University of California, Los Angeles (1990)

Submitted in Partial Fulfillment

of the Requirements for the

Degree of

Doctor of Philosophy

at the

Massachusetts Institute of Technology

February, 1997

Copyright © Massachusetts Institute of Technology 1997
All Rights Reserved

Signature of Author _____



Department of Chemistry
October 28, 1996

Certified by _____



Professor James R. Williamson
Thesis Chairman

Accepted by _____



Professor Dietmar Seyferth
Chairman, Departmental Committee on Graduate Students

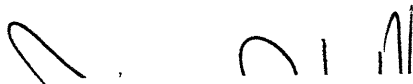
MASSACHUSETTS
OF TECHNOLOGY

MAR 3 1997

LIBRARIES

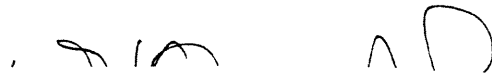
Science

This Doctoral thesis has been examined by a Committee of the Department of Chemistry as follows:



Professor James R. Williamson _____

Thesis Chairman and Supervisor

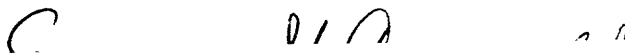


Professor William H. Orme-Johnson _____

Thesis Supervisor

Professor JoAnne Stubb _____

Thesis Supervisor



Professor Ernest G. Cravalho _____

Thesis Supervisor, Department of Mechanical Engineering

NMR Study of Peptide Derivatives in Cryoprotective Media and Dimethyl Sulfoxide

by

Robert Marius Bieganski

Submitted to the Department of Chemistry at the Massachusetts Institute of Technology on October 28, 1996 in partial fulfillment of the requirements for the Degree of Doctor of Philosophy

ABSTRACT

$\Delta\Delta G^\circ$ values for formation of antiparallel β -strand structure in the hairpin peptide-epindolidione model system have been measured for 14 natural and six synthetically-modified amino acid residues in dimethyl sulfoxide (DMSO). The DMSO $\Delta\Delta G^\circ$ values span a range of 1.51 Kcal/mole between the weakest and strongest β -strand formers, suggesting that amino acids have distinct and significant energetic preferences or propensities for β -strand formation in DMSO. The $\Delta\Delta G^\circ$ values (relative to alanine) show that the natural amino acid propensities from strongest to weakest are Val, Phe, Trp, Tyr, Thr, Leu, Lys, Arg, Glu, Ala, Gln, Gly, Asp, and Asn.

Nuclear Overhauser enhancement (NOE) experiments have been used to establish a second structure-reporting function of the peptide-epindolidione model system that is independent of chemical shift arguments, and that validates the original chemical shift-based reporter function of the epindolidione template.

$\Delta\Delta G^\circ$ values for formation of antiparallel β -strand structure in the hairpin peptide-epindolidione model system have been measured for 14 natural and six synthetically-modified amino acid residues in cryoprotective water-DMSO (CP) mixtures. The CP $\Delta\Delta G^\circ$ values span a range of at least 2.2 Kcal/mole between the weakest and strongest β -strand formers, suggesting that amino acids have distinct and significant energetic preferences for β -strand formation in CP mixtures. The CP $\Delta\Delta G^\circ$ values (relative to alanine) show that the natural amino acid

propensities from strongest to weakest are Phe, Trp, Val, Tyr, Thr, Leu, Glu, Gln, Lys, Arg, Ala, Asp, Asn, and Gly. Furthermore, thermodynamic analysis of the peptide-epindolidione derivatives showed that CP mixtures have a profound, residue-specific stabilizing effect on β -strand structure for both antiparallel and parallel derivatives, relative to pure DMSO and water.

Unique physicochemical properties of cryoprotective water-DMSO mixtures allowed detailed structural investigation of a number of peptide-epindolidione derivatives using two-dimensional (2D) Nuclear Magnetic Resonance (NMR) Spectroscopy. These NMR studies provide strong evidence that the peptide-epindolidione derivatives assume a robust β -strand-turn-template hairpin structure in the cryoprotective water-DMSO mixtures.

Thesis Supervisors:

Professor James R. Williamson

Title: Professor of Chemistry

Professor William H. Orme-Johnson

Title: Professor of Chemistry

Professor JoAnne Stubbe

Title: Professor of Chemistry and Biology

Professor Ernest G. Cravalho

Title: Professor of Mechanical Engineering and Health Sciences
and Technology

The author assumes sole and complete responsibility for the content of this thesis

Acknowledgements

I would like to thank the National Institutes of Health for research support (NIH grants GM 13453 and GM 40547).

Furthermore, I thank the following members of the MIT Faculty for serving as my Thesis Supervisors:

Prof. James R. Williamson (Thesis Chairman),

Prof. Ernest G. Cravalho,

Prof. William H. Orme-Johnson, and

Prof. JoAnne Stubbe.

Moreover, I would like to thank Prof. Wayne L. Hubbell, my undergraduate thesis advisor at the University of California, Los Angeles, for the opportunity to work in his laboratory, and for his enduring help, encouragement and inspiration.

I dedicate this thesis to my precious son Max
my wife Nancy and my Parents

Table of Contents

	Page
Chapter 1 Introduction	9
Chapter 2 Determination of Relative β -Strand Propensities ($\Delta\Delta G^\circ$ values) in Dimethyl Sulfoxide.....	39
Chapter 3 Investigation of Two Reporter Properties of Peptide- Epindolidione Conjugates in Dimethyl Sulfoxide. Correlation of a Ratio of NOE Intensities with Chemical Shift Changes.....	54
Chapter 4 Motives for Investigation of Peptide-Epindolidione Derivatives in Cryoprotective Water-DMSO Mixtures & Introduction to the Unique Physicochemical Properties of Cryoprotective Mixtures.....	82
Chapter 5 Determination of Relative β -Strand Propensities ($\Delta\Delta G^\circ$ values) in Cryoprotective Solvents.....	101
Experimental	145
Appendix A	186
Appendix B	205
Appendix C	218
Bibliography	254

Chapter 1
Introduction

The work described in this thesis builds upon the prior work of Drs. Bowen, Blanchard, and Arico-Muendel (Bowen, 1988; Blanchard, 1992; Arico-Muendel, 1992), Mr. Schaal & Giallourakis (Schaal, 1991; Giallourakis, 1992), and Ms. Link (Link, 1983) in this laboratory. The first systematic investigation of peptide-epindolidione conjugates was carried out by Dr. Bowen (Bowen, 1988; Kemp & Bowen, 1988). The peptide-epindolidione conjugate model system originally investigated by Bowen, and also the primary topic of this thesis is shown in Fig. 1-1. **1b** in Fig. 1-1 is a more convenient way of representing the full structure of **1a**, where Z denotes the duplicate peptide chain. This representation is possible due to the C₂ symmetry properties of the conjugate **1a**.

Dr. Bowen, building on preliminary experiments by Link (Link, 1983), developed a facile symmetrical synthesis of the 2,8-diamino-epindolidione tetracyclic template. This initial work was modeled on the general methods for preparation of epindolidiones reported by Jaffe & Matrick (Jaffe & Matrick, 1968). Subsequently, Bowen developed an efficient synthetic and purification procedures for derivatization of the 2,8-diamino-epindolidione template with peptides. Altogether, he prepared and characterized 12 peptide-epindolidione derivatives which are listed in Table 1-1. The three derivatives in the first column of Table 1-1 can be represented as XY:PdA where X and Y are variable residues corresponding to the fourth and third amino acid residues, respectively, counting from the template. The common structural motif of the derivatives in the first column is the structure of the dipeptide turn that links the epindolidione template with the dipeptide that is intended to mimic a β -strand, **1a** in Fig. 1-1, (see the footnote on p. #11). In this case, the turn is made of the residues l-Pro-d-Ala, which are thought to promote turn formation. The derivatives in the second column can be represented as XG:PG. In these derivatives, the d-Ala in the turn has been replaced with the achiral

amino acid residue glycine. In his thesis, Bowen showed that the replacement of d-Ala with Gly weakens the turn structure to a considerable degree. This is an important point, because as will be clear from the subsequent discussion, a robust turn structure is a necessary prerequisite for initiation of an extended β -strand structure¹ in the remaining portion of peptide-epindolidione conjugate.

Dr. Bowen was able to demonstrate this point by preparing the derivative FA: SarG listed in column three of Table 1-1. In this derivative, sarcosine (Sar) replaces the proline. Evidently, removing the structural constraint imposed by the five-membered ring of proline, and substituting d-alanine for glycine, weakens the turn, and results in no observable structure in the FA: SarG derivative, Fig. 1-6 (Bowen, 1988). The three derivatives in the fourth column of Table 1-1 are chirality-mismatch derivatives. These three, together with the two derivatives in column three, serve the purpose of "negative control derivatives", designed to test certain structural hypothesis about the behavior of the peptide-epindolidione derivatives.

Table 1-1.

Peptide-epindolidione conjugates prepared by Dr. Bowen (Bowen, 1988).

AG: PdA ¹	GG: PG	FA: SarG	dFA: PdA	dFdA: PdA
FA: PdA	AG: PG	FAib: PdA	FdA: PdA	
FG: PdA	FG: PG		dFG: PdA	

¹Single letter codes for amino acids are used in naming the derivatives. Thus, AG: PdA represents structure **1a** (Fig. 1-1) where d-alanine (dA) is the first residue covalently bound to the template, followed by l-proline. The colon symbolizes the chain-reversing urea functionality, followed by l-glycine and l-alanine which is functionalized with the N,N'-dimethylamide designed to minimize aggregation.

¹Prior researchers from this laboratory refer to the peptide-epindolidione conjugates as models for either antiparallel or parallel β -sheet formation. Due to the structural differences between actual β -sheets found in proteins and the peptide-epindolidione model, this researcher will not call these systems as models for sheet formation, but instead as models for "antiparallel" or "parallel" β -strand formation. β -strand is a polypeptide chain in a nearly extended conformation, and constitutes the basic unit of β -sheet structure in proteins (Creighton, 1993). The terms "antiparallel" or "parallel" β -strand will be retained in quotations, only to distinguish the two types of peptide-epindolidione structures studied by Blanchard & Arico-Muendel, respectively, (Blanchard, 1992; Arico-Muendel, 1992).

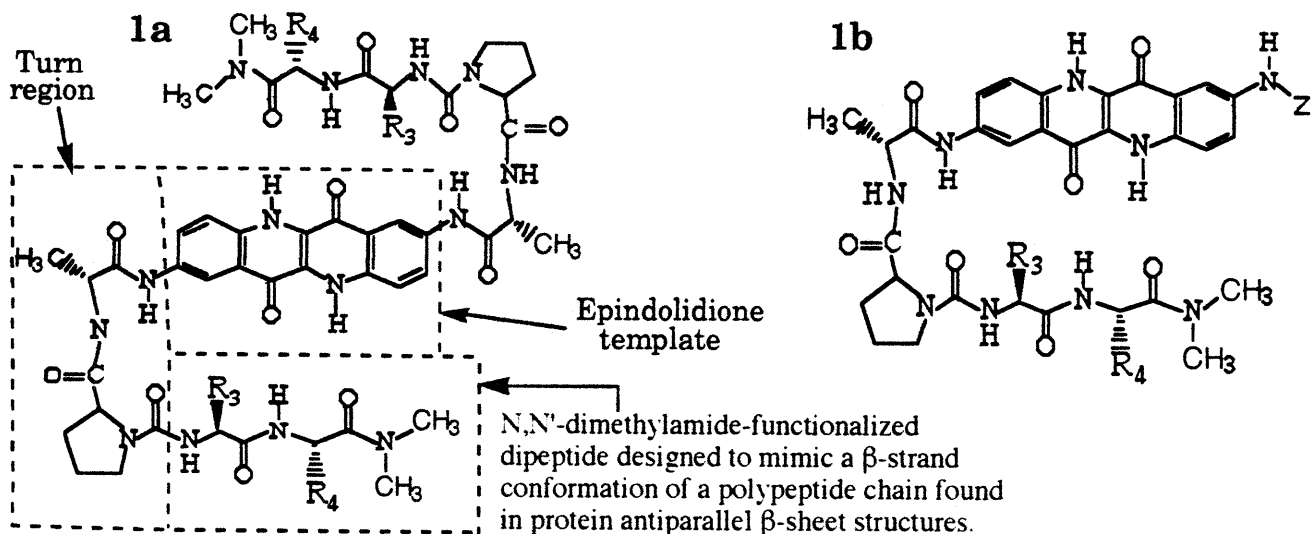


Figure 1-1. **1a)** Structure of peptide-epindolidione conjugate of the general formula XY:PdA. The variable residues X and Y correspond to the amino acid residues with side chains R_4 and R_3 , respectively, in the dipeptide portion of the molecule intended to mimic a β -strand conformation; The colon represents the chain-reversing urea functionality, followed by P and dA which are the single letter amino acid codes for l-proline and d-alanine, respectively, in the turn region. The Boxed regions represent the different parts of the peptide-epindolidione model system. **1b)** Simplified representation of the structure of the peptide-epindolidione conjugate shown in **1a**, where Z denotes the duplicated peptide chain of **1a**.

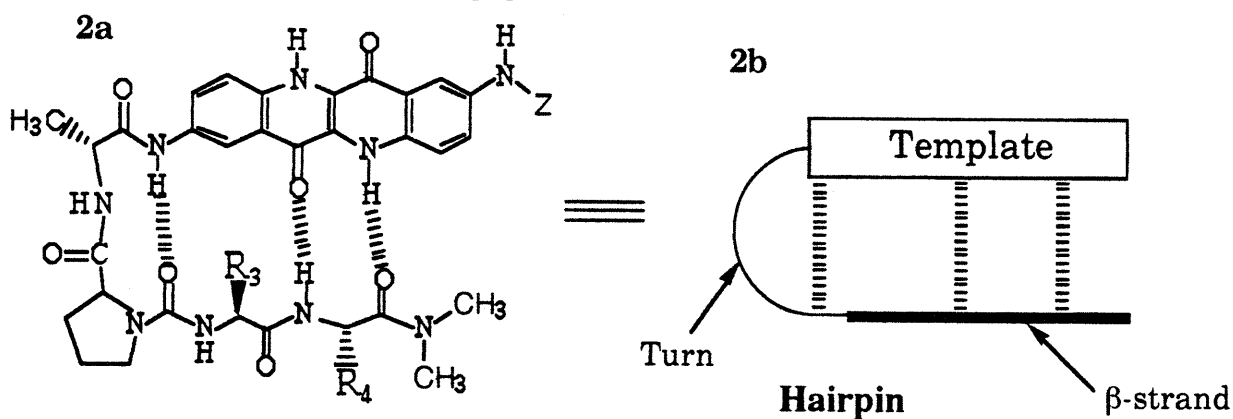


Fig. 1-2. **2a)** Template-hydrogen-bonded "antiparallel" β -strand structure representation of **1b**, clearly showing the three intramolecular peptide-template hydrogen bonds, and the overall hairpin conformation of the conjugate. **2b)** A schematic representation of **2a** in the structured "antiparallel" β -strand-turn-template hairpin conformation.

Bowen used the derivative FG:PdA as a test case for demonstrating that the peptide-epindolidione system can be used as a relatively simple system for the study of peptide derivatives that assume a β -strand-turn-template hairpin conformations (**2a & 2b** in Fig. 1-2) in DMSO-d₆. Furthermore, this derivative was important in determining which spectroscopic tools are likely to be most useful in conformational analysis of the peptide-epindolidione conjugates. ¹H-NMR was found to be the method best suited for these studies. In particular, predictable changes in chemical shifts, and detection of crucial NOEs were found the most useful. Fig. 1-3 shows the result of a series of NOE difference experiments performed by Bowen on the derivative FG:PdA in DMSO-d₆. These NOEs are consistent with the designed hairpin structure. In particular, the presence of the long-range NOE between the template proton H4 and the methyl protons of the N,N'-dimethylamide function, provides strong support for the extended β -strand conformation in the dipeptide part of the FG:PdA conjugate, as well as, its overall hairpin conformation indicated in Fig. 1-3. In this thesis we will refer to derivatives **1a** that exhibit the extended, β -strand-turn-template hairpin conformation of Fig. 1-3 (and Fig. **2a & 2b**) as "structured".

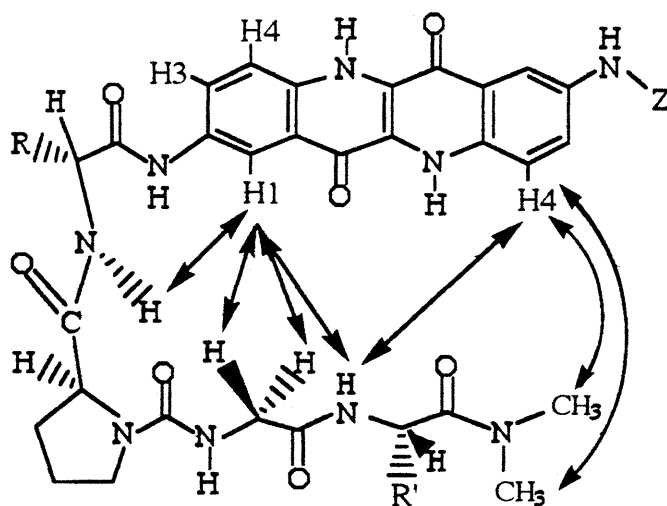


Figure 1-3. Difference NOEs observed for FG:PdA in DMSO-d₆ (Bowen, 1988).

Dr. Bowen also employed circular dichroism (CD) spectroscopy in the study of FG:PdA. Using CD, he was able to study the dimerization behavior of this derivative in solvents less polar than DMSO, (e.g. tetrahydrofuran, THF), and found that addition of only small amounts of DMSO or water inhibited dimer formation. Furthermore, he showed that dimerization is a property of derivatives with Gly in the first β -strand position (i.e. XG:PdA), and that the derivatives that exhibit this behavior also form crystals under suitable conditions. However, the crystals of FG:PdA obtained by Bowen, despite considerable effort, failed to yield good quality X-ray diffraction patterns. It was not until several years later when Dr. Flippen-Anderson (Naval Research Laboratories) was able to solve the X-ray crystal structure of FG:PdA using crystals provided by Dr. Blanchard (Blanchard, 1992).

The most important conclusions that emerged from the work of Dr. Bowen are:

- (1) the epindolidione template can induce extended (β -strand) peptide conformation in the conjugated peptide, provided a robust turn structure is present,
- (2) temperature gradients ($d\delta/dT$) of amide NH protons provide supporting evidence for the presence or lack of intramolecular hydrogen bonding for the study of the conjugates in DMSO- d_6 (**2a** & **2b** in Fig. 1-2),
- (3) chemical shift of the amide NH of the fourth residue (X in Fig. 1-1) correlates with the chemical shift of the H3 proton of the epindolidione template,
- (4) detected NOEs are consistent with and support the conclusion that at least some fraction of the conjugate FG:PdA exists in the conformation depicted in Fig. 1-3, and
- (5) using CD, Bowen was able to monitor dimerization behavior of some of the derivatives (e.g. FG:PdA), and worked out a procedure for its crystallization.

Observation (3) in the above list deserves special comment. The initial observation of Bowen that the chemical shift of the amide NH of the fourth residue

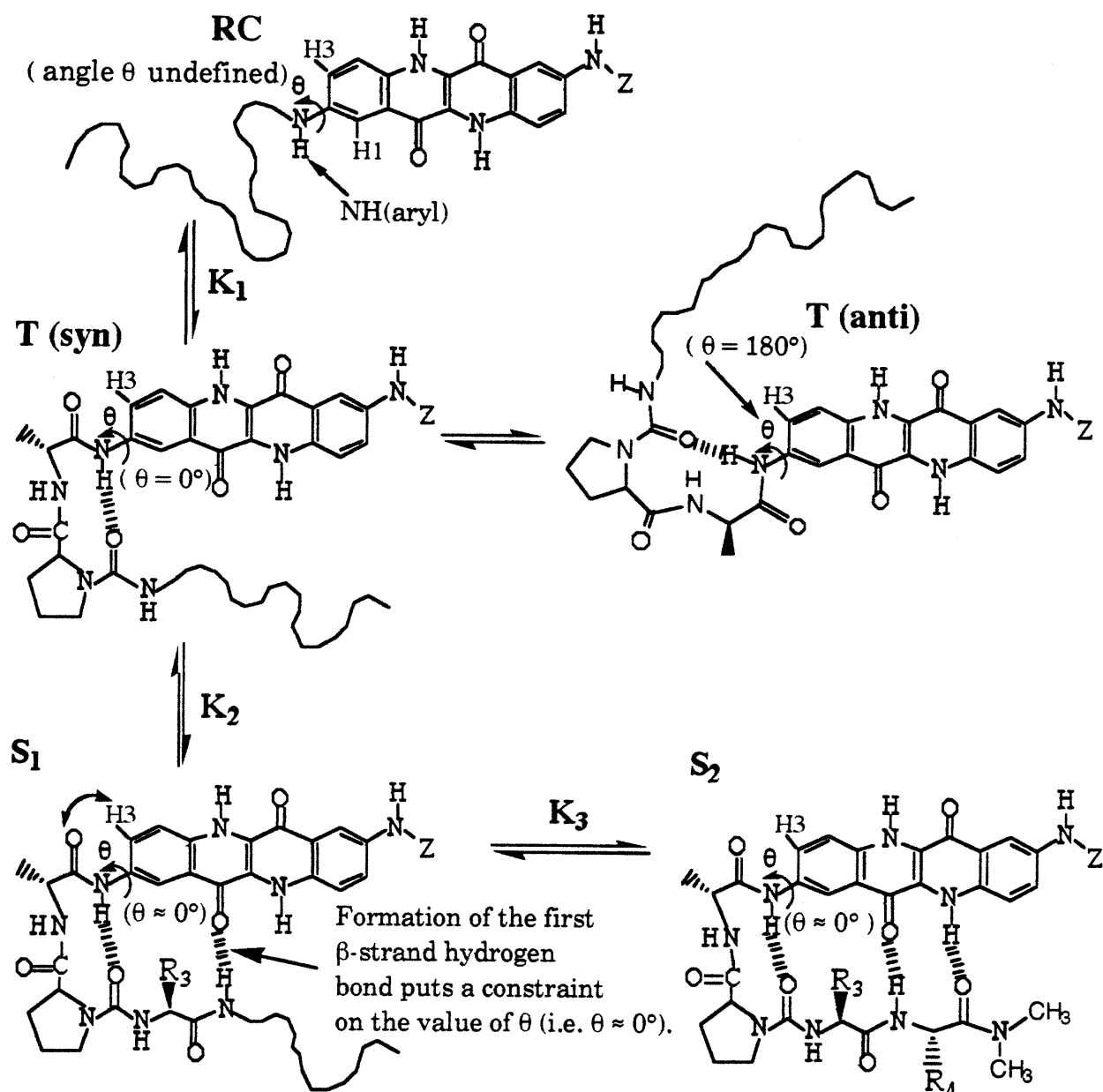


Figure 1-4. Peptide-epindolidione conjugate in the random coil, **RC**, Turn, **T(syn)**, with $\theta = 0^\circ$, **T(anti)**, with $\theta = 180^\circ$, "strand-1" or **S₁**, and "strand-2" or **S₂** conformational ensemble states. Formation of the "first β -strand" hydrogen bond forces the epindolidione and the turn region to be nearly coplanar ($\theta \approx 0^\circ$), thus constraining H3 to be proximal to the carbonyl oxygen of the d-alanine carbonyl, as shown by the curved arrow in **S₁**. The squiggly line represents a peptide in a random coil conformation. K_1 , K_2 , and K_3 represent the equilibrium constants for the formation of the **T**, **S₁**, and **S₂**, states, respectively. See text for more detail.

correlates with the chemical shift of the H3 proton of the epindolidione template, provided preliminary evidence that the H3 chemical shift can be used as a reporter function for the presence of the first intramolecular hydrogen bond in the β -strand region of the peptide-epindolidione conjugate (see **S₁** in Fig. 1-4). As will be seen from the subsequent discussion, this observation proved to be the most useful feature of the peptide-epindolidione system. This observation was only tentative at the time of Bowen, due to the limited number of derivatives prepared by Bowen (Table 1-1), but turned out to be an extremely useful and general property of the model system when the original data base of Bowen was expanded by subsequent researchers in this laboratory (Blanchard, 1992; Schaal, 1991; and the work in this thesis).

Based on structural arguments, one can rationalize why the H3 chemical shift (δ_{H3}) is likely to be sensitive to the formation of the first hydrogen bond in the β -strand region of the peptide-epindolidione model. Figure 1-4 shows a schematic diagram of the peptide-epindolidione conjugate in a number of conformational states that for convenience can be defined in terms of the intramolecular hydrogen bonding (Blanchard, 1992). In Fig. 1-4, **RC** represents the peptide-epindolidione conjugate with the peptide in a random coil conformation, forming no intramolecular hydrogen bonds with the template. From Fig. 1-4, it is apparent that in the **RC** state, there is free rotation (within any steric limitations) about the C2-aryl-N bond as indicated by the arrow, which leaves the angle θ largely undefined. K_1 is the equilibrium constant for the formation of the intramolecular turn hydrogen bond. As in the case of **RC**, formation of the turn hydrogen bond is not likely to significantly hinder rotation about the C2-aryl-N bond. This is indicated by the equilibrium arrows between the hypothetical **T(syn)** and **T(anti)** conformational states.

T(syn) state is defined by the presence of the turn hydrogen bond and $\theta \equiv 0^\circ$.

By definition, the torsional angle $\theta \equiv 0^\circ$, when the four atoms, NH(aryl) hydrogen, the aryl nitrogen, and the epindolidione carbons C2 and C3 are in the same plane. **T(anti)** results from a counterclockwise 180° rotation around the C2-aryl-N bond. K_2 is the equilibrium constant for the formation of the intramolecular hydrogen bond between the pyridone carbonyl oxygen of the epindolidione template and the peptide NH hydrogen of the fourth amino acid residue, counting from the epindolidione template. We will refer to this hydrogen bond as "the first strand hydrogen bond". The presence of the two intramolecular hydrogen bonds defines the "strand-1" or **S₁** state. As indicated in Fig. 1-4, formation of the first β -strand hydrogen bond puts a constraint on the allowed values of θ , as free rotation around the C2-aryl-N bond (as in the **T** state) is no longer possible. Furthermore, formation of the first strand hydrogen bond forces the epindolidione and the turn region to be nearly coplanar ($\theta \approx 0^\circ$), thus constraining H3 of the epindolidione to be proximal to the oxygen of the d-alanine carbonyl group, as indicated by the curved arrow in **S₁**. Evidently, this proximity results in a large chemical shift anisotropy of the ^1H NMR resonance corresponding to the proton of H3 (Bowen, 1988; Blanchard, 1992). K_3 in Fig. 1-4 represents the equilibrium constant for formation of the "second strand" or "strand-2" hydrogen bond between the pyridone NH of the epindolidione template and the carbonyl oxygen of the fourth amino acid residue, leading to formation of the "strand-2" or **S₂** state.

In summary, the value of the H3 chemical shift is likely to depend on the population fraction of the structured **S₁** and **S₂** " β -strand states"(Fig. 1-4). This effect has indeed been demonstrated experimentally (Blanchard, 1992; this thesis).

In order to study the conformation and energetics of peptide-epindolidione conjugates in solution, Dr. Blanchard addressed the issue of aggregation. Presence of aggregation presents considerable difficulties when one attempts the study of energetics of peptide structures. In the first place, the structure of an aggregate is usually not defined, which makes it impossible to draw meaningful conclusions from structural probes such as the NOE. Second, the forces that lead to aggregation may selectively stabilize certain undefined conformation(s), which may lead to incorrect energetic analysis in systems that exhibit aggregation. As a result, Blanchard conducted extensive studies regarding the issue of aggregation as pertaining to the peptide-epindolidione conjugates (Blanchard, 1992).

It is informative to review the key points of his work, as the aspect of aggregation is crucial to the work described in this thesis as well. The first observation made by Blanchard (and Bowen) was that the solvent plays a critical role when studying aggregation behavior of the conjugates. A second important aspect is the specific structure of the peptide-epindolidione conjugates (i.e. the nature of X and/or Y in XY:PdA). To give a specific example, the derivative FG:PdA is soluble in polar aprotic solvents such as DMSO or dimethylformamide (DMF). It is markedly less soluble in less polar solvents such as THF (millimolar solubility), and only sparingly soluble in solvents such as chloroform. It is virtually insoluble in pure water. Blanchard used vapor pressure osmometry (VPO) to investigate aggregation in solvents such as THF. Unfortunately, this technique was not applicable to solvents such as DMSO or water, due to their low vapor pressure. Furthermore, to confirm the conclusions obtained from the VPO experiments, Blanchard carried out dilution studies using $^1\text{H-NMR}$ as a probe for aggregation. From the experiments, he found $^1\text{H-NMR}$ to be the technique of choice for monitoring the aggregation behavior of the peptide-epindolidione conjugates. Furthermore, from NMR dilution

experiments, he was able to show that the peptide-epindolidione derivatives of the general structure **1a** (XY:PdA) shown in Fig. 1-1 are monomeric or free from association in DMSO-d₆ in the millimolar concentration range, which is suitable for both one-dimensional (1D) and two-dimensional (2D)-NMR work. To give a specific example, the derivative FG:PdA shows no detectable changes in resonance chemical shifts, resonance peak multiplicity, line widths, or coupling constants over the concentration range of 16 mM - 16 μ M in DMSO-d₆. This behavior was found consistent with FG:PdA being in the monomeric state over this whole concentration range. This behavior seems to be the characteristic of all derivatives of the general structure XY:PdA (**1a** in Fig. 1-1). This conclusion is important, as many of the energetic arguments about the peptide-epindolidione conjugates are derived from studies in DMSO-d₆.

With the issue of aggregation in DMSO put to rest, it was possible to fully explore the conformational and energetic behavior of derivatives **1a** in DMSO.

A major obstacle encountered in conformational analysis of small peptides is due to their inherent flexibility. In other words, most flexible (linear) peptides exist in solution in a number of quickly (on the NMR time scale) interconverting states (Kessler, 1982). The peptide-epindolidione conjugates are no exception, and are also very likely to exist in a large number of conformations with comparable energetic profiles. To obtain a rough estimate, Blanchard in his thesis (Blanchard, 1992) assumes that if each rotatable bond in **1a** (Fig. 1-1) is allowed three orientations (i.e. *gauche*⁺, *gauche*⁻, and *trans*), and neglecting the *cis* and *trans* conformations of the amide bonds, he estimates that there are 3⁸ or 6561 potential backbone conformations. This estimate does not take into consideration the individual conformations of the side chains of the amino acids, which would obviously increase

the number of possible conformers. Furthermore, Blanchard correctly argues that the majority of these conformations are not distinguishable by NMR spectroscopy. Thus, in effect, the spectrum that one obtains is a time-averaged (or "smeared") picture of the conformational ensemble of the conjugate being studied. The solution to this problem is to subdivide all the possible conformational states of a conjugate into distinct states ("superstates") that can be distinguished by NMR spectroscopy (Blanchard, 1992). This is possible in the case of the peptide-epindolidione conjugates because of the structuring and reporting properties of the epindolidione template. Blanchard selected the formation of intramolecular hydrogen bonds within the turn and the β -strand forming region of the peptide-epindolidione conjugate model as the critical factors that define each of the possible superstates. Based on this operational definition, Figure 1-5 shows that there are eight possible conformational superstates, each of which is defined by the position and number of the hydrogen bond(s) present.

As mentioned previously, Bowen found that the derivative FA: SarG lacks the expected β -strand-turn-template hairpin structure (**2a** or **2b** in Fig. 1-2; Bowen 1988). He concluded from this evidence that a robust turn structure is necessary for formation of a β -strand-turn-template hairpin structure in the XY: PdA derivatives. This conclusion is further supported by the synthesis and conformational analysis of urethane-based peptide-epindolidione derivatives reported by Arico-Muendel (Arico-Muendel, 1992). Arico-Muendel replaced the urea functionality in FA: PdA with a urethane. He reports that a change from urea to urethane results in a loss of the usual hairpin structure observed for the original FA: PdA. Since the urethane carbonyl oxygen is likely to be less basic than the corresponding urea carbonyl oxygen, this change in basicity is expected to weaken the turn hydrogen bond in the urethane model, which is exactly what was found by Arico-Muendel (Fig. 1-6).

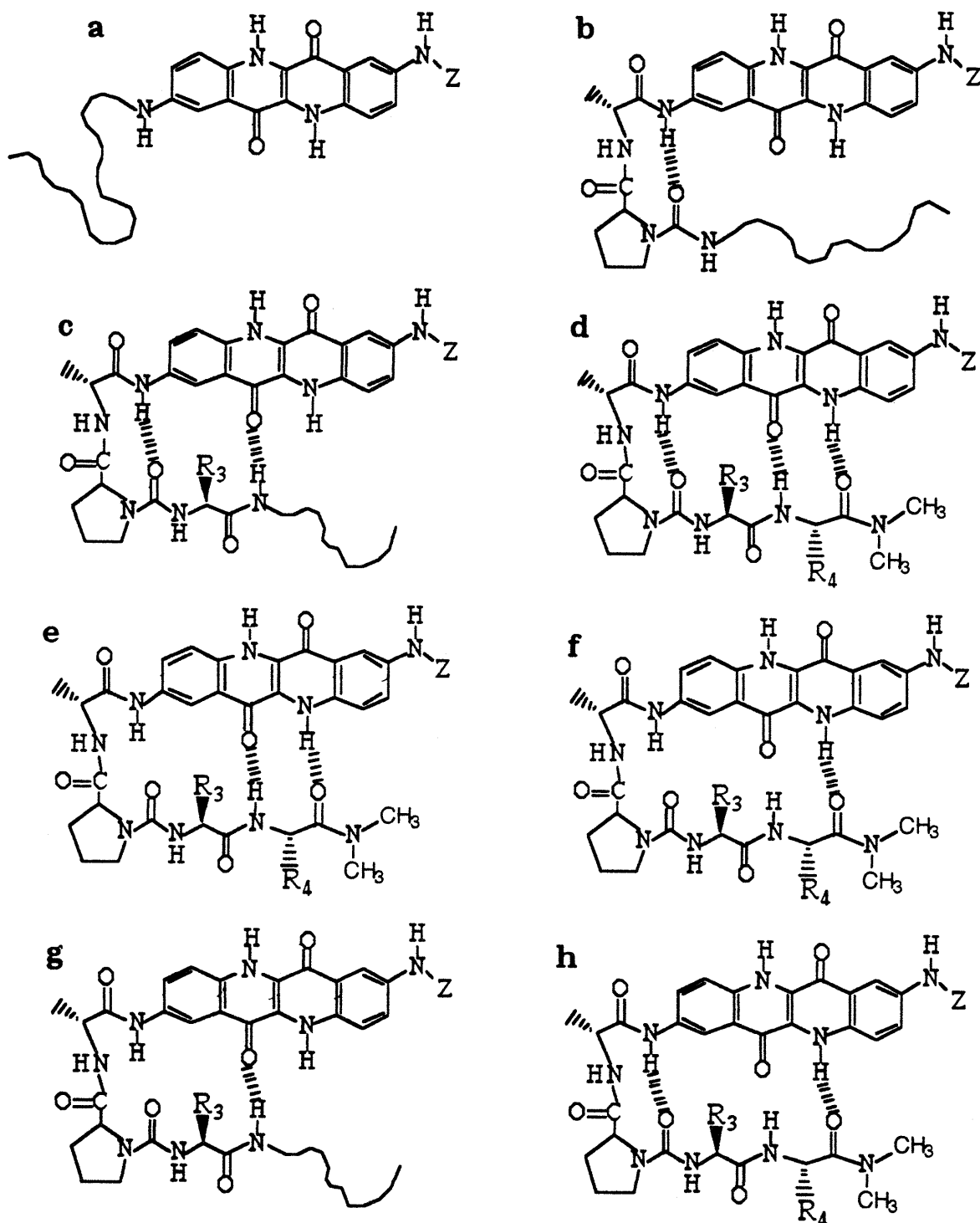


Figure 1-5. Schematic diagram representing the eight conformational "superstates" defined by the position and number of hydrogen bond(s) that each contains (Blanchard, 1992). The squiggly line represents the peptide.

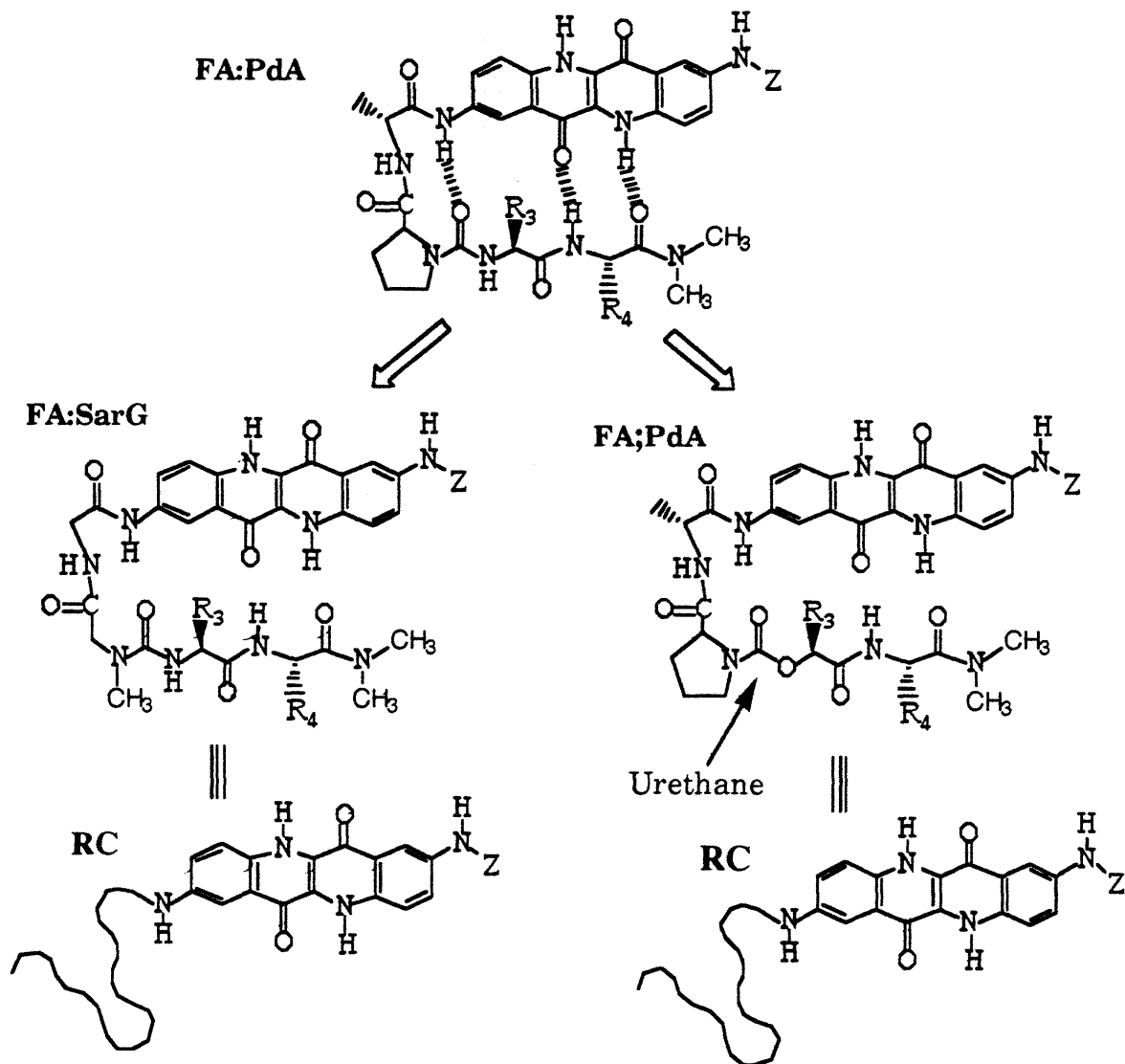


Figure 1-6. Schematic diagram summarizing the experimental results of Bowen and Arico-Muendel (Bowen, 1988; Arico-Muendel, 1992). Change in the turn structure from FA:PdA to FA:SarG results in loss of structure, represented by **RC** (Bowen, 1988). Change in the turn structure from FA:PdA to FA;PdA, where the semicolon ";" represents the urethane, also results in loss of structure, **RC** (Arico-Muendel, 1992).

Fig. 1-6 summarizes the two experimental results of Bowen & Arico-Muendel (Bowen, 1988; Arico-Muendel, 1992) that provided strong support for the hypothesis that a robust turn structure is a necessary prerequisite for formation of the β -strand-turn-template hairpin structured state otherwise observed for FA:PdA.

Based on the FA:SerG and FA;PdA urethane results mentioned above (Fig. 1-6), one can eliminate the hydrogen-bonded states in Fig. 1-5 that do not also contain the turn hydrogen bond (i.e. states **e**, **f** & **g**). This leaves us with only five states. In his thesis, Blanchard argues from correlation data observed between the chemical shifts of H3 and the NH proton of the fourth amino acid residue, that the superstate that contains the third hydrogen bond without the second one (i.e. superstate **h** in Fig. 1-5) is not populated to a significant degree, and can be ignored (Blanchard, 1992). Blanchard takes the correlation data as an evidence for the absence of superstate **h**. Blanchard points out that another test of this hypothesis would be the synthesis of ester derivatives in which the fourth residue amide hydrogen is removed by replacement of the peptide amide NH with an ester oxygen. If such derivatives show no structure, it would provide additional evidence that superstate **h** can be ignored. This researcher has done this experiment by synthesizing three such ester derivatives (Appendix **B**), and the results fully confirm the hypothesis that superstates that do not contain the first β -strand hydrogen bond (i.e. **h**, Fig. 1-5) also do not contain the second β -strand hydrogen bond. Thus, from the original eight states shown in Fig. 1-5, one is left with only four states, which are shown in Figure 1-7. Fig. 1-7 also includes the relevant equilibrium constants that relate the four states shown.

The goal of this research project is to obtain quantitative propensities of amino acid residues to adopt an extended β -strand structure as defined by either the **S₁** or **S₂** superstates of Figs. 1-4 or 1-7. This can be accomplished by applying the formalism of equilibrium thermodynamics. The equilibrium formulation of Fig. 1-7 in terms of the equilibrium constants K_1 , K_2 , and K_3 allows us to obtain such quantitative amino acid propensities.

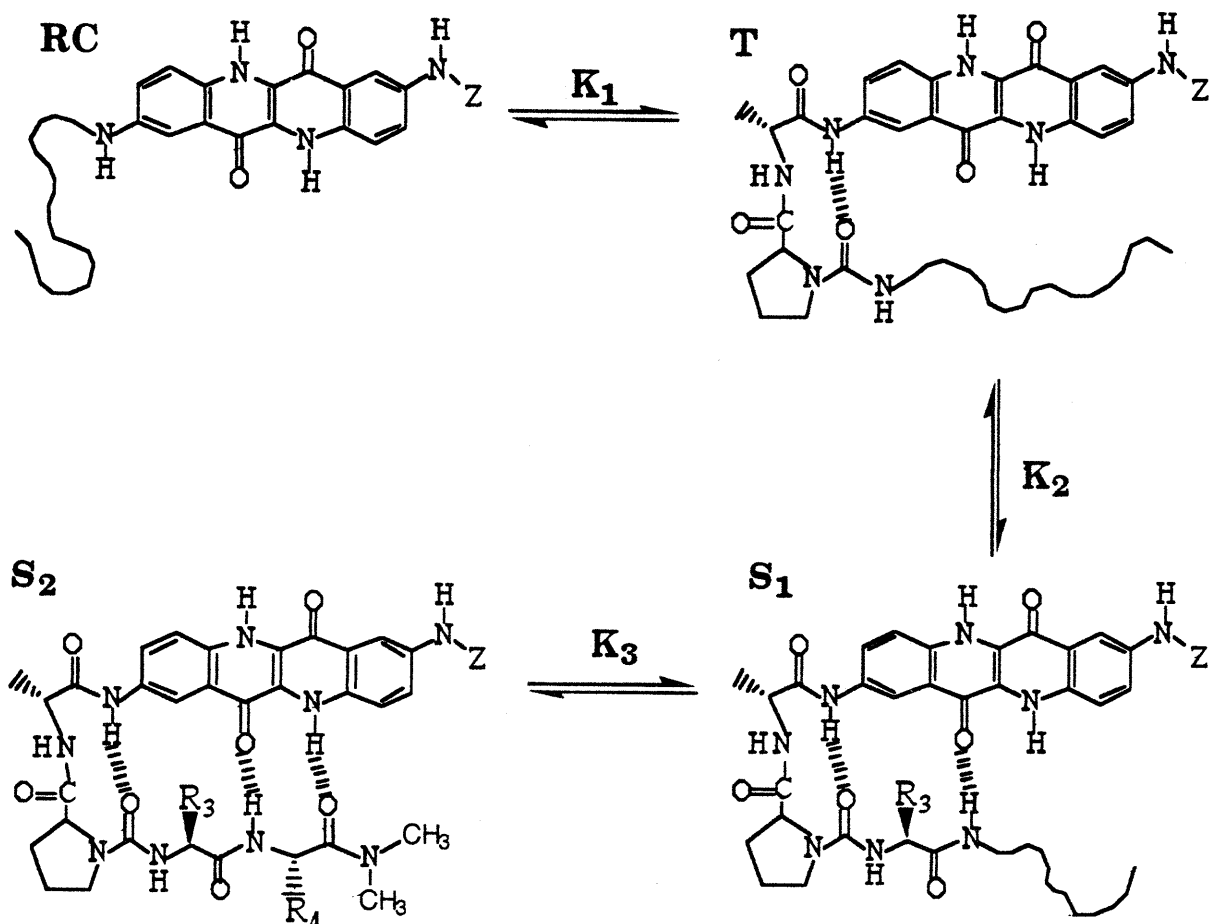


Figure 1-7. Equilibrium expressions relating the four superstates (Blanchard, 1992). The squiggly line represents the peptide in a random coil conformation. K_1 , K_2 , and K_3 represent the equilibrium constants for the formation of the T, S₁, and S₂ superstates, respectively.

In Fig. 1-7, K_1 , K_2 , and K_3 represent the equilibrium constants for formation of the first, second, and the third hydrogen bond, respectively. K_1 , K_2 , and K_3 are defined as follows:

$$K_1 = \frac{P_t}{P_{rc}}, \quad K_2 = \frac{P_{s1}}{P_t}, \quad \text{and} \quad K_3 = \frac{P_{s2}}{P_{s1}} \quad (\text{Eq. 1-1})$$

where P_{rc} , P_t , P_{s1} , and P_{s2} represent the population states of the random coil,

turn, first β -strand and second β -strand hydrogen-bonded states, respectively. Since equilibrium constants reflect the difference in free energy between the states [i.e., $K_{eq} = \exp(-\Delta G^\circ/RT)$], they are a proper choice for determination of the propensities of amino acid residues for β -strand formation in the peptide-epindolidione model.

In order to make use of the equilibrium expressions defined by Fig. 1-7 and Eq. 1-1, it is necessary to find a NMR parameter that is exclusively sensitive to the formation of the β -strand hydrogen bonds shown in Fig. 1-7.

Several NMR parameters can be used to monitor hydrogen-bonded hairpin formation (S_1 and S_2 states in Fig. 1-7) in the peptide-epindolidione conjugates. Among the most useful, are temperature gradients ($d\delta/dT$) of amide NH protons which provide support for the presence or absence of intramolecular hydrogen bonding (Kessler, 1982), chemical shift changes in amide NH's and the proton H3 of the epindolidione template, and detection of critical NOEs that confirm the presence of structured hairpin states (i.e. S_1 and S_2 states in Fig. 1-7).

In his thesis, Blanchard demonstrated that temperature gradients ($d\delta/dT$) of amide NH protons are useful in confirming the presence or absence of intramolecular hydrogen bonds. However, Blanchard found that there is a relatively large scatter in the individual ($d\delta/dT$) values of amide NH protons, relative to the average value (Blanchard, 1992). This scatter suggests that there is a substantial variation, from derivative to derivative, which may be due to local structural effects besides the presence or absence of an intramolecular hydrogen bond. In other words, the specific nature of an amino acid side chain may be influencing the value of

($d\delta/dT$) due to differences in solvent access, for example. Thus, even though the temperature gradients ($d\delta/dT$) of the NH resonances observed in DMSO- d_6 tend to support the hydrogen bonding model that we expect (Fig. 1-7), they are not sensitive or specific enough to be useful as parameters for description of the thermodynamic model of Figure 1-7.

The 3J coupling constants between the $C\alpha H$ and the amide NH are often used in peptide conformational analysis, as they can be related through the Karplus equation to the ϕ angle. However, coupling constants are not very useful for determining torsional angles for very flexible peptides, and especially for peptides that assume the extended structures characteristic of β -strands. This statement is due to the fact that the range of ϕ angles expected for a peptide residue in an extended β -strand ($\approx -120^\circ$ to -150°) corresponds to the values of coupling constants in the range of 8.0-9.5 Hz, which is very close to the accepted value for the random coil of 7.5 Hz (Kessler, 1982). Indeed, examination of the average J-values for "antiparallel" peptide-epindolidione conjugates clearly shows that the coupling constants exhibit only small variation over the range of derivatives presented, and that all are rather close to the average value of the random coil model (Blanchard, 1992). From this perspective, while useful in confirming that the peptide is in an extended, or β -strand-compatible conformation, the coupling constants are essentially useless for more precise determination of the conformational state of a given peptide-epindolidione derivative (Blanchard, 1992).

Next it is worth examining the variation in the chemical shifts of some of the various protons in the peptide-epindolidione conjugates that may be sensitive enough to be used to measure the populations of the structured states depicted in

Fig. 1-7. First, the aryl NH which is expected to be involved in the turn, exhibits a mean displacement of 0.39 ± 0.05 ppm upfield from the value of 10.18 ppm, which is the chemical shift for aryl NH in the derivative 2,8-bis-(Boc-d-Ala-NH)-epindolidione which is thought to be a good model for the random coil state of the peptide-epindolidione conjugates (Blanchard, 1992). In a similar fashion, the pyridone NH exhibits a mean displacement of 0.16 ± 0.10 ppm upfield from its value of 12.03 ppm value in 2,8-bis-(Boc-d-Ala-NH)-epindolidione. In addition, the peptide NH that is thought to form the first β -strand hydrogen bond displays a mean displacement of 0.50 ± 0.28 ppm from the random coil values reported by Bundi et al. (Bundi et al. 1975). Also the NH of d-Ala shows a mean displacement of 0.20 ± 0.06 ppm from the value obtained in the derivative Boc-Pro-d-Ala-*p*-cresyl ester, which is not expected to form a turn structure (Arico-Muendel, 1992).

Even though each of the above-mentioned chemical shift displacements provides a strong support that the peptide-epindolidione conjugates do exist in structured, or non-random-coil conformations, they are not the best suited for determining the various state populations shown in Fig. 1-7 because the variation in the chemical shifts that one observes in these protons is likely to involve contributions from magnetic anisotropies caused by the specific nature of an amino acid side chain, in addition to those that reflect changes in population states. To give a specific hypothetical example, the exact value of the chemical shift of the fourth amino acid NH may be modulated by the precise chemical nature of the fourth residue side chain in, addition to that caused by the formation of the first β -strand hydrogen bond. This possibility makes protons that are proximal to the loci to be varied in the peptide-epindolidione model (i.e. X and Y in 1a) not reliable as reporters of state populations necessary to evaluate the thermodynamic system shown in Fig. 1-7.

On the other hand, the situation is quite different if we consider the H3 proton of the epindolidione template. Unlike the other protons that exhibit large displacements in chemical shifts relative to the random coil models, the H3 hydrogen is well-removed from the amino acid loci that are varied in the β -strand model (i.e. the X & Y in XY:PdA). Therefore, any magnetic anisotropies caused by such variations are not likely to be transmitted to H3. Clearly, as Figure 1-4 shows, formation of the first (as well as the second) β -strand hydrogen bond is expected to result in a significant deshielding of H3 due to approach by the carbonyl oxygen of the d-Ala carbonyl, which is expected due to the planar geometry necessary to accommodate the β -strand hydrogen bond(s). Indeed, one observes a mean displacement of 0.53 ± 0.15 ppm in the chemical shift of H3 over the random coil model represented by the derivative 2,8-bis-(Boc-d-Ala-NH)-epindolidione (Blanchard, 1992).

Based on these observations, the H3 chemical shift was chosen as the primary reporter proton whose chemical shift can be used to analyze the population states shown in Fig. 1-7.

The experimentally observed H3 chemical shift, δ_{H3} , is a weighted average of the chemical shift values of each of the four states shown in Fig. 1-7 (Blanchard, 1992),

$$\delta_{H3} = \frac{\delta_{rc}P_{rc} + \delta_t P_t + \delta_{s1}P_{s1} + \delta_{s2}P_{s2}}{P_{tot}}, \quad (\text{Eq. 1-2})$$

where $P_{tot} = P_{rc} + P_t + P_{s1} + P_{s2}$ and δ_{rc} , δ_t , δ_{s1} , and δ_{s2} are the H3 chemical shifts for the random coil, turn, first β -strand, and second β -strand hydrogen-bonded

states, respectively. Furthermore, we can simplify the treatment if we let $\delta_o = \delta_{rc} + \delta_t$, where δ_o is the combined random coil/turn H3 chemical shift. Moreover, from Fig. 1-4 it is apparent that $\delta_{s1} = \delta_{s2} = \delta_\beta$. This is true because formation of the second β -strand hydrogen bond is not expected to further limit rotation about the C2-aryl-N bond since the constraint that it induces is expected to be identical to the one caused by the first β -strand hydrogen bond. δ_β here represents the H3 chemical shift for the structured states (i.e. S_1 or S_2 states in Fig. 1-4) with either one or two β -strand hydrogen bonds. Dr. Daniel Blanchard (Blanchard, 1992) was able to estimate the values for both δ_o and δ_β using appropriate model systems and solvent extrapolation. Equation 1-2 can therefore be rewritten as

$$\delta_{H3} = \frac{\delta_o(P_{rc} + P_t) + \delta_\beta(P_{s1} + P_{s2})}{P_{tot}} \quad (\text{Eq. 1-3})$$

Algebraic manipulation of the above equations given in Dr. Blanchard's thesis (Blanchard, 1992) leads to the following key equation

$$\frac{P_{s1} + P_{s2}}{P_{tot}} = \frac{\delta_{H3} - \delta_o}{\delta_\beta - \delta_o} \quad (\text{Eq. 1-4})$$

This is an expression for the fraction of total β -strand population states in terms of experimentally measurable quantities δ_{H3} , δ_o , and the quantity δ_β estimated by Blanchard. δ_o is obtained from model derivatives that cannot form either the first nor the second β -strand hydrogen bonds. Blanchard used the averaged value of the H3 chemical shift for the intermediate tripeptide ester derivatives RO-X:PdA which

is 7.97 ppm. Estimation of the value of δ_{β} proved more difficult. As pointed out by Blanchard, due to the aggressive hydrogen bond acceptor properties of DMSO, it is unlikely that even the most robust derivatives in the data base are fully structured in DMSO. However, a number of observations led to the conclusion (Blanchard, 1992) that the derivatives are 100% structured in chloroform, which is a much weaker hydrogen bond donor in comparison to DMSO. Blanchard found that in chloroform-d (CDCl_3), the H3 chemical shifts for a number of peptide-epindolidione derivatives XY:PdA converge (from the values in DMSO-d6) to an average value of 9.00 ppm. Thus, $\delta_{\text{H3}}(\text{CDCl}_3) = 9.00$ ppm represents the H3 chemical shift for an average, fully-structured derivative **1a** (Fig. 1-1) in chloroform-d. However, the question remained how this value, determined in chloroform, can be related to an analogous value in DMSO-d6? Blanchard prepared model compounds that were designed to mimic the environment of H3 proton in a fully structured derivative **1a**. Using these models, and correcting for solvent change, Blanchard estimated that the value of δ_{β} is 8.91 ppm in DMSO-d6.

It must be emphasized at this point that the accuracy of the quantitative analysis of β -strand propensities of amino acids (which is the main goal of this project) is dependent on the accuracy of the limiting values δ_{α} and δ_{β} . Since the value of δ_{α} is obtained directly from peptide-epindolidione model systems that lack structure in DMSO-d6, it is expected to be sufficiently accurate. The need to use model systems and correction for solvent change, however, puts some degree of uncertainty in the δ_{β} value estimated by Blanchard (Blanchard, 1992). In Chapter three of this thesis we will see that it is possible to estimate the value of δ_{β} in a completely independent way based on NOE ratio arguments. Furthermore, this

newly estimated value will be found to be within experimental error of the value reported above (8.91 ppm), that had been estimated by Blanchard using model systems and solvent corrections.

With the values of δ_{α} and δ_{β} , Blanchard used Eq. 1-4 to calculate the fraction of total β -strand² for the derivatives of the general structure **1a** (XY:PdA) in the data base available at that time (Blanchard, 1992). These are listed in Table 1-2. Some useful trends emerge from the data in Table 1-2. If one looks at the derivatives in which one amino acid in either β -strand position (either X or Y) is held constant, while the other is varied, the mole fraction of the β -strand increases in the order Gly, Ala, Leu, Phe, and Val. To give a specific example, if Val is the constant residue in the fourth position, and the third position is varied, we get VG, VA, VL, VF, and VV, with respective β -strand mole fractions of 0.25, 0.44, 0.52, 0.72, and 0.74. This implies that Gly is the weakest β -strand former and Val is the strongest, within this data base. Another point that is obvious from Table 1-2 is that none of the derivatives in the data base is either 100% structured or 0% structured. Instead, the range is from 21% to 74%. As we mentioned above, this behavior is expected in DMSO-d₆, due to its strong hydrogen-bond donor properties. Furthermore, as Blanchard pointed out in his thesis, the lack of either fully structured or structureless derivatives is fortunate, as it allows one to estimate β -strand forming propensities for all of the amino acid residues in the data base.

²See the footnote on page 11 in this Chapter.

Table 1-2Mole fraction of total β -strand

4 th Residue (X)	3 rd Residue (Y)	$(P_{s1} + P_{s2})/P_{tot}$
L	G	0.21 ¹
F	G	0.23 ²
V	G	0.25 ¹
G	A	0.31
L	A	0.33
A	A	0.34
A	L	0.38
L	L	0.38
F	A	0.38 ²
F	M	0.43 ³
V	A	0.44 ¹
F	S	0.46 ²
F	L	0.48 ¹
V	L	0.52
G	V	0.53
A	F	0.54
F	S(OtBu)	0.55 ³
L	F	0.56 ¹
L	V	0.63
F	F	0.63
A	V	0.64
I	F	0.66 ³
F	V	0.67 ¹
F	I	0.71 ³
V	F	0.72 ¹
V	V	0.74

¹As reported by Dr. Blanchard in his Doctoral thesis.²Calculated by Blanchard from data reported by Dr. Bowen in his Doctoral thesis.³Calculated by Blanchard from data reported by Mr. Schaal in his Master's thesis.

Although the mole fraction of total β -strand formed by a given derivative as reported in Table 1-2 gives the first quantitative estimate of β -strand structures using the peptide-epindolidione conjugates, this list does not provide information on the intrinsic propensities of amino acid residues for formation of β -strand structure. In order to obtain such quantities, it is necessary to consider the thermodynamic system depicted in Fig. 1-7 in more detail.

One can obtain another useful expression if one subtract "1" from both sides of Eq. 1-4 (Blanchard, 1992),

$$1 - \frac{P_{s1} + P_{s2}}{P_{tot}} = 1 - \frac{\delta_{H3} - \delta_o}{\delta_\beta - \delta_o} \quad \text{or} \quad \frac{P_{rc} + P_t + P_{s1} + P_{s2} - P_{s1} - P_{s2}}{P_{tot}} = \frac{\delta_\beta - \delta_o - \delta_{H3} + \delta_o}{\delta_\beta - \delta_o}$$

$$\text{or} \quad \frac{P_{rc} + P_t}{P_{tot}} = \frac{\delta_\beta - \delta_{H3}}{\delta_\beta - \delta_o} \quad (\text{Eq. 1-5})$$

Furthermore, one can divide Eq. 1-4 by Eq. 1-5 to obtain

$$\frac{P_{s1} + P_{s2}}{P_{rc} + P_t} = \frac{\delta_{H3} - \delta_o}{\delta_\beta - \delta_{H3}} \quad (\text{Eq. 1-6})$$

Now, since $P_{tot} = P_{rc} + P_t + P_{s1} + P_{s2}$, using the expressions for K_1 , K_2 , and K_3 in Eq. 1-1, one can write

$$P_{tot} = P_{rc} + K_1 P_{rc} + K_2 P_t + K_3 P_{s1}, \quad (\text{Eq. 1-7})$$

which is equivalent to

$$P_{tot} = P_{rc}(1 + K_1 + K_1 K_2 + K_1 K_2 K_3) \quad (\text{Eq. 1-8}).$$

Eq. 1-8 can be rewritten to express the mole fraction of the random coil states, or

$$P_{rc}/P_{tot} = 1/(1 + K_1 + K_1 K_2 + K_1 K_2 K_3) \quad (\text{Eq. 1-9}).$$

In a similar way, one can write expressions for the mole fractions of the turn, strand-1, and strand-2 states (Blanchard, 1992),

$$P_t/P_{tot} = K_1/(1 + K_1 + K_1K_2 + K_1K_2K_3) \quad (\text{Eq. 1-10})$$

$$P_{s1}/P_{tot} = K_1K_2/(1 + K_1 + K_1K_2 + K_1K_2K_3) \quad (\text{Eq. 1-11})$$

$$P_{s2}/P_{tot} = K_1K_2K_3/(1 + K_1 + K_1K_2 + K_1K_2K_3) \quad (\text{Eq. 1-12}).$$

Now, using Eq. 1-6 and Eqs. 1-11 - 1-12, one can rewrite Eq. 1-6 as

$$\frac{P_{s1} + P_{s2}}{P_{RC} + P_T} = \frac{\delta_{H3} - \delta_o}{\delta_\beta - \delta_{H3}} = \frac{K_1K_2 + K_1K_2K_3}{1 + K_1}, \text{ which can be simplified to}$$

$$\frac{\delta_{H3} - \delta_o}{\delta_\beta - \delta_{H3}} = \frac{K_2(1 + K_3)}{1 + \frac{1}{K_1}} \quad (\text{Eq. 1-13}).$$

In his thesis, Blanchard defines the ratio expressed by Eq. 1-13 as χ . Since χ is expressed in terms of the known parameters δ_{H3} , δ_o and δ_β , one can assign a χ value to every derivative in the data base. In other words, every derivative XY:PdA can be identified with the corresponding χ value or $\chi(\text{XY:PdA})$. Using the definition of χ , Blanchard was able to test the independence hypothesis which is a crucial step toward finding the intrinsic propensities of amino acids. To test the hypothesis of independence, he measured the ratios of pairs of χ values for derivatives with the same fourth amino acid. In symbolic terms,

$$\frac{\chi(\text{XY:PdA})}{\chi(\text{XZ:PdA})} = \frac{\frac{K_{2Y}(1 + K_{3X})}{1 + \frac{1}{K_1}}}{\frac{K_{2Z}(1 + K_{3X})}{1 + \frac{1}{K_1}}} = \frac{K_{2Y}}{K_{2Z}} \quad (\text{Eq. 1-14})$$

In a similar fashion, the ratios of pairs of χ values for derivatives with the same third residue should yield the following expression (Blanchard, 1992)

$$\frac{\chi(\text{XY:PdA})}{\chi(\text{ZY:PdA})} = \frac{\frac{K_{2Y}(1 + K_{3X})}{1 + \frac{1}{K_1}}}{\frac{K_{2Y}(1 + K_{3Z})}{1 + \frac{1}{K_1}}} = \frac{1 + K_{3X}}{1 + K_{3Z}} \quad (\text{Eq. 1-15})$$

The result of these measurements showed that the deviation for the majority of the ratios in both cases (i.e., Eqs. 1-14 & 1-15) are within 20% of the average. However, derivatives that contain Gly residue proved to be less consistent. Blanchard attributed this to the unusual flexibility of the glycine residue. Based on these measurements, and excluding derivatives containing Gly, Blanchard concluded that the value of K_2 for a given amino acid residue is largely independent of the nature of the fourth amino acid (X), and the value of K_3 is largely independent of the nature of the third amino acid (Y). This constitutes the proof of independence, and the fact that the equilibrium constants as defined by either K_2 or K_3 should reflect the intrinsic propensity for an amino acid to assume a β -strand structure in the peptide-epindolidione model.

It must be emphasized that obtaining Equations 1-14 & 1-15 is based on the assumption that the value of the equilibrium constant K_1 is independent of the

nature of either the third or the fourth amino acid residue in the peptide-epindolidione models. Furthermore, the accuracy of these results rests on the accuracy with which the values of δ_o and δ_β were obtained. In this respect, our ability to independently estimate the value of δ_β in Chapter three of this thesis, puts Blanchard's conclusions of independence on much more solid grounds.

Subsequent to proving independence, Blanchard attempted to evaluate the actual numerical values of the equilibrium constants K_1 , K_2 , and K_3 . However, to do so, he had to assume that for at least two of the amino acids used in the data base, their respective intrinsic propensities are independent of the actual position in the peptide-epindolidione model. In other words, Blanchard had to assume that for at least two amino acid residues X and Y, $K_{2X} = K_{3X}$, and $K_{2Y} = K_{3Y}$. As discussed by Blanchard, the validity of this assumption depends on the equivalency of the first and second β -strand positions in the peptide-epindolidione model. This implies that the first and second β -strand hydrogen bond are equal in strength, and that there is no structural bias in either position. Blanchard furthermore states: "Both of these conditions are reasonable, but it is difficult to conceive of experiments able to test them". However, the experimental work to be described in Appendix **B** of this thesis provides strong evidence that Blanchard's assumption that $K_{2X} = K_{3X}$, and $K_{2Y} = K_{3Y}$ is not true. It is therefore important to emphasize that Blanchard's analysis to obtain the individual values of the equilibrium constants (Blanchard, 1992) is not correct, and that the values that he obtained are different from the values that will be reported in this thesis (Appendix **B**).

Chapter two will present $\Delta\Delta G^\circ$ values for formation of "antiparallel" β -strand structure using the hairpin peptide-epindolidione model system for 14 natural and six synthetically-modified amino acid residues in dimethyl sulfoxide (DMSO). The DMSO $\Delta\Delta G^\circ$ values span a range of 1.51 Kcal/mole between the weakest and strongest β -strand formers, suggesting that amino acids have distinct and significant energetic preferences or propensities for β -strand formation in DMSO.

Chapter three will provide results from nuclear Overhauser enhancement (NOE) experiments that have been used to establish a second structure-reporting function of the peptide-epindolidione model system that is independent of chemical shift arguments, and that validates the original chemical shift-based reporter function of the epindolidione template.

Chapter four reviews the difficulties encountered by other researchers in this laboratory with the water soluble version of the epindolidione model, and provides an introduction to the unique physical and biological properties of cryoprotective water-DMSO mixtures, which were found very useful in the study of the peptide-epindolidione model in aqueous-like media.

Chapter five provides $\Delta\Delta G^\circ$ values for formation of "antiparallel" β -strand structure in the hairpin peptide-epindolidione model system that have been measured for 14 natural and six synthetically-modified amino acid residues in cryoprotective water-DMSO (CP) mixtures. The CP $\Delta\Delta G^\circ$ values will be shown to span a range of at least 2.2 Kcal/mole between the weakest and strongest β -strand formers, suggesting that amino acids have distinct and significant energetic preferences for β -strand formation in CP mixtures. Furthermore, thermodynamic

analysis of the peptide-epindolidione derivatives will show that CP mixtures have a profound, residue-specific stabilizing effect on β -strand structure for both "antiparallel" and "parallel" derivatives, relative to pure DMSO and water. Chapter five will also demonstrate that the unique physicochemical properties of cryoprotective water-DMSO mixtures allowed detailed structural investigation of a number of peptide-epindolidione derivatives using two-dimensional (2D) Nuclear Magnetic Resonance (NMR) Spectroscopy. These NMR studies provide strong evidence that the peptide-epindolidione derivatives assume a robust β -strand-turn-template hairpin structure in the cryoprotective water-DMSO mixtures.

Chapter 2

Determination of Relative β -Strand Propensities ($\Delta\Delta G^\circ$ values) in Dimethyl Sulfoxide

The review of the work of Drs. Bowen and Blanchard (Bowen, 1988; Blanchard, 1992) described in the last Chapter provided strong evidence that the chemical shift of the H3 proton of the epindolidione template, δ_{H3} , can be used as a sensitive reporter function of the conformational state of the peptide-epindolidione derivatives. Furthermore, Bowen and Blanchard provided NOE evidence that shows that some of the peptide-epindolidione derivatives exhibit the expected "antiparallel" β -strand-turn-template hairpin structure¹ (1b, Fig. 2-1) in DMSO-d6.

This Chapter provides new relative quantitative measures of amino acid propensities for the formation of "antiparallel" β -strand in DMSO-d6 which significantly extend the work reported by Blanchard (Blanchard, 1992). The $\Delta\Delta G^\circ$ values that have been measured for 14 natural and six synthetically-modified amino acid residues span a range of 1.51 Kcal/mole between the worst and best β -strand formers, indicating that, even in a simple synthetic peptide model, amino acids have distinct and significant energetic preferences for β -strand formation. Since DMSO-d6 as a solvent has properties very different from that of water, the significance of the $\Delta\Delta G^\circ$ values reported in this Chapter to energetics of β -strand formation in water is uncertain. However, Chapter five will provide analogous $\Delta\Delta G^\circ$ values for β -strand formation in a cryoprotective water-DMSO solvent which is thought to share many properties unique to water.

¹Prior researchers from this laboratory refer to the peptide-epindolidione conjugates as models for either antiparallel or parallel β -sheet formation. Due to the structural differences between actual β -sheets found in proteins and the peptide-epindolidione model, this researcher will not call these systems as models for sheet formation, but instead as models for "antiparallel" or "parallel" β -strand formation. β -strand is a polypeptide chain in a nearly extended conformation, and constitutes the basic unit of β -sheet structure in proteins (Creighton, 1993). The terms "antiparallel" or "parallel" β -strand will be retained in quotations, only to distinguish the two types of peptide-epindolidione structures studied by Blanchard & Arico-Muendel, respectively, (Blanchard, 1992; Arico-Muendel, 1992).

Table 1-2 in Chapter one lists the mole fractions of total β -strand, $(P_{s1} + P_{s2})/P_{tot}$, for 28 "antiparallel" peptide-epindolidione derivatives of general structure **1a** (XY:PdA, Fig. 2-1) prepared by Bowen, Schaal, and Blanchard (Bowen, 1988; Schaal, 1991; Blanchard, 1992). The 28 XY:PdA derivatives of Table 1-2 are generated by pair combinations of only eight amino acid residues, Gly, Ala, Leu, Ile, Val, Phe, Met, and Ser in the XY:PdA model **1a**. Mr. Schaal (Schaal, 1991) attempted to incorporate other amino acid residues in the peptide-epindolidione model **1a**, however, one of the synthetic steps that was used at that time in this laboratory to prepare derivatives **1a**, proved not suitable for incorporation of other amino acid residues into the peptide-epindolidione model **1a**. Thus, Schaal attempted the synthesis of derivative **1a** containing threonine, but with no success (Schaal, 1991).

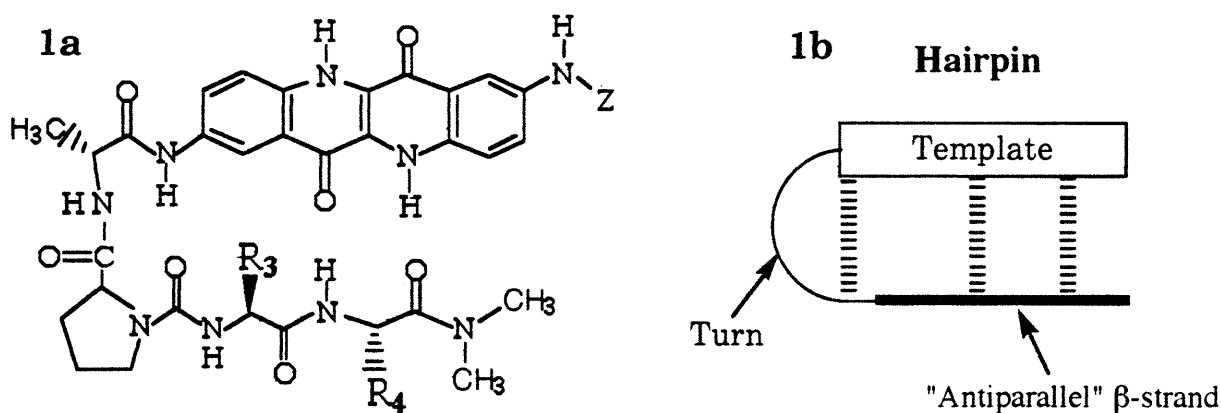


Figure 2-1. **1a**) Structure of the "antiparallel" peptide-epindolidione conjugate of the general formula XY:PdA where X and Y designate single-letter amino acid codes for the variable "antiparallel" β -strand positions with the side chains R_4 , and R_3 , respectively. The colon in XY:PdA designates the urea function, followed by l-proline (P) and d-alanine (dA) which is covalently linked to the epindolidione template. Z denotes the duplicated peptide chain (see also Fig. 1-1 in Chapter one). **1b**) A schematic representation of **1a** in the structured "antiparallel" β -strand-turn-template hairpin conformation showing the presence of the three intramolecular hydrogen bonds between the peptide and the template as represented in the S_2 superstate of Figs. 1-4 & 1-7 in Chapter one.

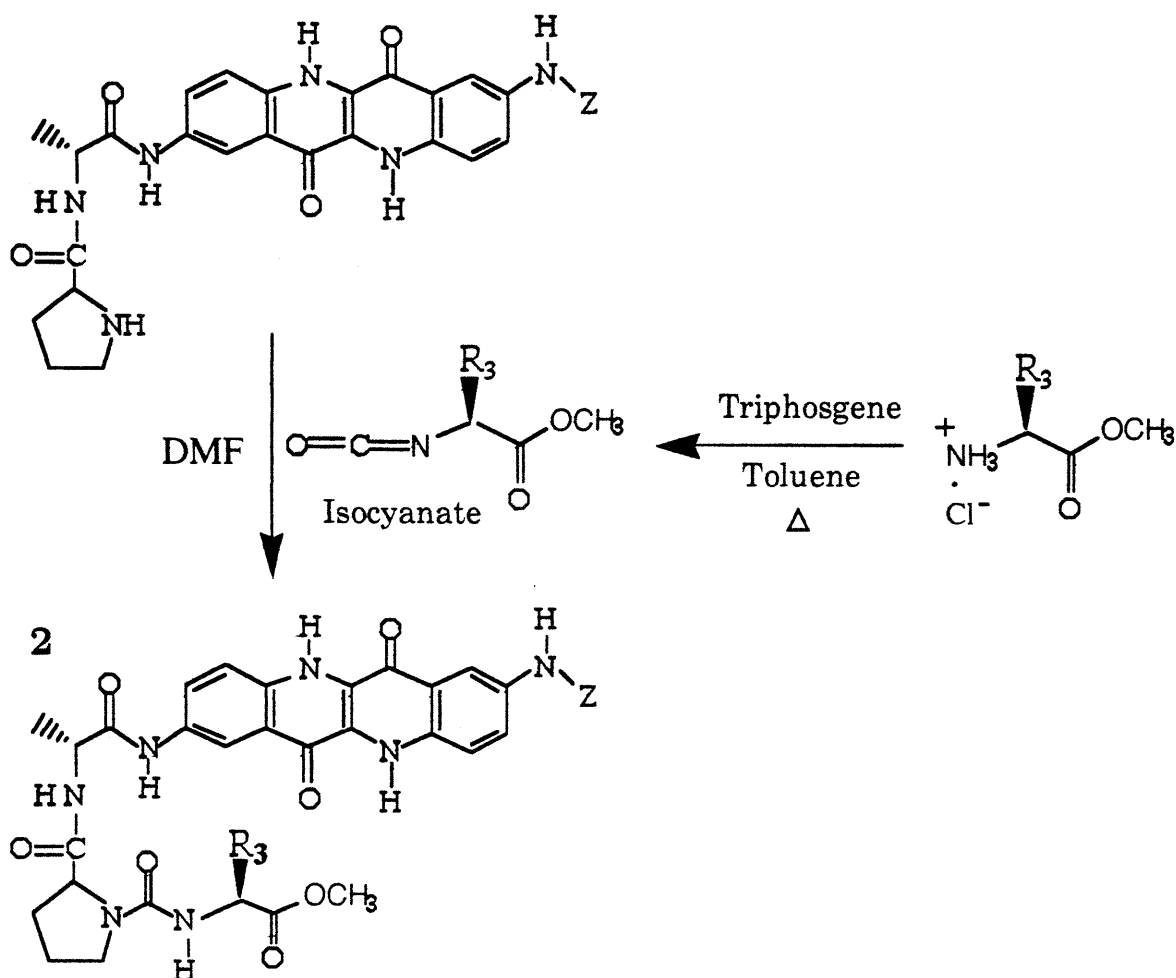


Figure 2-2. The urea-coupling synthetic step that employs the isocyanate intermediate that was originally used by Bowen, Schaal, and Blanchard to prepare the tripeptide-epindolidione ester intermediates (2) on the way to the tetrapeptide-epindolidione derivatives XY:PdA (1a, in Fig. 2-1).

The synthetic step that proved not suitable for expansion of the data base of Table 1-2 is the step that leads to the isocyanate intermediate that is later used in a urea-coupling step (Blanchard, 1992). Both steps are shown in Fig. 2-2. The triphosgene step of Fig. 2-2 that yields the isocyanate intermediate is not suitable in the synthesis of intermediates containing acid-sensitive functional groups (e.g. tryptophan) due to the harsh acid conditions present in the step.

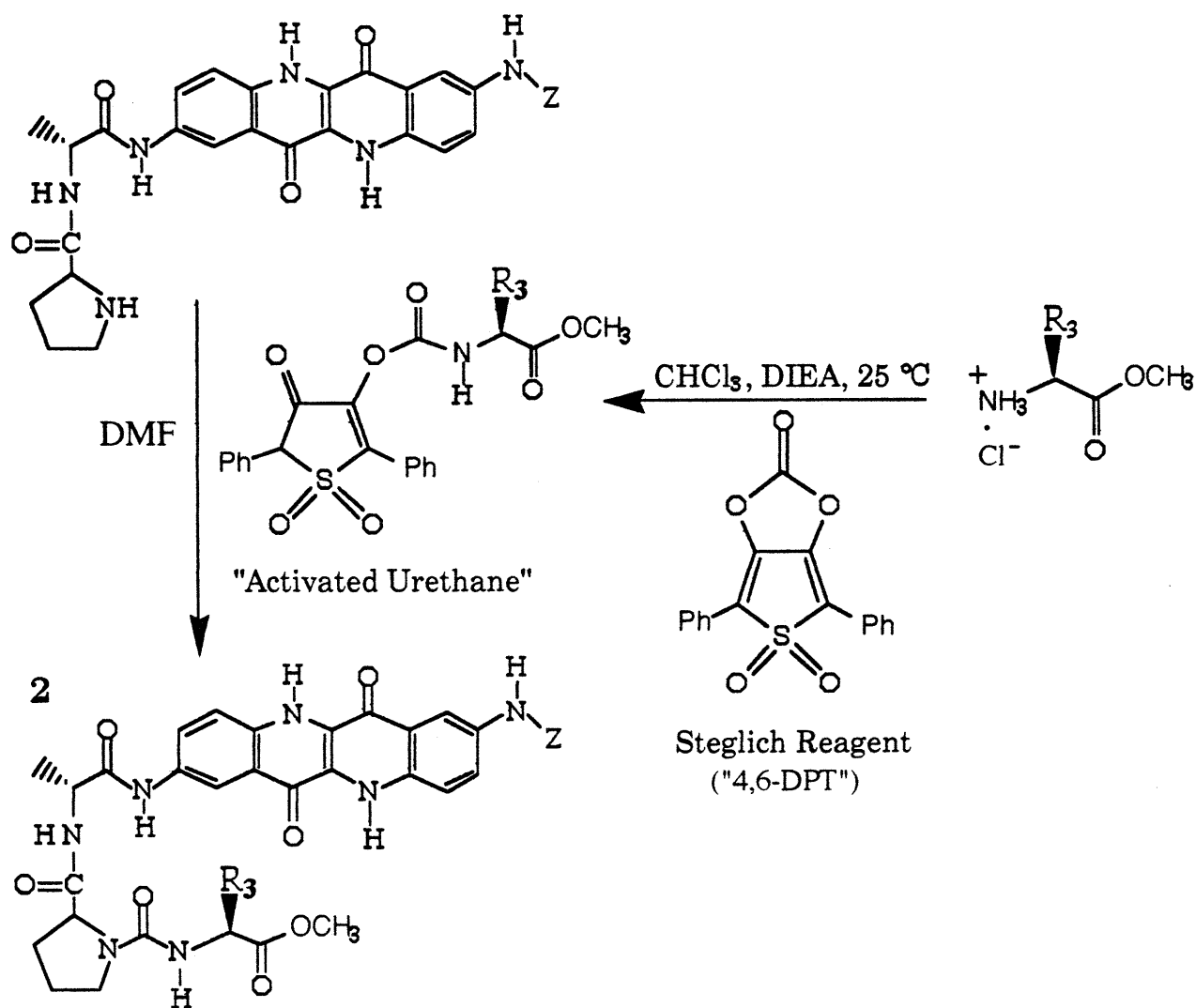


Figure 2-3. The urea-coupling synthetic step that employs an "activated urethane" instead of an isocyanate as shown in Fig. 1-2. "4,6-DPT" is an abbreviation for the reagent developed by Steglich (Schmidt et al. 1979), 4,6-diphenylthieno[3,4-d]-1,3-dioxol-2-one 5,5-dioxide which is used to activate an amino acid, and thus plays the role of triphosgene in Fig. 2-2.

This researcher solved the problem by replacing the isocyanate step with a synthetic step shown in Fig. 2-3. Using this modified synthetic step, this researcher successfully prepared the following 15 tetrapeptide-epindolidione derivatives: VT: PdA, VT(OtBu): PdA, VW: PdA, VK(ϵ -BOC): PdA, VK: PdA, VN: PdA, VD: PdA,

VD(OtBu):PdA, VE:PdA, VE(OtBu):PdA, VQ:PdA, VQ(DOD):PdA, VR:PdA, VY:PdA, and VY(OtBu):PdA, as well as, five tripeptide-epindolidione ester derivatives: MeO-K(ϵ -BOC):PdA, MeO-K:PdA, MeO-K:PdK, MeO-D(OtBu):PdA, and MeO-E(OtBu):PdA. In naming these derivatives, single-letter amino acid codes are used. Thus, for example, VK(ϵ -BOC):PdA designates a tetrapeptide-template conjugate where d-Ala, l-Pro, l-Lys(ϵ -BOC), and l-Val are the first, second, third, and fourth amino acid residues, respectively, counting from the template (1a in Fig. 2-1). The colon represents the sequence-reversing urea function. Furthermore, the symbols in the parentheses refer to side chain protection. Thus, (ϵ -BOC) designates tertiary-butyloxycarbonyl-protected epsilon-amino group of lysine, and (OtBu) designates a tertiary-butyl-protected side chain carboxyl group; (DOD) represents dimethoxydityl-protected side chain of glutamine (Fig. 2-8). The new procedure for preparation of the "activated urethane" that is subsequently used in the urea coupling reaction is very mild, goes rapidly to completion at room temperature, and in contrast to the previously used isocyanate procedure, it is thought to be much safer.

Besides the 15 tetrapeptide derivatives prepared via the activated urethane step, this researcher prepared the tripeptide-epindolidione ester derivative EtO-G:PdA (for TOE study, Chapter three), and a relatively large quantity (300 mg) of the derivative VG:PdA (both via the isocyanate procedure) intended for growing crystals for X-Ray structure determination. As was mentioned in the review of Chapter one, Blanchard prepared the crystals of FG:PdA whose X-Ray structure (after a large amount of work) was solved by Dr. Flippen-Anderson of the Naval Research Laboratory in Bethesda. This researcher prepared crystals of VG:PdA which were send to Dr. Flippen-Anderson for X-Ray structure determination. However, technical and time constraint problems prevented solution of the X-Ray structure by Dr. Flippen-Anderson.

All of the 21 peptide-epindolidione derivatives mentioned above have been subjected to detailed one-dimensional (1D) and two-dimensional (2D) NMR analysis in DMSO-d₆ at room temperature, 25 °C. The 1D-NMR spectra have been completely assigned using 2D-COSY analysis, and when necessary, a combination of 2D-COSY and NOESY analysis. Furthermore, as we will see in Chapter three, some of the derivatives were subjected to kinetic truncated NOE (TOE) experiments.

From the set of 16 tetrapeptide-epindolidione derivatives, six have been subjected to a detailed 2D-NOESY analysis in DMSO-d₆ at room temperature in order to confirm the presence of the expected β -strand-turn-template hairpin structure (1b in Fig. 2-1). Figure 2-4 shows the most important NOE results from a representative NOESY spectrum for VK(ϵ -BOC):PdA in DMSO-d₆, 25 °C which is shown in Fig. 2-5.

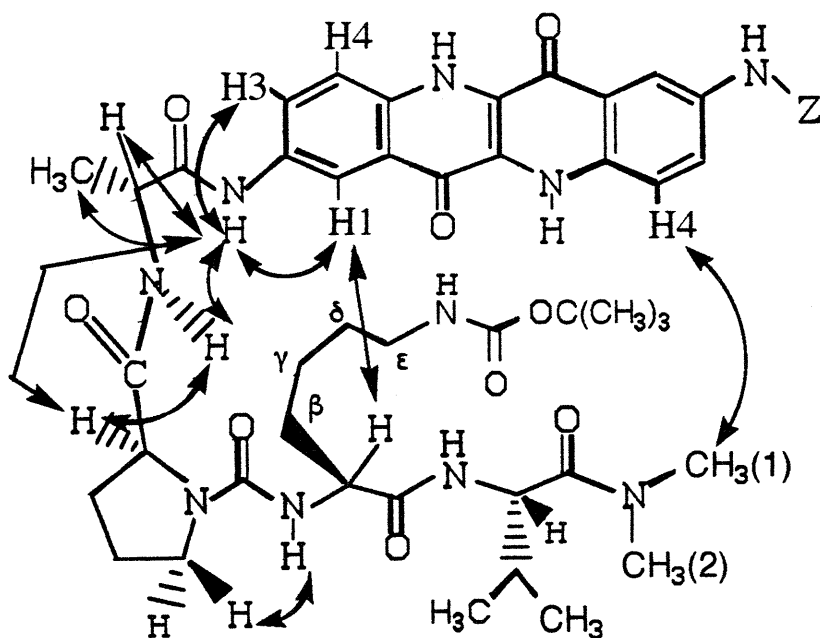


Figure 2-4. Phase-sensitive NOESY results for VK(ϵ -BOC):PdA in DMSO-d₆, 25 °C. The double-headed arrows indicate the observed, non-trivial NOEs. Z, as before, denotes the duplicated peptide chain.

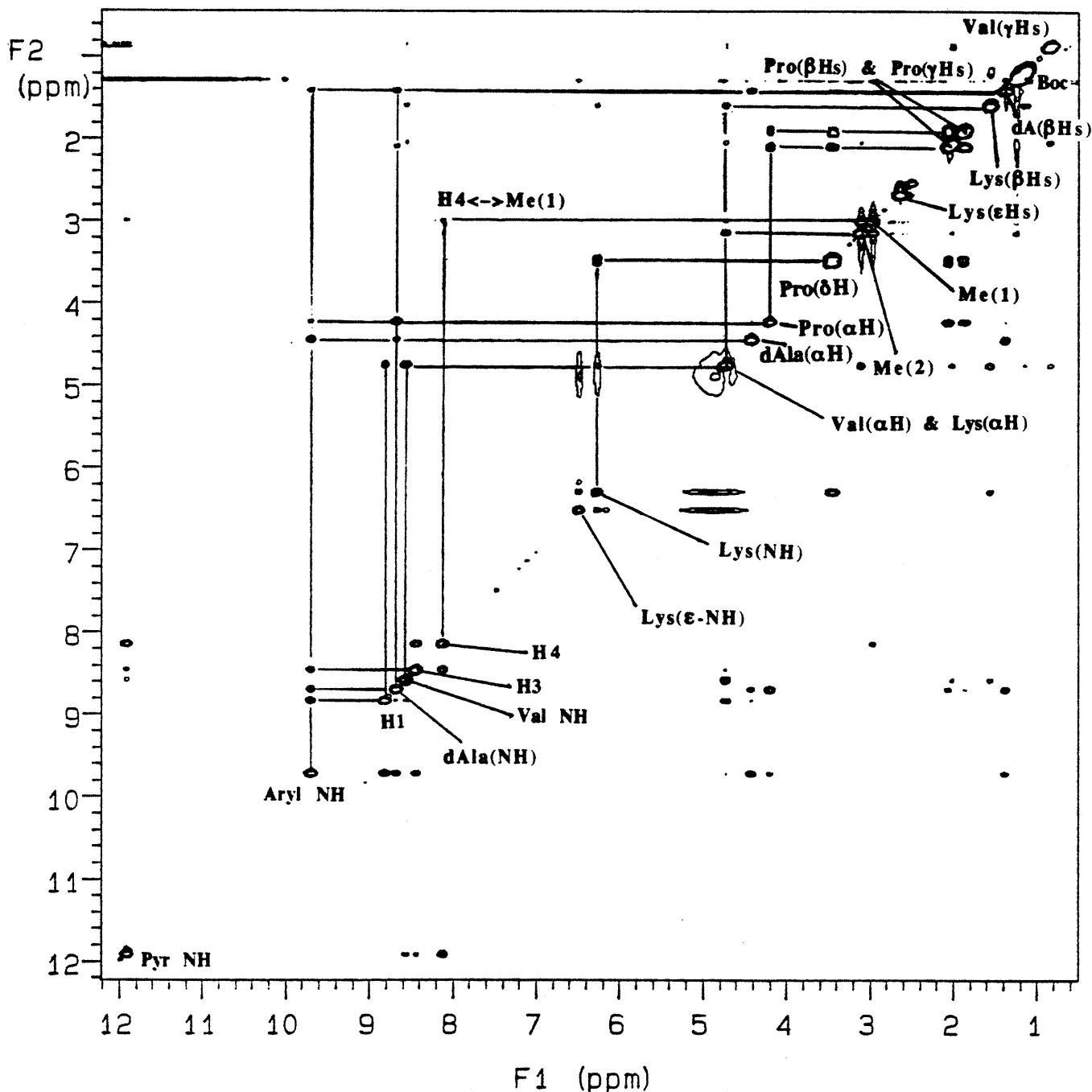


Figure 2-5. Phase-sensitive NOESY spectrum of VK(ϵ -BOC):PdA in DMSO- d_6 , 25°C, acquired on a 500 MHz spectrometer ("Bullwinkle"). Mixing time is 500 msec. with 32 scans per increment. The spectrum is not symmetrized with 270 points in t_1 , and 2K points in t_2 , zero-filled to a 2K X 1K data matrix. The crucial long-range NOE between the epindolidione template proton H4 and the methyl group of the N,N'-dimethylamide function is indicated in the spectrum as H4 \leftrightarrow Me(1).

The long-range NOEs between H4 of the template and the methyl group of the N,N'-dimethylamide moiety, and between H1 and the alpha hydrogen of lysine(ϵ -BOC), provide strong support that at least some fraction of the molecule occupies the β -strand-turn-template hairpin conformation (**1b**, Fig. 2-1) shown in Fig. 2-4.

As was mentioned in Chapter one, the long-range NOE between H4 proton of the template and the methyl group, [CH₃(1)], of the N,N'-dimethylamide moiety is the most important NOE indicating presence of structured β -strand-turn-template hairpin states (**1b** in Fig 2-1; **2a** & **2b**, Fig. 1-2). In fact, this NOE is present in the NOESY spectra of all the tetrapeptide-epindolidione derivatives examined by this researcher in DMSO-d₆, (VW:PdA, VY:PdA, VT:PdA, VK(ϵ -Boc):PdA, VG:PdA, and VN:PdA), as well as in the derivatives examined by Drs. Bowen and Blanchard (FG:PdA, examined by Bowen, 1988; FG:PdA, FV:PdA, and GA:PdA, examined by Blanchard, 1992). These NOE results provide strong evidence that the tetrapeptide-epindolidione derivatives occupy structured β -strand-turn-template hairpin conformations in DMSO-d₆ at room temperature. Furthermore, in all the NOESY spectra examined, there are no NOEs that contradict the predicted peptide-epindolidione derivative conformations.

Having justified that the peptide-epindolidione derivatives **1a** (Fig. 2-1) assume the expected β -strand-turn-template hairpin conformation in DMSO-d₆, we can now turn our attention to examination of the energetics of derivatives **1a** in DMSO-d₆.

Figure 2-6 represents a schematic diagram of the four conformational states ("superstates") that were chosen by Blanchard (Blanchard, 1992) to analyze the conformational behavior of the peptide-epindolidione derivatives **1a** (Fig. 2-1).

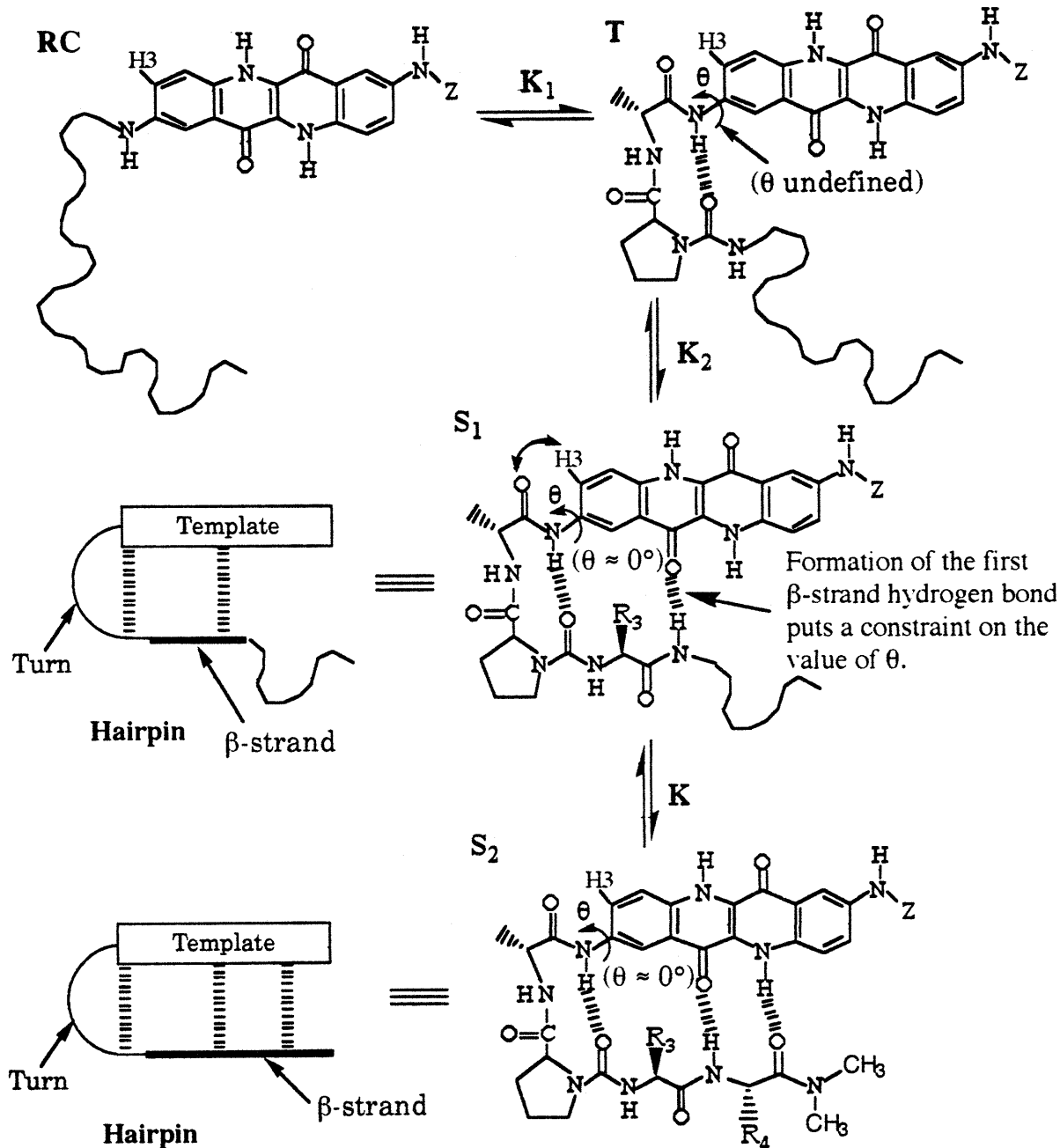


Figure 2-6. Schematic diagram depicting equilibria between the four conformational superstates (**RC**, **T**, **S₁**, & **S₂**) that were discussed in Chapter one (Figs. 1-4 & 1-7, Chapter one; Blanchard, 1992). The squiggly line represents the peptide in a random coil conformation. The dashed lines represent hydrogen bonds. K_1 , K_2 , and K_3 represent equilibrium constants between the given states. To the left of the **S₁**, & **S₂** superstates, a schematic "hairpin" representation of the superstates is given.

In the Figure, **RC** represents derivative **1a** in which the peptide assumes a random coil conformation; **T** represents the peptide in the turn conformation, which is defined by the presence of the turn hydrogen bond; **S₁** represents **1a** with the turn and the first β -strand hydrogen bonds, and **S₂** represents **1a** in a completely structured, β -strand-turn-template hairpin state (**1b** in Fig. 2-1), with all three intramolecular hydrogen bonds present. As we discussed in Chapters one (and will further elaborate in Chapter three), formation of the first β -strand hydrogen bond puts a constraint on the rotation around the C2-aryl-N bond (angle θ in Fig. 2-6), which places the carbonyl oxygen of d-alanine in proximity to the epindolidione H3 hydrogen (double-sided arrow in **S₁**). The constraint caused by formation of the first β -strand hydrogen bond is thought to be the reason why the chemical shift of H3 [and the (aryl NH-H3)/(aryl NH-H1) NOE ratio, see Chapter three] is found useful as a NMR reporter function for the conformational states of **1a** (Chapters one & three; Blanchard, 1992).

In Chapter one, Equation 1-13 defined a quantity named χ , that can be expressed in terms of experimentally accessible quantities δ_{H3} , δ_O , and δ_β . For convenience, χ is given below as Equation 2-1.

$$\chi \equiv \frac{\delta_{H3} - \delta_O}{\delta_\beta - \delta_{H3}} = \frac{K_2(1 + K_3)}{1 + \frac{1}{K_1}} \quad (\text{Eq. 2-1}).$$

In Eq. 2-1, K_1 , K_2 , and K_3 are the equilibrium constants as defined in Fig. 2-6.

As discussed in Chapter one, every derivative **1a** can be assigned a χ value based on its specific value of the H3 chemical shift, δ_{H3} . Furthermore, one can take ratios of χ

values, which result in very useful expressions if the fourth residue of the derivatives used in the ratio is the same. This ratio is given in Eq. 2-2, which suggests that for a pair of derivatives **1a**, with the same fourth residue (*Z* in Eq. 2-2), the ratio of χ 's reduces to the ratio of the equilibrium constants (K_{2X}/K_{2Y}), where *X* and *Y* represent variable amino acid residues in the first β -strand position of **1a**.

$$\frac{\chi(\text{ZX:PdA})}{\chi(\text{ZY:PdA})} = \frac{\frac{K_{2X}(1 + K_{3Z})}{1 + \frac{1}{K_1}}}{\frac{K_{2Y}(1 + K_{3Z})}{1 + \frac{1}{K_1}}} = \frac{K_{2X}}{K_{2Y}} \quad (\text{Eq. 2-2})$$

Table 2-1 gives a list of the H₃ chemical shifts, δ_{H_3} , for 20 derivatives of the general structure *VX:PdA*, along with the corresponding $\chi(\text{VX:PdA})/\chi(\text{VA:PdA}) = K_{2X}/K_{2A}$, and $\Delta\Delta G^\circ_{\text{Ala-X}}$ values (see below), where *X* is the variable third residue.

We can recast the ratio of the equilibrium constants K_{2X}/K_{2A} into free energy difference, or $\Delta\Delta G^\circ$ values using Eq. 2-3. In Eq. 2-3, $\Delta\Delta G^\circ_{\text{Ala-X}}$ represents the free energy change when the derivative *VA:PdA* is "mutated" to *VX:PdA*. Table 2-1 lists the $\Delta\Delta G^\circ_{\text{Ala-X}}$ values calculated using Equation 2-3 and the K_{2X}/K_{2A} data from the third column of Table 2-1.

$$-RT \ln \left(\frac{K_{2X}}{K_{2\text{Ala}}} \right) = -RT \ln (K_{2X}) + RT \ln (K_{2\text{Ala}}) =$$

$$- [RT \ln (K_{2X})] - [-RT \ln (K_{2\text{Ala}})] = \Delta G^\circ_{2X} - \Delta G^\circ_{2\text{Ala}} \equiv \Delta\Delta G^\circ_{\text{Ala-X}} \quad (\text{Eq. 2-3})$$

Table 2-1.

H3 chemical shifts, δ_{H3} , $K_{2\text{X}}/K_{2\text{A}}$, and $\Delta\Delta G^\circ_{\text{Ala-X}}$ values for 20 derivatives of the general formula VX:PdA, where X is a variable amino acid residue.

3 rd Residue (X)	δ_{H3} ¹	$K_{2\text{X}}/K_{2\text{A}}$ ²	$\Delta\Delta G^\circ_{\text{Ala-X}}$ (Kcal/mol) ⁷
N	8.14 ³	0.28 ³	0.75 ⁵
D	8.16	0.31	0.69
G	8.21	0.43	0.50
D(OtBu)	8.29	0.65	0.26
Q(DOD)	8.31	0.71	0.20
Q	8.33	0.78	0.15
A	8.39 ⁴	1.00 ⁴	0.00 ⁶
E	8.40 ³	1.05 ³	-0.03 ⁵
R	8.41	1.10	-0.06
K(ϵ -Boc)	8.44	1.25	-0.13
K	8.45	1.30	-0.16
L	8.46 ⁴	1.35 ⁴	-0.18 ⁶
E(OtBu)	8.46 ³	1.35 ³	-0.18 ⁵
T(OtBu)	8.48	1.49	-0.24
T	8.52	1.76	-0.33
Y	8.55	2.01	-0.41
W	8.61	2.66	-0.58
Y(OtBu)	8.63	2.95	-0.64
F	8.65 ⁴	3.23 ⁴	-0.69 ⁶
V	8.67	3.59	-0.76

¹H3 chemical shifts (ppm) relative to tetramethylsilane (TMS) for derivatives VX:PdA (1a, Fig. 2-1), where X is the variable third residue, and valine (V) is the constant fourth residue, obtained in DMSO-d6 at room temperature (25 °C). (DOD) designates the dimetoxydityl glutamine side chain-protecting group (Fig. 2-8), (ϵ -BOC) designates the tertiary-butylloxycarbonyl epsilon-amino protecting group, and (OtBu) represents the tertiary-butyl side chain protecting group.

² $K_{2\text{X}}/K_{2\text{A}}$ values calculated from δ_{H3} values (second column) using Eqs. 2-1 & 2-2.

³Calculated from derivatives prepared by this researcher.

⁴As reported by Dr. Blanchard in his Doctoral thesis (Blanchard, 1992).

⁵Calculated from derivatives prepared by this researcher using Eq. 2-3.

⁶Calculated from the $K_{2\text{X}}/K_{2\text{A}}$ Blanchard (Blanchard, 1992) data using Eq. 2-3.

⁷In Eq. 2-3, $R = 1.987 \text{ cal K}^{-1}\text{mol}^{-1}$, and $T = 298 \text{ K}$.

The $\Delta\Delta G_{\text{Ala-X}}^{\circ}$ data in Table 2-1 provides a thermodynamic scale for the relative "antiparallel" β -strand forming propensities in DMSO-d6 for a wide range of amino acid residues, including ones with modified side chains. The free energy range spanned by all the derivatives in the data base is 0.75- (-0.76) or 1.51 Kcal/mol.

From the data of Table 2-1, several interesting trends emerge. The first striking observation is that the amino acid residues asparagine (N) and aspartic acid (D) are weaker β -strand formers than glycine (G). This can be rationalized by hypothesizing that Asn and Asp are very weak β -strand-formers due to the ability of their hydrophilic side chains to form intramolecular hydrogen bonding interactions with the peptide backbone, that interferes with the β -strand-promoting hydrogen bonding with the epindolidione template. One such hypothetical interaction is illustrated in the case of VN:PdA in Figure 2-7. In the case of VD:PdA, a similar intramolecular hydrogen bond can form between the side chain carboxyl oxygen of the aspartate residue and the peptide backbone NH. From Table 2-1 we see that the best β -strand former is valine, followed by phenylalanine, tryptophan, tyrosine, threonine, etc. Another trend that emerges from Table 2-1 is that blocking a hydrophilic side chain with a bulky tertiary-butyl group in the case of Asp, Glu, and Tyr leads to higher β -strand-turn-template hairpin stability. The ϵ -BOC-protected lysine appears to be slightly less β -strand-promoting than the free lysine residue. However, lysine differs from the other residues because its side chain is very long. Therefore, since the protecting group is far-removed from the peptide backbone, its effect may be negligible. The slightly lower β -strand stability of derivatives VQ(DOD):PdA and VT(OtBu), relative to the unprotected ones, can be rationalized based on steric hinderance arguments. VQ(DOD):PdA is slightly less stable than VQ:PdA, which may be caused by the difficulty to accommodate the bulky dimethoxydityl (DOD) group within the constraints of the peptide-epindolidione β -strand model, Fig. 2-8. Analogous argument can be used to explain why VT(OtBu) is slightly less stable than VT:PdA.

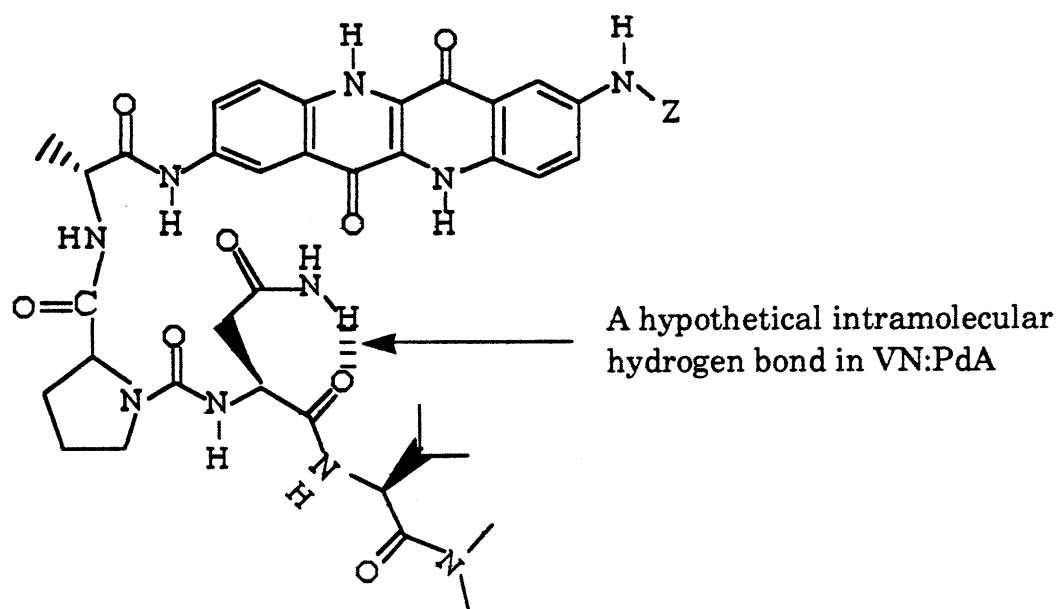


Figure 2-7. Hypothetical structure of peptide-epindolidione conjugate VN:PdA in which an intramolecular hydrogen bond between the side chain of asparagine and the peptide backbone carbonyl leads to loss of β -strand structure. Z denotes the duplicated peptide chain.

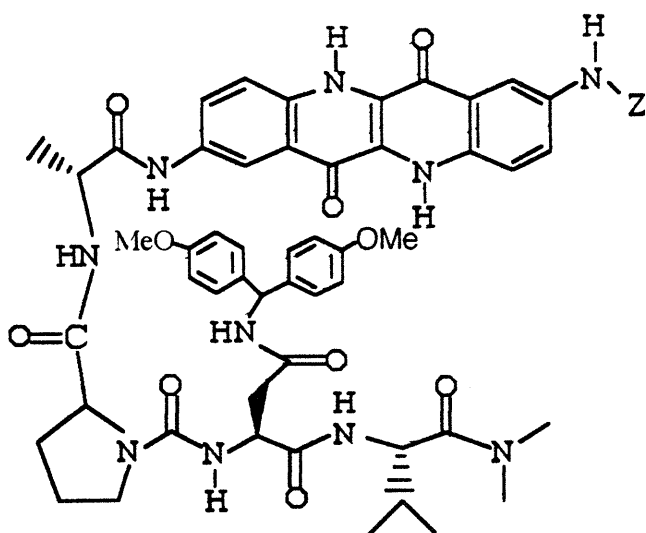


Figure 2-8. Structure of the derivative VQ(DOD):PdA. The bulky nature of the dimethoxydityl (DOD) glutamine side chain-protecting group may not be well accommodated in the peptide-epindolidione β -strand-turn-template hairpin model.

Chapter 3

Investigation of Two Reporter Properties of Peptide-Epindolidione Conjugates in Dimethyl Sulfoxide. Correlation of a Ratio of NOE Intensities with Chemical Shift Changes

From review of the work of Drs. Bowen and Blanchard in Chapter one, we have seen that the chemical shift of proton H3, δ_{H3} , of the epindolidione template proved most useful for conformational analysis of the "antiparallel" peptide-epindolidione β -strand models. In other words, Chapter one demonstrated that changes in chemical shift of H3 can be related to conformational mole fractions if the reference points for limiting conformations (i.e. δ_{O} and δ_{B}) are known. Alternatively, measurement of a ratio of state populations allows independent assessment of conformational mole fractions. For a two-state system that meets stringent structural conditions, conformational mole fractions can in principle be calculated from quantitative NOE measurements (Neuhaus & Williamson, 1989). The main topic of this Chapter is determination of the conformational mole fractions of the peptide-epindolidione conjugates based on quantitative NOE measurements that are independent of chemical shift arguments. This Chapter, therefore, provides evidence for a second reporter property of the peptide-epindolidione conjugates. However, before we discuss this system, we will review the work from two studies that employ principles that are analogous to the ones to be discussed here.

Neuhaus & Williamson (Neuhaus & Williamson, 1989) present an elegant theoretical NOE analysis of the problem of determining the methoxy conformer ratio represented by the equilibrium shown in Fig. 3-1. This investigation has been initially carried out by Mersh & Sanders (Mersh & Sanders, 1981) and further studied by Kruse and collaborators (Kruse et al., 1985). From the NOE analysis, Neuhaus & Williamson (Neuhaus & Williamson, 1989) estimate that the conformer ratio **1a/1b** is about 15. This preference is presumed to be the result of a stereoelectronic effect between the methoxy oxygen lone pair and the C-C σ^* antibonding orbital of the olefin in conformer **1a** (Fig. 3-1).

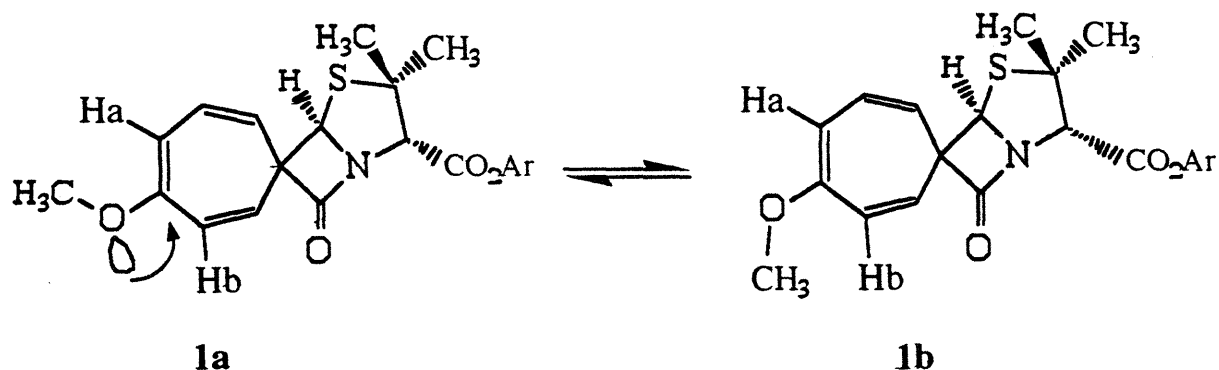
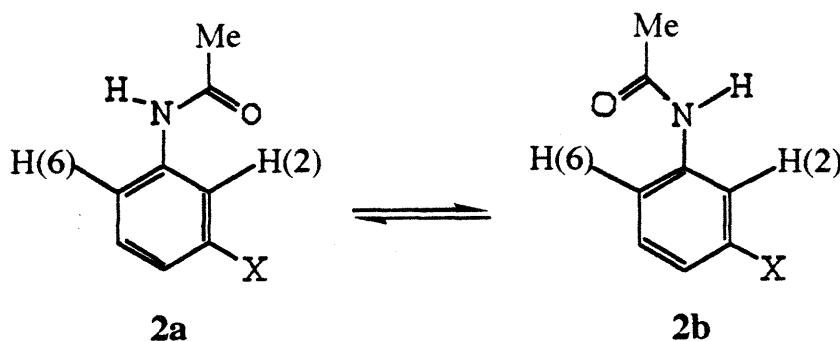


Figure 3-1. Methoxy conformer equilibrium diagram. Conformer **1a** is more stable than **1b**, probably due to the stereoelectronic effect indicated by the curved arrow (Neuhaus & Williamson, 1989).

Another example which is of central importance to the work presented in this Chapter, is that of Camilleri and coworkers (Camilleri et al., 1988). In this work, the authors show that certain meta-substituted anilides show a distinct preference for one particular conformer. This is illustrated by the conformer equilibrium shown in Fig. 3-2, where X indicates the structure of the meta-substituent. NOE difference experiments have been used to rationalize the unexpectedly large difference between the chemical shifts of protons H(2) and H(6) in Fig. 3-2. In particular, H(2) was found to be more deshielded than expected based on the electronegativity of the substituent X. The NOE evidence suggests that this effect can be justified if the anilides show a preference for conformer **2a**.



X = H, Me, OMe, Cl, CN, and NO₂.

Figure 3-2. Conformer equilibrium for meta-substituted anilides; In the equilibrium there is a preference for conformer **2a** (Camilleri et al., 1988).

These two literature examples clearly show that although in most cases it is very difficult to draw quantitative conclusions based solely on NOE measurements in small molecules (Neuhaus & Williamson, 1989), there are special cases when this is possible, especially when there is other collaborative evidence (e.g. structurally predictable changes in chemical shifts) to support such conclusions. This Chapter explores such an issue in great detail by providing a correlation between measured NOE ratios and chemical shift changes in the H3 proton of the epindolidione template that confirm and enforce important conclusions about the conformational behavior of the peptide-epindolidione models studied in this work.

In 1992, Cosmas Giallourakis (Giallourakis, 1992) in this laboratory suggested from NOESY spectral analysis that the (aryl NH-H3)/(aryl NH-H1) NOE ratio (estimated by Giallourakis through cross-peak volume integration of NOESY spectra) can be used as a potential new reporter of β -strand structure for peptide-epindolidione derivatives **3** (Fig. 3-3), in addition to the chemical shift of the H3 proton. In this Chapter, his initial results have been extended and theoretically justified. Furthermore, carefully designed kinetic NOE experiments have been performed to accurately determine the (aryl NH-H3)/(aryl NH-H1) NOE ratios.

It is possible to obtain some insight as to why the (aryl NH-H3)/(aryl NH-H1) NOE ratio may be useful as a new reporter function from examination of Figure 3-4. Peptide-epindolidione β -strand states represented as **S₁** or **S₂** (Fig. 3-4) position the aryl NH adjacent to H1 (open arrow in **S₁** or **S₂**). Measurement of their abundance relative to states that position the NH adjacent to H3, open arrow in **T(Anti)** should provide an independent measure of β -strand stabilization. Furthermore, Fig. 3-4 suggests that the NOE ratio should be correlated to the value of δ_{H3} , because when the aryl NH is closest to H1 in **S₁** or **S₂**, the H3 proton is closest to the carbonyl oxygen of d-Ala (curved arrow in **S₁** or **S₂**) which causes its chemical shift anisotropy,

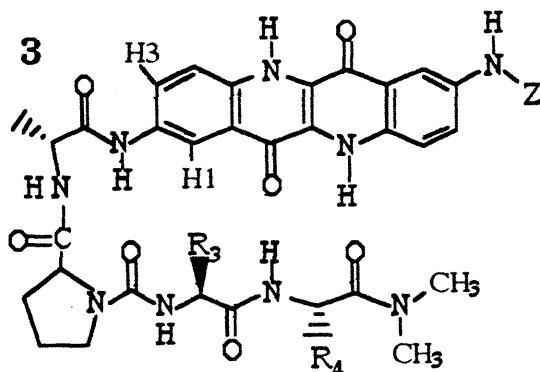


Figure 3-3. Structure of the "antiparallel" peptide-epindolidione conjugate of the general formula XY:PdA (see Figs. 1-1 & 1-2 in Chapter one for more detail).

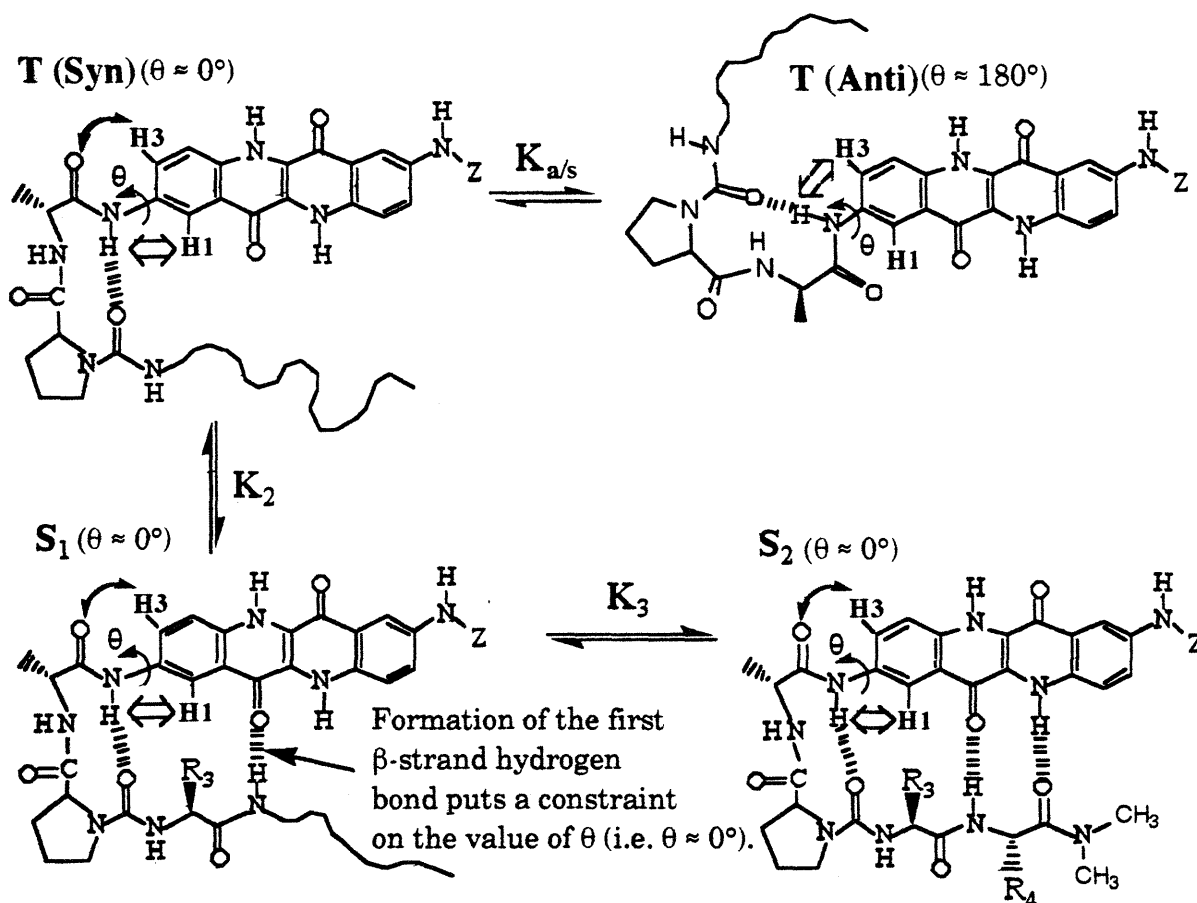


Figure 3-4. Schematic diagram of peptide-epindolidione conjugate in four conformational superstates. The structured superstates **S₁** and **S₂** position the aryl NH in close proximity to H1 (open arrow). In contrast, the **T (Anti)** superstate positions the aryl NH in proximity to H3. $K_{a/s}$ represents the equilibrium constant between the **T (Anti)** and the other superstates with $\theta \approx 0^\circ$. The squiggly line represents peptide in the random coil conformation. See text for more details.

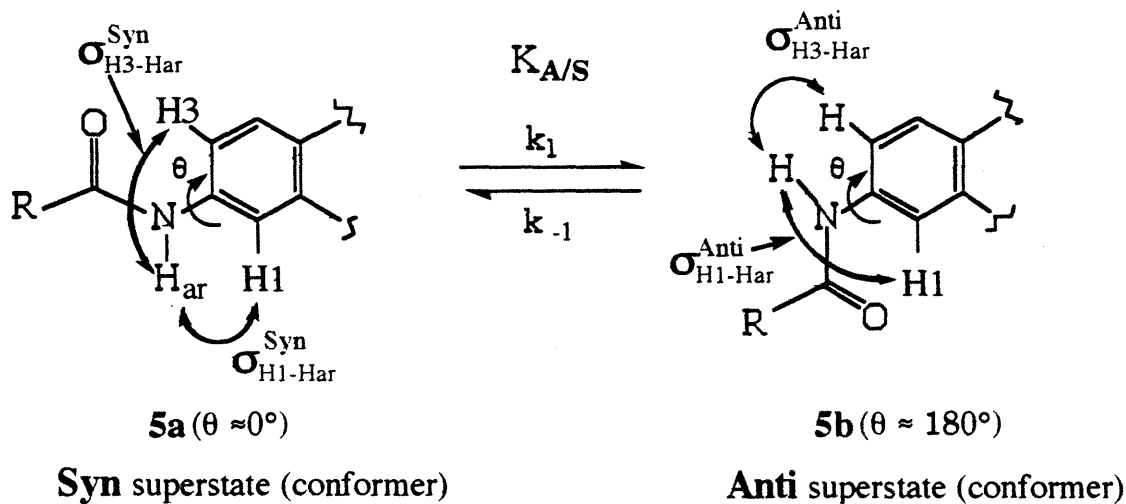


Figure 3-5. The acylanilide region of two superstates, **5b(Anti)**, with $\theta \approx 180^\circ$, and **5a(Syn)**. R representing the peptide. k_1 and k_{-1} represents the forward and reverse rate constants for interconversion of the **5a(syn)** and **5b(anti)** conformers. The relevant NOE interactions are indicated by the curved arrows and represent cross-relaxation rate constants, $\sigma_{i,j}$. (See Appendix A for more detail).

as discussed in Chapter one. On the other hand, in the non- β -strand-initiating conformation **T(Anti)**, the aryl NH is closest to H3, while the carbonyl oxygen of d-Ala is furthest removed from H3.

Figure 3-5 shows an enlarged representation of the acylanilide region of peptide-epindolidione conjugate in the **Syn (5a)** and **Anti (5b)** superstates or conformers, with the R group representing the peptide. $K_{A/S}$ represents the equilibrium constant for interconversion of the **Syn** and **Anti** conformers. The relevant NOE interactions are indicated by the curved arrows and represent cross-relaxation rate constants, $\sigma_{i,j}$. A more detailed exposition of the NOE theory that underlies the analysis given in this Chapter is reviewed in Appendix A that belongs to this Chapter. Appendix A also shows that the cross-relaxation rate constant, $\sigma_{i,j}$ is proportional to the product of the distance between the protons i and j times the correlation time (τ_c) for the vector joining the protons.

The equilibrium constant depicted in Figure 3-5 is defined by the following equation

$$K_{A/S} \equiv \frac{N_{\text{Anti}}}{N_{\text{Syn}}}, \text{ where} \quad (\text{Eq. 3-1})$$

N_{Anti} = mole fraction of the Anti conformer, and

N_{Syn} = mole fraction of the Syn conformer, (i.e. $N_{\text{Syn}} + N_{\text{Anti}} = 1$).

Figures 3-4, 3-5 and Eq. 3-1 assume that the **Syn** and **Anti** conformers are the major species present in solution. In other words, that the system can be approximated to behave as a two-state system. We have seen from the above two literature examples that both Neuhaus & Williamson (Neuhaus & Williamson, 1989), as well as Camilleri et al. (Camilleri et al., 1988) had to make the same assumption in order to analyze their systems. In fact the meta-substituted acetanilide system of Camilleri et al. (Fig. 3-2) is structurally very similar to the acylanilide region of the peptide-epindolidione conjugate depicted in Fig. 3-5. Based on this close structural analogy, we expect our system (Fig. 3-5) to conform to the assumptions that Camilleri et al. had to make to analyze their system.

Besides the two-state assumption mentioned above, two more assumptions are necessary in order to translate the NOE ratios into conformer ratios. It is necessary to assume that superstates or conformers **5a** and **5b** are in fast exchange on both the chemical shift and T_1 time scales, i.e. $k_1, k_{-1} \gg \delta, R_1$ [where $R_1 = (T_1)^{-1}$]. This assumption is very reasonable, since we expect the rotation around the bond C2-N (Fig. 3-5) to be fast due to lack of significant rotational energy barriers. This point is further justified in the next paragraph. The second assumption is that there are no magnetic spins (protons) present in the immediate region between either H1 or H3 and the aryl NH (NH_{ar}) in either the **Syn** or **Anti** conformers. In other words,

to a first approximation, we neglect the effect of the group R in Fig 3-5. This assumption is also very reasonable. Since the NHar to H1 or H3 distances in either the **Syn** or **Anti** conformations, respectively, are both equal and only 2.19 Å (see below), it is highly unlikely that other protons (e.g. from the peptide chain) would violate this assumption.

The derivation of abundance ratios from measured NOE intensities is dependent on knowledge of interproton distances for the states used in the model. For the **Syn** conformer with $\theta = 0^\circ$, the H1 to NHar distance must equal the H3 to NHar distance for the **Anti** conformer with $\theta = 180^\circ$ (2.19 Å from molecular mechanics simulation). The molecular mechanics-calculated dihedral angle θ for acetanilide is $\pm 30.2^\circ$, but rotation to planarity results in an energy increase of only +0.45 kcal/mol. Systematic distortion of this torsional angle θ in **S₂** (Fig. 3-4) demonstrated that $\pm 15^\circ$ changes increased the in-vacuum energy by only 0.2 kcal/mol. θ change of $\pm 15^\circ$ in **5a** of Fig. 3-5 results in a change in NHar-to-H1 distance of $(2.22 - 2.19) = 0.02\text{Å}$, which corresponds to a change of only 8% in $(r/r_0)^6$. The **S₁** and **S₂** superstates are therefore expected to be energetically tolerant within this angular window, and the ratios of NOE intensities are expected to be similarly insensitive. Another important point that can be argued based on distance considerations can be seen from examination of Fig. 3-5. Because the distance between the NHar and H3 in the **Syn** conformer **5a** (3.7 Å from molecular mechanics simulation) is substantially greater than the NHar-to-H1 distance (2.19 Å), we expect that the experimental NOE ratio, $[(\text{aryl NH-H3})/(\text{aryl NH-H1})]_{\text{exper.}}$, or simply $[(\text{NHAr-H3})/(\text{NHAr-H1})]_{\text{exper.}} \approx 0$ for pure **S₁** and **S₂** states. This approximation can be justified based on the 6th power distance dependence of the NOE; Thus, $(r_{\text{H3-Har}}/r_{\text{H1-Har}})^6 = 0.04 \approx 0.0$, where $r_{\text{H3-Har}}$ and $r_{\text{H1-Har}}$ represent the

distances between H3-NHar, and H1-NHar, respectively in S_1 , S_2 or $5a$ (Fig. 3-5).

Based on the discussion in the above paragraph, we can obtain an expression which shows that the experimentally derived, $[(\text{NHAr-H3})/(\text{NHAr-H1})]_{\text{exper}}$, NOE ratio is directly proportional to δ_{H3} . To arrive at such an expression, we need Eq. 1-5 from Chapter one of this thesis which states,

$$\frac{P_{\text{rc}} + P_{\text{t}}}{P_{\text{tot}}} = \frac{\delta_{\beta} - \delta_{\text{H3}}}{\delta_{\beta} - \delta_{\text{O}}}, \quad (\text{Eq. 1-5})$$

where the symbols have the same meaning as defined in Chapter one. Furthermore, we define $N_0 \equiv [(\text{NHAr-H3})/(\text{NHAr-H1})]_{\text{exper}}$ for peptide-epindolidione derivatives that lack the β -strand-turn-template hairpin structure, (i.e. peptide-epindolidione derivatives that only populate the random coil and turn states). With this definition, and the approximation that $[(\text{NHAr-H3})/(\text{NHAr-H1})]_{\text{exper}} \approx 0$ for pure S_1 and S_2 states (Fig. 3-4), we can write

$$\left[\frac{(\text{NHAr-H3})}{(\text{NHAr-H1})} \right]_{\text{exper.}} = N_0 \left(\frac{P_{\text{rc}} + P_{\text{t}}}{P_{\text{tot}}} \right) = N_0 \left(\frac{\delta_{\beta} - \delta_{\text{H3}}}{\delta_{\beta} - \delta_{\text{O}}} \right) \quad (\text{Eq. 3-2})$$

Eq. 3-2 clearly satisfies the above definition of N_0 , and the approximation that $[(\text{NHAr-H3})/(\text{NHAr-H1})]_{\text{exper.}} \approx 0$ for pure states S_1 and S_2 . If $P_{\text{rc}} + P_{\text{t}} = P_{\text{tot}}$,

$[(\text{NHAr-H3})/(\text{NHAr-H1})]_{\text{exper.}} = N_0$. Furthermore, when $P_{\text{rc}} + P_{\text{t}} = 0$,

$[(\text{NHAr-H3})/(\text{NHAr-H1})]_{\text{exper.}} = 0$ as required above.

Algebraic manipulation of Eq. 3-2 (given below) gives Eq. 3-3. Equation 3-3 shows that the chemical shift of proton H3 (δ_{H3}) is a linear function of the experimental NOE ratio.

$$(\delta_{\beta} - \delta_{H3})N_o = (\delta_{\beta} - \delta_o) \left[\frac{(NHAr - H3)}{(NHAr - H1)} \right]_{\text{exper.}}, \text{ or}$$

$$\delta_{\beta} - \delta_{H3} = \frac{1}{N_o} (\delta_{\beta} - \delta_o) \left[\frac{(NHAr - H3)}{(NHAr - H1)} \right]_{\text{exper.}}, \text{ or}$$

$$\delta_{H3} = \delta_{\beta} - \frac{1}{N_o} (\delta_{\beta} - \delta_o) \left[\frac{(NHAr - H3)}{(NHAr - H1)} \right]_{\text{exper.}} \quad (\text{Eq. 3-3})$$

This equation is central to the topic of this Chapter as it shows that based on the assumptions outlined above, we expect the experimental NOE ratio represented by $[(NHAr-H3)/(NHAr-H1)]_{\text{exper.}}$ to be directly proportional to δ_{H3} which, as we have seen from Chapter one, proved to be the most useful reporter property of the peptide-epindolidione derivatives.

The rest of this Chapter will briefly review the initial work of Giallourakis (Giallourakis, 1992) pertinent to the topic of this Chapter, and subsequently will provide detailed experimental evidence in support of Eq. 3-3, as well as some important conclusions that have emerged from this analysis.

In 1992, as part of study of β -turns in peptide-epindolidione conjugates, Giallourakis (Giallourakis, 1992) studied NOESY spectra of tripeptide-epindolidione ester derivatives whose general structure is shown in Figure 3-6. **6a** shows a tripeptide-template conjugate in the **Syn** conformation. The terminal ester group ensures that the tripeptide is capable of forming only the turn hydrogen bond but neither the first nor the second strand bonds. In our abbreviated notation, the tripeptide-template conjugates are name as RO-X:PdA, where RO represents the ester functionality, X is the third amino acid residue, the colon represents the chain-reversing urea functionality followed by proline and d-alanine which is covalently linked to the epindolidione template. From analysis of the NOESY spectra,

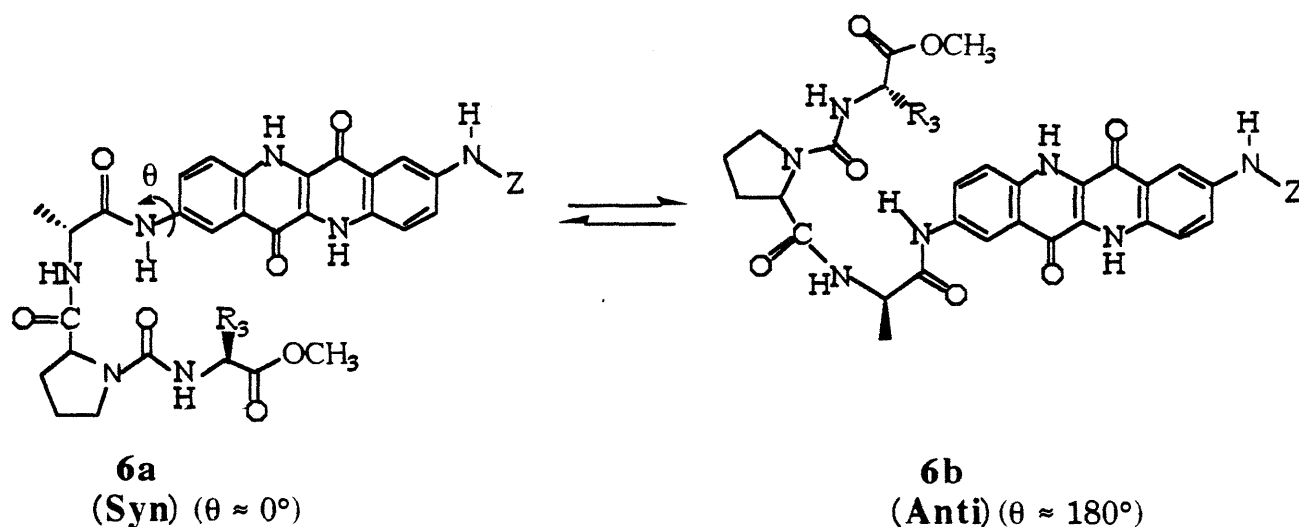


Figure 3-6. **6a**) Tripeptide-epindolidione methyl ester in the **Syn** conformation. **6b**) Tripeptide-epindolidione methyl ester in the **Anti** conformation. The two conformations are interconvertible through rotation about the C2-N aryl bond. Z duplicates the peptide chain.

Giallourakis observed that the experimental NOE ratio, $[(\text{NH}_{\text{ar}}\text{-H3})/(\text{NH}_{\text{ar}}\text{-H1})]_{\text{exper}}$ for the tripeptide-epindolidione ester derivatives is substantially greater than the corresponding NOE ratio measured for tetrapeptide-epindolidione conjugates of general structure **3** (Fig. 3-3). He used cross-peak volume

integration of the NOESY spectra to estimate the NOE ratios. Based on qualitative arguments regarding the distances between H1, H3, and aryl NH, Giallourakis suggested that the NOESY spectral data indicates that the tripeptide-epindolidione esters favor the **Anti** conformation shown in **6b** against the **Syn** conformation **6a**. Giallourakis studied tripeptides with the bulky Val and Ile residues in the third position (X in RO-X:PdA), and estimated the NOE ratios to be about 3:1 in favor of **Anti** conformation. Based on this data, Giallourakis suggested the hypothesis that the preference for the **Anti** conformation may be the result of a steric interaction between the epindolidione template and the side chain of the third residue. This hypothesis is not trivial because the central assumption of the template-peptide system as a model system for β -strand formation is that the template has minimal steric interaction with the conjugated peptide, and that the first β -strand position is equivalent to the second position (Chapter one; Blanchard, 1992).

To test this hypothesis, this researcher prepared the following additional tripeptide derivatives: EtO-G:PdA, MeO-D(OtBu):PdA, MeO-E(OtBu):PdA, and MeO-K(ϵ -BOC):PdA for study in DMSO- d_6 (Chapter, two). The first derivative, EtO-G:PdA was synthesized to test the hypothesis raised by Giallourakis that it may be the steric nature of the side chain of the third residue that results in the preference for the **Anti** conformation. Since the derivative EtO-G:PdA has glycine in the third position, it is expected to exhibit the least amount of steric interaction with the epindolidione core. On the other hand, examination of the derivatives MeO-D(OtBu):PdA and MeO-E(OtBu):PdA with the bulky, tertiary-butyl-protected side chains should provide an important test as to the effect of steric bulk in the third position of the tripeptide derivatives on the experimental NOE ratio.

In order to determine the $[(\text{NHAr-H3})/(\text{NHAr-H1})]_{\text{exper}}$ NOE ratio accurately, a series of truncated driven NOE or TOE kinetic experiments were carried out on three of the above-mentioned tripeptide derivatives, EtO-G:PdA, MeO-D(OtBu):PdA, and MeO-E(OtBu):PdA. Furthermore, NOESY experiments were also performed on these three derivatives to see how the NOE ratios estimated from NOESY cross-peak integration compare with the results obtained from the TOE experiments. For the remaining derivative MeO-K(ϵ -BOC):PdA, NOESY cross-peak integration was used to estimate the $[(\text{NHAr-H3})/(\text{NHAr-H1})]_{\text{exper}}$.

One can compute $[(\text{NHAr-H3})/(\text{NHAr-H1})]_{\text{exper}}$ from NOE experiments in two ways¹ (Neuhaus & Williamson, 1989). The first relies on the linearity of NOE buildup over short irradiation times. In this case let $f_{\text{H3}}\{\text{NHAr}\}(t)$ be the NOE enhancement for proton H3 if the NHAr proton is irradiated for a time t . Then we can write,

$$\left[\frac{(\text{NHAr-H3})}{(\text{NHAr-H1})} \right]_{\text{exper.}} = \frac{f_{\text{H3}}\{\text{NHAr}\}(t)}{f_{\text{H1}}\{\text{NHAr}\}(t)} = K_{A/S} \equiv K_{\text{eq}} \quad (\text{Eq. 3-4})$$

The required NOE enhancements are obtained from a truncated driven NOE (TOE) experiment (Wagner & Wüthrich, 1979), or from a 2D-NOESY experiment with a short mixing time.

Figure 3-7 shows results of the entire TOE experiment obtained on the tripeptide-epindolidione ethyl ester derivative EtO-G:PdA. Figure 3-8 shows the early time dependence of the data points from Figure 3-7. One obvious feature of the

1) A more detailed exposition of the NOE theory that underlies the analysis given in this Chapter, together with Tables of experimental results, are given in Appendix A.

plot in Figure 3-8 is the linearity of the initial NOE buildup for both protons H1 and H3 when the aryl NH is irradiated for only a short time. The ratio of the initial slopes from Figure 3-8 is the conformer ratio that we seek. If we let $m(\text{H3})$ denote the slope of the least-square regression line through the experimental data points for the NOE buildup observed for proton H3 in Fig. 3-8, and $m(\text{H1})$ the analogous slope for proton H1, then

$$\left[\frac{(\text{NHAr} - \text{H3})}{(\text{NHAr} - \text{H1})} \right]_{\text{exper.}} = \frac{m(\text{H3})}{m(\text{H1})} = K_{\text{eq}} = \frac{16.7}{10.7} = 1.6. \quad (\text{Eq. 3-5})$$

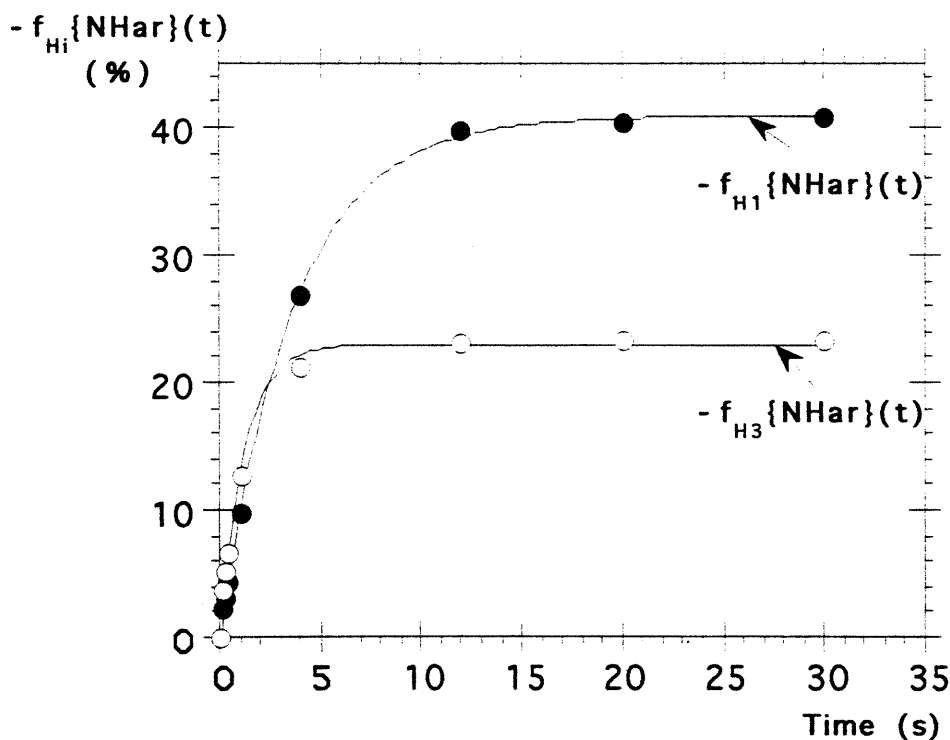


Figure 3-7. Plot of the time-dependent NOE buildup for protons H1 and H3 from a TOE experiment performed on the EtO-G:PdA tripeptide-epindolidione ethyl ester derivative in DMSO-d₆, 30 °C. See text for further details.

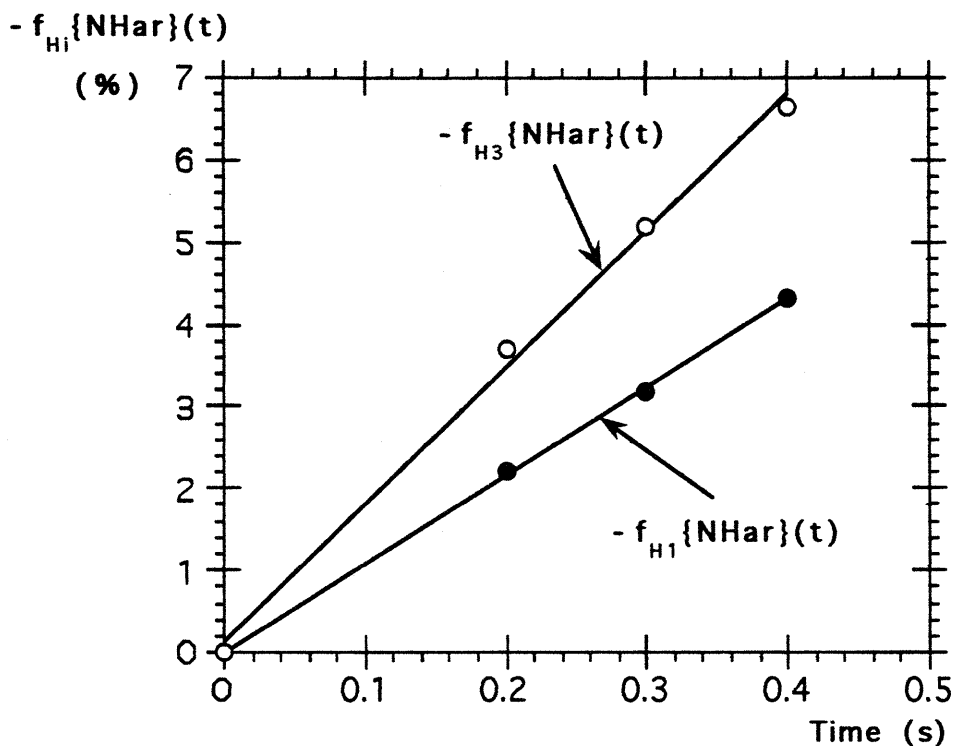


Figure 3-8. Plot of the early time-dependent NOE buildup for protons H1 and H3 from the TOE experiment shown in Figure 3-7.

The result of Eq. 3-5 tells us that the tripeptide-epindolidione derivative EtO-G:PdA prefers the **Anti** versus the **Syn** conformation by a factor of 1.6. This estimation is not as accurate as the one that can be derived from steady-state enhancements that will be discussed below. This is due to the rather small value of the NOE enhancements (see Fig. 3-8) during the early NOE buildup phase of the TOE experiment.

We can estimate the conformer ratio in a second way that employs steady-state enhancements (Neuhaus & Williamson, 1989). The relevant equation that comes out of the theory is Equation 3-6, given below (see Appendix A to this Chapter for more details).

$$K_{\text{eq}} \equiv \frac{N_{\text{Anti}}}{N_{\text{Syn}}} = \frac{f_{\text{H3}}^{\text{ss}} \{H_{\text{ar}}\} \cdot R_{\text{H3}} \cdot \tau_{\text{c,Anti}} \cdot (r_{\text{H3-Har}}^{\text{Anti}})^{-6}}{f_{\text{H1}}^{\text{ss}} \{H_{\text{ar}}\} \cdot R_{\text{H1}} \cdot \tau_{\text{c,Syn}} \cdot (r_{\text{H1-Har}}^{\text{Syn}})^{-6}}, \quad (\text{Eq. 3-6}).$$

In Equation 3-6, $f_{\text{H3}}^{\text{ss}} \{NH_{\text{ar}}\}$ is the steady-state NOE of proton H3 that results from saturation of the aryl NH proton, NHar. $f_{\text{H1}}^{\text{ss}} \{NH_{\text{ar}}\}$ is the steady-state NOE of proton H1 resulting from saturation of Har. R_{H3} and R_{H1} represent the relaxation rate constants for protons H3 and H1, respectively. $\tau_{\text{c,Anti}}$ and $\tau_{\text{c,Syn}}$ are the correlation times for the **Anti** and **Syn** conformers, respectively. $r_{\text{H3-Har}}^{\text{Anti}}$ and $r_{\text{H1-Har}}^{\text{Syn}}$ represent the distances between protons H3 and NHar in the **Anti**, and H1 and NHar in the **Syn** conformations, respectively (see Fig. 3-5). Assuming that (see Appendix A and the Fig. 3-5 regarding the validity of these assumptions)

$$\frac{\tau_{\text{c,Anti}}}{\tau_{\text{c,Syn}}} \approx 1, \text{ and } \left(\frac{r_{\text{H3-Har}}^{\text{Anti}}}{r_{\text{H1-Har}}^{\text{Syn}}} \right)^{-6} \approx 1, \text{ we can finally write,}$$

$$K_{\text{eq}} \equiv \frac{N_{\text{Anti}}}{N_{\text{Syn}}} = \frac{f_{\text{H3}}^{\text{ss}} \{H_{\text{ar}}\} \cdot R_{\text{H3}}}{f_{\text{H1}}^{\text{ss}} \{H_{\text{ar}}\} \cdot R_{\text{H1}}}, \quad (\text{Eq. 3-7}).$$

Thus, according to this treatment, in order to calculate K_{eq} we need to measure

$f_{\text{H3}}^{\text{ss}} \{NH_{\text{ar}}\}$, $f_{\text{H1}}^{\text{ss}} \{NH_{\text{ar}}\}$, R_{H3} , and R_{H1} . The steady state enhancements $f_{\text{H3}}^{\text{ss}} \{NH_{\text{ar}}\}$,

$f_{\text{H1}}^{\text{ss}} \{NH_{\text{ar}}\}$, and the rate constants R_{H3} , and R_{H1} are obtained by fitting the time

dependence of Fig. 3-7 to equation 3-8 given below,

$$F_{\text{Hi}}(t) = f_{\text{Hi}}^{\text{ss}} \{\text{NH}_{\text{ar}}\} [1 - \exp(-R_{\text{Hi}} t)]. \quad (\text{Eq. 3-8})$$

From this fit, we obtain the following estimate for K_{eq} ,

$$K_{\text{eq}} \equiv \frac{N_{\text{Anti}}}{N_{\text{Syn}}} = \frac{f_{\text{H3}}^{\text{ss}} \{\text{NH}_{\text{ar}}\} \cdot R_{\text{H3}}}{f_{\text{H1}}^{\text{ss}} \{\text{NH}_{\text{ar}}\} \cdot R_{\text{H1}}} = \frac{(0.22997) (0.81068 \text{ sec}^{-1})}{(0.40877) (0.2702 \text{ sec}^{-1})} = 1.69. \quad (\text{Eq. 3-9})$$

From Eqs. 3-5 and 3-9, one can see that the conformer ratios obtained by the two methods are identical within experimental error, which is estimated to be within 10% of the reported value. The steady-state results confirm the earlier observation that the derivative EtO-G:PdA prefers the anti conformation by a factor of about 1.7.

An analogous TOE experiment has been performed on the tripeptide methyl ester peptide-epindolidione derivative MeO-D(OtBu):PdA to compare the results with those for the tripeptide EtO-G:PdA discussed above. In contrast to EtO-G:PdA, the third residue of the derivative MeO-D(OtBu):PdA is a bulky tertiary-butyl-protected aspartate. This derivative, therefore, is a good model system to test the hypothesis whether it is the bulk of the side chain of the third residue that causes the tripeptide ester derivatives to favor the **Anti** conformation **6b** (Fig. 3-6). As in the case of the TOE experiments for EtO-G:PdA, we obtained the following data for the derivative MeO-D(OtBu):PdA (Fig. 3-10),

$$\left[\frac{(\text{NH}_{\text{ar}} - \text{H3})}{(\text{NH}_{\text{ar}} - \text{H1})} \right]_{\text{exper.}} = \frac{m(\text{H3})}{m(\text{H1})} = K_{\text{eq}} = \frac{23.6}{9.68} = 2.4. \quad (\text{Eq. 3-10})$$

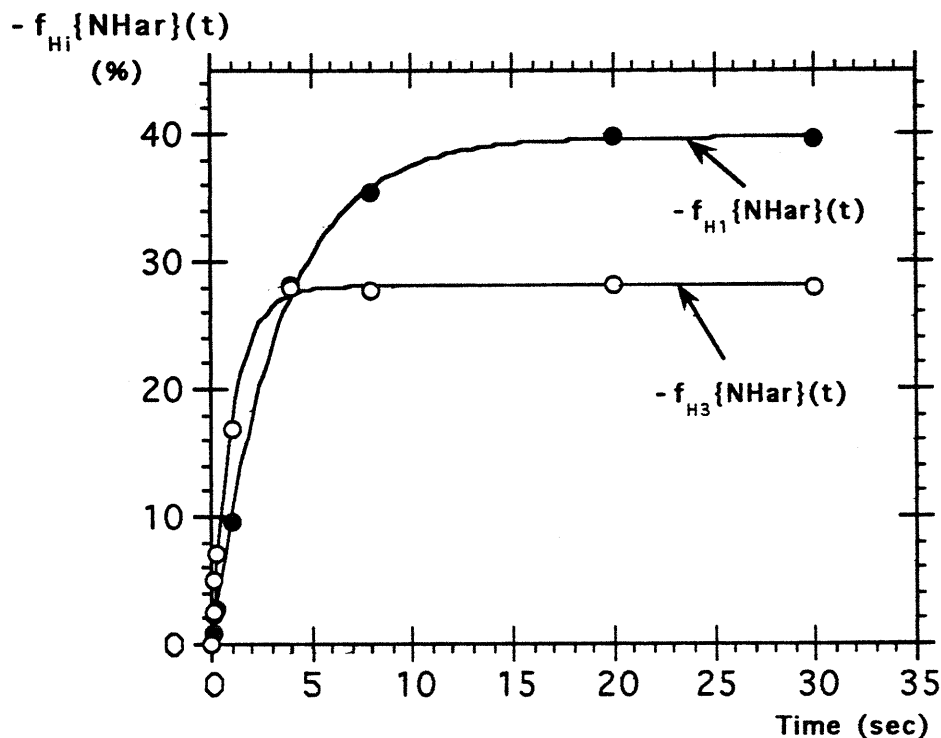


Figure 3-9. Plot of the time-dependent NOE buildup for protons H1 and H3 from a TOE experiment performed on the MeO-D(OtBu):PdA tripeptide methyl ester peptide-epindolidione derivative in DMSO-d₆, 30 °C. See text for further details.

Eq. 3-10 gives the conformer ratio from the ratio of the initial-slopes of the least-square regression line through the experimental points of Fig. 3-10. As before, we can fit the data from the full TOE experiment shown in Fig. 3-9 into Eq. 3-8 to obtain the relevant parameters which are then used to compute the conformer equilibrium using Eq. 3-9. Such a fit gives us the result shown in Eq. 3-11.

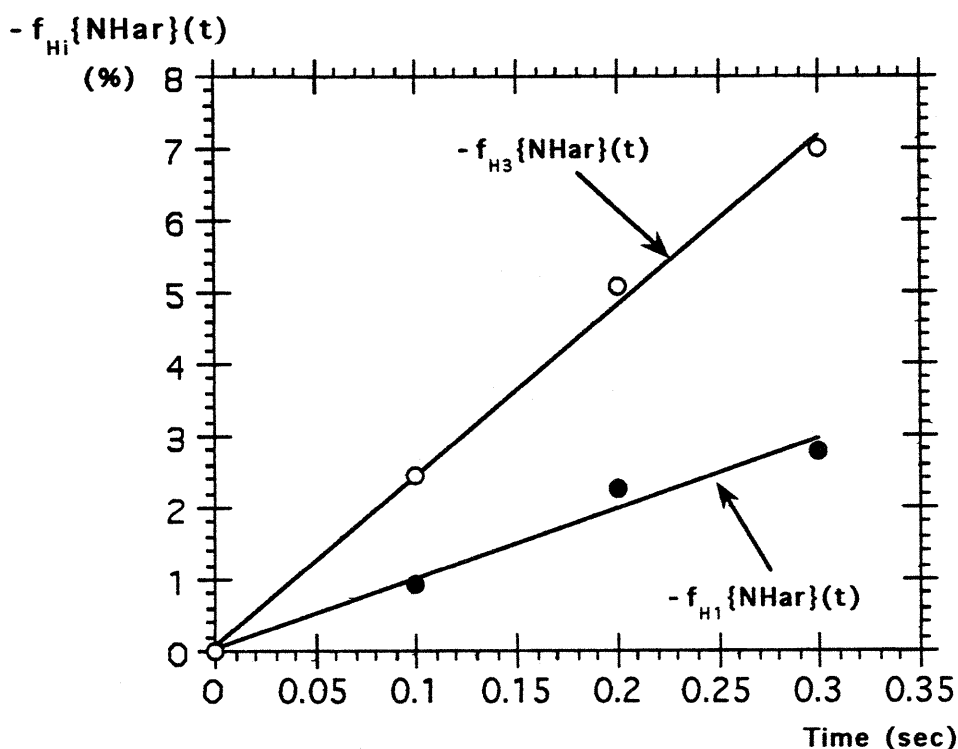


Figure 3-10. Plot of the early time-dependent NOE buildup for protons H1 and H3 from the TOE experiment shown in Figure 3-9.

$$K_{eq} = \frac{N_{Anti}}{N_{Syn}} = \frac{f_{H3}^{ss}\{NH_{ar}\} \cdot R_{H3}}{f_{H1}^{ss}\{NH_{ar}\} \cdot R_{H1}} = \frac{(0.28078)(0.94129 \text{ sec}^{-1})}{(0.3972)(0.2919 \text{ sec}^{-1})} = 2.28. \quad (\text{Eq. 3-11})$$

As was noted in the case of EtO-G: PdA, both the initial-slope approximation and the steady-state data for the MeO-D(OtBu): PdA derivative give a consistent value for the conformer equilibrium constant, K_{eq} . This value is 2.3 in favor of the **Anti** conformation. An additional TOE experiment performed on the derivative MeO-E(OtBu): PdA, which also has a very bulky third-residue side chain, gave

K_{eq} of 2.4. Thus, within experimental error, the K_{eq} values for the two derivatives MeO-D(OtBu):PdA and MeO-E(OtBu):PdA are essentially identical and somewhat larger than the K_{eq} value of 1.7 for the derivative EtO-G:PdA.

The results from the TOE experiments agree with the results obtained from the NOESY spectra using cross-peak integration. They are also consistent with the initial results reported by Giallourakis, who estimated from cross-peak integration of NOESY spectra that derivatives MeO-Val:PdA and MeO-Ile:PdA favor the **Anti** conformation by a factor of about 3:1 (Giallourakis, 1992). This researcher also estimated the K_{eq} for MeK(ϵ -BOC):PdA from NOESY cross-peak volume integration and found it to be 2.6.

From these derivatives we can conclude that there seems to be some influence on the population of the **Syn** and **Anti** states that depends on the nature (size) of the side chain of the third residue (X) in the tripeptide peptide-epindolidione ester derivatives RO-X:PdA. However, this effect is not very large. Nevertheless, since the free energy difference between the various conformations of the peptide-epindolidione conjugates is most likely small (on the order of kT , Blanchard, 1992), this effect may be significant, at least for some of the derivatives with bulky side chains in the first β -strand position.

Earlier in this Chapter, we derived Equation 3-3 which shows that the chemical shift of proton H3 (δ_{H3}) is a linear function of the experimental NOE ratio. The NOE theory that was used to derive conformer ratios from measured NOE intensities for the tripeptide ester derivatives RO-X:PdA can also be employed to derive conformer ratios for the tetrapeptide-epindolidione derivatives **3** (Fig. 3-3) from experimentally measured NOE ratios. Figure 3-11 shows data from the entire TOE experiment obtained on the tetrapeptide-epindolidione derivative VK(ϵ -Boc):PdA. Figure 3-12 shows the early time dependence of the data points from Figure 3-11. As in the case of the tripeptide-epindolidione ester derivatives (Figs. 3-8 & 3-10), the plot in Fig. 3-12 shows the linear nature of the initial NOE buildup for both protons H1 and H3 of derivative VK(ϵ -Boc):PdA when the aryl NH is irradiated for only a short time. The initial-slope approximation gives the $N_{\text{Anti}}/N_{\text{Syn}}$ conformer ratio of 0.6 for VK(ϵ -Boc):PdA, (Eq. 3-12),

$$\left[\frac{(\text{NH}_{\text{ar}} - \text{H3})}{(\text{NH}_{\text{ar}} - \text{H1})} \right]_{\text{exper.}} = \frac{m(\text{H3})}{m(\text{H1})} = K_{\text{eq}} = \frac{17.09}{30.85} = 0.6. \quad (\text{Eq. 3-12}).$$

The steady-state equation that employs the data from the full TOE experiment of Fig. 3-11 gives the conformer ratio of 0.50 (Eq. 3-13),

$$K_{\text{eq}} = \frac{N_{\text{Anti}}}{N_{\text{Syn}}} = \frac{f_{\text{H3}}^{\text{ss}} \{\text{NH}_{\text{ar}}\} \cdot R_{\text{H3}}}{f_{\text{H1}}^{\text{ss}} \{\text{NH}_{\text{ar}}\} \cdot R_{\text{H1}}} = \frac{(0.22497) (0.80287 \text{ sec}^{-1})}{(0.36468) (0.99219 \text{ sec}^{-1})} = 0.50. \quad (\text{Eq. 3-13}).$$

The two results are in good agreement and suggest that the derivative VK(ϵ -Boc):PdA favors the **Syn** conformation by a factor of about 2 to 1. This result is in contrast to the results obtained with the tripeptide-epindolidione ester derivatives which were shown to favor the **Anti** conformation (Eqs. 3-9 & 3-11).

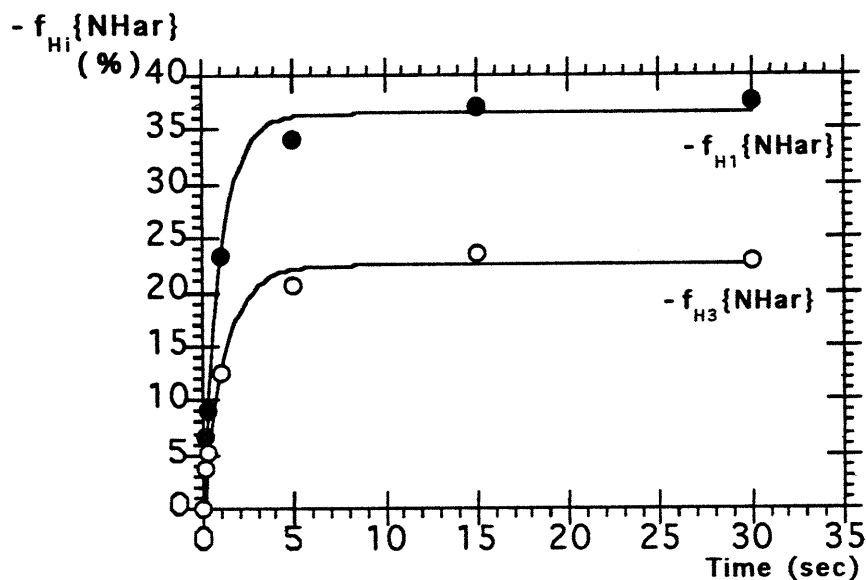


Figure 3-11. Plot of the time-dependent NOE buildup for protons H1 and H3 from a TOE experiment performed on the VK(ϵ -BOC):PdA peptide-epindolidione derivative in DMSO-d₆, 30 °C.

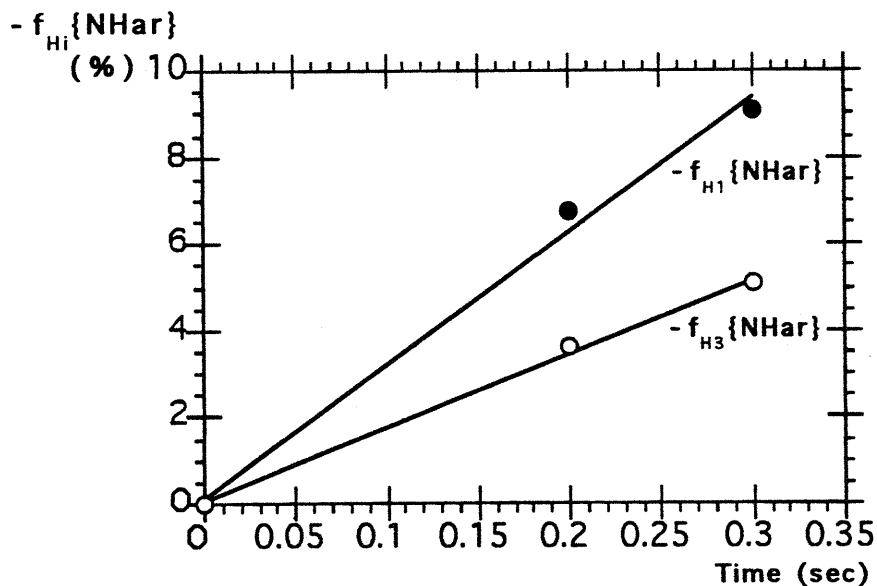


Figure 3-12. Plot of the early time-dependent NOE buildup of Fig. 3-11.

Figure 3-13 plots the H3 chemical shift (δ_{H3}) for 10 tetrapeptide-epindolidione derivatives as a function of the conformer equilibrium constant, K_{eq} , derived from experimental NOE ratios. Eight of the ten derivatives whose data is plotted in

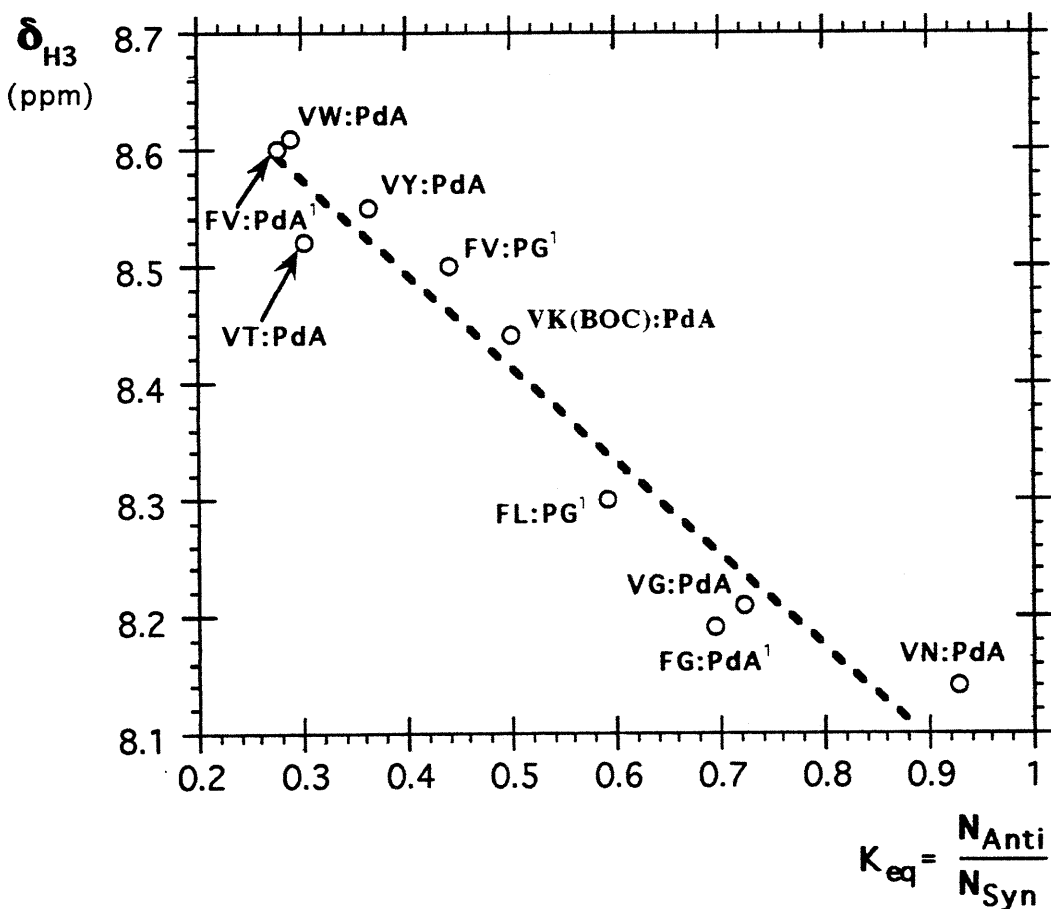


Figure 3-13. Plot of the H3 chemical shift from eight peptide-epindolidione derivatives of general structure **3** (Fig. 3-3), and two derivatives in which Gly replaces d-Ala in **3**, as a function of the conformer equilibrium constant derived from experimental NOE ratios obtained by the methods outlined in the text. Derivatives with a superscript (1) report data obtained by Giallourakis (Giallourakis, 1992). The dashed line represents least-square regression fit through the data points.

Fig. 3-13 are of the general structure XY:PdA (**3** in Fig. 3-3). The other two derivatives differ with respect to the turn structure, where glycine replaces the d-alanine of XY:PdA. Examination of Fig. 3-13 shows that all 10 derivatives have K_{eq} values that favor the **Syn** conformation. Furthermore, the least-square regression line through the data points in Fig. 3-13 has the mathematical form

$$\delta_{H3} = 8.81 - 0.79K_{eq} \quad (\text{Eq. 3-14})$$

with a correlation coefficient of 0.97. Eq. 3-14 clearly validates the prediction of Eq. 3-3 which suggested that δ_{H3} is directly proportional to the experimental NOE ratio, $[(NHAr-H3)/(NHAr-H1)]_{\text{exper}}$.

Figure 3-14 shows a plot of the same data as in Fig. 3-13 except that this graph clearly shows the results of extrapolation of the least square linear regression line to the two axes. According to Eq. 3-3, the "y-intercept" value of 8.81 ppm should correspond to δ_{β} . As we discussed in Chapter one of this thesis, Blanchard (Blanchard, 1992) estimated the value of δ_{β} to be 8.91 ppm. However, Blanchard had to use model systems, solvent extrapolation, and correction for solvent changes in order to arrive at his estimate of δ_{β} . The fact that we were able to obtain an independent estimate for δ_{β} , which is in satisfactory agreement with the estimate of Blanchard, is a very important result. We have seen from the discussion in Chapter two that an accurate estimate of the value of δ_{β} is essential in order to calculate the β -strand propensities of amino acids. Ability to estimate this value using two independent experimental methods adds much more confidence as to the accuracy of the amino acid β -strand propensities that are reported in this thesis.

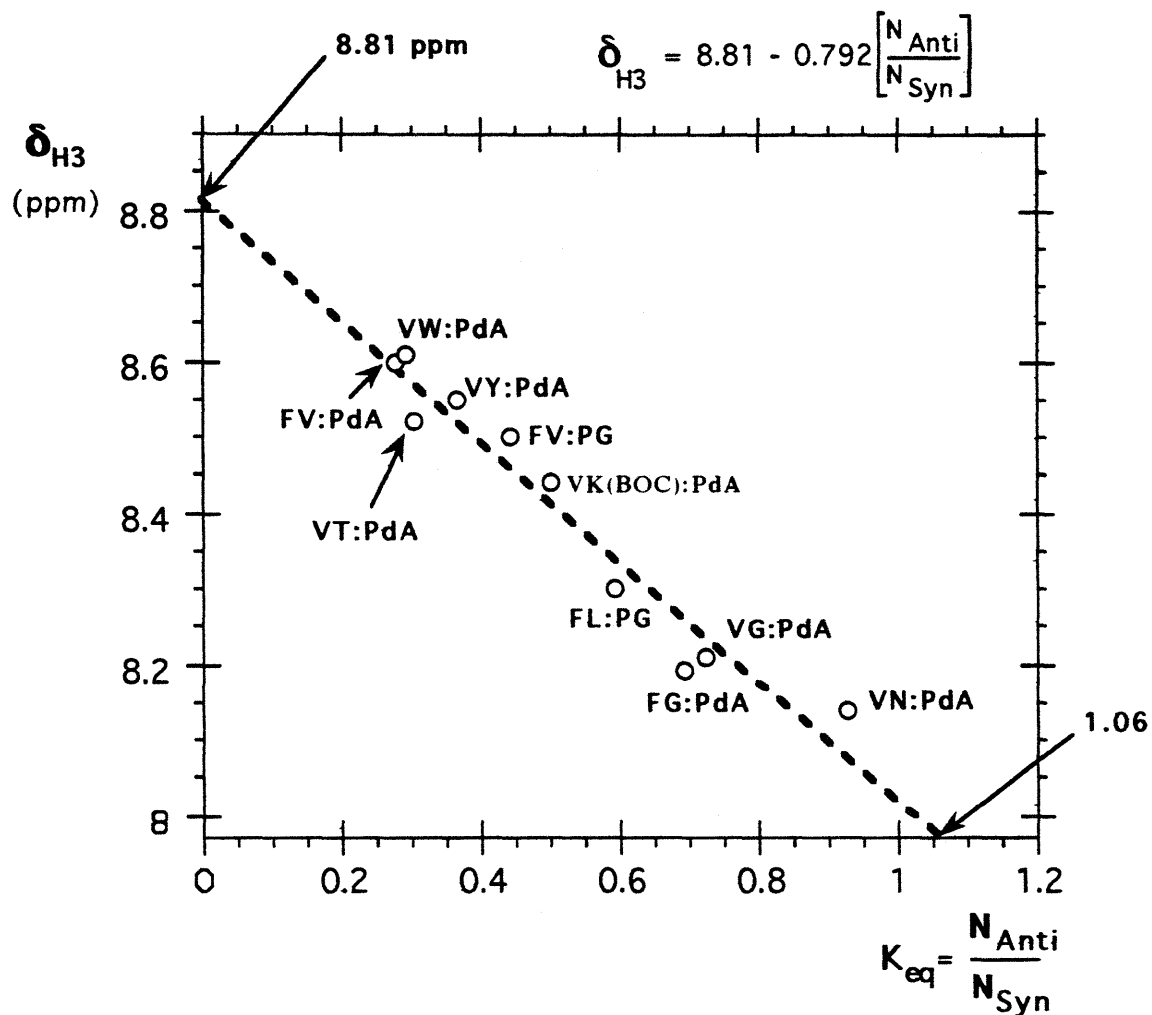


Figure 3-14. Plot of the same data as in Fig. 3-13, except that this graph shows the result of extrapolation of the least square linear regression line to the two axes. The equation that appears above the graph is the equation obtained from a least square fit to the data points.

Figure 3-14 demonstrates another essential point. As we have seen from the discussion of Chapter two, Blanchard used the tripeptide-epindolidione derivatives RO-X: PdA that cannot form β -strand structure to evaluate the lower-limit of the H3 chemical shift (δ_o) for derivatives of general structure **3** (Fig. 3-3). Blanchard

assigned the value of 7.97 ppm to δ_{O} . In Fig. 3-14, at 7.97 ppm, the extrapolated value of $N_{\text{Anti}}/N_{\text{Syn}}$ is 1.06. This is a significant result since it suggests that in the absence of hydrogen bonding interactions, the epindolidione template of **3** (Fig. 3-3) induces no local bias toward the β -strand-initiating **Syn** conformation (Fig. 3-4). This result strongly suggests that the β -strand propensities observed for hydrogen bonding peptide-epindolidione conjugates of structure **3** (Fig. 3-3) are unlikely to arise from an intrinsic affinity between the hydrophobic bulk of the epindolidione template and the attached peptide, either in an unstructured or in a β -turn conformation, but are more likely due to the hydrogen bonding effect of the epindolidione template. This conclusion is in agreement with the initial design objective of the peptide-epindolidione model system, where the epindolidione template was designed to initiate β -strand structure in the conjugated peptide through formation of hydrogen bonds with the peptide. Furthermore, the flat, aromatic epindolidione functionality was chosen to minimize any possible interaction with the peptide, other than that due to hydrogen bonding. The results presented above are clearly consistent with the original design objectives.

The importance of hydrogen bonding is further supported by examination of the striking correlation between the chemical shift of the NH of the fourth amino acid residue (X in **3**, Fig. 3-3) and the chemical shift of H3 (δ_{H3}). This correlation is shown in Figure 3-15. The correlation of Fig. 3-15 is expected on purely structural ground. As we mentioned before, formation of the first β -strand hydrogen bond between the NH of the fourth amino acid residue (X in **3**, Fig. 3-3) and the epindolidione pyridone carbonyl oxygen forces the epindolidione and the turn region to be approximately coplanar, thus constraining H3 to be proximal to the carbonyl oxygen of the d-Ala carbonyl (**S**₁ or **S**₂ in Fig. 3-4).

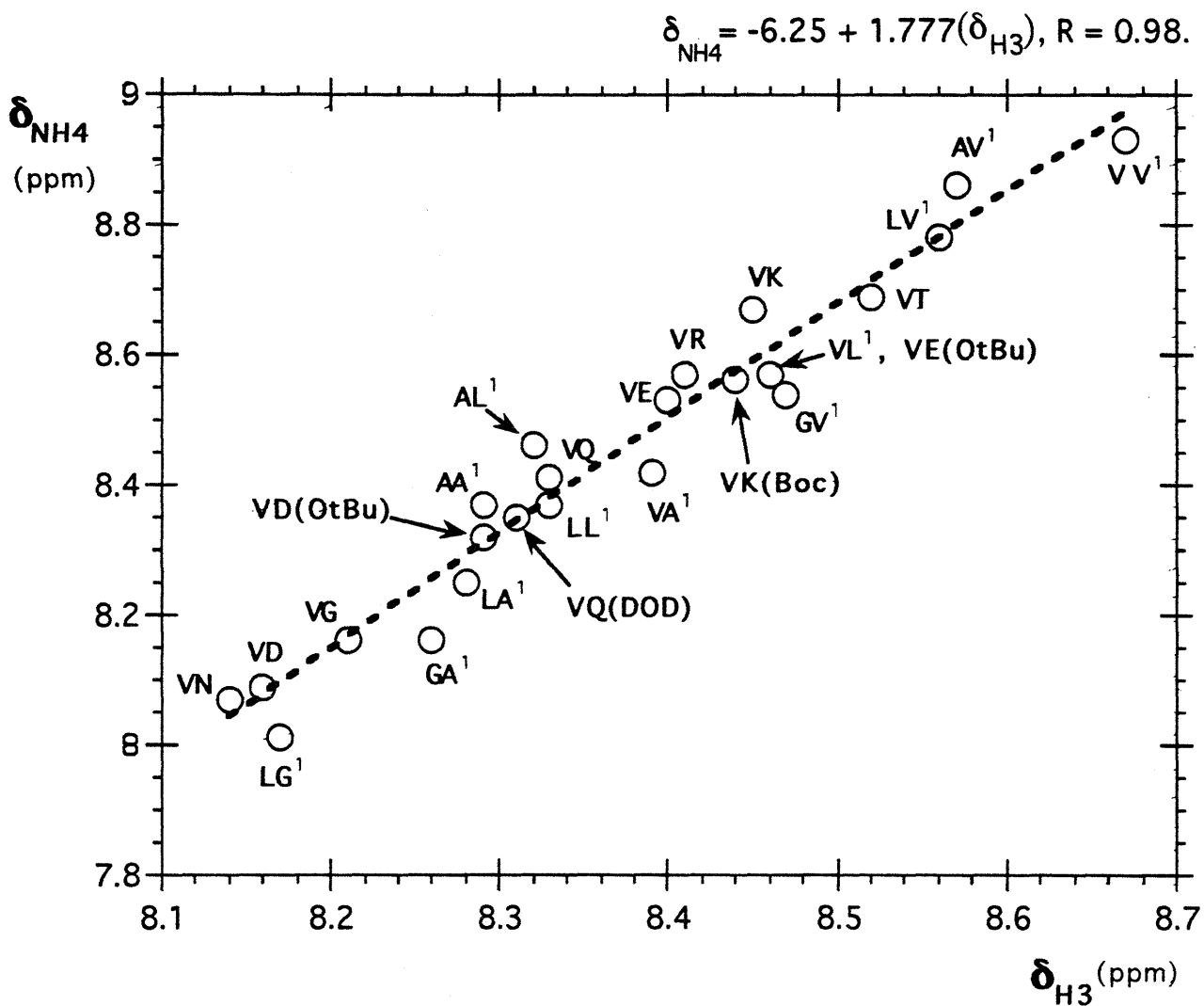


Figure 3-15. Plot of the chemical shift of NH4 (the amide NH of the fourth residue, X in XY:PdA, Fig. 3-3) as a function of the chemical shift of H3 for peptide-epindolidione conjugates of the general structure 3 (Fig. 3-3), in DMSO-d₆, 25 °C. Derivatives with a superscript (1) report data obtained by Blanchard (Blanchard, 1992). The equation that appears above the graph resulted from a least square fit to the data points represented by the dashed line.

Summary and Conclusion

In this Chapter, nuclear Overhauser enhancement (NOE) experiments have been used to establish a second structure-reporting function of the peptide-epindolidione model system that is independent of chemical shift arguments, and therefore validates the original chemical shift-based reporter function of the epindolidione template.

Figures 3-14 and 3-15 demonstrate two independent reporter features of the epindolidione function. Figure 3-15 strikingly demonstrates correlation of a pair of physically separated chemical shifts, and thus reflects global structure. The correlation seen in Figure 3-14 reflects only the local environment of aryl NH, H1, and H3 of the acylanilide function of the epindolidione (Fig. 3-5). Nevertheless, as we have seen from the above discussion, the correlation of Fig. 3-14 demonstrates the essential β -strand-stabilizing role played by the hydrogen bonds formed between the epindolidione template and the conjugated peptide. Taken together the two reporter features (i.e., NOE ratios & H3 chemical shift) confirm the accuracy of measured β -strand propensities, and provide a remarkably detailed characterization of the conformational states of **3** (Fig. 3-3).

Chapter 4

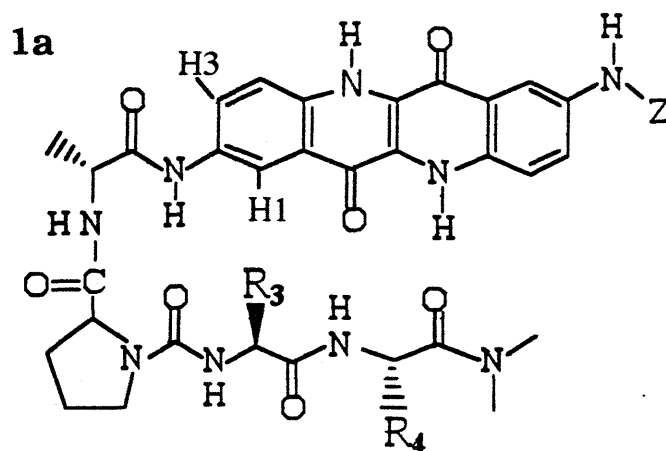
Motives for Investigation of Peptide-Epindolidione Derivatives in Cryoprotective Water-DMSO Mixtures & Introduction to the Unique Physicochemical Properties of Cryoprotective Mixtures

Chapter two provided quantitative estimates of relative β -strand propensities for a wide range of natural and synthetically modified amino acid residues in dimethyl sulfoxide (DMSO). These propensities provide a considerable data base of information regarding the factors responsible for β -strand formation and stability in DMSO. DMSO was chosen as an initial solvent for the study of peptide-epindolidione model systems, because like water it competes strongly for hydrogen bonds, and therefore, as a solvent provides a good test for the effectiveness of the epindolidione template in initiation of β -strand structure. The "antiparallel" DMSO results described in Chapter two, together with the analogous "parallel" propensities determined by Arico-Muendel (Arico-Muendel, 1992), are the first quantitative β -strand propensities determined using a simple synthetic model system. However, from a biological perspective one can argue that these propensities are irrelevant for understanding the energetic factors responsible for β -strand formation in water, because water is a solvent with properties very distinct from that of DMSO. Thus, the ultimate goal of this project is to determine β -strand propensities for amino acids in aqueous media. Unfortunately, the peptide-epindolidione model system designed for DMSO studies (1a in Fig. 4-1 below) is not soluble in pure water. However, as will be shown in the next Chapter, it is soluble in cryoprotective water-DMSO mixtures.

This Chapter will review the initial progress made by other researchers in this laboratory that addresses the study of peptide-epindolidione model system in aqueous media (Arico-Muendel, 1992; Blanchard, 1992), and then will provide an overview of the unique properties of cryoprotective mixtures. As will be seen from the subsequent discussion, cryoprotective mixtures have found widespread application in biology and biochemistry due to their special properties, some of

which are their ability to protect biological structures at cryogenic temperatures (Douzou & Petsko, 1984; Karlsson et al., 1993; Karlsson & Toner, 1995), high viscosity that is useful for detailed NOE characterization of peptides and that also mimics an important property of cytoplasm (Amodeo et al., 1991).

Based on the insights obtained by Arico-Muendel who was the first researcher in this laboratory to study the "parallel" β -strand version of the peptide-epindolidione model in water (Arico-Muendel, 1992), Blanchard redesigned the DMSO-soluble peptide-epindolidione model to render it soluble enough for aqueous studies (Blanchard, 1992). **1a** in Fig. 4-1 gives the structure of the original peptide-epindolidione model used for DMSO studies. **1b** shows the "antiparallel" peptide-epindolidione model redesigned by Blanchard for water studies. **1c** shows the water-soluble version of the "parallel" peptide-epindolidione model that was used originally by Arico-Muendel. In his thesis, Arico-Muendel found that it is necessary to introduce six positive charges into the peptide-epindolidione molecule (**1c** in Fig. 4-1) in order to make it soluble enough for NMR studies in water. Surprisingly, even with six charges per molecule, most of the parallel derivatives studied by Arico-Muendel (with one exception, KFVPdK) require dilution below 10 μM in order to attain convergence in NMR spectra that indicates unassociated or monomeric state.



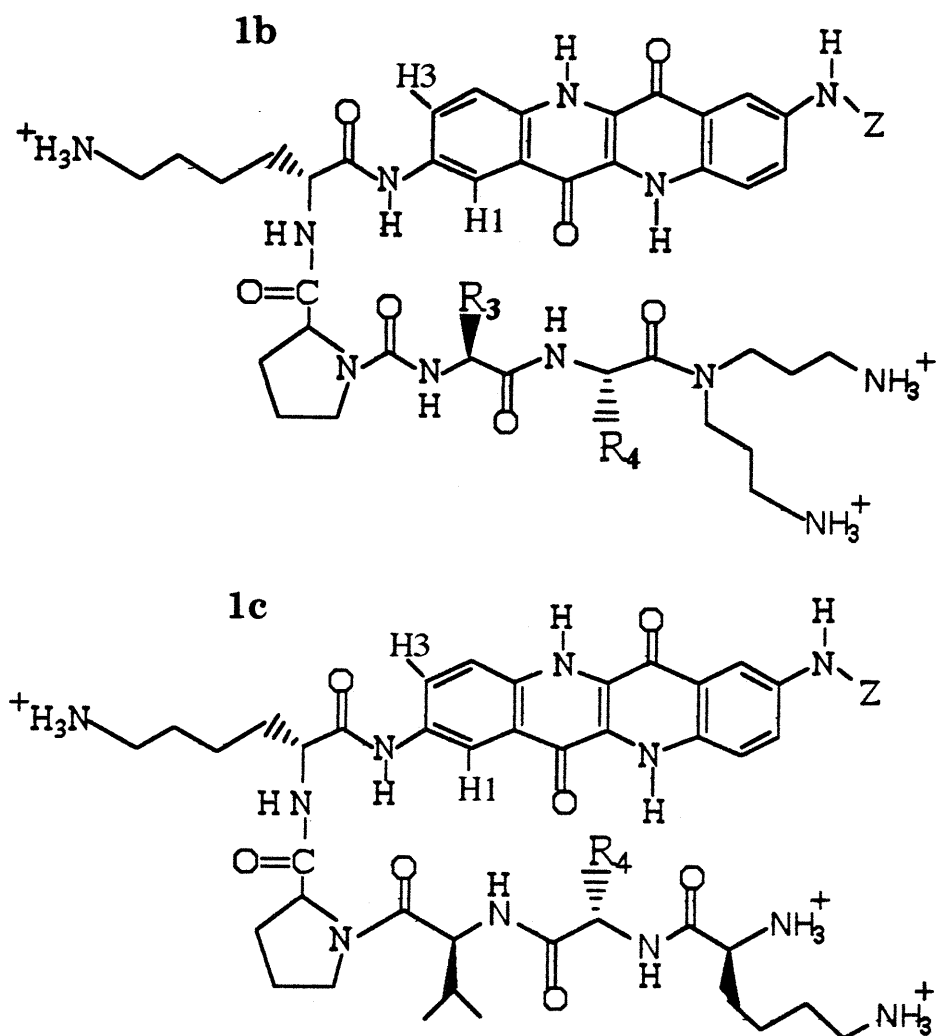


Figure 4-1. **1a)** The original DMSO-soluble peptide-epindolidione model XY:PdA (also see Fig 1-2 of Chapter one). **1b)** Blanchard's water-soluble version of **1a** named wsXY:PdK, where "ws" designates the water-solubilizing *bis*-propylamine, X and Y are the variable fourth and third amino acid residues, respectively, counting from the template; The colon, as before, represents the chain-reversing urea function, followed by Pro and d-Lys which replaces d-Ala in **1a** to maximize water-solubility. **1c)** "Parallel" version of **1b** named KXVPdK (Arico-Muendel, 1992). Z duplicates the peptide chain in all cases (**1a**, **b**, & **c**).

As we discussed in Chapter one of this thesis, proof of the absence of aggregation is a necessary prerequisite before one undertakes conformational studies of these model systems. Blanchard prepared 10 water soluble peptide-epindolidione

derivatives of the general structure **1b** shown in Fig. 4-1. Using NMR-monitored dilution studies, Blanchard determined a criterion under which the general derivative **1b** in Fig 4-1 can be considered monomeric. According to this criterion, a derivative can be considered monomeric in aqueous solution when a 100% dilution of an NMR sample results in the shifts of the aromatic protons of the epindolidione template to be less than 3 Hz (Blanchard, 1992). Table 4-1 lists the 10 water soluble derivatives prepared by Blanchard together with his estimated concentration at which each derivative is thought to be monomeric.

Table 4-1

Blanchard's water soluble peptide-epindolidione derivatives wsXY:PdK (Blanchard, 1992).

4th residue (X)	3rd residue (Y)	Monomeric concentration (mM)
V	V	0.18
V	F	0.20
V	M	0.19
V	L	0.09
V	A	0.19
F	M	0.56
M	V	0.20
L	V	0.22
L	L	0.09
A	V	0.06

From Table 4-1, we can see that even with six charges per molecule (**1b**, Fig. 4-1), the most soluble derivative, wsFM:PdK, is monomeric only at concentration below 0.56 mM. Good quality two-dimensional or 2D-NMR (e.g. 2D-NOESY), usually requires NMR sample concentration of at least 1 mM. As a result, Blanchard was only able to obtain 1D-NMR spectra on the derivatives listed in Table 4-1 (Blanchard, 1992). Furthermore, Blanchard carried out trifluoroethanol-d₂ (TFE) titration experiments on two of the derivatives in Table 4-1 (wsVV:PdK and wsVF:PdK). Based solely on chemical shift arguments, Blanchard concluded that the

derivatives of Table 4-1 become 100% structured in water mixtures with more than 20 mole % TFE. With this information, he proceeded in a manner analogous to that used in the case of the DMSO-soluble derivatives (**1a** in Fig. 4-1) to estimate the χ values, as well as, the equilibrium constants K_2 and K_3 for the derivatives of Table 4-1 (Blanchard, 1992). However, as mentioned above, all the estimates that Blanchard made were based solely on chemical shift arguments. Furthermore, no attempt was made at the time to provide structural evidence (e.g. in the form of NOE experiments) that the derivatives **1b** in Fig. 4-1 (Table 4-1) do indeed assume the predicted β -strand structure in water or water/TFE mixtures. Due to lack of structural data, Blanchard's conclusions of 1992 (Blanchard, 1992) regarding the energetics of the water soluble derivatives in Table 4-1 are tentative at best.

Dr. Roger Kautz, a postdoctoral fellow in this laboratory, undertook 1D and 2D-NMR investigation on the derivatives listed in Table 4-1 with the aim of providing the structural information that was necessary to confirm Blanchard's 1992 conclusions. However, Kautz found out that the NOE experiments in water at room temperatures resulted in inherently weak Overhauser enhancements between even short-range contacts (Kautz, unpublished data). Dr. Kautz attributed this lack of NOEs in water to an intermediate tumbling correlation time, τ_c (see Fig. 4-2 and the discussion that follows). Furthermore, the unusually short relaxation time ($T_{1\rho}$) in the rotating frame prevented the use of rotating frame experiments (e.g. 2D-ROESY) that are specifically designed to investigate NOE behavior of molecules with tumbling correlation times in an intermediate tumbling regime that lead to weak, or zero NOEs in conventional 2D-NOESY or 1D-NOE experiments (Kautz, unpublished data). Moreover, the necessity to carry out the NOE experiments at low concentrations (e.g. < 1 mM, see Table 4-1) in order to avoid aggregation, further added to the above-mentioned problems, resulting in low

sensitivity and the need for very long acquisition times. In order to obtain any useful structural information from NOESY experiments on the derivatives of Table 4-1, Kautz found out that it was necessary to slow down the molecular tumbling through lowering the temperature, and increasing the viscosity of the solvent by addition of trifluoroethanol-d₂ (TFE) to water. Using such conditions, Kautz obtained NOE data which provided evidence that at least some of the derivatives of Table 4-1 (e.g. wsFV:PdK and wsVV:PdK) do assume the required β -strand structure. However, the small size of the data base examined by Kautz is a serious limitation of his study, especially if one wants to draw quantitative conclusions regarding the energetics of the water soluble derivatives.

The difficulties encountered with the NOE work for the derivatives **1b** (Fig. 4-1 & Table 4-1) in water, and water/TFE mixtures stand in sharp contrast to the NOE work in DMSO-d₆ with the DMSO-soluble peptide-epindolidione analogues (**1a** in Fig. 4-1). As we have seen from the discussion in Chapter one of this thesis, all peptide-epindolidione conjugates of structure **1a** (Fig. 4-1) are freely soluble and monomeric at millimolar concentrations in DMSO-d₆. Furthermore, the higher viscosity of DMSO (relative to water) results in tumbling correlation times that lead to relatively strong, negative NOEs for the DMSO-soluble derivatives in DMSO-d₆ at room temperature. As a result, in contrast to the water soluble derivatives **1b** (Fig. 4-1), it was possible to obtain detailed NOE characterization for a number of the DMSO-soluble derivatives **1a** (Fig. 4-1) in DMSO-d₆ (Bowen, 1988; Blanchard, 1992; Chapters two and three in this thesis).

The rest of this Chapter will discuss in some detail the unique properties of cryoprotective mixtures which is the reason why these were chosen as a solvent system of choice for the conformational analysis of the peptide-epindolidione conjugates.

There are four main reasons why the cryoprotective water-DMSO mixtures were chosen as the solvent system of choice for the conformational analysis of peptide-epindolidione conjugates.

- 1) A large number of biochemical and crystallographic studies with proteins in other laboratories have demonstrated that cryomixtures are completely bio-compatible (Douzou & Petsko, 1984). Furthermore, besides biochemical and crystallographic studies, water-DMSO mixtures have found widespread application as solutions used to protect the integrity of biological structure at cryogenic temperatures (Karlsson et al., 1993; Karlsson & Toner, 1995).
- 2) Cryoprotective water-DMSO mixtures are characterized by relatively high viscosities in comparison to both pure DMSO and especially water (Cowie & Toporowski, 1961; Schichman & Amey, 1971). As will be seen from the discussion below, solvents with high viscosities are ideal for NOE study of molecules in the so-called "intermediate" molecular weight size range. Furthermore, the high viscosity of cryoprotective mixtures is thought to mimic an important property of the cytoplasm (Amodeo et al., 1991; Temussi et al., 1992).
- 3) In this study (Chapter five), water-DMSO cryomixtures were found to significantly enhance the energetic stability of β -strand-turn-template hairpin structure (Fig. 1-2, Chapter one) in the peptide-epindolidione model.
- 4) The large set of peptide-epindolidione derivatives synthesized for DMSO studies (1a in Fig. 4-1) proved to be monomeric in cryoprotective water-DMSO mixtures at millimolar concentrations, which allowed extensive 2D-NOESY structural characterization of a number of such derivatives (Chapter five).

Cryoprotective mixtures or cryomixtures can be defined as mixtures of certain organic solvents with water. The best examples are mixtures of water with dimethyl sulfoxide (DMSO) or water with a variety of alcohols and polyols (e.g. ethylene glycol or glycerol). In Biochemistry, cryomixtures have been extensively investigated by Douzou and collaborators (Douzou, 1977; Douzou & Petsko, 1984). Specifically, cryomixtures were employed in the study of enzymatic reactions at low temperatures in order to take advantage of the slower reaction rates at lower temperatures (Douzou, 1977; Douzou & Petsko, 1984). Furthermore, cryomixtures were employed in the crystallography of a variety of proteins (Douzou & Petsko, 1984). The studies of the research groups of Douzou & Petsko have demonstrated that cryomixtures are fully bio-compatible. In other words, cryomixtures were found to have a minimal and predictable effect on a large number of enzyme systems and reactions (Douzou & Petsko, 1984).

Besides the studies mentioned above, cryomixtures have found widespread application in the study of bio-active peptides by NMR spectroscopy (Motta et al., 1987; Verheyden et al., 1990; Amodeo et al., 1991; Temussi et al., 1992). All these studies support the hypothesis that cryomixtures have properties very similar to that of water, and are well-suited for a wide range of biochemical studies.

Cryomixtures have also been widely used in cryopreservation of cells and tissues (Karlsson et al., 1993; Karlsson & Toner, 1995). Cryopreservation is a technique used to maintain biological materials (e.g. cells, tissues, etc.) at cryogenic temperatures. It takes advantage of the fact that most biochemical reactions and physical processes are dramatically reduced in rate at cryogenic temperatures (i.e. at the boiling point of liquid nitrogen, $-196\text{ }^{\circ}\text{C}$).

Since the serendipitous discovery by Polge and collaborators in 1949, which demonstrated that addition of glycerol can protect sperm during cryopreservation (Polge et al., 1949), the use of cryoprotectants such as DMSO and alcohols has become routine in cryopreservation of a large variety of biomaterial (Karlsson et al., 1993). The exact nature of the mechanism by which cryoprotectants such as DMSO work is not known at the present time, but a number of hypotheses have been proposed (Fink, 1986; Fahy et al., 1987; Karlsson et al., 1993; Karlsson & Toner, 1995). One likely mechanism why cryoprotectants are beneficial during low temperature storage of biological structures is that they invariably lower the equilibrium melting point of the mixture, and thus can prevent ice crystal formation which is thought to be deleterious to cells and tissues (Karlsson et al., 1993; Karlsson, Cravalho, & Toner, 1993). Another aspect of the protective effect of cryoprotectants when added to water is the high viscosity of cryomixtures which can dramatically reduce both the rates of nucleation and growth of ice crystals in the intra and extracellular space (Karlsson et al., 1993). Indeed, this phenomenon is employed in the widely used process of vitrification in which one uses large concentrations of cryoprotectants (e.g. DMSO) to totally prevent ice formation during cryopreservation (Fahy et al., 1987).

From the above discussion, it is clear that not only "simple" enzymes and reactions, but whole cells and complex multicellular assemblies or tissues can survive and function after exposure to cryomixtures. Since the functioning of cells and tissues is a highly integrated and complex process that is extremely sensitive to most changes in physical or chemical conditions, the fact that these systems can survive exposure to concentrated cryoprotectants such as DMSO is a strong evidence that cryomixtures are fully bio-compatible and therefore must share many properties in common with the milieu of the cytoplasm.

As we have seen from the review of the work of Dr. Kautz, he found that the peptide-epindolidione derivatives of structure **1b** (Fig. 4-1) exhibit few or no useful NOEs in water. One can see the origin of this effect more clearly by examining the graph in Figure 4-2. Figure 4-2 plots the maximal theoretical homonuclear NOE enhancement, $f_I\{S\}_{\max}$, as a function of the product $\omega\tau_c$, where ω is the spectrometer frequency (e.g. 500 MHz for ^1H), and τ_c is the rotational correlation time of the molecule under investigation. For clarity, $\omega\tau_c$ is plotted in a log scale.

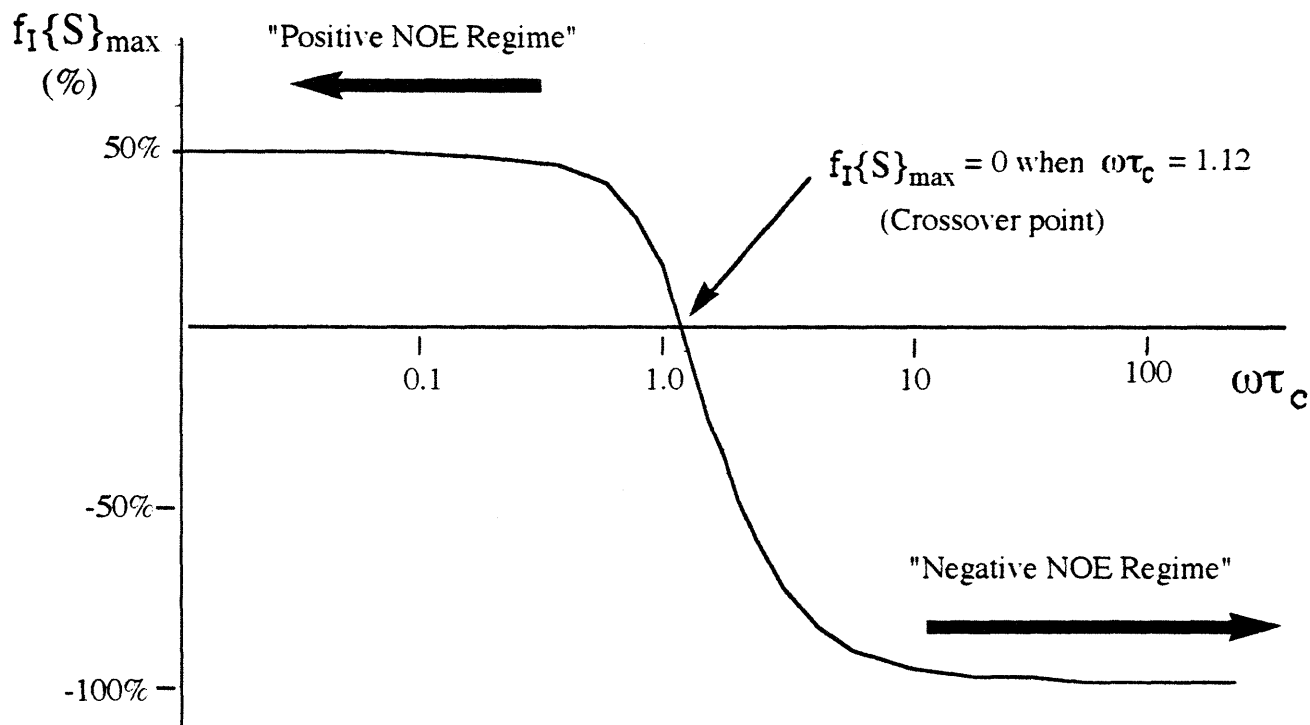


Figure 4-2. Schematic plot of the maximum theoretical homonuclear NOE enhancement, $f_I\{S\}_{\max}$, as a function of $\omega\tau_c$. Depending on the sign of $f_I\{S\}_{\max}$, one can define the "positive NOE regime" where $f_I\{S\}_{\max} \approx +50\%$, and the "negative NOE regime" where $f_I\{S\}_{\max} \approx -100\%$. The region where $f_I\{S\}_{\max} \approx 0\%$ is usually referred to as the "crossover point" (Neuhaus & Williamson, 1989).

The maximum theoretical homonuclear NOE enhancement function has the form given by Eq. 4-1 below (Neuhaus & Williamson, p. 36).

$$f_{\text{I}}\{\text{S}\}_{\text{max}} = \frac{5 + (\omega\tau_c)^2 - 4(\omega\tau_c)^4}{10 + 23(\omega\tau_c)^2 + 4(\omega\tau_c)^4} \quad (\text{Eq. 4-1}).$$

In Eq. 4-1, $f_{\text{I}}\{\text{S}\}_{\text{max}}$ represents the maximum theoretical homonuclear NOE enhancement observed at proton I when proton S has been saturated. From Eq. 4-1 and Fig. 4-2 we can see that for small organic molecules in non-viscous solvents (e.g. acetone), the rotational correlation time is very short, which results in a vanishingly small value for the product $\omega\tau_c$. This leads to $f_{\text{I}}\{\text{S}\}_{\text{max}}$ of 0.5 or 50% under such limiting conditions. In the other extreme, for molecules of large molecular weight (e.g. small proteins), molecular tumbling is slow, hence τ_c is relatively long, and $\omega\tau_c$ becomes large. In the limit of very slow tumbling, $f_{\text{I}}\{\text{S}\}_{\text{max}}$ has the value of -1 or -100%. From Fig. 4-2 we can see that there are two regions or regimes that are frequently referred to in the NMR literature. The so-called "negative NOE regime" refers to relatively large molecules, or smaller molecules in viscous solvents (see below). On the other hand, "the positive NOE regime" or "the extreme narrowing regime" refers to small organic molecules in non-viscous solvents such as acetone. From a practical viewpoint, it is most convenient to run NOE experiments (e.g. 2D-NOESY) in the negative NOE regime. The main reason for this is that competing relaxation processes (which are mostly due to the presence of dissolved molecular oxygen) are much more efficient in the positive NOE regime. This results in decrease in the observed positive NOE enhancements, well below the maximum theoretical value of 50% (Neuhaus & Williamson, 1989). Thus, work in the negative NOE regime is often much more convenient from a practical point of view. For our purposes, and especially relevant to the NOE work with the water soluble peptide-indolizone derivatives **1b** (Fig 4-1), is the central region in Fig. 4-2 between the

positive and negative NOE regimes. From Fig. 4-2 we can see that $f_1\{S\}_{\max}$ is zero when the numerator of Eq. 4-1 is zero. Solving $5 + (\omega\tau_c)^2 - 4(\omega\tau_c)^4 = 0$ for $\omega\tau_c$, gives $\omega\tau_c = (5/4)^{1/2} \approx 1.12$. At the high magnet fields (e.g. corresponding to $\omega = 300\text{-}600$ MHz for ^1H) that are required to resolve the spectra of even the simplest peptide systems, it so happens that for peptides in the molecular weight range of 1000-2000 amu in water, the product of $\omega\tau_c \approx 1.12$, and the NOEs vanish. The region of the curve in Fig. 4-2 where the NOE crosses from positive to negative is often referred to as the "crossover point". This is thought to be the reason why Dr. Kautz was not able to observe any useful NOEs for the water soluble derivatives **1b** (Fig. 4-1 & Table 4-1) in water. It is generally known that this difficulty has been overcome with the introduction of the rotating-frame or ROESY pulse sequence (Bax & Davis, 1985). However, the 2D-ROESY spectra are often more difficult to interpret than the corresponding 2D-NOESY spectra due to the presence of undesirable artifacts (e.g. the presence of Homonuclear Hartmann-Hahn, or HOHAHA (TOCSY) effects, see Neuhaus & Williamson, 1989, p. 319)). Furthermore, as we have seen from the above discussion, Dr. Kautz found that the unusually short relaxation time ($T_{1\rho}$) for the aromatic epindolidione template protons of the peptide-epindolidione conjugates of Table 4-1 in water in the rotating frame prevented the use of rotating frame experiments such as the 2D-ROESY. As a result, Kautz had to find conditions under which the derivatives of Table 4-1 could be studied in the negative NOE regime. As we have seen, he accomplished this by lowering the NMR sample temperature, and adding TFE to water (Kautz, unpublished data).

In Fig. 4-2, we see that it is possible to move away from the "crossover point" to the "negative NOE regime" by either increasing the spectrometer frequency ω , or the correlation time of the molecule, τ_c . Since most modern NMR spectrometers

operate at ^1H frequencies of 250-600 MHz, and the highest available fields correspond to 750-1000 MHz, it is easy to see that one cannot gain much by increasing ω , and in cases when one already works at the highest fields available in practice, manipulation of ω is clearly of no help. On the other hand, it is clear that one can increase the product $\omega\tau_c$ by increasing τ_c . One way to increase the value of τ_c is to increase the viscosity of the solvent and/or decrease its temperature. For the isotropic rigid rotor model (which can be used to approximate the rotational, or tumbling motion of spherical molecules) one can use the Stokes-Einstein relationship (Eq. 4-2), which predicts that τ_c is directly proportional to the macroscopic solvent viscosity, and inversely proportional to the sample temperature T . This is expressed by Eq. 4-2, where η is the solvent viscosity, d is the diameter of the spherical solute molecule, k is the Boltzmann constant, and T is the absolute temperature (Tobias & Markley, 1986).

$$\tau_c = \frac{8\pi d^3}{6k} \frac{\eta}{T} \quad (\text{Eq. 4-2.})$$

Water-DMSO cryomixtures are very unusual with respect to the strong dependence of their viscosities on both the temperature and composition of the mixture (Cowie & Toporowski, 1961; Schichman & Amey, 1971). Figure 4-3 shows a plot of the viscosity as a function of composition of the water-DMSO mixture at several different temperatures. Notice that for each isotherm, the viscosity of the binary mixture has a maximum near the molar ratio range of 2:1 water:DMSO, respectively. Another striking feature of the graph is the progressive increase in the sharpness of the viscosity maximum as the temperature of the mixture is lowered.

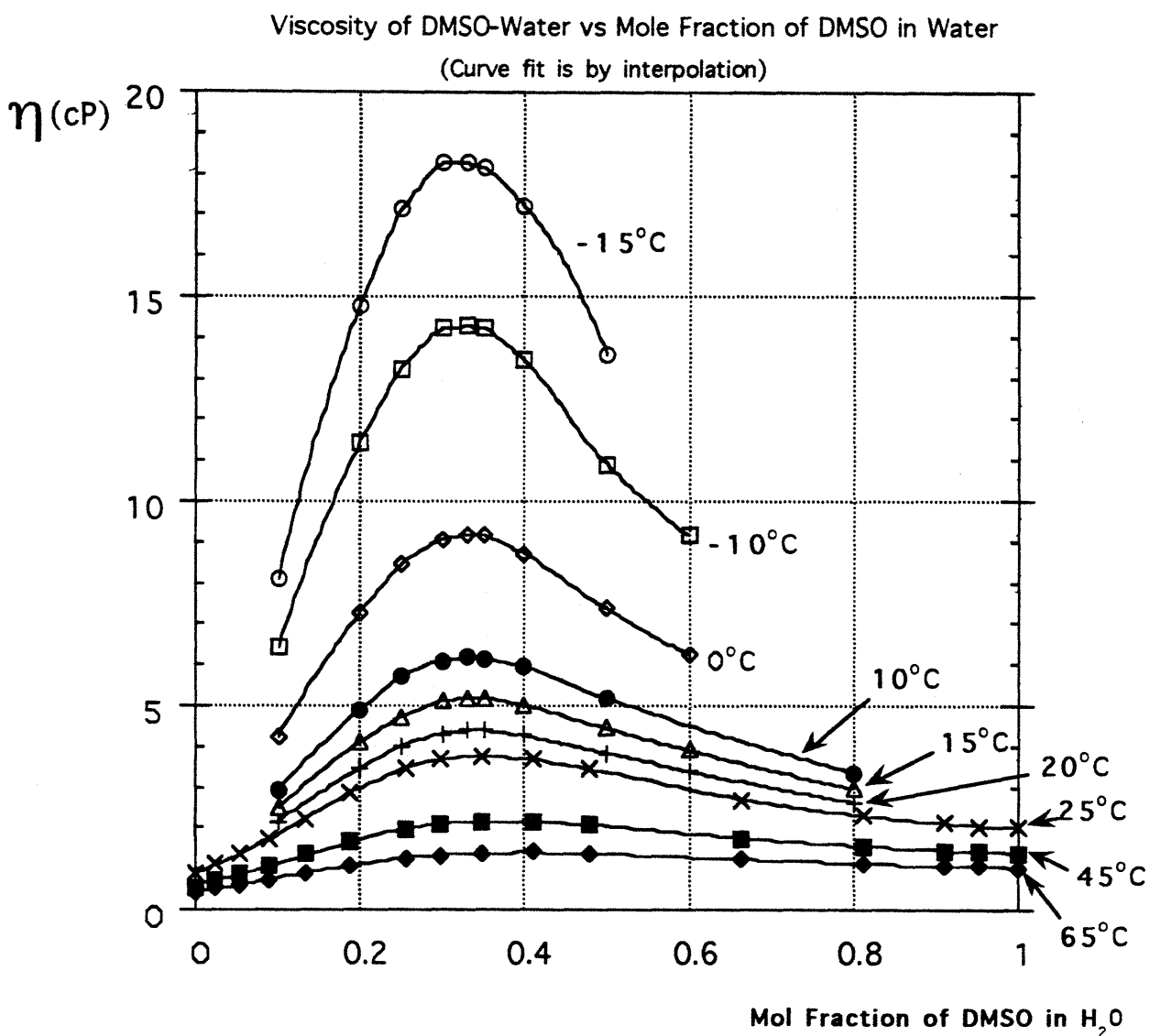


Figure 4-3. Plot of the macroscopic viscosity of DMSO-water binary mixture as a function of mole fraction of DMSO in water. Data points for the isotherms of 65, 45, and 25 °C are from Cowie & Toporowski, 1961; The remaining data points are from Schichman & Amey, 1971. The curve fit that connects the data points has been obtained by interpolation using KaleidaGraph™ software program.

The NMR utility of DMSO-water cryoprotective mixtures becomes obvious if one makes a direct comparison between the relative viscosities of pure water, DMSO, and the cryomixture. Thus, at room temperature (25 °C), the viscosity of pure water is 0.90 centipoise (cP), while that of neat DMSO is 2.0 cP. In contrast, for the cryomixture with a mole fraction of water of 0.65, the viscosity is 3.8 cP (Cowie & Toporowski, 1961). As we mentioned above, this effect becomes more pronounced with decreasing temperature. Thus, at the temperature of -10 °C, the viscosity of the cryomixture with the same mole fraction of water (0.65) is 14.2 cP, or nearly 16 times that of water at room temperature (Schichman & Amey, 1971). We can use Eq. 4-2 and the data in Fig. 4-3 to estimate the effect of the increased viscosity of a cryomixture on the correlation time, τ_c of a solute molecule. According to Eq. 4-2 and the data plotted in Fig. 4-3, if we do NMR experiments in the cryomixture with mole fraction of water = 0.65 at room temperature, τ_c of a solute molecule should be over four times that of the τ_c of the same molecule in pure water. This difference becomes nearly 16 if we lower the temperature of the cryomixture to -10 °C. Thus, for example, if one is working with NMR spectrometer operating at ^1H frequency of 500 MHz at room temperature in pure water, in order to obtain the same effect on the value of the product $\omega\tau_c$, it would be necessary to obtain NMR spectrometer operating at ^1H frequency of 16 x 500 or 8 GHz ! This is obviously not possible at the present time. However, this comparison clearly demonstrates the usefulness of cryomixtures when one wants to alter an unfavorable value of $\omega\tau_c$ for spectroscopic convenience.

Besides viscosity, other bulk properties such as density and heat of mixing show maxima for mixtures in the molar ratio range of 2:1 water-DMSO (Luzar & Chandler, 1993; Schichman & Amey, 1971). Furthermore, the freezing point of

cryoprotective water-DMSO mixtures is dramatically depressed, especially in the molar ratio range of 2:1 water-DMSO (Schichman & Amey, 1971; Gordalla & Zeidler, 1991). Thus, for example, the cryomixture of composition 68 mole % water and 32 mole % DMSO can be cooled down to 180 K (-93 °C) without freezing (Gordalla & Zeidler, 1991).

Besides the macroscopic properties mentioned above, microscopic properties such as proton NMR relaxation rates, chemical exchange (Gordalla & Zeidler, 1991), and orientational relaxation times (Templeton & Kenney-Wallace, 1986) also exhibit pronounced anomalies, especially in the molar ratio range of 2:1 water-DMSO. In this context, the work of Gordalla & Zeidler (Gordalla & Zeidler, 1991) who used ^{17}O -enriched water to calculate NMR proton relaxation rates as a function of temperature for water-DMSO mixture of the composition 68 mole % water and 32 mole % DMSO, is of special interest. From the NMR proton relaxation rates, Gordalla & Zeidler estimated that the rotational correlation time of water molecule in the 68 mole % water - 32 mole % DMSO composition range has the value of 16.8 ps at 298 K. This correlation time (τ_c) is much longer than that computed for pure water at 298 K, which is 1.95 ps (Van der Maarel et al., 1985), and suggests that when added to water, DMSO decreases the mobility of water by a factor of 8.6 at the 68 mole % water - 32 mole % DMSO composition range (Gordalla & Zeidler, 1991). This experimental data suggests that addition of DMSO to water modifies the hydrogen bonding properties of water, resulting in the above-described anomalous behavior. This hypothesis is supported by recent neutron diffraction studies combined with molecular dynamics simulations which have been used to probe the intrinsic solution structure of the water-DMSO cryoprotective mixtures (Luzar & Chandler, 1993; Soper & Luzar, 1992). These studies suggest that in the 2:1 water-DMSO mixture, water retains the local tetrahedral water-water hydrogen bonding network characteristic of pure water, but at a reduced abundance.

In summary, the neutron diffraction and computer simulation studies support the hypothesis that the major elements of the structure of liquid water that are unique to pure water appear to be retained in the cryoprotective mixture. Furthermore, these data provide a microscopic picture that illuminates the unusual properties of cryomixtures, and agrees with the extensive biological and biochemical evidence reviewed above, which strongly suggest the full bio-compatibility of cryomixtures.

From a series of NOE experiments, Temussi and coworkers (Amodeo et al., 1991; Temussi et al., 1992) have recently argued that the high viscosities of the water-DMSO cryoprotective mixtures strongly and selectively stabilizes compact peptide structures in the studied bio-active peptides. However, from the NOE data of Temussi and coworkers, it is difficult to separate effects attributable to changes in NMR correlation time from intrinsic stability changes. Furthermore, Temussi and coworkers argue that the high viscosity property of cryomixtures may have an important biological significance. In particular, based on the typical range of viscosities reported for cellular cytoplasm, which is between 5-30 cP (Pollard, 1976), Temussi and coworkers argue that with respect to viscosity, cryoprotective media may mimic the cellular cytoplasm better than pure water does (Amodeo et al., 1991; Temussi et al., 1992). This hypothesis, if true, could be of some significance to the work to be reported in the next Chapter, since it suggests that cryoprotective water-DMSO mixtures may be of potential interest in the study of the energetics of peptide secondary structure formation in solvent media that resemble the milieu of the cytoplasm.

The next Chapter will provide relative quantitative β -strand propensities of amino acids in cryoprotective media derived using the peptide-epindolidione models. These β -strand propensities will demonstrate that cryoprotective mixtures have a profound stabilizing effect on both the "antiparallel" and "parallel" β -strand structure relative to both pure DMSO and water. To our knowledge, the data presented in the next Chapter provides the first account ever made for the dramatic stabilizing properties of water-DMSO cryomixtures on both "antiparallel" and "parallel" β -strand structure. The next Chapter will also examine some potential practical applications that the peptide-stabilizing effect of cryomixtures can have in the fields of cryobiology and medicine.

Chapter 5

Determination of Relative β -Strand Propensities ($\Delta\Delta G^\circ$ values) in Cryoprotective Solvents

The work described in this Chapter will provide relative quantitative amino acid propensities ($\Delta\Delta G^\circ$ values) for β -strand formation in the β -strand-turn-template hairpin peptide-epindolidione models (**1c** & **1d** in Fig. 5-1) in cryoprotective water-DMSO media. These propensities will demonstrate that cryoprotective water-DMSO mixtures have a profound stabilizing effect on β -strand-turn-template hairpin structures (**1c** & **1d** in Fig. 5-1), relative to both pure DMSO and water. To our knowledge, this effect has not been previously reported in the literature, and suggests the hypothesis that cryoprotective water-DMSO mixtures may be of potential interest in the study of the energetics of peptide secondary structure formation in cryoprotective solvent media that resemble the milieu of the cytoplasm.

The discovery that synthetic peptide-epindolidione conjugates are strongly stabilized by cryoprotective water-DMSO mixtures may have potential practical value with respect to rational design of peptide derivatives capable of protecting cells and tissues during cryopreservation processes, by binding to and inhibiting ice growth, which is thought to be deleterious to cells and tissues (Karlsson et al., 1993).

This Chapter will also demonstrate that NMR work in cryoprotective mixtures allowed detailed structural characterization of a number of peptide-epindolidione derivatives, providing strong support that the peptide-epindolidione conjugates assume a robust β -strand-turn-template hairpin structure (**1c** & **1d** in Fig 5-1) in the cryoprotective water-DMSO mixtures.

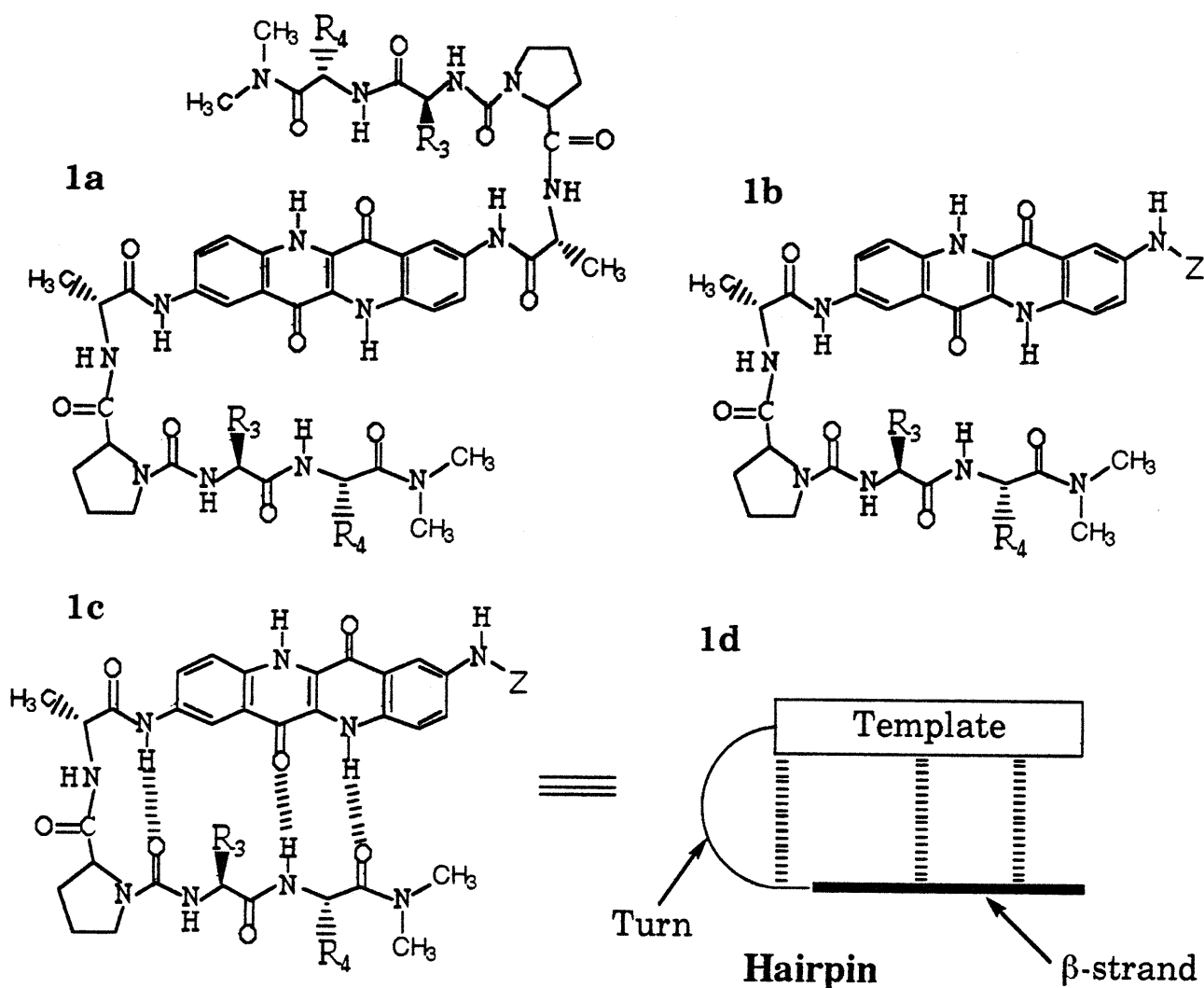


Figure 5-1. 1a) Structure of peptide-epindolidione conjugate of the general formula XY:PdA. The variable residues X and Y correspond to the amino acid residues with side chains R_4 and R_3 , respectively, in the dipeptide portion of the molecule intended to mimic a β -strand conformation; The colon represents the chain-reversing urea functionality, followed by P and dA which are the single letter amino acid codes for l-proline and d-alanine, respectively, in the turn region.

1b) Simplified representation of the structure of the peptide-epindolidione conjugate shown in **1a** where Z denotes the duplicated peptide chain of **1a**.

1c) Template hydrogen-bonded "antiparallel" β -strand structure representation of **1b**, clearly showing the three intramolecular peptide-template hydrogen bonds and the overall hairpin conformation of the conjugate.

1d) A schematic representation of **1c** in the structured "antiparallel" β -strand-turn-template hairpin conformation.

The structure-enhancing effect of cryoprotective mixtures was discovered during addition of D₂O to DMSO-d₆ solutions of VK:PdA and VR:PdA. As we have seen from the review discussion in Chapter one, these derivatives are fully soluble and monomeric in the millimolar concentration range in DMSO-d₆. However, unlike other derivatives of the general structure VX:PdA (1a in Fig. 5-1), the derivatives VK:PdA and VR:PdA possess the positively-charged residues lysine and arginine. With two charges per molecule, these derivatives are expected to have limited solubility in water. Figure 5-2 plots the H₃ chemical shifts of VK:PdA and VR:PdA as a function of the mole% of DMSO-d₆ in D₂O, pD = 2.0, 25 °C. Notice that both curves go through a maximum around 50 mole % DMSO-d₆. Another striking feature of the plot in Fig. 5-2 is the large decrease in the chemical shift of H₃ for both derivatives when the cryoprotective solution reaches higher mole % of water (e.g. above 80 mole % water). In particular, in neat DMSO-d₆, the H₃ shifts are 8.45 ppm and 8.41 ppm for VK:PdA and VR:PdA, respectively; It reaches a maximum of 8.56 ppm for both derivatives at X_{DMSO} = 51 mole %, and decreases to 7.57 ppm and 7.95 ppm for VK:PdA, and VR:PdA, respectively, in pure D₂O (Fig. 5-2). As will be demonstrated below, the large drop in the H₃ chemical shifts for both derivatives is most likely due to two separate phenomena. The first is a progressive increase in the degree of association (aggregation) of the derivatives as the mole fraction of water increases. The other reflects the stabilizing effect of the binary cryomixture relative to either pure D₂O or DMSO-d₆.

To probe the association process in more detail, a series of NMR dilution experiments were carried out on both derivatives in pure D₂O, pD = 2.0, 25 °C, and the resultant data is plotted in Figures 5-3a and 5-3b.

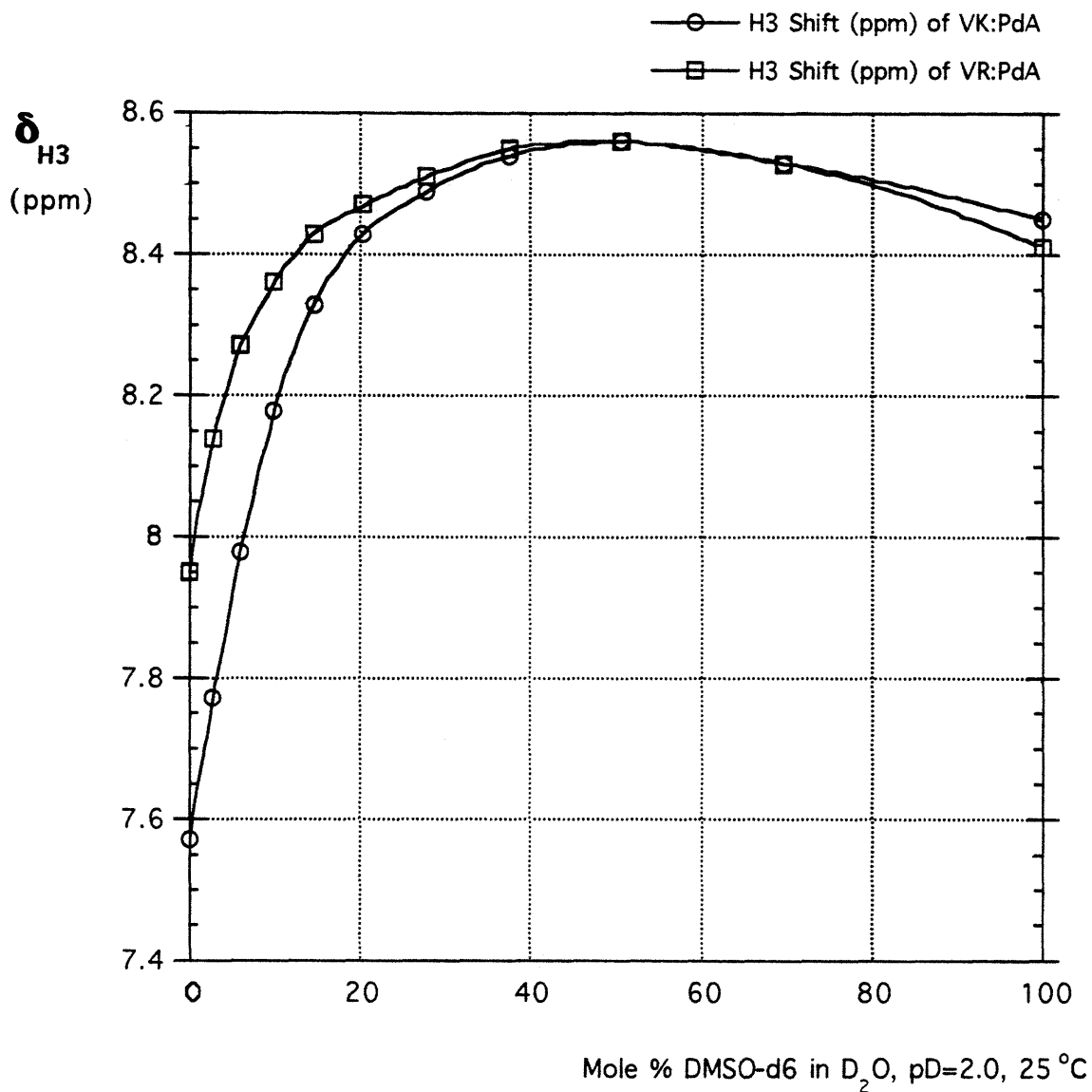


Figure 5-2. Plot of the H3 chemical shifts of VK:PdA and VR:PdA as a function of the mole % of DMSO-d6 in D₂O, pD = 2.0, 25 °C. Curve fit is by interpolation between the data points. The approximate concentrations of VK:PdA and VR:PdA are 2 mM and 1 mM, respectively.

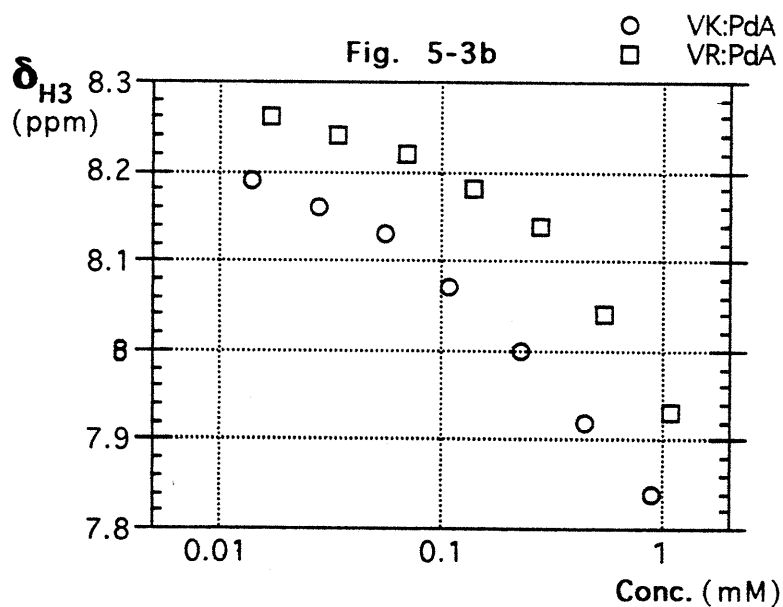
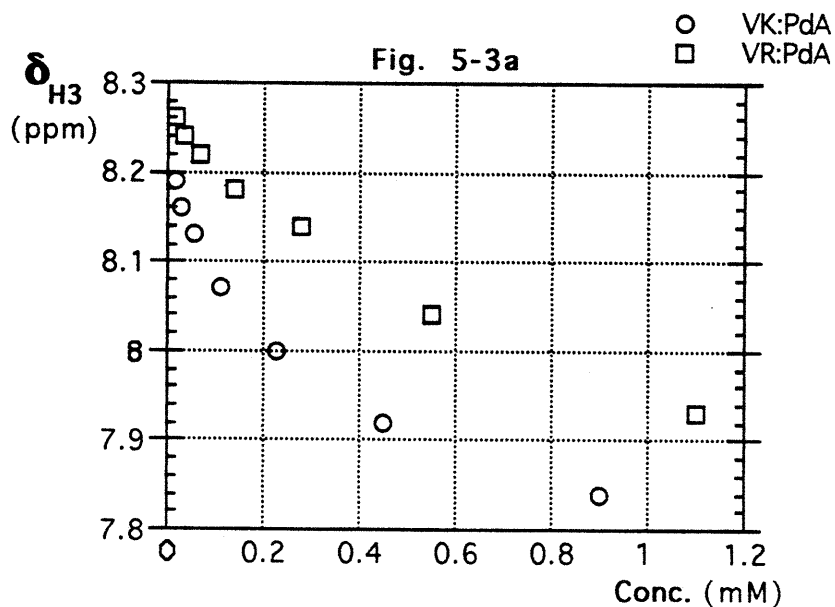


Figure 5-3a) H₃ chemical shifts of VK:PdA and VR:PdA as a function of the respective approximate concentrations in D₂O, pD = 2.0, 25 °C in a series of sequential (two-fold) NMR dilution experiments. **5-3b)** The same data as in Fig. 5-3a except that the concentration is plotted in a logarithmic scale, which clearly demonstrates convergence of δ_{H3} for both derivatives.

Figure 5-3a plots δ_{H3} of VK:PdA and VR:PdA as a function of the respective concentrations of the derivatives in pure D_2O , $\text{pD} = 2.0$, $25\text{ }^\circ\text{C}$ in a series of sequential (two-fold) NMR dilution experiments. Figure 5-3b gives a semi-log plot of the same data as in Fig. 5-3a. From Fig. 5-3b, it is clear that the H3 chemical shifts for both derivatives are beginning to converge with increasing dilution. However, in the case of both derivatives, the last two-fold dilution does not fulfill Blanchard's criterion for lack of association that was mentioned in the last Chapter (Chapter four). To give a specific example, a two-fold (or 100 %) dilution of VK:PdA from a concentration of $28\text{ }\mu\text{M}$ to $14\text{ }\mu\text{M}$ (Fig. 5-3), leads to a $\Delta\delta_{\text{H3}} = 0.03\text{ ppm}$, which corresponds to a $\Delta\delta_{\text{H3}}$ of 15 Hz at the spectrometer frequency of 500 MHz.

$\Delta\delta_{\text{H3}}$ of 15 Hz exceeds the Blanchard's criterion for the lack of association, which suggests that a 100% dilution of an NMR sample should result in $\Delta\delta_{\text{H3}} < 3\text{ Hz}$ in order for the derivative to be considered monomeric (Blanchard, 1992). It should be emphasized that even though both derivatives VK:PdA and VR:PdA exhibit pronounced association as determined by NMR-monitored dilution studies of Figs. 5-3a & b, nevertheless both derivatives have an appreciable water solubility due to the presence of two positively charged residues per molecule. The presence of association for both derivatives, even below the concentration of $20\text{ }\mu\text{M}$, should not be surprising if we remember that the wsXY:PdK derivatives (1b of Fig. 4-1, Chapter four) with six charges per molecule still exhibit association at higher concentrations (see Table 4-1 in Chapter 4). The semi-log plot of Fig. 5-3b is useful because it allows us to estimate the approximate value of δ_{H3} for both derivatives in the limit of infinite dilution. Roughly speaking, one can argue that the limiting value for δ_{H3} for both derivatives should fall between 8.2 - 8.3 ppm. This result, even though approximate, allows us to re-examine the data plotted in Fig. 5-2. Since separate NMR dilution experiments indicate that the peptide-epindolidione derivatives of structure VX:PdA (1a, Fig. 5-1) do not associate appreciably above 30 mole % DMSO

(see below), we can generate Figure 5-4 which plots the same data as Figure 5-2, in addition to the two approximate curves (designated as "corrected") which employ the limiting value for δ_{H3} for both derivatives VK:PdA and VR:PdA in pure D_2O , in the absence of aggregation, (i.e. in the limit of infinite dilution).

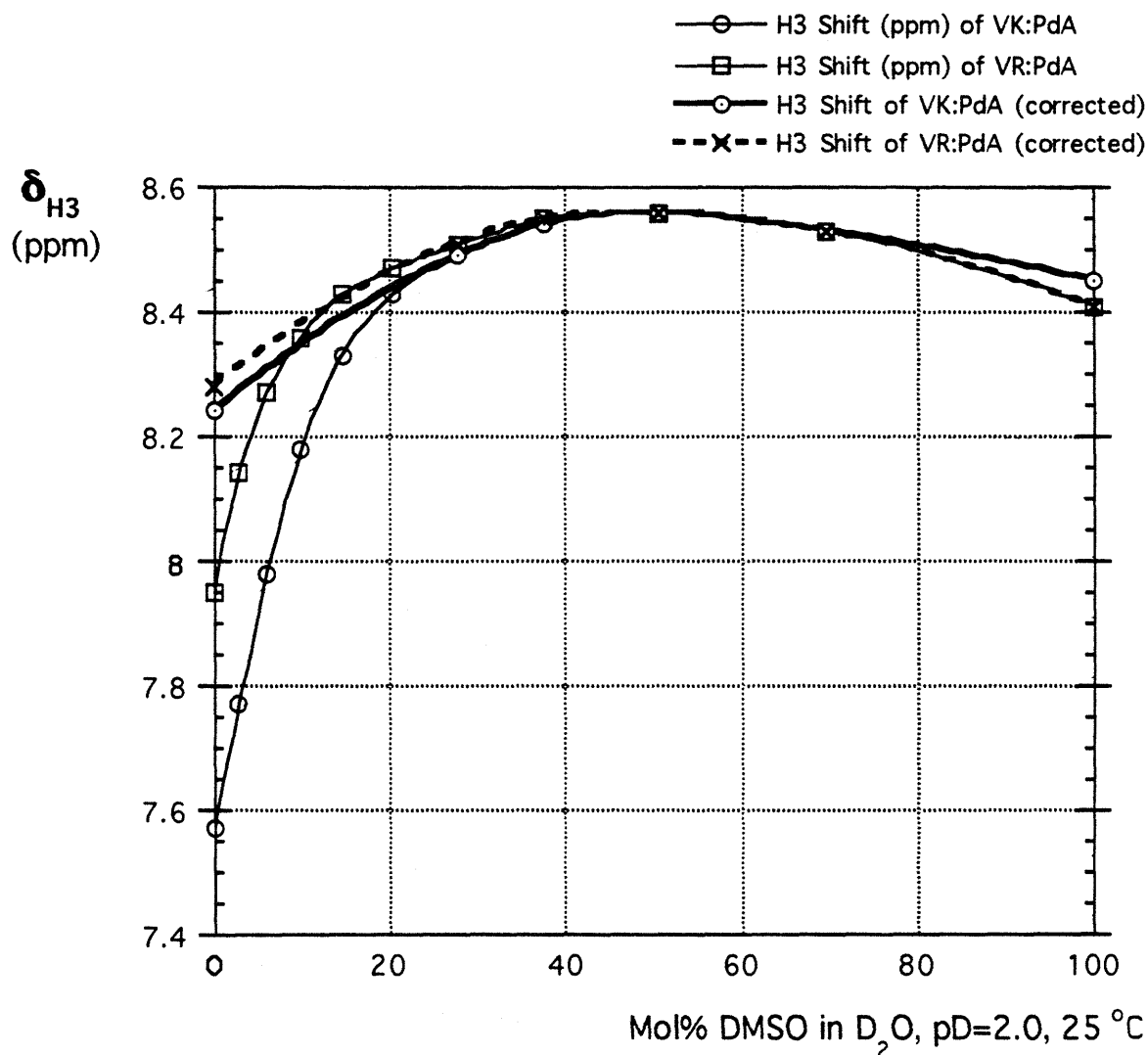


Figure 5-4. Replot of the data in Fig. 5-2 with additional data in D_2O estimated from limiting dilution data of Fig. 5-3b and labelled as "corrected". The curve fits are generated through interpolation.

The data plotted in Fig. 5-4 allows us to deconvolute two effects that act together to increase the H3 chemical shifts of the derivatives VK:PdA and VR:PdA as DMSO-d6 is added to D₂O. The downfield shift in the H3 chemical shift in the "corrected" curves reflects the increase in the stability of β -strand-turn-template hairpin structure (1b & 1c in Fig. 5-1) for both derivatives, as DMSO-d6 is added to D₂O. On the other hand, the larger downfield shift in the H3 chemical shift in the remaining two curves has an additional component due to the progressive loss of association of the derivatives as DMSO-d6 is added to D₂O. Since aggregation is an undesirable effect (Chapter one; Blanchard, 1992), we are exclusively interested in the changes in H3 chemical shift represented by the "corrected" curves in Fig. 5-4.

From Fig. 5-4 we can draw two conclusions, which as we will demonstrate below, can be generalized to all of the VX:PdA derivatives (1a in Fig. 5-1) studied in this Chapter. The first important conclusion is that δ_{H3} has a higher value (i.e. H3 is more deshielded) in the binary cryomixture, relative to either pure D₂O or DMSO-d6. We will demonstrate below that this is equivalent to the statement that the peptide-epindolidione derivatives VX:PdA are more stable in the cryomixtures than in either pure DMSO-d6 or D₂O. The second conclusion is that addition of DMSO-d6 to D₂O breaks-up the association between the peptide-epindolidione derivatives. As will be shown below, this loss of association is highly advantageous, since it allows detailed structural and energetic characterization of the peptide-epindolidione derivatives in the cryomixtures in the absence of association.

Figure 5-5 plots the H3 chemical shift of the derivative VN:PdA as a function of the mole % of DMSO-d6 in D₂O, pD = 2.0, 25 °C at three different concentrations of VN:PdA. Unlike the derivatives VK:PdA and VR:PdA, VN:PdA is not charged, therefore, one would predict that it would be less soluble in pure water than the derivatives that carry a net positive charge. Indeed, titration to pure D₂O results in

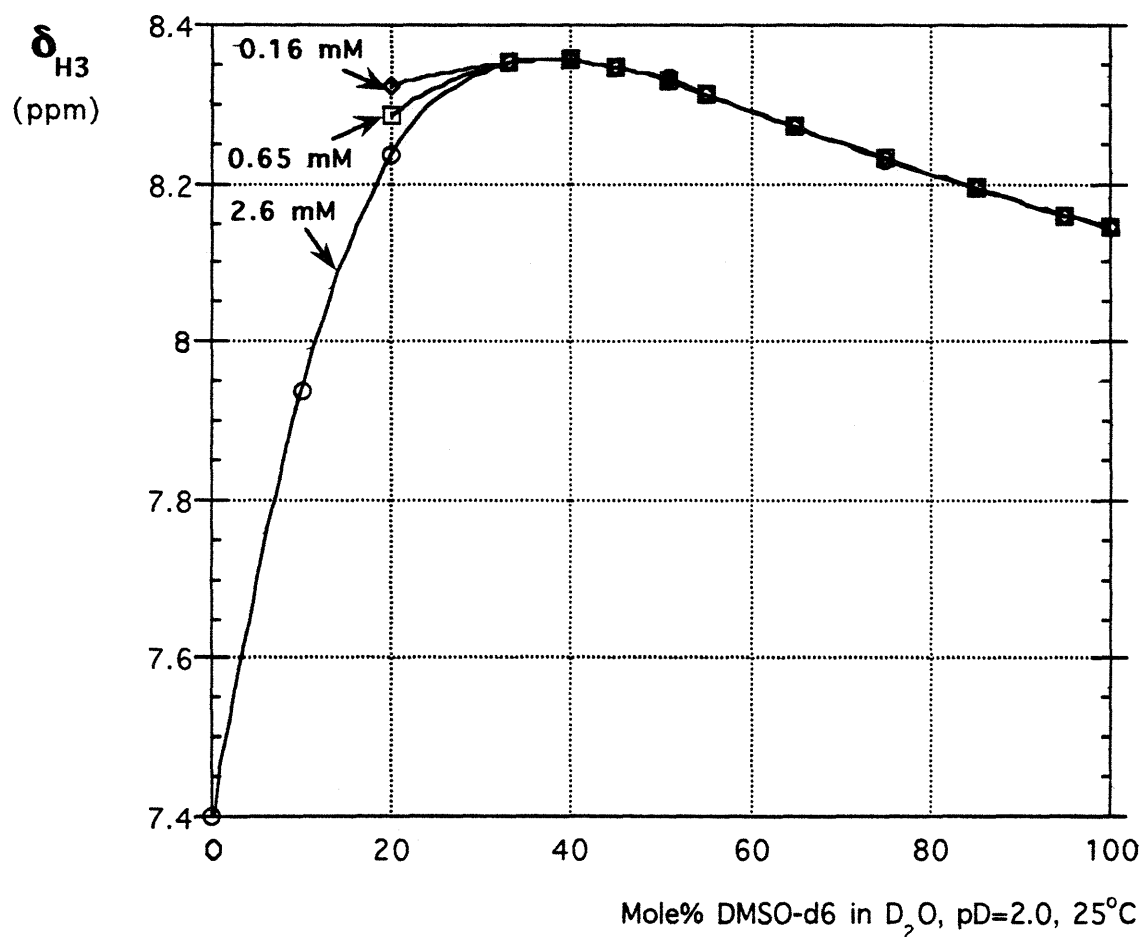


Figure 5-5. Plot of the H3 chemical shifts of VN:PdA as a function of the mole % of DMSO-d6 in D₂O, pD = 2.0, 25 °C. Curve fit is by interpolation between the data points. The three different curves that diverge from the point at 33 mole % DMSO-d6 indicate the effect of dilution, or the loss of association of the derivative reflected in the H3 chemical shift value in the cryomixture.

a dramatic upfield shift in H3, no doubt the result of extensive aggregation in addition to the β -strand-structuring effect mentioned above. The most striking feature of the graph in Fig. 5-5 is the overlap of the data points with the indicated concentrations of VN:PdA down to about 30 mole % DMSO-d6. After that, one observes divergence in the value of δ_{H3} which clearly depends on the concentration of the derivative. The overlap in δ_{H3} in Figure 5-5 down to about 30 mole % DMSO-d6 clearly demonstrates that there is no association of the derivative in the cryomixture above 30 mole % DMSO-d6 at derivative concentration below ≈ 2 mM. As was mentioned above, this property is shared by all the derivatives to be examined in the rest of this Chapter.

Figure 5-6 presents another example of a plot of δ_{H3} versus the mole % of DMSO-d6 in D_2O , this time using the derivatives VN:PdA and VT:PdA. The purpose of Figure 5-6 is to clearly indicate the unique behavior of the chemical shift of the epindolidione proton H3 in comparison to that of H1 and H4. From Fig. 5-6, it is clear that only the H3 chemical shift exhibits the pronounced maximum with the changing mole fraction of D_2O . This behavior is consistent with H3 having the properties of a reporter proton. This aspect of the H3 proton was discussed at length in the previous Chapters of this thesis. As will be shown below, the unique behavior of the chemical shift of H3 in Fig. 5-6 is a general property of the other derivatives VX:PdA (**1a** in Fig. 5-1) that will be discussed in this chapter, and reflects the increased stability of the β -strand-turn-template hairpins (**1c** & **1d** in Fig. 5-1) in the cryoprotective water-DMSO mixtures relative to both water and DMSO.

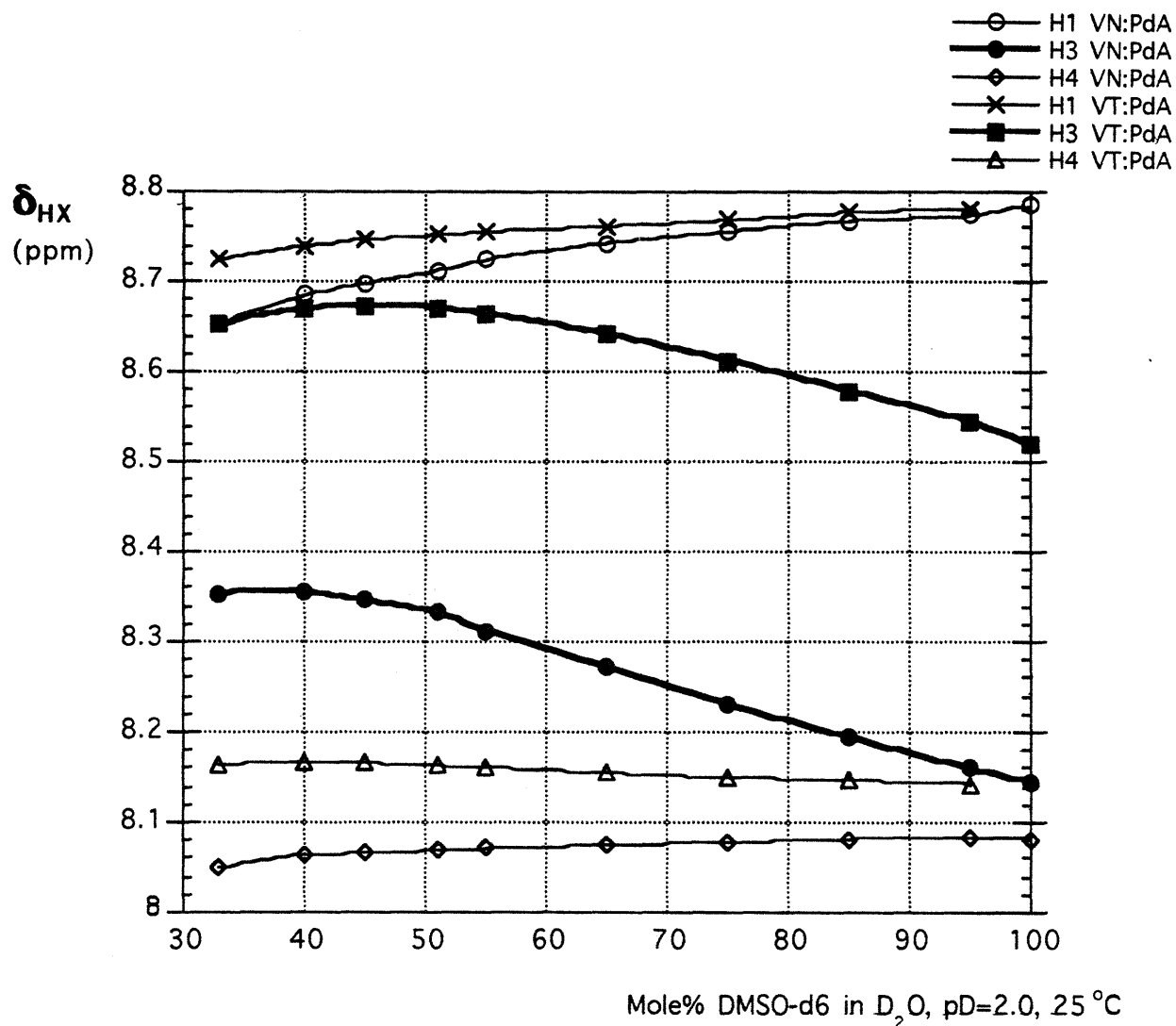


Figure 5-6. Plot of the chemical shifts for the aromatic epindolidione protons H1, H3, and H4 of VT:PdA (0.6 mM) and VN:PdA (2.3 mM) as a function of the mole % of DMSO-d6 in D₂O, pD = 2.0, 25°C from 33 mole% DMSO-d6 to 100 mole % DMSO-d6. Curve fit is by interpolation between the data points. From the plot it is clear that for both derivatives, only the H3 chemical shift (heavy curves) exhibits the pronounced maximum with the changing mole fraction of D₂O. This behavior is consistent with H3 being the reporter proton for the energetic stability of the β -strand-turn-template hairpin peptide-epindolidione model system (1c & 1d, Fig. 5-1).

In Fig. 5-7, H3 chemical shift data is plotted against the mole % of DMSO-d6 in D₂O, pD = 2.0, 25 °C from 33 to 100 mole% DMSO-d6 for 19 derivatives of the general structure VX:PdA (Fig. 5-1), where X is a variable amino acid residue.

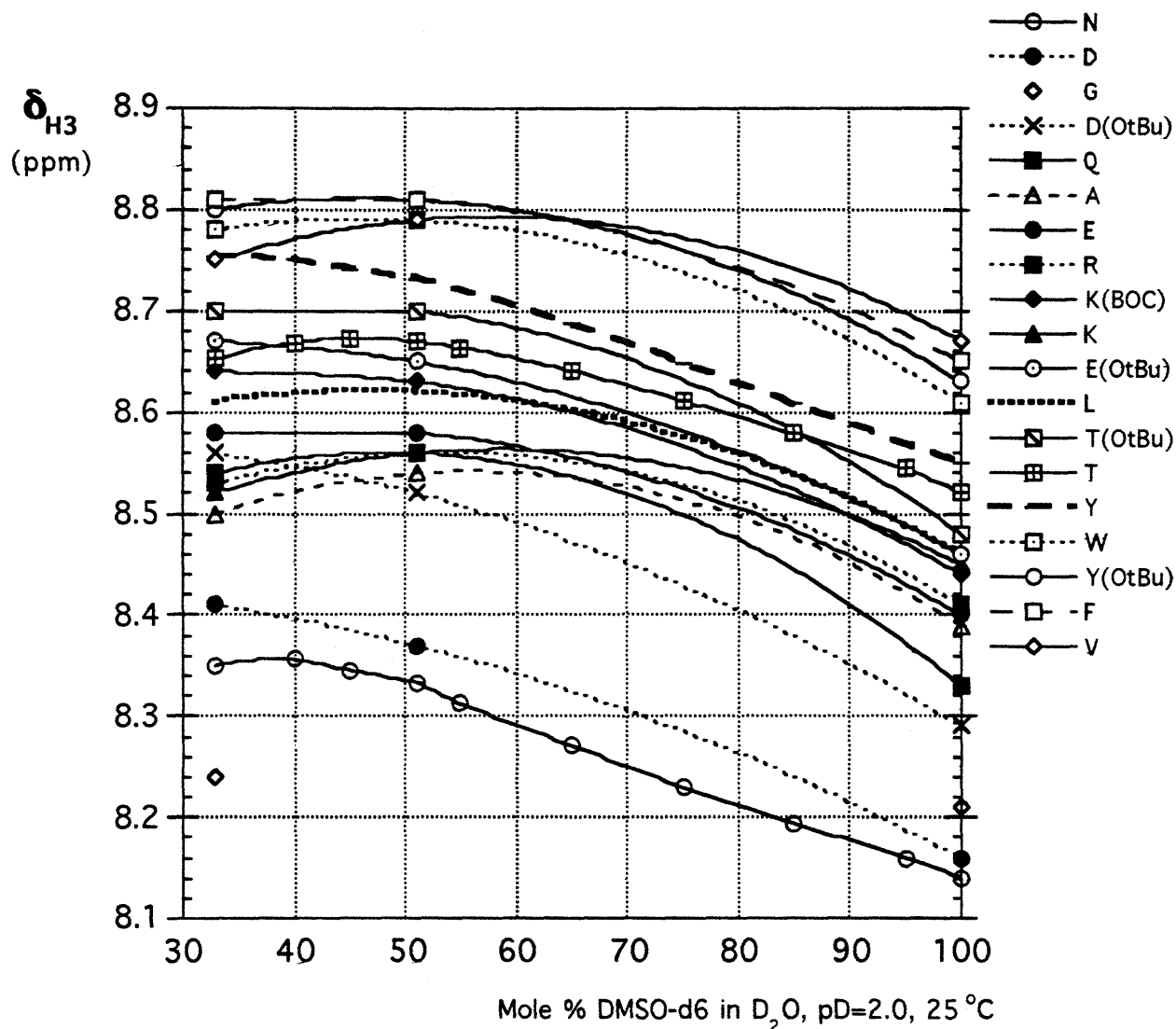


Figure 5-7. Plot of the H3 chemical shifts of VX:PdA as a function of the mole % of DMSO-d6 in D₂O, pD = 2.0, 25 °C. X is the variable third amino acid residue for a derivative of structure shown in Fig. 5-1. Single-letter codes are used to designate the variable residue X. X(OtBu) designates a side chain protected by a *tert*-butyl group; K(Boc) designates a Lys side chain protected with a Boc group, and DOD designates the dimetoxydityl protecting group. (Curve fit is by interpolation).

From Fig. 5-7, it is clear that for every derivative, δ_{H3} increases upon addition of D_2O to DMSO-d6. An analogous D_2O titration performed on the tripeptide-epindolidione ethyl ester derivative EtO-G:PdA, that cannot form β -strand structure, resulted in essentially no change in δ_{H3} (see below), indicating that the changes in δ_{H3} observed for the derivatives of Fig. 5-7 are not due to solvent effects, but instead reflect the increasing β -strand stability for a given derivative as D_2O is added to DMSO-d6. This conclusion was confirmed by analyzing the solvent dependence of the chemical shift of the 7-hydrogen of 1-formyl-1,2,3,4-tetrahydroquinoline during D_2O titration experiment (from pure DMSO-d6). The 7-hydrogen of 1-formyl-1,2,3,4-tetrahydroquinoline was originally used by Blanchard as a model system for the chemical shift of the H3 epindolidione in a 100 % structured derivative. In fact, in his thesis, Blanchard used this model compound to estimate the value of δ_{β} (Blanchard, 1992). From the chemical shift of the 7-hydrogen of the above-mentioned model compound, we obtained $\delta_{\beta}(33 \text{ mole\% DMSO}) = 8.82 \text{ ppm}$, and $\delta_{\beta}(51 \text{ mole\% DMSO}) = 8.84 \text{ ppm}$. As was mentioned before, the value of δ_{β} in pure DMSO is 8.91 ppm. δ_{O} for the cryomixtures was obtained from the H3 chemical shift of the tripeptide-epindolidione ethyl ester derivative EtO-G:PdA at the appropriate water-DMSO mole fractions. Thus, $\delta_{\text{O}}(33 \text{ mole\% DMSO}) = \delta_{\text{O}}(51 \text{ mole\% DMSO}) = 8.00 \text{ ppm}$. (Note that δ_{O} for neat DMSO-d6 is 7.97 ppm).

In summary, all evidence supports the conclusion that the variation in the H3 chemical shift observed in Fig. 5-7 (and the other Figures above), reflects the structuring effect of the cryoprotective mixture on the peptide-epindolidione derivative. As will be seen later in this Chapter, extensive 2D-NOESY analysis of the derivatives confirms the presence of a robust hairpin (1c & 1d, Fig. 5-1) structure for some of the derivatives in Fig. 5-7, when placed in cryomixtures.

We can proceed in a fashion analogous to that of Chapter two in order to obtain the $\Delta\Delta G^\circ$ values for the derivatives VX:PdA (Fig. 5-1) in cryomixture. Then we can compare the $\Delta\Delta G^\circ$ obtained in the cryomixture with the $\Delta\Delta G^\circ$ obtained in pure DMSO-d6 reported in Chapter two. For this purpose, we choose the cryoprotective mixture with a 2:1 water : DMSO molar ratio (i.e. 33 mole % DMSO-d6, 67 mole % water). We choose this cryoprotective ratio for several important reasons. First, as we have seen from Fig. 4-3 in Chapter four, the viscosity of the water-DMSO cryomixture reaches a maximum in the concentration range of 2:1 water : DMSO; As we have seen from the discussion of Chapter four, high viscosity is advantageous for maximizing NOEs. The second reason is that the 2:1 water : DMSO cryomixture has the highest water concentration at which the derivatives VX:PdA are soluble enough to allow acquisition of 2D-NOESY experiments. As will be shown later in this Chapter, the 2D-NOESY experiments fully confirm the presence of a well-defined β -strand-turn-template structure in all cases studied. Another reason for choosing the 2:1 water:DMSO molar ratio has to do with the wealth of the experimental and theoretical studies performed by other laboratories with the water-DMSO cryomixture at this particular concentration range. From the review in Chapter four, we have seen that the majority of studies on the properties of water-DMSO mixtures have been conducted in the 2:1 water : DMSO concentration range (Gordalla & Zeidler, 1991; Luzar & Chandler, 1993).

In manner analogous to that in Chapter two, we can obtain the ratios of equilibrium constants K_2 by taking ratios of χ values defined by Equation 5-1 (see also Eq. 2-1 in Chapter 2). As in Chapter two, we take the ratios of χ values as given

$$\chi \equiv \frac{P_{s1} + P_{s2}}{P_{RC} + P_T} = \frac{\delta_{H3} - \delta_O}{\delta_\beta - \delta_{H3}} = \frac{K_1}{1 + K_1} K_2 (1 + K_3) \quad (\text{Eq. 5-1}).$$

$$\frac{\chi(\text{VX:PdA})}{\chi(\text{VA:PdA})} = \frac{\left(\frac{K_1}{1 + K_1}\right) K_{2X} (1 + K_{3V})}{\left(\frac{K_1}{1 + K_1}\right) K_{2A} (1 + K_{3V})} = \frac{K_{2X}}{K_{2A}} \quad (\text{Eq. 5-2})$$

by Equation 5-2 in order to obtain the corresponding ratio K_{2X}/K_{2A} , where K_{2X} represents the equilibrium constant of a variable residue X for formation of the first β -strand hydrogen bond in VX:PdA. K_{2A} represents the equilibrium constant for formation of the first β -strand hydrogen bond for the amino acid residue Ala in VA:PdA. Table 5-1 gives the values of χ and K_{2X}/K_{2A} calculated for the indicated 19 derivatives using Eqs. 5-1 and 5-2, with $\delta_\beta(33 \text{ mole\% DMSO-d6}) = 8.82 \text{ ppm}$ and $\delta_\alpha(33 \text{ mole\% DMSO-d6}) = 8.00 \text{ ppm}$, estimated from the model compounds 1-formyl-1,2,3,4-tetrahydroquinoline and EtO-G:PdA, as discussed above.

From the H3 chemical shifts observed for VX:PdA, where X = Phe, Tyr(OtBu), Trp, and Tyr, it is clear that within experimental error these derivatives are completely structured in the cryoprotective mixture; only lower bounds can be estimated for their $\chi_{X,\text{Val}}$ or $\chi(\text{DMSO-d6})$ parameters as indicated in Table 5-1. As will be seen later in this Chapter, these results are in accord with 2D-NOESY data which show intense negative cross-peaks expected for the β -strand hairpin structure. Figure 5-8 plots as a function of $\chi_{X,\text{Val}}$ in DMSO-d6, $\chi(\text{DMSO-d6})$, the ratio of $\chi(\text{CP})$ observed in the cryoprotective solvent to that seen in DMSO-d6.

Table 5-1

δ_{H3} (DMSO-d6), δ_{H3} (CP), and the values of χ (DMSO-d6), χ (CP), and K_{2X}/K_{2A} calculated for derivatives VX:PdA (X variable) using Eqs. 5-1 & 5-2.

3 rd Residue (X)	$\delta_{\text{H3}}(\text{D})^1$	$\delta_{\text{H3}}(\text{CP})^1$	$\chi(\text{D})^2$	$\chi(\text{CP})^3$	K_{2X}/K_{2A}^4
N	8.14	8.35	0.22	0.74	0.46
D	8.16	8.41	0.25	1.0	0.63
G	8.21	8.24	0.34	0.41	0.26
D(OtBu) ⁵	8.29	8.56	0.52	2.2	1.4
Q	8.33	8.54	0.62	1.9	1.2
A	8.39	8.50	0.80	1.6	1.0
E	8.40	8.58	0.84	2.4	1.5
R	8.41	8.53	0.88	1.8	1.1
K(ϵ -Boc)	8.44	8.64	1.00	3.6	2.3
K	8.45	8.52	1.04	1.7	1.1
L	8.46	8.61	1.08	2.9	1.8
E(OtBu)	8.46	8.67	1.08	4.5	2.8
T(OtBu)	8.48	8.70	1.19	5.8	3.6
T	8.52	8.65	1.41	3.8	2.4
Y	8.55	8.75	1.61	11 ⁶	6.9
W	8.61	8.78	2.13	14 ⁶	9
Y(OtBu)	8.63	8.80	2.36	17 ⁶	11
F	8.65	8.81	2.58	18 ⁶	11
V	8.67	8.75	2.87	11	6.9

¹H3 chemical shifts in pure DMSO-d6, $\delta_{\text{H3}}(\text{D})$, and the cryomixture, $\delta_{\text{H3}}(\text{CP})$, are reported in ppm relative to tetramethylsilane (TMS), and were obtained at 25 °C.

² $\chi(\text{D})$ represents the χ value computed in pure DMSO-d6, 25 °C.

³ $\chi(\text{CP})$ represents the χ value computed in the 2:1 D₂O:DMSO-d6 cryomixture, pD = 2.0, 25 °C.

⁴ Calculated using Eq. 5-2 with the listed $\chi(\text{CP})$ values.

⁵ The expression in parentheses next to a residue X indicate the nature of side chain protection. Thus, X(OtBu) represents a residue X with a *tertiary*-butyl protecting group; K(ϵ -Boc) represents lysine side chain protected with a *tertiary*-butyloxycarbonyl (BOC) group.

⁶Estimated lower bound (see text for more detail).

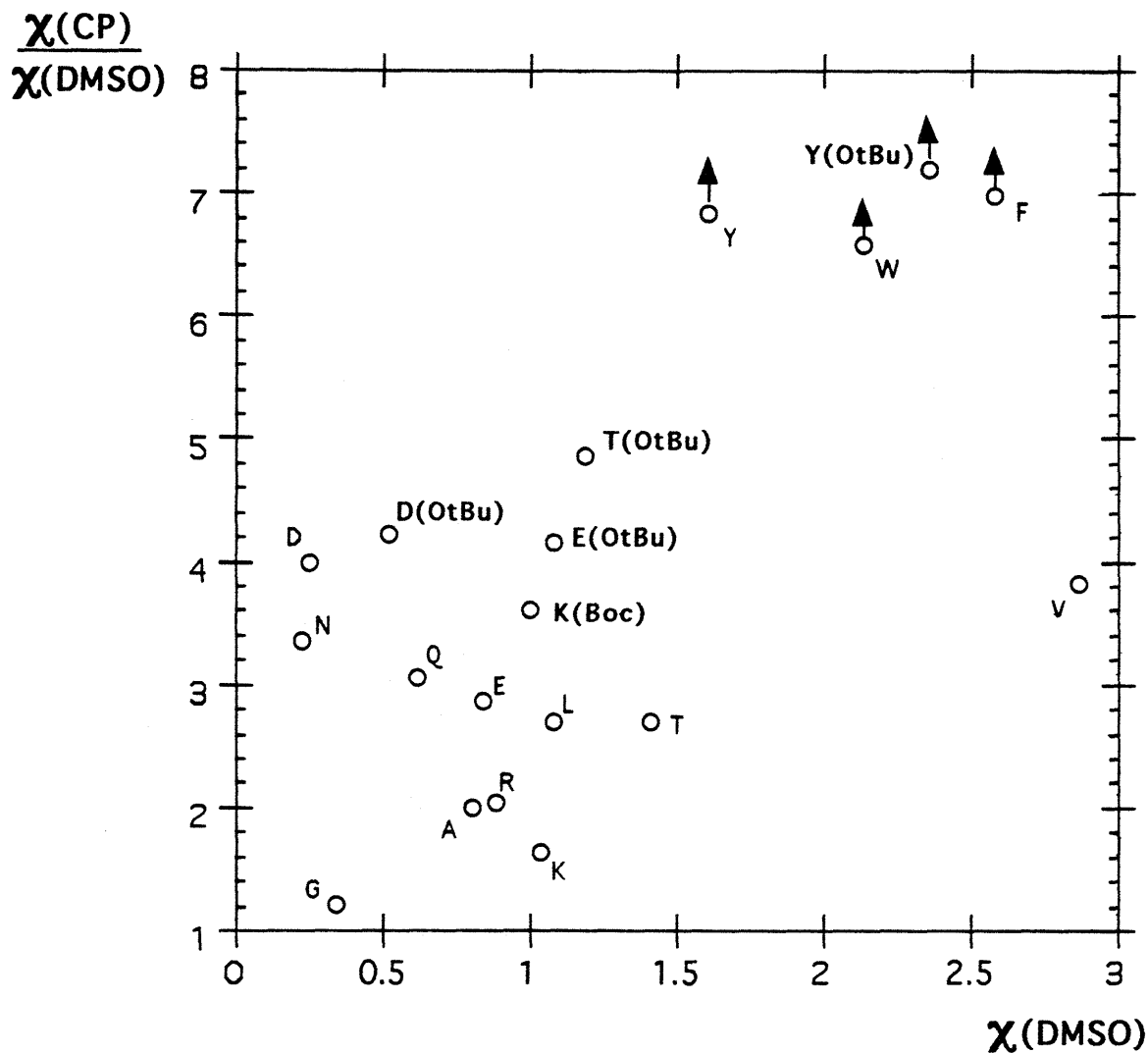


Figure 5-8 Plot of the ratios of $\chi_{X,Val}$ in the cryomixture, $\chi(\text{CP})$, to $\chi_{X,Val}$ in DMSO-d6, $\chi(\text{DMSO})$, expressed as a function of $\chi(\text{DMSO})$. X represents the variable amino acid residue. The magnitude of the ratios expresses the degree to which the cryomixture stabilizes a strand residue X relative to its stability in DMSO-d6. The $\chi_{X,Val}$ values are computed using Eq. 5-1. Amino acid residues are named by their single-letter codes. The remaining data points represent residues blocked by a *tertiary*-butyl group. A circle with an arrow signifies an estimated lower bound for that residue.

An amino acid side chain R_3 (Fig 5-1) of residue X that is strongly stabilized by the change to the cryoprotective solvent is expected to have an unusually high value of the $\chi(\text{CP})/\chi(\text{DMSO})$ ratio. The plot in Fig. 5-8 shows that glycine, alanine, and the charged amino acids lysine and arginine show the smallest ratio, while the amino acids bearing aromatic side chains show ratios that are at least four-fold larger. Also included in Fig. 5-8 are data for five peptide-epindolidione derivatives in which a polar or charged side chain function has been blocked by a *tertiary*-butyl protecting group. Strikingly, the *tertiary*-butyl-protected derivatives have significantly higher ratios relative to the unprotected ones. This suggests that addition of non-polar, hydrophobic bulk increases the susceptibility to stabilization by the cryoprotective solvent, relative to the behavior seen in DMSO itself.

From the values of K_{2X}/K_{2A} in Table 5-1, we can calculate the values of $\Delta\Delta G^\circ_{\text{Ala-X}}$ using Eq. 5-3. These are listed in Table 5-2.

$$-RT \ln \left(\frac{K_{2X}}{K_{2\text{Ala}}} \right) = -RT \ln (K_{2X}) + RT \ln (K_{2\text{Ala}}) =$$

$$- \left[RT \ln (K_{2X}) \right] - \left[-RT \ln (K_{2\text{Ala}}) \right] = \Delta G^\circ_{2X} - \Delta G^\circ_{2\text{Ala}} \equiv \Delta\Delta G^\circ_{\text{Ala-X}} \quad (\text{Eq. 5-3})$$

The data in Table 5-2 provides a thermodynamic scale for the relative β -strand forming propensities of 19 derivatives VX:PdA in the 2:1 $\text{D}_2\text{O}:\text{DMSO-d}_6$ cryoprotective mixture (CP). The free energy range spanned by all the derivatives in the data base is 0.80- (-1.4) or 2.2 Kcal/mol which is larger than the analogous range of 1.51 Kcal/mol spanned by the VX:PdA derivatives in DMSO-d₆ (Chapter 2 and the third column in Table 5-2).

Table 5-2

$\Delta\Delta G^\circ_{\text{Ala-X}}$ (CP) values calculated using Eq. 5-3 and data of Table 5-1.

3 rd Resid. (X)	$\Delta\Delta G^\circ_{\text{Ala-X}}$ (CP) (Kcal/mol) ¹	$\Delta\Delta G^\circ_{\text{Ala-X}}$ (DMSO) ² (Kcal/mol)
G	0.80	0.50
N	0.46	0.75
D	0.27	0.69
A	0.00	0.00
R	-0.06	-0.06
K	-0.06	-0.16
Q	-0.11	0.15
D(OtBu)	-0.20	0.26
E	-0.24	-0.03
L	-0.35	-0.18
K(ϵ -BOC)	-0.49	-0.13
T	-0.52	-0.33
E(OtBu)	-0.61	-0.18
T(OtBu)	-0.76	-0.24
Y	-1.1 ³	-0.41
V	-1.1	-0.76
W	-1.3 ³	-0.58
Y(OtBu)	-1.4 ³	-0.64
F	-1.4 ³	-0.69

¹In Eq. 5-3, $R = 1.987 \text{ cal K}^{-1} \text{ mol}^{-1}$, and $T = 298 \text{ K}$.

²As given in Table 2-1 of Chapter 2, excluding the derivative VQ(DOD):PdA

³Estimated upper bound

We can obtain a useful comparison of the propensity differences between the VX: PdA derivatives in the 2:1 D₂O:DMSO-d₆ cryomixture and pure DMSO-d₆ by considering the thermodynamic cycle shown in Fig. 5-9. In this hypothetical cycle, the derivative VA: PdA is "mutated" to VX: PdA (X variable) in DMSO-d₆. This results in a free energy change corresponding to $\Delta\Delta G^\circ_{\text{Ala-X}}$ (DMSO). The next step in the cycle is the transfer of the derivative VX: PdA from pure DMSO to the cryoprotective

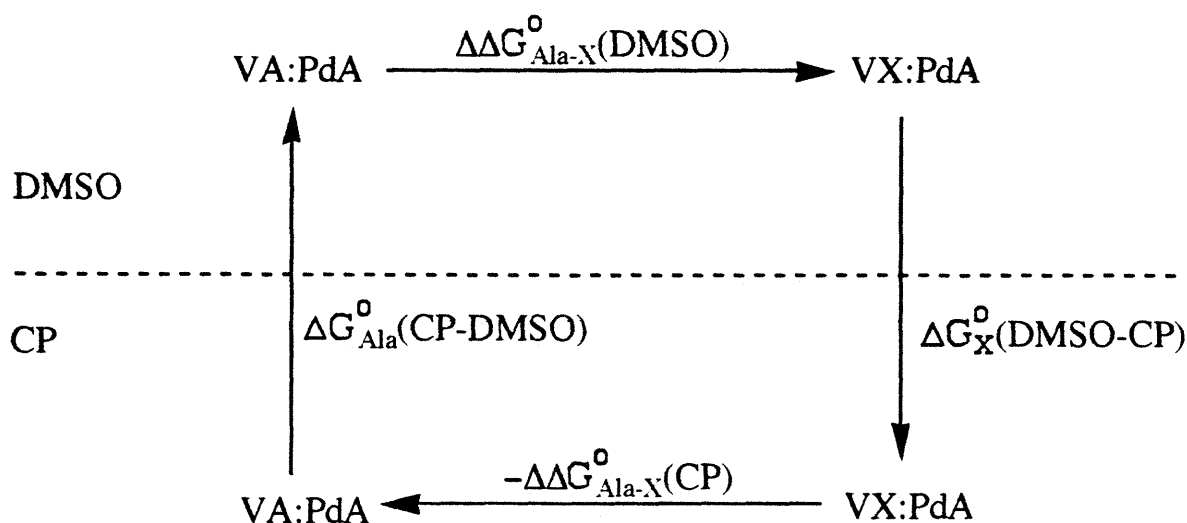


Figure 5-9. A hypothetical thermodynamic cycle where the peptide-epindolidione derivative VA: PdA is "mutated" to VX: PdA in DMSO-d₆ (upper arrow). This structural change in DMSO-d₆ corresponds to free energy change $\Delta\Delta G_{Ala-X}^{\circ}$ (DMSO) which is given in Table 5-2. The next arrow depicts the transfer of a derivative VX: PdA from the DMSO-d₆ phase to the 2:1 D₂O:DMSO-d₆ phase (CP). The corresponding transfer free energy change is ΔG_X° (DMSO \rightarrow CP). The next arrow represents the structural change whereby VX: PdA is changed back to VA: PdA, but this time in the cryomixture. The corresponding free energy change is $-\Delta\Delta G_{Ala-X}^{\circ}$ (CP), Table 5-2. Finally, the last process that completes the cycle is the transfer of the derivative VA: PdA from the cryomixture (CP) to DMSO-d₆. The corresponding free energy change is ΔG_{Ala}° (CP \rightarrow DMSO).

mixture (CP). This transfer is represented by a free energy change of

ΔG_X° (DMSO \rightarrow CP). Subsequently, the VX: PdA derivative is "mutated" in the

cryomixture back to the reference derivative VA: PdA. This results in free energy

change of $-\Delta\Delta G_{Ala-X}^{\circ}$ (CP), Table 5-2. Finally, the last step that completes the cycle

is the transfer of the derivative VA: PdA from the cryomixture back to DMSO-d₆.

This process is associated with the energy change of ΔG_{Ala}° (CP \rightarrow DMSO), Fig. 5-9.

Next we utilize the principle that the sum of free energy changes in any thermodynamic cycle is zero. This leads to Equation 5-4 from which we obtain the transfer free energy change from DMSO-d6 to the cryomixture, or

$\Delta\Delta G_{Ala-X}^{\circ}$ (DMSO \rightarrow CP). This transfer free energy is exactly what we need to compare the relative strand propensities in the cryomixture with those in DMSO-d6.

$$\Delta\Delta G_{Ala-X}^{\circ}(\text{DMSO}) + \Delta G_X^{\circ}(\text{DMSO} - \text{CP}) - \Delta\Delta G_{Ala-X}^{\circ}(\text{CP}) + \Delta G_{Ala}^{\circ}(\text{CP} - \text{DMSO}) = 0$$

or

$$\Delta G_X^{\circ}(\text{DMSO} - \text{CP}) - \Delta G_{Ala}^{\circ}(\text{DMSO} - \text{CP}) = \Delta\Delta G_{Ala-X}^{\circ}(\text{CP}) - \Delta\Delta G_{Ala-X}^{\circ}(\text{DMSO})$$

or

$$\Delta\Delta G_{Ala-X}^{\circ}(\text{DMSO} - \text{CP}) = \Delta\Delta G_{Ala-X}^{\circ}(\text{CP}) - \Delta\Delta G_{Ala-X}^{\circ}(\text{DMSO}) \quad (\text{Eq. 5-4}).$$

Table 5-3 provides the list of the $\Delta\Delta G_{Ala-X}^{\circ}$ (DMSO-CP) values calculated with Eq. 5-4 and the data from Table 5-2. The relative DMSO-CP transfer free energies of Table 5-3 clearly show that only glycine has an unfavorable or positive free energy of transfer. Furthermore, the charged amino acids lysine and arginine have transfer free energies comparable to alanine. In contrast, the amino acids bearing aromatic side chains have the most favorable or negative transfer free energies in the data base. Moreover, for all the five peptide-epindolidione derivatives in which a polar or charged side chain function has been blocked by a *tert*-butyl-derived protective group, the free energy of transfer to the cryomixture is more favorable relative to the unprotected ones. This suggests that addition of non-polar, hydrophobic bulk increases the susceptibility to stabilization by the cryoprotective solvent, relative to the behavior seen in DMSO-d6 itself.

Table 5-3.

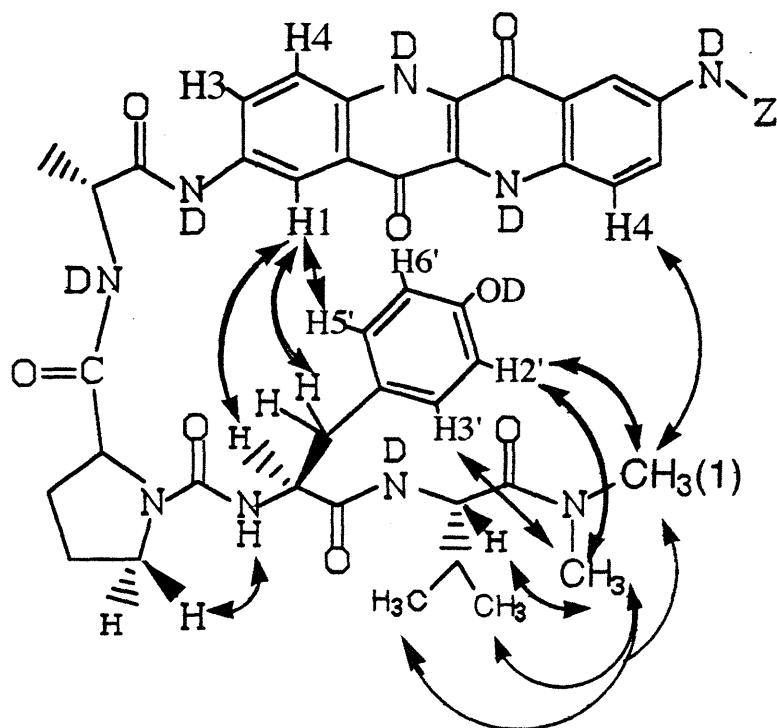
$\Delta\Delta G_{Ala-X}^{\circ}$ (DMSO \rightarrow CP) values calculated with Eq. 5-4.

Third Residue (X)	$\Delta\Delta G_{Ala-X}^{\circ}$ (DMSO \rightarrow CP) (Kcal/mol)
Y(OtBu)	-0.76 ^a
W	-0.72 ^a
F	-0.71 ^a
Y	-0.69 ^a
T(OtBu)	-0.52
D(OtBu)	-0.46
E(OtBu)	-0.43
D	-0.42
K(ϵ -BOC)	-0.36
V	-0.34
N	-0.29
Q	-0.26
E	-0.21
T	-0.19
L	-0.17
R	0.00
A	0.00
K	0.10
G	0.30

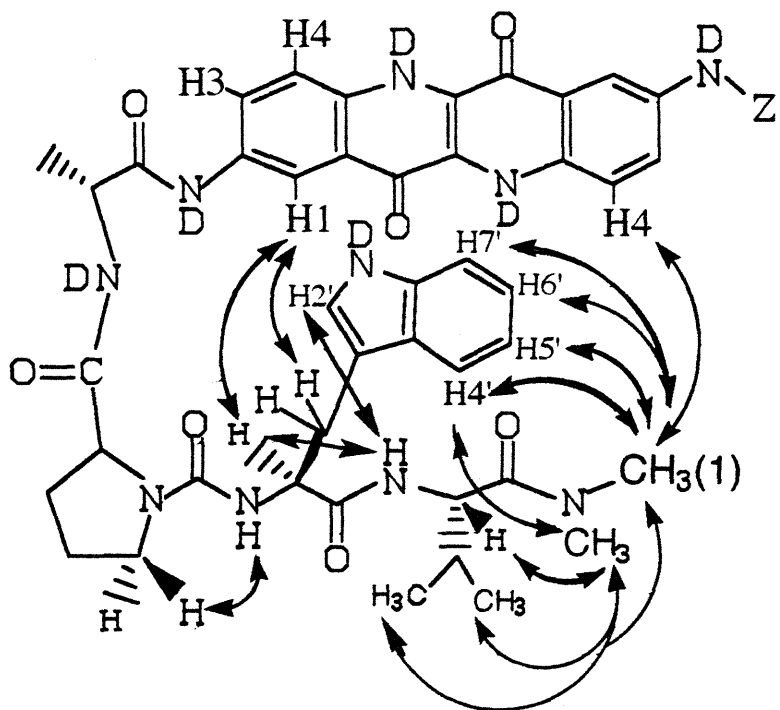
^a Estimated upper bound

It is clear that the ranking of Table 5-3 is essentially identical to that obtained from Fig. 5-8. The usefulness of the data in Table 5-3 is that it provides direct quantitative measure of the relative free energies of transfer from DMSO-d₆ to the cryomixture. Such values can be of practical significance in estimating the relative stability of a β -strand in the two solvent systems.

A series of 2D-NOESY experiments in cryoprotective D_2O -DMSO- d_6 indicates that derivatives **1a** (Fig. 5-1) have the required β -strand-turn-template hairpin structure.



5-10a
VY:PaA



5-10b
VW:PaA

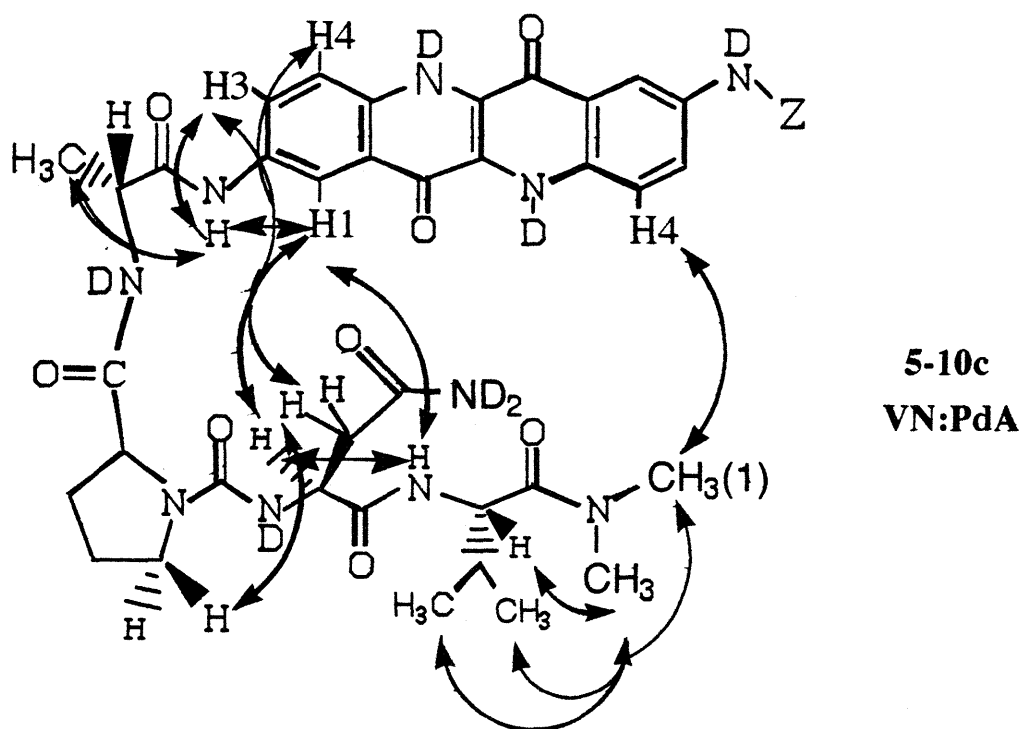


Figure 5-10. Representative 2D-SCUBA-NOESY results for a) VY: PdA (≈ 0.7 mM), b) VW: PdA (≈ 1.2 mM), and c) VN: PdA (≈ 2 mM) in 80/20 v/v DMSO- d_6 /D $_2$ O (51 mole%/49 mole% DMSO- d_6 /D $_2$ O), pD = 2.0, ≈ 6 °C, acquired on a 500 MHz spectrometer at the Francis Bitter National Magnet Laboratory at MIT. In each case note the absence of detectable NOEs between the side chains of R $_3$ and Val.

Figure 5-10 shows the NOE results from three representative NOESY spectra acquired on a 500 MHz spectrometer located at the Francis Bitter National Magnet Laboratory (NML) at MIT for three different derivatives in 80/20 v/v DMSO- d_6 /D $_2$ O (51 mole%/49 mole% DMSO- d_6 /D $_2$ O), pD = 2.0, 6 °C. Figure 5-11 shows the actual SCUBA-NOESY spectrum of VY: PdA including the assignment of the diagonal resonances as well as several of the crucial NOEs that indicate the presence of a robust β -strand-turn-template hairpin structure for this derivative. In Figs. 5-10a and 5-11 we can see the presence of the long-range NOE between the H4 proton of the epindolidione template and the methyl group of the N,N'-dimethylamide functionality designated as "Me(1)". Another long-range NOE shown in Figs. 5-10a

and 5-11 is that between the alpha proton of tyrosine, Tyr(α H) and the epindolidione H1 proton. These two long-range NOEs, and the absence of any detectable NOEs between the side chains of tyrosine and valine, strongly support the hairpin conformation as shown in Fig. 5-10a. The other NOEs shown in Figs. 5-10a and 5-11 help to define the conformation of the tyrosine side chain with respect to the epindolidione template and the rest of the peptide chain. In the review provided in Chapter four, we have seen that Dr. Kautz was not able to see any significant NOEs in pure water for the water soluble derivatives **1b** (Fig. 4-1 & Table 4-1, Chapter four). The large, negative NOE cross-peaks that can be seen in Fig. 5-11 clearly demonstrate the practical utility of doing NOE experiments in the viscous water-DMSO cryomixtures on peptide derivatives in the "intermediate" molecular weight range. Fig. 5-10b shows the results of a SCUBA-NOESY for the derivative VW:PdA. As in the case of derivative VY:PdA, Fig. 5-10b indicates the presence of the crucial long-range NOEs, and the absence of any detectable NOEs between the side chains of tryptophan and valine, which clearly support the hairpin conformation shown in Fig. 5-10b. Furthermore, the additional NOEs shown in Fig. 5-10b help to define the conformation of the tryptophan (indole) side chain with respect to the epindolidione template and the rest of the peptide chain. Fig. 5-10c shows the results of a SCUBA-NOESY for the derivative VN:PdA. As in the case of derivatives VY:PdA and VW:PdA, one can see the presence of the long-range NOEs supporting the hairpin structure depicted in Fig. 5-10c. However, Fig. 5-10c shows that in the case of VN:PdA, there are extra NOEs that are not present in the NOESY spectra of VY:PdA and VW:PdA (Fig. 10a & b). These extra NOEs are those between the alpha and beta-protons of asparagine and the H3 and H4 protons of the epindolidione template. The likely origin of the extra NOEs in the case of VN:PdA will be discussed below.

Figure 5-12 shows the NOESY spectrum of VN:PdA acquired in 33 mole% DMSO-d₆ - 67 mole% D₂O, pD = 2.0, - 15 °C on a 500 MHz spectrometer located at the MIT Chemistry Spectroscopy Laboratory. In this spectrum, the long-range NOE between the H4 proton of the epindolidione and the Me(1) is clearly indicated, and is consistent with the required hairpin conformation. In addition to these NOESY spectra, analogous NOESY spectra for VW:PdA and VY:PdA in 33 mole % DMSO-d₆- 67 mole % D₂O, pD = 2.0, at - 10 °C, and -5 °C, respectively, gave results that are fully consistent with the NOESY spectra taken at the cryoprotective concentration of Fig. 5-10. The presence of the long-range NOEs between the epindolidione H4 proton and the methyl protons of the N,N'-dimethylamide function, "Me(1)", for each of the derivatives VY:PdA, VW:PdA, and VN:PdA at two different cryoprotective concentrations (i.e. 33 & 51 mole % DMSO-d₆ in D₂O, and at several different temperatures) is the most emphatic indication supporting the presence of the β-strand-turn-template hairpin structure in the cryomixtures. In addition, as mentioned above, other long-range NOEs (e.g. between the alpha proton of residue X and H1 of the template, Fig. 5-10), and the absence of detectable NOEs between the side chains of R₃ and Val, are fully consistent with the conclusion that the derivatives VY:PdA and VW:PdA assume a robust β-strand-turn-template hairpin structure in the cryomixtures. As mentioned above, the results of the NOESY spectrum for VN:PdA (Fig. 5-10c) show the presence of extra NOEs that are not consistent with the indicated strand conformation for VN:PdA (Fig. 5-10c). However, these extra NOEs are consistent with the hypothesis that the derivative VN:PdA exists in the **Anti** conformation in addition to the β-strand-initiating **Syn** conformation shown in Fig. 5-10c. Figure 5-13 shows the derivative VN:PdA in the **Syn** and **Anti** conformations, and indicates how the **Anti** conformation can contribute to the presence the extra NOEs observed in Fig. 5-10c.

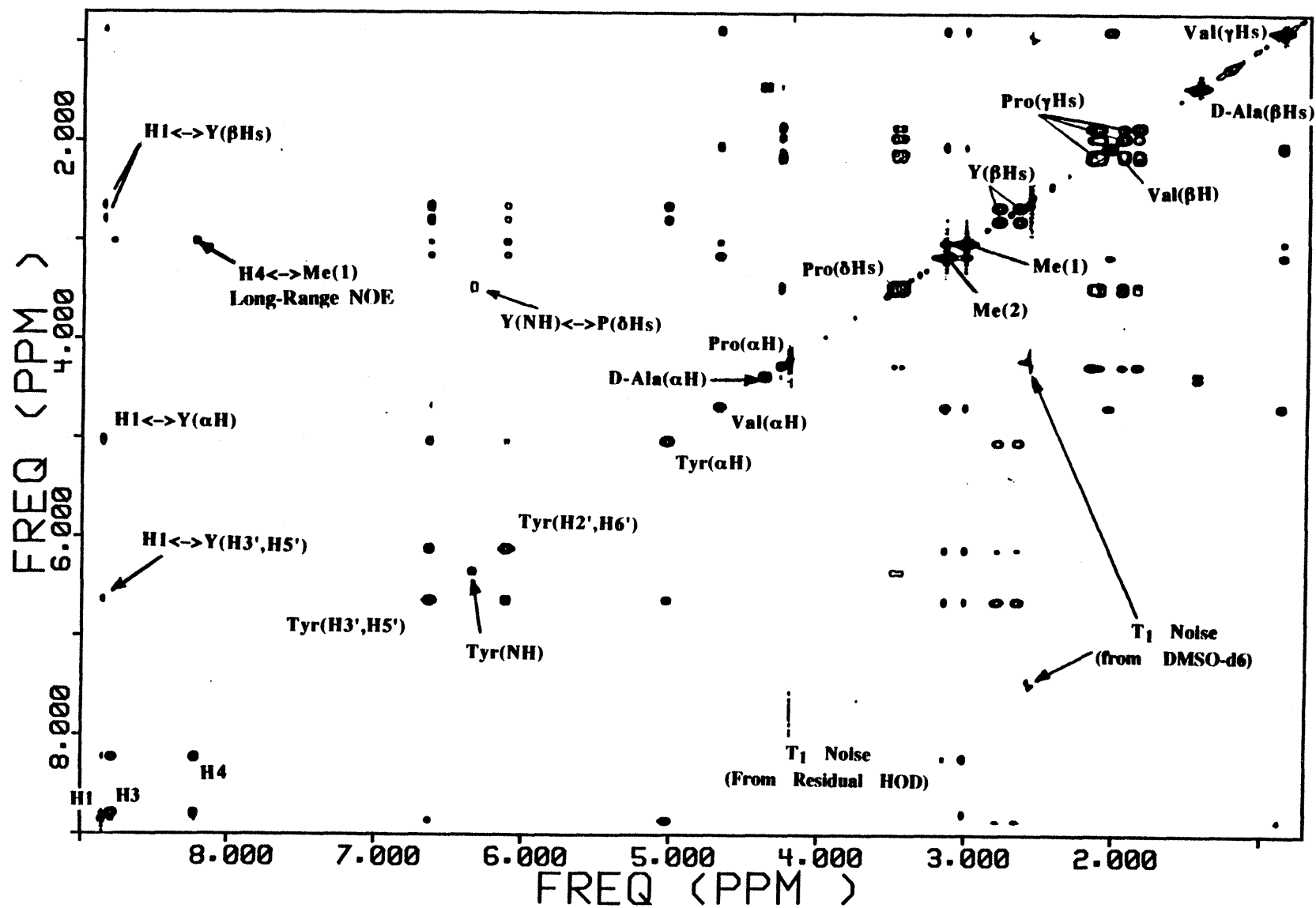


Figure 5-11. Phase-sensitive SCUBA-NOESY spectrum of VY:PdA (≈ 0.7 mM) in 51 mole % DMSO-d₆ - 49 mole % D₂O, pD = 2.0, 6 °C, acquired on a 500 MHz spectrometer located at the NML. The mixing time is 300 msec. The arrow indicates the crucial long-range NOE between the template H4 and Me(1), H4 \leftrightarrow Me(1).

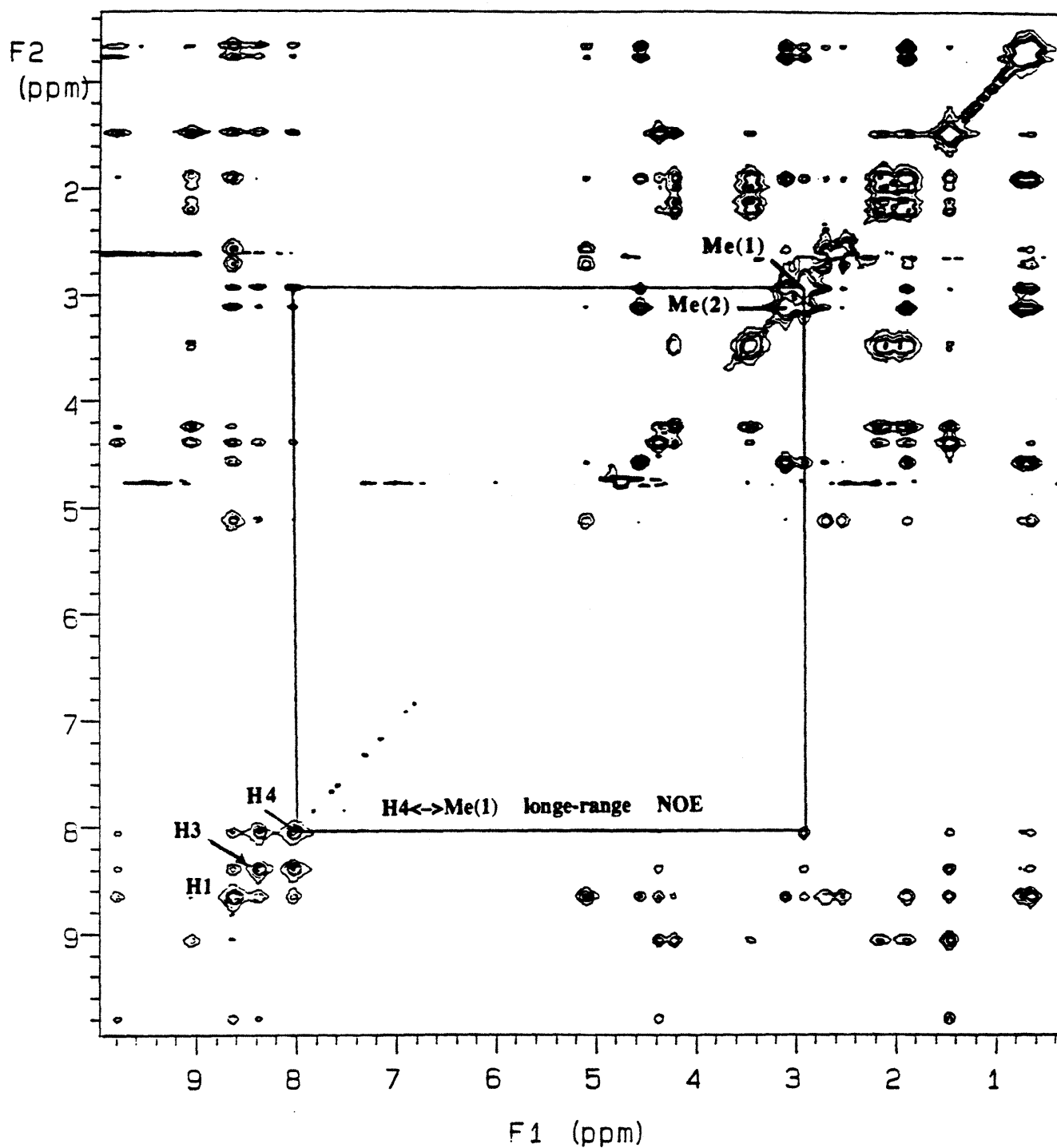


Figure 5-12. Phase-sensitive NOESY spectrum of VN:PdA in 33 mole % DMSO- d_6 /67 mole % D_2O , pD = 2.0, $-15^\circ C$, acquired on a 500 MHz spectrometer. Mixing time is 200 msec. The spectrum is not symmetrized with a 2K X 2K data matrix. For clarity, only the critical long-range NOE between the H4 of the epindolidione template and the methyl of the N,N'-dimethylamide cap is indicated in the spectrum.

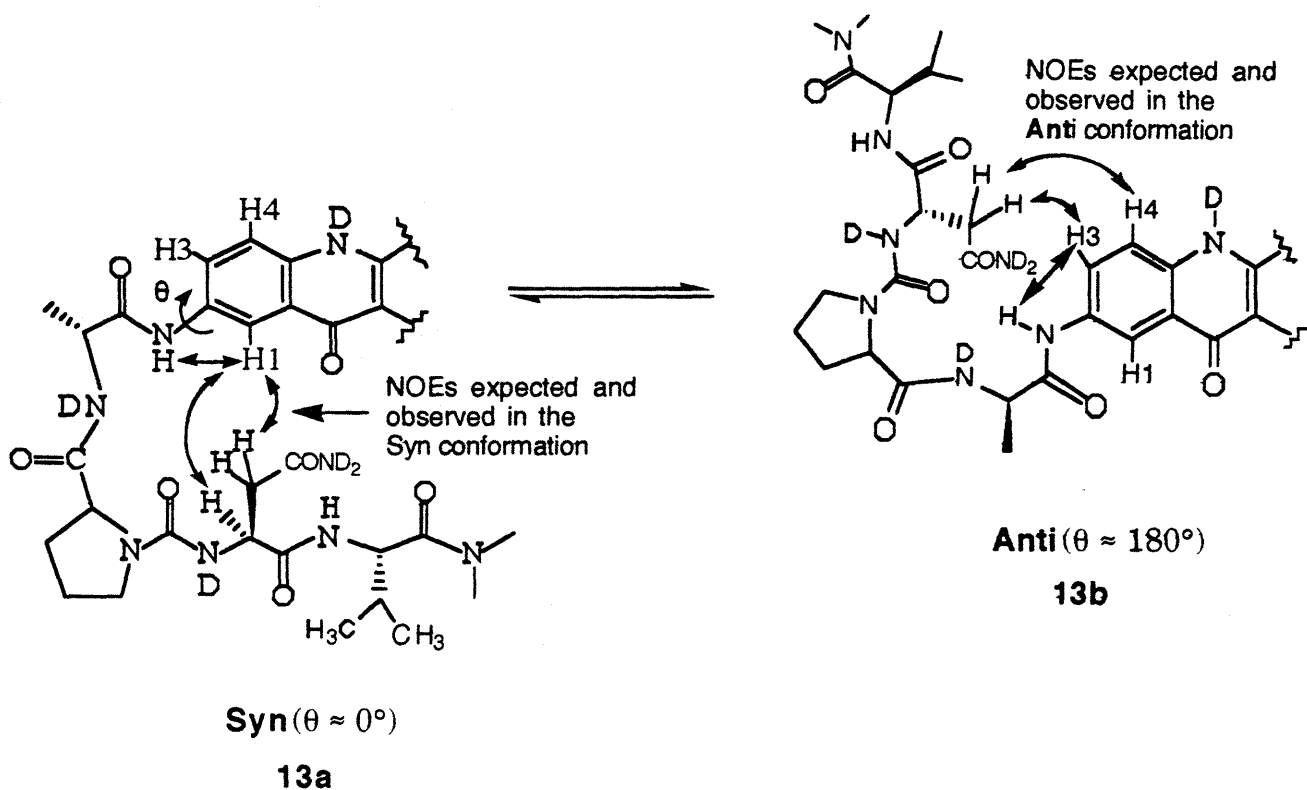


Figure 5-13. a) Peptide-epindolidione derivative VN:PdA in the **Syn** conformation. b) VN:PdA in the **Anti** conformation which results from a 180° rotation around the epindolidione C2-Aryl-N bond. The double-sided arrows indicate the expected and observed NOEs in the **Syn** and **Anti** conformations.

From Fig. 5-8 we can see that the derivative VN:PdA is predicted to be much less stable in the cryomixture than either derivatives VY:PdA or VW:PdA. As we have seen from the discussion of Chapter three in this thesis, the mole fraction that a given derivative spends in the **Syn** conformation is directly related to its stability in DMSO. This trend apparently persists in the cryomixtures. Thus, we can explain the presence of the extra NOEs consistent with the **Anti** conformation in the case of VN:PdA (Fig. 5-10c and Fig. 5-13b), and the absence of analogous NOEs for VW:PdA and VY:PdA, by suggesting that VY:PdA and VW:PdA possess very robust hairpin structures, and hence exist predominantly in the **Syn** conformation. On the other hand, VN:PdA has a much weaker structure (Fig. 5-8), and therefore the extra NOEs indicate the presence of the **Anti** conformation, Fig. 5-13b.

Another observation that can be made from the NMR data for the derivatives VX:PdA, is the relatively slow exchange of some of the NH protons in the cryomixture, especially at low temperatures. Thus, the pyridone NH exchanges to ND very fast (within the limit of 1D-NMR measurement, ≈ 5 min.) On the other hand, NH protons that are more sterically hindered, or otherwise are expected to be involved in intramolecular hydrogen bonds (e.g. the aryl NH or the ValNH), exchange more slowly (with a half-life on the order of hours). This behavior is consistent with the slow rates of hydrogen chemical exchange measured by Gordalla and Zeidler in water-DMSO cryomixtures, relative to pure water (Gordalla & Zeidler, 1991).

In summary, from the above discussion it is clear that the derivatives VX:PdA (Fig. 5-1) are stabilized by water-DMSO cryomixtures relative to pure DMSO-d₆ (Fig. 5-8 and Table 5-3). Furthermore, the NOESY data clearly show that the derivatives predicted to be the most stable (e.g. VW:PdA or VY:PdA) based on H₃ chemical shift arguments (Fig. 5-8) assume robust hairpin structures (Fig. 5-10a, and b). On the other hand, less stable derivatives such as VN:PdA (Fig. 5-8) show NOEs that are consistent with a less robust structure (Fig. 5-10c and 5-13b). Moreover, in all the NOESY spectra examined, there are no NOEs that contradict the predicted peptide-epindolidione derivative conformations.

In the rest of this Chapter, we will examine the behavior of the water-soluble "antiparallel" and "parallel" peptide-epindolidione derivatives in cryoprotective media. As the data will show, cryoprotective water-DMSO mixtures stabilize both "parallel" and "antiparallel" peptide-epindolidione β -strand-turn-template hairpin structures relative to pure water.

Earlier in this Chapter it was demonstrated that even the derivatives VK:PdA and VR:PdA, which possess two charges per molecule, associate extensively in pure D₂O (Figs. 5-3 and 5-4). Nevertheless, as Figs. 5-3 and 5-4 show, because of the positive charge, in the case of these two derivatives we were able to estimate the H₃ chemical shift in the limit of infinite dilution in pure D₂O (Fig. 5-4). Based on the

H3 chemical shift of Fig. 5-4, it was possible to conclude that both derivatives VK:PdA and VR:PdA are more stable in D₂O-DMSO-d6 cryomixtures relative to either pure D₂O or DMSO-d6. However, in the case of other derivatives VX:PdA that (unlike VR:PdA and VK:PdA) do not possess a net positive charge, limited water solubility prevented analogous estimation of limiting H3 chemical shifts in pure D₂O. Therefore, for the other derivatives VX:PdA, we could not make a similar comparison regarding the relative stability in D₂O and D₂O-DMSO-d6 mixtures.

We have seen from the discussion in Chapter four that Blanchard prepared "antiparallel" peptide-epindolidione derivatives designed for aqueous studies (wsXY:PdK in Fig 4-1b & Table 4-1, Chapter four). This researcher used some of the wsXY:PdK derivatives prepared by Blanchard in order to examine their behavior in water-DMSO cryomixtures relative to pure water. Table 5-4 lists the H3 chemical shifts of four wsXY:PdK derivatives in pure D₂O, pD = 2.0, 25 °C, and in the 33 mole % DMSO-d6 - 67 mole % D₂O, pD = 2.0, 25 °C cryomixture. For comparison, Table 5-4 also gives the H3 chemical shifts of the corresponding DMSO soluble derivatives VX:PdA. Figure 5-14 plots the data of Table 5-4. From the Table and the Figure, it is clear that in each case the H3 of a given wsXY:PdK derivative is significantly increased in the cryomixture relative to pure D₂O. This observation, therefore, confirms the conclusion derived from the derivatives VK:PdA and VR:PdA (Fig. 5-4). Thus, based on the H3 chemical shifts of derivatives VK:PdA and VR:PdA in Fig. 5-4 together with the H3 chemical shifts of the four wsXY:PdA derivatives listed in Table 5-4, we can conclude that "antiparallel" peptide-epindolidione derivatives are stabilized by the cryomixture relative to both D₂O, and DMSO-d6.

Table 5-4.

H3 shift for wsXY:PdK in D₂O, D₂O-DMSO-d₆, and XY:PdA in D₂O-DMSO-d₆.

Derivative	δ_{H3} (D ₂ O, ppm)	δ_{H3} (CP, ppm) ¹
wsVA:PdK	8.03 ²	8.34 ³
wsVL:PdK	8.16	8.54
wsFV:PdK	8.15	8.65
wsVV:PdK	8.33	8.69
VA:PdA	-	8.50
VL:PdA	-	8.61
VV:PdA	-	8.75

¹CP indicates cryoprotective mixture with 33 mole % DMSO-d₆ - 67 mole % D₂O (i.e., 2:1 DMSO-d₆:D₂O) pD = 2.0, 25 °C.

²As reported by Blanchard (Blanchard, 1992).

³Determined by this researcher using Blanchard's derivatives.

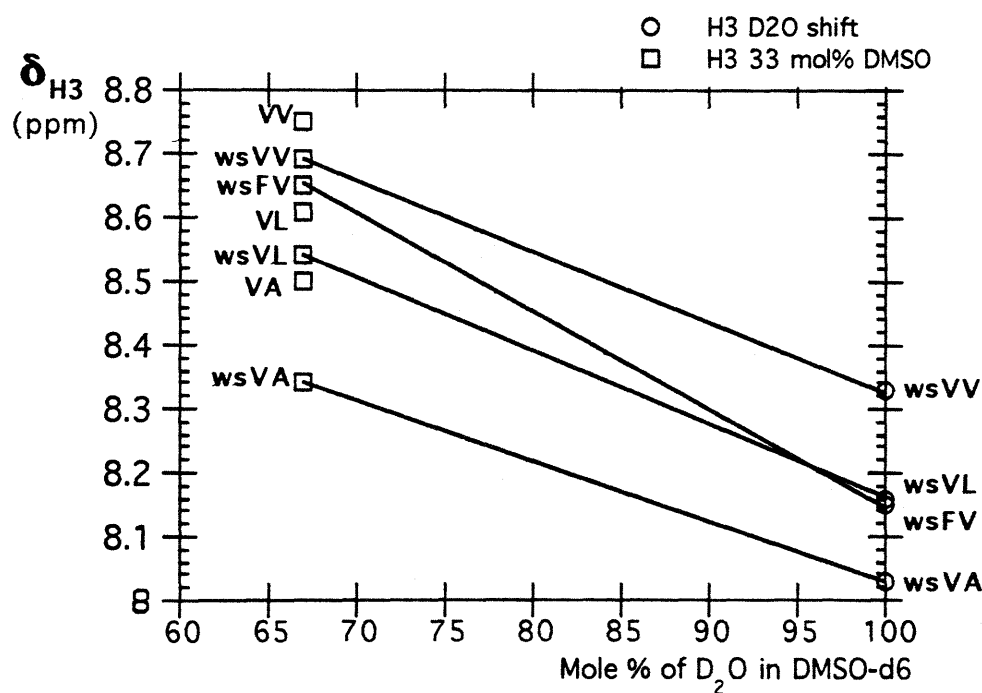


Figure 5-14. Plot of the data listed in Table 5-4 as the H3 chemical shift versus the mole percent of D₂O in DMSO-d₆, pD = 2.0, 25 °C.

Another point obvious from Table 5-4 and Fig. 5-14 is the higher stability of the VX:PdA derivatives relative to the analogous wsVX:PdK derivatives. This observation is puzzling, because the only difference in the two derivatives (i.e. VX:PdA and wsVX:PdK) is the alteration of the turn structure (i.e. change of d-Ala to d-Lys), and the presence of six positive charges per molecule in the case of the wsVX:PdK derivatives. We can attribute this stability difference to either or both of the following reasons. It is possible that the structural change of d-Ala to d-Lys weakens the turn structure, and thus results in the weaker structure of the wsVX:PdK derivatives. Indeed this hypothesis was originally proposed by Blanchard to explain the weaker strand propensities that he estimated in water relative to those in DMSO-d₆ (Blanchard, 1992). Another possibility is that the presence of the six positive charges per molecule in the wsVX:PdK derivatives has a destabilizing effect on their hairpin structure. This hypothesis is supported by the data of Fig. 5-8 and Table 5-3, which clearly show that the charged derivatives VK:PdA and VR:PdA (that possess only two charges per molecule) are the least stable (besides VG:PdA), and are comparable in stability to VA:PdA. As we will see from the subsequent discussion, the same trend is observed in the case of "parallel" peptide-epindolidione derivatives. Thus, it is likely that the presence of charge is inherently destabilizing for β -strand-turn-template hairpin structures.

Figure 5-15 shows the crucial long-range NOEs from a NOESY experiment performed at the Francis Bitter National Magnet Laboratory (NML), on the derivative wsFV:PdK (≈ 0.5 mM) in 33 mole % DMSO-d₆ - 67 mole % D₂O, pD = 2.0, 6 °C. The Figure shows the crucial long-range NOEs between the H4 proton of the epindolidione template and the alpha and beta protons of the propylamine cap. Furthermore, there are also NOEs between the H1 and the Val γ methyls, the alpha hydrogen of Val, and the H2' (and/or H6') protons of the Phe side chain.

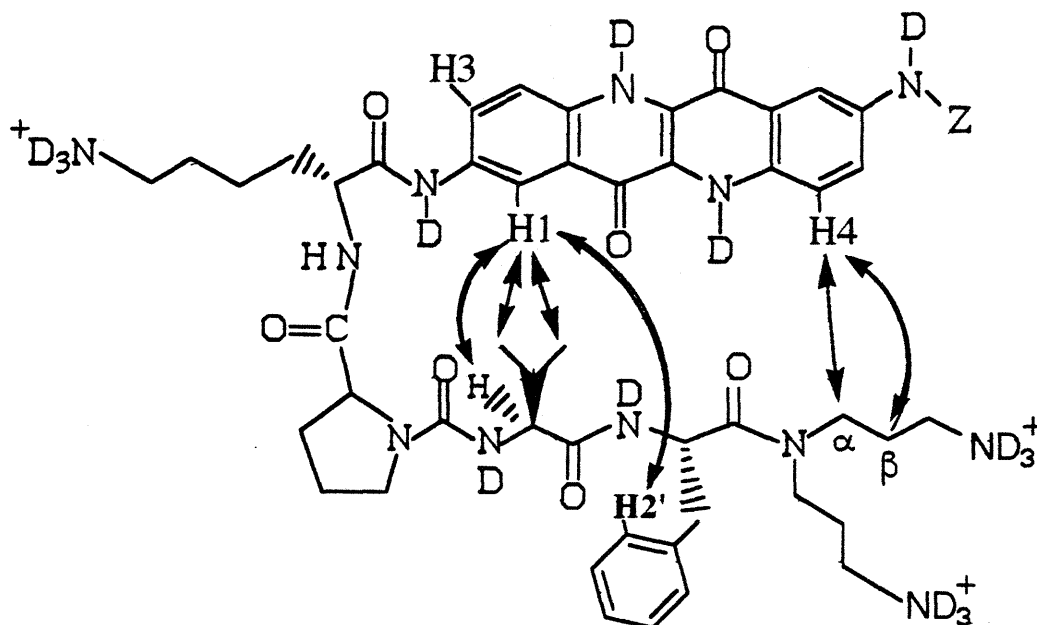


Figure 5-15. Crucial long-range NOEs obtained from a NOESY experiment on the derivative wsFV:PdK (0.5 mM) in 2:1 D₂O:DMSO-d₆ (molar ratio), pD = 2.0, 6 °C, on a 500 MHz spectrometer located at the Francis Bitter National Magnet Laboratory.

These NOEs are clearly consistent with the structure shown, and confirm that the water soluble "antiparallel" peptide-epindolidione derivatives also assume the required β -strand-turn-template hairpin structure in the 2:1 D₂O:DMSO-d₆.

The data presented above provides strong evidence that cryoprotective water-DMSO mixtures stabilize "antiparallel" β -strand-turn-template hairpin structure relative to both pure water and DMSO-d₆. Next we will examine evidence that suggests a similar stabilizing effect of cryomixtures on "parallel" peptide-epindolidione derivatives.

The first "parallel" peptide-epindolidione derivative studied in cryomixtures was KFVPdK, and its structure is shown in Fig. 5-16. As we briefly mentioned in Chapter four, this derivative is unusual in comparison to other water soluble

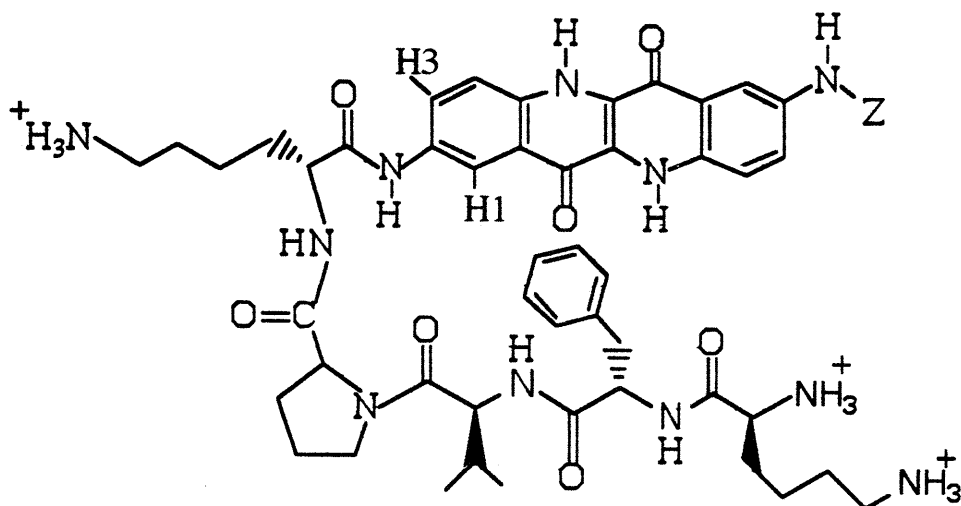


Figure 5-16. Structure of the water soluble parallel peptide-epindolidione derivative KFVPdK prepared by Arico-Muendel (Arico-Muendel, 1992).

"parallel" peptide-epindolidione derivatives of the general structure KXVPdK with respect to its relatively high water solubility. In his thesis, Arico-Muendel demonstrated that the derivative KFVPdK is monomeric at a concentration of 1 mM in water (Arico-Muendel, 1992). This favorable solubility profile allowed Arico-Muendel to conduct 2D-NOESY and ROESY experiments in water, which confirmed the predicted "parallel" structure.

As a prelude to the study of KFVPdK in water-DMSO cryomixtures, this researcher performed DMSO-d₆ titration experiments for this derivative in D₂O, pD = 2.0, 25 °C. Figure 5-17 shows a plot of the H3 chemical shift of KFVPdK as a function of the mole % of DMSO-d₆ in D₂O. From the Figure it is obvious that the H3 chemical shift increases upon addition of DMSO-d₆. Furthermore, from the

slope of the curve, it is clear that the rate of change of δ_{H3} is largest at the beginning of the titration and then begins to level off. The curve in Fig. 5-17 is a fit to the data

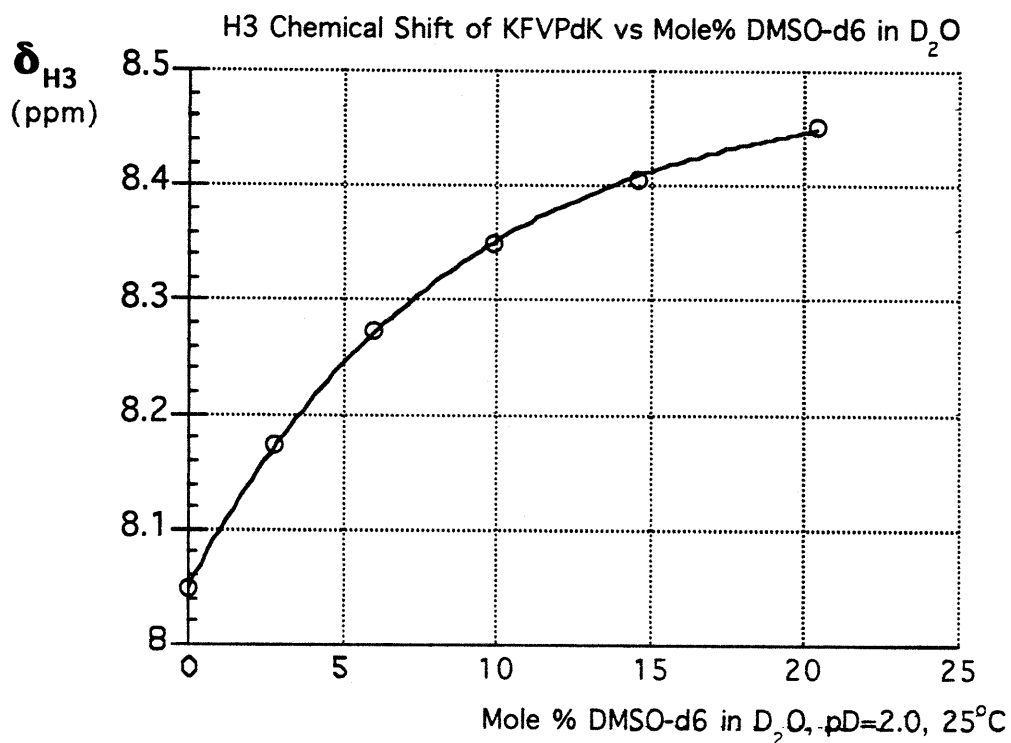


Figure 5-17. H3 chemical shift of the water soluble parallel peptide-epindolidione derivative KFVPdK as a function of mole % DMSO-d6 in D₂O, pD=2.0, 25 °C. The curve is a fit ($R = 0.9998$) to the data points obtained with the equation $\delta_{\text{H3}} = 8.488 - 0.439\exp(-0.117 \cdot X_{\text{DMSO}})$ where X_{DMSO} is the mole % of DMSO-d6.

points obtained using Equation 5-5. Equation 5-6 shows that the slope of the

$$\delta_{\text{H3}} = 8.488 - 0.439 \cdot \exp(-0.117 \cdot X_{\text{DMSO}}) \quad (\text{Eq. 5-5})$$

curve at $X_{\text{DMSO}} = 0$ is 0.051. However, at $X_{\text{DMSO}} = 20$ mole %, the slope is

$0.051 \cdot \exp(-0.117 \cdot 20) = 0.051 \cdot (0.096)$, which is only 9.6 % of the initial slope.

$$\left. \frac{\partial \delta_{\text{H3}}}{\partial X_{\text{DMSO}}} \right|_{X_{\text{DMSO}} = 0} = 0.051 \exp(-0.117 X_{\text{DMSO}}) = 0.051 \text{ ppm/mol\% DMSO} \quad (\text{Eq. 5-6})$$

Since H3 shift is expected to reflect the stability of the derivative, the plot in Fig. 5-17 suggests that the increase in stability of KFVPdK is largest during the initial stages of titration. As we will see below, we used the data of Fig. 5-17 to help choose a suitable mole % of DMSO-d6 in D₂O for NOESY study.

Figure 5-18 shows the NOE data derived from a series of NOESY experiments acquired on a 600 MHz spectrometer located at the NML. The crucial NOEs sought were the long-range NOEs between the pyridone NH and/or H4 of the template and the alpha proton of phenylalanine. The assignment shown in Fig. 5-18 is the result of three separate NOESY experiments. The first NOESY was performed in 90 mole % D₂O, 10 mole % DMSO-d6, pD = 2.0, 5 °C. The other two NOESY spectra were performed in 90 mol% H₂O, 10 mol% DMSO-d6, pH = 2.0, 5 °C. A NOESY that employed presaturation of the water signal was not satisfactory, because presaturation of the broad water signal in the cryomixture at 5 °C resulted in a simultaneous presaturation of the resonance due to the Phe alpha proton (i.e., the water peak is very close to the Phe alpha H). Therefore, it was necessary to run a jump-return (JR) NOESY to obtain the weak long-range NOEs between the Phe alpha H and the H4 and pyridone NH of the template. The other significant long-range NOEs shown in Fig. 5-18 are those between the H1 and the H3',H4', and H5' of the benzyl ring and the β-protons of Phe. In addition, one could observe NOEs between the H1 and the methyl groups of Val, with one being weaker than the other, which suggests the conformation of the isopropyl group as shown in Fig. 5-18. This conformation is consistent with the additional three NOEs of different strengths between the δ proton of Pro, and the Val side chain, Fig. 5-18. Furthermore, it is

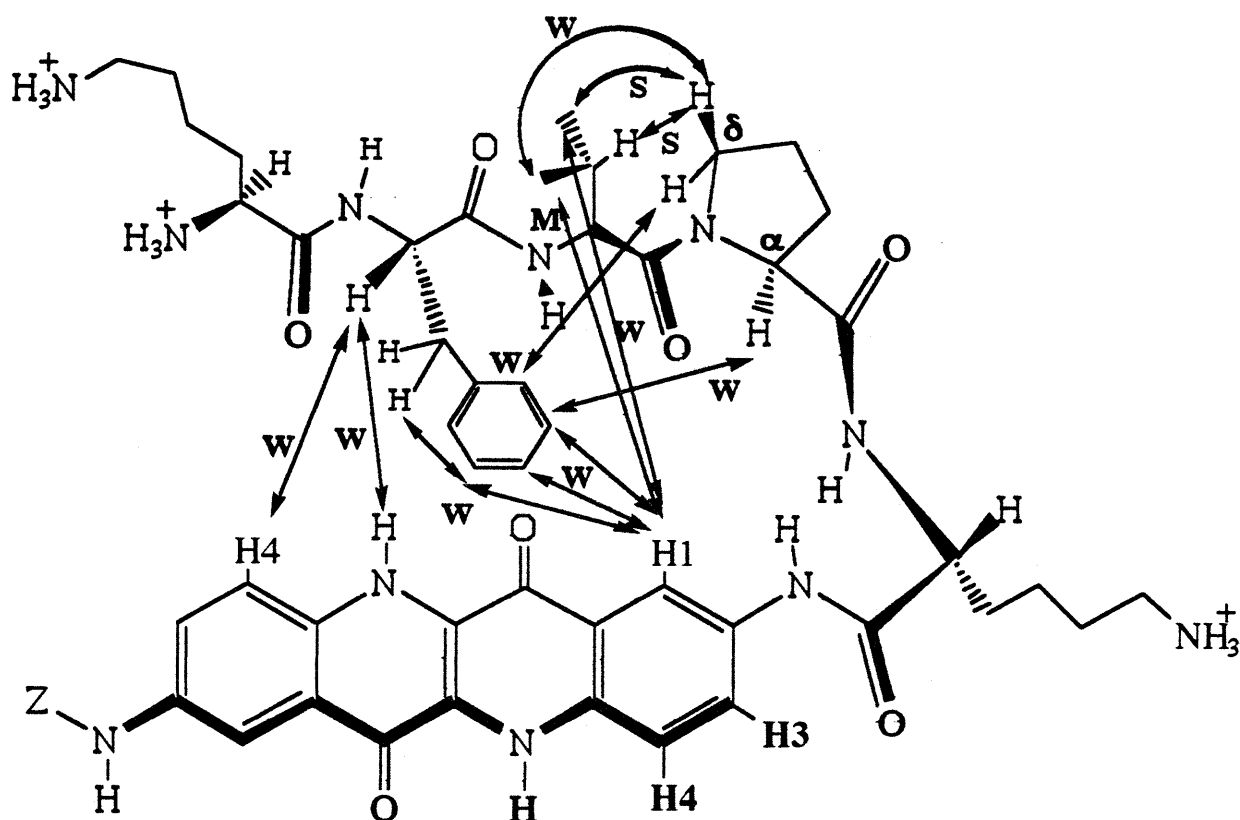


Figure 5-18. NOE data obtained from a series of NOESY experiments in 90 mole % D₂O, 10 mole % DMSO-d₆, pD = 2.0, and 90 mole % H₂O, 10 mole % DMSO-d₆, pH = 2.0, 5 °C. The mixing time was 300 msec. in each case. It was necessary to run a jump-return NOESY to obtain the long-range NOEs between the phenylalanine alpha H and the H4 and pyridone NH of the template. W = weak, M = medium, and S = strong denote the qualitative magnitudes of the NOEs observed for the derivative. Note the absence of NOEs between the Val and Phe side chains which is consistent with the indicated strand conformation. See text for more detail.

important to note the absence of any detectable NOEs between the Val and Phe side chains which is consistent with the strand structure. In summary, the NOESY data on KFVPdK in the cryomixture fully confirm the conformation shown in Fig. 5-18 which is also consistent with the conformation derived from the NOESY and ROESY experiments of Arico-Muendel in pure water (Arico-Muendel, 1992).

In Figure 5-19, H3 chemical shift data is plotted against the mole % of DMSO-d6 in D₂O, pD = 2.0, 25 °C for 13 derivatives of the general structure KXVPdK (Fig. 5-16), where X is a variable amino acid residue. From the Figure, it is clear that for every derivative, δ_{H3} increases upon addition of DMSO-d6 to D₂O. Table 5-5 gives the ranking based on the H3 chemical shift for each derivative of Fig. 5-19 for pure D₂O, as well as, 10 mole % DMSO-d6 - 90 mole % D₂O. The most striking feature of Fig. 5-19 is the divergence of δ_{H3} upon change to the cryoprotective mixture, which is clearly dependent on the specific nature of the amino acid residue X in KXVPdK. The most dramatic divergence in δ_{H3} upon change from D₂O to 10 mole % DMSO-d6 cryomixture occurs for derivatives KKVPdK and KFVPdK (Fig. 5-19). From the Figure it is clear that the increase in the δ_{H3} of KFVPdK is much larger than the corresponding increase in the δ_{H3} of KKVPdK upon change to the 10 mole % DMSO-d6 cryomixture. We can make this comparison more quantitative by computing the numerical values of the slopes joining the two data points for each derivative KXVPdK between 0 and 10 mole % DMSO-d6. We can then divide each slope value by the smallest slope value, which is that for KKVPdK. The results are given in Table 5-6. From the data in Table 5-6, it is clear that KFVPdK experiences the largest increase in the value of δ_{H3} , and KKVPdK the smallest. This suggests that the change to the cryomixture has the largest stabilizing effect on the derivative KFVPdK, and least on KKVPdK. In fact Table 5-6 provides ranking for each derivative KXVPdK based on the relative magnitude of stabilization upon change from D₂O to the cryomixture. This ranking indicates that in cryomixture, "parallel" derivatives containing a positively charged residue (i.e., lysine) are least stable, while those containing aromatic, or hydrophobic residues (i.e. F, L, I, and V) are most stabilized by change to the cryomixture.

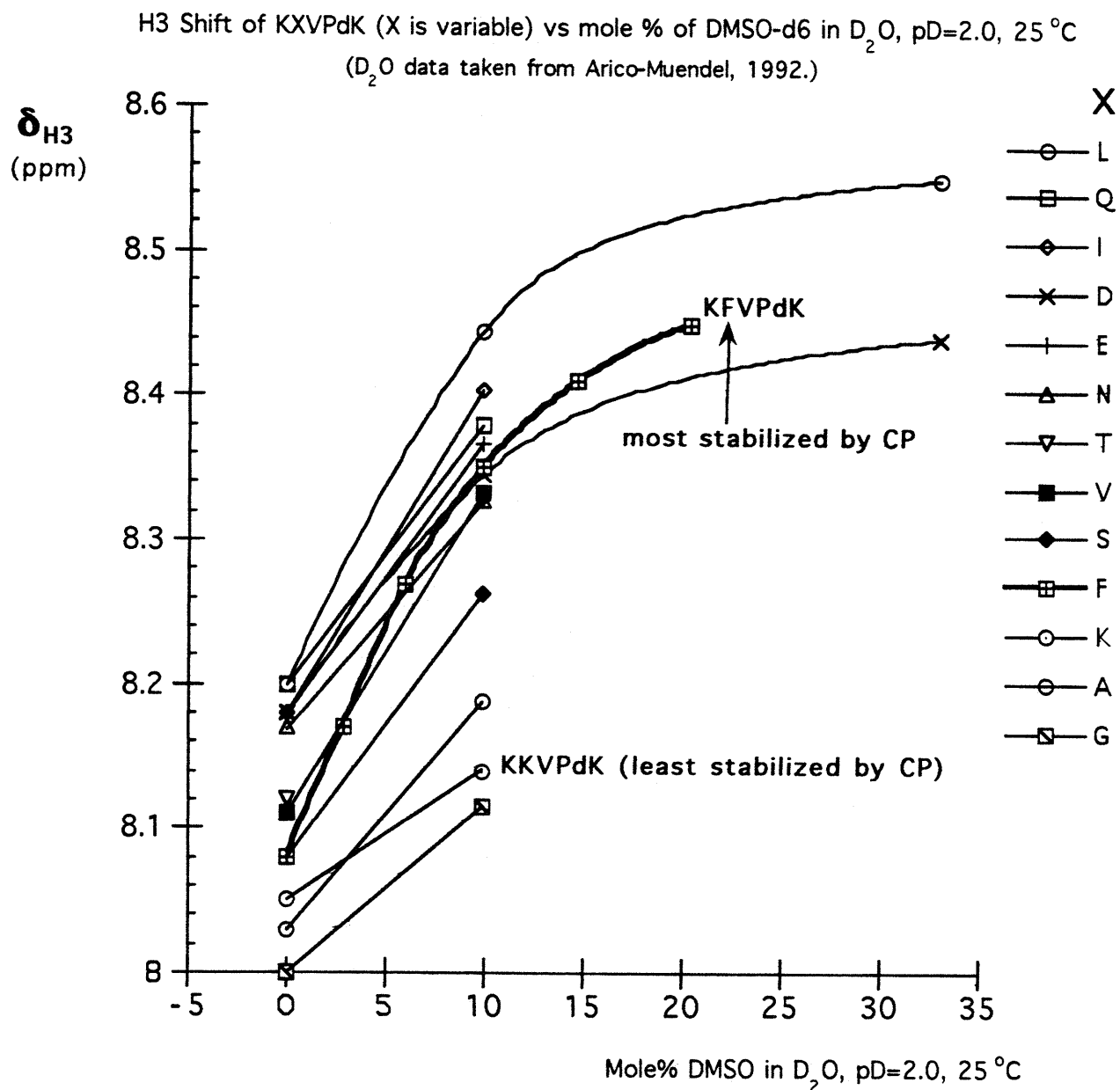


Figure 5-19. Plot of the chemical shift of the H3 proton of water soluble, parallel peptide-epindolidione derivatives KXVPdK synthesized by Arico-Muendel (Arico-Muendel, 1992) as a function of the mole % of DMSO-d6 in D₂O, pD = 2.0, 25 °C. X is the variable amino acid residue in KXVPdK. The chemical shift data for pure D₂O is taken from the thesis of Arico-Muendel (Arico-Muendel, 1992). Curve Fit is by interpolation between data points.

Table 5-5.

KXVPdK stability Ranking in D₂O (Arico-Muendel, 1992) and cryomixture (CP) based on the corresponding H₃ chemical shifts.

Residue X	$\delta_{H3}(D_2O)^1$	Residue X	$\delta_{H3}(CP)^2$
L, Q	8.20	L	8.45
I, D, E	8.18	I	8.40
N	8.17	Q	8.38
T	8.12	E	8.37
V	8.11	F, D	8.35
S, F	8.08	V, T, N	8.33
K	8.05	S	8.26
A	8.03	A	8.19
G	8.00	K	8.14
		G	8.12

¹D₂O data taken from thesis of Arico-Muendel (Arico-Muendel, 1992).

²CP denotes 10 mole % DMSO-d₆ - 90 mole % D₂O, pD = 2.0, 25 °C cryomixture.

Table 5-6.

Normalized slope values between the 0 and 10 mole % DMSO-d₆ data points for each derivative KXVPdK of Fig. 5-19.

Residue X	Normalized Slope ¹
F	2.97
L	2.75
I, V	2.53
T	2.31
E	2.09
Q, S	1.98
A	1.76
G	1.32
K	1.00

¹The normalized slope value is the result of the division of the actual slope value for derivative KXVPdK by the value of the slope for KKVPdK obtained from Fig. 5-19.

The data presented in this Chapter provided the first account ever made of the dramatic stabilizing properties of water-DMSO cryomixtures on both "antiparallel" and "parallel" β -strand-turn-template hairpin structure. Furthermore, besides demonstrating an overall stabilizing effect of cryomixtures on hairpin structure, this Chapter provided quantitative ranking of relative β -strand propensities of individual amino acid residues in both "antiparallel" and "parallel" peptide-epindolidione β -strand models. These ranking presented in Figures 5-8, 14 and 19 allows one to draw some interesting conclusions. For both "parallel" and "antiparallel" β -strands, charged residues (e.g. Lys or Arg) seem least stabilizing in cryomixtures. On the other hand, hydrophobic and especially aromatic residues (e.g. Phe) appear to provide the highest degree of stabilization on β -strand structure in cryoprotective media. This point is made clear by the dramatic increase in β -strand stability due to blocking of charged or polar side chains of amino acid residues as shown in Fig. 5-8. To give a specific example, removing a positive charge from lysine, by blocking with a BOC group, results in a dramatic increase in "antiparallel" β -strand stability in the cryomixture, but has essentially no effect in pure DMSO-d₆ (Fig. 5-8). Furthermore, as Fig. 5-19 and Table 5-6 show, the "parallel" derivative KKVPdK experiences the lowest level of stabilization upon change from D₂O to the cryomixture, while KFVPdK is most stabilized by the cryomixture. It must be emphasized that the destabilizing effect of charged residues on β -strand structure in water is much less obvious than in the cryomixture (Fig. 5-19), and is not observable in DMSO-d₆ (Fig. 5-8).

The data obtained from the study of peptide-epindolidione models in cryoprotective water-DMSO mixtures can be of potential practical value for rational design of stable peptide structures in cryosolvents. As we have seen from the review

provided in Chapter four, cryoprotective solvents such as water-DMSO have found widespread application in cryobiology and medicine in the cryopreservation process of cells and tissues. In nature, certain species of polar fish and insects produce peptides and proteins known as "antifreeze proteins" that help them survive exposure to low environmental temperatures. Such proteins were first identified by DeVries in Antarctic Fish (DeVries & Wohlschlag, 1969). Subsequent research has shown that these proteins help survival in low-temperature environments by non-colligative depression of the freezing temperature of aqueous solutions, presumably by binding to and inhibition of ice growth (Davies & Hew, 1990; Wen & Laursen, 1992).

Ice formation in cells and tissues during exposure to sub-zero temperatures is thought to contribute significantly to cryoinjury (Karlsson, Cravalho, & Toner, 1993). The discovery presented in this thesis that cryoprotective water-DMSO media can dramatically stabilize synthetic peptide derivatives can have potential applications in the rational design of peptide derivatives that can efficiently bind to and inhibit ice growth in cryosolvents. Such molecules can have potentially enormous beneficial effects during the process of cryopreservation of cells and tissues in cryobiology and medicine.

Experimental

NMR Spectroscopy

General

High resolution ^1H Nuclear Magnetic Resonance (NMR) spectroscopy was carried out on the Varian Spectrometers located at the MIT Chemistry Department Spectroscopy Laboratory, or at the Francis Bitter National Magnet Laboratory also at MIT. Routine, one-dimensional (1D) NMR spectra were acquired on the Unity-300, XL-300, or the Gemini-300 spectrometers located at the MIT Chemistry Department Spectroscopy Laboratory. Two-dimensional (2D) experiments, temperature studies, and 1D nuclear Overhauser effect (1D NOE) experiments were run on either the Varian VXR-500S ("Bullwinkle"), or VXR-501S ("Rocky") 500 MHz spectrometers at the MIT Chemistry Department Spectroscopy Laboratory. NMR time at the Francis Bitter National Magnet Laboratory was reserved exclusively for 2D NMR experiments run on either the 500 or 600 MHz spectrometers. The probe was allowed to equilibrate for at least ten minutes for variable-temperature experiments. At the MIT Chemistry Department Spectroscopy Laboratory, the FIDs (Free Induction Decays) after being saved to either the 3M DC 6150 Data Cartridge tape (150 Mbytes) or the HEWLETT® PACKARD 90 meters DDS-1 Data Cartridge (2 Gbytes) tape, were processed on either the Sun Microsystems Sparc 2 workstation using the Varian Instruments 3.1 VNMR software version, or on the Silicon Graphics Personal Indigo IRIS® workstation using the Varian Instruments revised 4.3 VNMR software version. At the Francis Bitter National Magnet Laboratory, the FIDs were initially saved to the HEWLETT® PACKARD 90 meters DDS-1 Data Cartridge tape, and then were processed on the VAX computer RNMRP software (Ruben's NMR Processing software.)

A note on the computer setup at the NML: all of the NMR spectrometers at the Francis Bitter National Magnet Laboratory belong to a network of VAX computers. The 500 MHz instrument is called RNMRC, and the 600 MHz spectrometer is called RNMRE. The software at the NML is divided into two parts in order to save magnet time:

1. The acquisition software, called RNMR (Ruben's NMR)
2. The processing software, called RNMRP (Ruben's NMR Processing software.)

This form of networking was designed to make off-line data processing possible. This is desirable because modern NMR experiments frequently require lengthy data processing.

Chemical shifts are reported in parts per million (ppm, δ) relative to tetramethylsilane (TMS) for organic solvents (e.g., DMSO- d_6 or CDCl_3), and trimethylsilylpropionic acid (TSP)

for aqueous and cryoprotective (DMSO/water) samples. Splitting patterns are abbreviated as: s, singlet; d, doublet; t, triplet, q, quartet; dd, doublet of doublets; m, unresolved multiplet; b, broad.

Cryoprotective Samples

DMSO/H₂O mixtures are often called cryoprotective mixtures due to their special biological properties (Douzou & Petsko, 1984.) In this work, ¹H-NMR experiments carried out in DMSO-d₆/D₂O and DMSO-d₆/H₂O are reported as mole percentages of DMSO-d₆

($X_{\text{DMSO-d}_6}$.) For routine preparation of NMR samples of a given $X_{\text{DMSO-d}_6}$, it was

necessary to obtain a relationship between the volume and mole fraction in the DMSO-d₆/D₂O binary mixtures:

DMSO-d₆ : MW=84.18 g•mol⁻¹, ρ=1.190 g•cm⁻³ (data taken from the Aldrich catalogue.)

D₂O: MW=20.03 g•mol⁻¹, ρ=1.107 g•cm⁻³ (data taken from the Aldrich catalogue.)

Let $V_{\text{DMSO-d}_6}^{\circ}$ = the molar volume of DMSO-d₆ = 84.18/1.19 = 70.7395cm³•mol⁻¹

Let $V_{\text{D}_2\text{O}}^{\circ}$ = the molar volume of D₂O = 20.03/1.107 = 18.0939cm³•mol⁻¹ ;

$$\text{Since } X_{\text{DMSO-d}_6} = \frac{n_{\text{DMSO-d}_6}}{(n_{\text{DMSO-d}_6} + n_{\text{D}_2\text{O}})}, \text{ and } n_{\text{DMSO-d}_6} = \frac{V_{\text{DMSO-d}_6}}{V_{\text{DMSO-d}_6}^{\circ}};$$

after some simple algebra we get

$$X_{\text{DMSO-d}_6} = \frac{V_{\text{DMSO-d}_6}}{V_{\text{DMSO-d}_6} + (3.9096)V_{\text{D}_2\text{O}}} \text{ (equation 1.)}$$

Since the peptide-epindolidione conjugates are freely soluble in pure DMSO, the most convenient way of preparing NMR samples of the conjugates in DMSO-d₆/D₂O cryomixtures was

to dissolve the conjugates in a given volume of DMSO- d_6 and then add the appropriate volume of D₂O (or H₂O) to obtain the desired mole fraction of DMSO- d_6 . For example, during a typical titration experiment, the sample (\approx 1 mg) would be dissolved in at least 700 μ l of DMSO- d_6 , and then the appropriate volume of D₂O or H₂O was added. To give a specific example, to prepare a peptide-epindolidione conjugate sample in 33 mol% DMSO- d_6 , equation (1) solved for V_{D_2O}

tells us that if we use 700 μ l of DMSO- d_6 to dissolve the conjugate, then we need to add

$$V_{D_2O} = \frac{(V_{DMSO-d_6})(1 - X_{DMSO-d_6})}{(3.9096) X_{DMSO-d_6}} = \frac{(700\mu l)(1 - 0.33)}{(3.9096)(0.33)} = 364 \mu l \text{ of } D_2O.$$

In all of the NMR experiments, the D₂O (or H₂O) used was always pD (or pH) 2.0. The pD (or pH) was adjusted by adding enough of 1N DCL (or HCL) to make the solution pD 2.0. A series of calibration measurements were carried out to determine the precision of the method used for determining the aliquots of D₂O, H₂O, or DMSO- d_6 . From the calibration measurements, one can estimate the accuracy of the measurements to be within $5.2\% \pm 1.4\%$ of the value reported.

NOE Difference Spectroscopy

1D NOE Difference Spectroscopy experiments were performed exclusively on either the Varian VXR-500S ("Bullwinkle"), or VXR-501S ("Rocky") 500 MHz spectrometers according to the standard methods outlined by Neuhaus & Williamson (Neuhaus & Williamson, Chapter 7, 1989.) Pure DMSO- d_6 samples were degassed by at least five freeze-thaw cycles using a dry ice-isopropanol cold bath while under nitrogen or high vacuum. After the final freeze-thaw cycle, nitrogen was introduced into the NMR tube, and the tube was capped. The cryoprotective samples were more difficult to degas than the pure DMSO- d_6 samples, and care had to be taken not to crack the NMR tube when freezing the sample in liquid nitrogen. The use of liquid nitrogen was necessary due to the very low freezing point of the cryoprotective samples. Except for this difference, the degassing of the cryoprotective samples was performed in the same way as described above for the pure DMSO- d_6 samples.

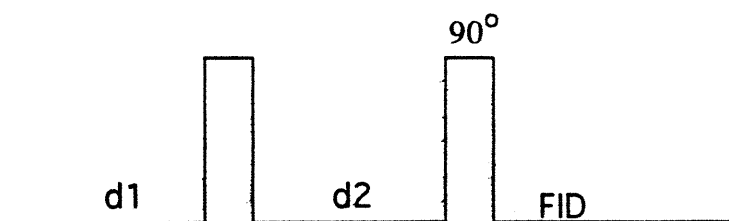
In order to achieve good presaturation selectivity, special setup instructions were

followed for most of the 1D NOE experiments. The following setup instructions were provided by Mr. Jim Simms, the Director of the MIT Chemistry Department Spectroscopy Laboratory.

Normally, ^1H 1D NOE experiments are performed using the parameters for ^1H NMR. However, much better decoupler selectivity was achieved by using the following procedure:

-
1. Load in the ^1H parameters.
 2. Write down the exact ^1H transmitter frequency (e.g., 499.843 MHz)
 3. Load the ^{13}C parameters (i.e., set up for regular ^{13}C work)
 4. After the ^{13}C parameters have been loaded, change the "sfrq" parameter to the frequency noted under #2 above (i.e., 499.843 MHz.)
 5. Set "homo"='n'
 6. Switch a knob on the spectrometer console to "narrow line"
 7. Set "dm"='nyn', and "dmm"='c'
 8. "d2" = variable (decoupling time); "d1" must be set > 0, to protect the receiver.
 9. must set "tn"='H1'
-

The sketch below illustrates the simple pulse sequence showing the time delays represented by "d1" and "d2". FID represents the acquisition time. The filled rectangles represent the pulses to be applied. For example, the right one represents a 90° transmitter pulse.



For NOE work on the Varian VXR-500S ("Bullwinkle"), the console temperature was always set to 30.0°C . Following that, the usual procedures of locking, tuning the probe, and shimming were performed. Initial shimming involved adjusting Z1 for a maximum value of the lock level. Subsequently, Z2 was adjusted for a maximum value of the lock level. The initial shimming was finished by re-adjusting Z1. It must be emphasized that the process of shimming

is very dependent on the volume of solution. This is why all NMR samples (except those for routine purity checks) had at least 700 μl of solvent. Next, the pulse width for the 90° ($\pi/2$) pulse ($\text{pw}90^\circ$) was determined. Subsequently, careful shimming was performed to obtain the width at half height ($\Delta_{1/2}$) on either the TMS or TSP peaks below 1 Hz, but often was able to achieve $\Delta_{1/2} < 0.5$ Hz for a spinning sample. Since all NOE experiments were done with the spinner turned 'off' (sample spinning may introduce unwanted artifacts, and generally lowers the reproducibility of NMR experiments), following the initial shimming with the spinner 'on', careful shimming using both the Z1-Z2 and the X1, Y1, XZ, YZ, XY, and X2-Y2 was performed with the spinner 'off'. The following procedure was followed for this shimming, adapted from the RNMR&U customer handbook written by Dr. Christopher J. Turner of the Francis Bitter National Magnet Laboratory at MIT (Turner, 1993.)

-
1. Adjust Z1 for a maximum value of the lock level. then adjust Z2. Finish off by readjusting Z1.
 2. Write down the current values of all the shims. Adjust X1 and Y1 for a maximum value of the lock signal.
 3. Optimize the combination of X1 and XZ for a maximum value of the lock signal.
 4. Optimize the combination of Y1 and YZ for a maximum value of the lock signal.
 5. Optimize the combination of XY and X2-Y2 for a maximum value of the lock signal.
 6. If any large shim changes were observed, then the phase of the lock signal should be optimized again and the whole process repeated from step 1.
-

Truncated Version of 1D NOE Experiment

The most commonly used 1D NOE experiments are 1D NOE difference experiments where the presaturation time ($d2$) is long ($d2 > 5 \times T_1$ for optimal results) and $d1$ is usually very short (e.g., 10 ms.) Also the strength of the B_1 (decoupler field) does not matter very much except it must not be too strong in order not to presaturate unwanted peaks. The truncated version of the 1D NOE difference experiment (TOE) differs only in the following ways:

1. $d2$ time parameter is a variable
2. B_1 field strength must be carefully calibrated, and

3. d_1 time must be long ($> 5 \times T_1$) to restore spin equilibrium.

Therefore, prior to TOE experiments, it is essential to perform decoupler calibration (Neuhaus & Williamson, Chapter 7, 1989.) Decoupler calibration involves determining the decoupler field strength (B_1) for a particular setting of the “dpwr” parameter. To give a specific example, decoupler calibration on the Varian VXR-500S (“Bullwinkle”) spectrometer was performed by running the experiment with an arrayed “d2” time parameter at a given “dpwr” setting. Thus, for

“dpwr”=36, the experiment gives $\gamma B_1 \approx 25$ Hz, or $pw(180^\circ) = 40$ ms; for

“dpwr”=37, $\gamma B_1 \approx 33$ Hz, or $pw(180^\circ) = 30$ ms, and for

“dpwr”=38, $\gamma B_1 \approx 170$ Hz, or $pw(180^\circ) = 5.9$ ms.

For this particular TOE experiment, $\gamma B_1 \approx 33$ Hz, with $pw(180^\circ) = 30$ ms was judged to be optimal, and was used to run the TOE experiment.

Another essential experiment that should be done before any NOE experiments are to be run is the determination of the T_1 for the protons of interest. Determination of T_1 is a relatively straightforward and commonly used procedure, hence will not be described in here.

The truncated NOE experiments generally consisted of 128 on and off-resonance irradiation transients recorded in an interleaved fashion. d_2 time was a variable (in one TOE experiment it ranged from 50 ms to 30 sec.), and the read pulse was 90° . d_1 time was usually set to 30 seconds (which satisfies the $d_1 > (5 \times T_1)$ requirement for most protons of interest.) The difference FID was transformed with 1.0 Hz line broadening. For integration of the transformed difference spectrum, a 15 Hz offset from the center of a resonance of interest was used for the sake of consistency. This offset had sometimes to be modified depending on the broadness of the resonance in question. The estimated accuracy of the integrals ranged from $\pm 5\%$ to $\pm 10\%$ of the value reported, mostly depending on the duration of the presaturation applied (d_2) and the number of the on and off-resonance irradiation transients recorded.

Two-Dimensional (2D) NMR

All 2D experiments were run with temperature control and without sample spinning. The probe was allowed to equilibrate for at least 15 minutes at a given temperature before beginning an experiment. These are crucial to avoid unwanted artifacts that sample spinning or even slight changes in temperature may introduce during the usually lengthy acquisition times.

Total Correlation Spectroscopy or TOCSY experiments (Braunschweiler & Ernst, 1983; Bax & Davis, 1985; Rucker & Shaka, 1989) were run at the Francis Bitter National Magnet Laboratory in the phase-sensitive mode according to the general method of States et al. (States et al., 1982.) A new, windowless sequence called DIPSI-2 was employed instead of the conventional broadband spin decoupling sequences such as MLEV-16 or WALTZ-16 (Rucker & Shaka, 1989.) The new DIPSI-2 sequence leads to a more rapid and complete cross polarization at a given expenditure of radiofrequency power (Rucker & Shaka, 1989.) Furthermore, a SCUBA (Stimulated Cross peaks Under Bleached Alphas) sequence was incorporated into the above TOCSY pulse sequence when water suppression was necessary (Brown, Weber, & Mueller, 1988.) Usually a 5 KHz spin lock transmitter field was used with a 70 ms spin lock period. Typically, for a 1-5 mM sample, we collected 0.5K x 2K data points with either 32, 64, or 128 scans per increment. An usual relaxation delay used was 2.0 sec. with spectral width of 6000 Hz in both dimensions. 2D-data processing typically involved linear prediction in t_1 (usually doubling the number of points in t_1), and zero filling to a symmetric data matrix of 2K x 2K. The 2K x 2K data matrix was then transformed with a Lorentzian-to-Gaussian exponential multiplication that was optimized for a given spectrum.

Homonuclear 2D Correlation Spectroscopy or COSY spectra (Aue et al., 1976; Bax & Freeman, 1981) were run either on the Varian VXR-500S ("Bullwinkle"), or VXR-501S ("Rocky") 500 MHz spectrometers at the MIT Chemistry Department Spectroscopy Laboratory in the absolute value mode. Typically 256 increments with 16 or 32 scans per increment were collected. The usual recycle delay time used was 1.0 s. The 2K x 0.25K data matrix was then zero-filled to a symmetric 2K x 2K matrix which was transformed with a sine-bell apodization.

Nuclear Overhauser Enhancement Spectroscopy or NOESY experiments (Wüthrich et al., 1984; Wüthrich, 1986; Neuhaus & Williamson, Chapter 8, 1989) were run at the MIT Chemistry Department Spectroscopy Laboratory and also at the Francis Bitter National Magnet Laboratory in the phase-sensitive mode according to the general method of States et al. (States et al., 1982.) At the Francis Bitter National Magnet Laboratory, the NOESY experiments incorporated the above-mentioned SCUBA sequence which is helpful in recovering peptide or protein α H resonances, which are usually lost due to the need to presaturate the large water resonance (Brown, Weber, & Mueller, 1988.) In general 32-64 transients were collected for each of 256-512 increments in t_1 . The mixing time most often used was 300 ms, but other mixing times (150, 200 ms) were used either to check for spin diffusion, or to follow NOE buildup. Typically, for a 1-5 mM sample, we collected 0.5K x 2K data points. As for the TOCSY spectra, spectral width of 6000 Hz in both dimensions was usually used. Typically 0.5K x 2K data points were collected with a relaxation delay of 2.0 sec. 2D-data processing typically involved linear prediction in t_1 (usually doubling the number of points in t_1), and zero filling to a symmetric data matrix of 2K x 2K. The 2K x 2K data matrix was then transformed with a Lorentzian-to-Gaussian exponential multiplication that was optimized for a given spectrum. We avoided symmetrization of the final spectrum, as it is likely to introduce unwanted artifacts.

Solvents

Dimethyl sulfoxide (dry) was distilled under high vacuum and stored over 4Å sieves. Dimethylformamide (dry) was distilled from ninhydrin under high vacuum and stored over 4Å sieves. Other solvents used for peptide synthesis were purchased from Mallinkrodt, Merck, and Maker. Acetonitrile used for preparative HPLC was Baker HPLC grade. Diisopropylethylamine (DIEA), triethylamine (TEA), and trifluoroacetic acid (TFA) were all Pierce Sequanal grade. Distilled water was deionized with Millipore Milli-Q water filtering system. Deuterated solvents for NMR were purchased from either Cambridge Isotope Laboratories, MSD Isotopes, or from Aldrich chemical company.

Chromatography

Preparative High Pressure Liquid Chromatography (HPLC) was run on a system that consisted of an Autochrom® OPG/S pre-pump solvent mixer with a Waters Associates model 590 pump fitted with preparative heads and a Waters Associates model 484 variable wavelength detector. The column was a C₁₈ reverse-phase Vydac 218TP1022. The solvent flow rate was usually run at 18 ml per min for the Vydac C₁₈ column. A Waters Associates model 484 tunable absorbance detector was used, with a Houston Instrument OmniScribe recorder. Analytical thin layer chromatography (TLC) was performed on silica gel 60, 250 μ glass-backed plates from E.M. Science. Preparative TLC was run using a 20 cm X 20 cm plates coated with a 0.25, 0.5, 1.0, or 2.0 mm thick layer of silica gel from Analtech G or GF Uniplates®. Gell filtration chromatography was run using a Sephadex LH-20 resin, which was swelled and eluted with DMF in a 2.5 cm (inner diameter), 50 cm Bio-Rad Econ-Column. The column wa eluted by a LKB equipment which consisted of a model 2132 Microperpex peristaltic pump with a model 2138 Uvicord S UV absorbance detector. The elution rate was usually set to about 0.5 ml/min., except during column washing, when the flow rate was usually doubled.

Preparation of 2,8-diacylamino-epindolidione Derivatives

The following procedures describe the preparation of peptide-epindolidione derivatives of the general formula VX:PdA, where X is the variable amino acid residue. In contrast to the general synthetic procedure for the synthesis of the peptide-epindolidione derivatives developed and described in the Doctoral Theses of Benjamin Bowen, Daniel Blanchard, and the Master's Thesis of Wesley Schaal, in this work it was necessary to modify the synthetic step leading to the chain-reversing urea function. This modification was needed because the older procedure for preparation of the amino acid isocyanates was not appropriate for some of the functionalized amino acid residues that had to be prepared in this work. Nevertheless, the majority of the other steps are patterned after the general syntheses developed by the other researchers mentioned above. The major purpose of this part of the experimental is to describe the new urea-forming reactions, and to describe in detail each step involved in preparation of the new derivatives. As the reader may notice, some of the synthetic procedures will be adopted from the other theses in essentially unchanged way, however, many differ in one or more important details.

Preparation of 2,8-diamino-epindolidione

Most of the steps in this synthesis are adopted from the original work of Drs. Bowen, Blanchard, and Arico-Muendel. This researcher has repeated this synthesis three times and found that it is essential for optimal results to have as detailed description of each step as possible. It is with this in mind that the following description is given.

Preparation of Dimethyl Dihydroxyfumarate

To an oven-dried 300 mL round-bottom flask equipped with a magnetic stirbar was added 21.44 g (0.145 mol) of dihydroxyfumaric acid hydrate¹ followed by 100 mL of anhydrous methanol. The solution was stirred for 20 minutes resulting in a dark-brown solution. At this point the flask was chilled in an ice bath (for \approx 15 min.) and 22.0 ml (302

¹) dihydroxyfumaric acid hydrate (FW= 148.07 g \cdot mol⁻¹) was obtained from Aldrich Chemical Company; Aldrich cat. # D11,320-4.

mmol, 2.1 eq.) thionyl chloride² was added slowly (over 10 min. period) under the surface of the chilled methanolic solution (with constant vigorous stirring) with a Hamilton syringe. During the slow addition of thionyl chloride, bubbling (of HCl) occurred. After initial addition of approximately 5 mL of thionyl chloride, the color of the dark-brown solution changed to a yellow-clear solution and subsequently after 10-15 mL more thionyl chloride was added, the clear yellow solution started to cloud-up, and soon became a rather viscous suspension of milky-yellow (“eggnog”) texture at the end of the thionyl chloride addition period. After addition of thionyl chloride was complete, the ice-bath was left for an additional five minutes and then was removed. Throughout the five minutes period, a stream of nitrogen was blown over the surface of the solution and, after the ice bath was removed, a nitrogen-filled balloon was attached. With the progression of time, the reaction became more viscous (eggnog color.) The solution was left with stirring under a nitrogen atmosphere for 48 hours. As the reaction progresses in time, the mixture becomes so thick that stirring becomes difficult, and towards the end of the reaction, the stirring actually stops. After 48 hrs., the reaction mixture was poured on a large glass frit (medium porosity) using a water suction-aspirator. The solid, after the solvent was drained, was of an eggnog color. Subsequently, it was washed (on the frit) with 20 mL cold methanol (portion of the 20 mL MeOH was used to remove the remnants of the solid from the reaction flask) and thereafter with 80 mL of distilled water. After the washing steps, the solid remaining on the frit was of a snow-white color. The yellow (eggnog) color was washed-away with the 20 mL MeOH and 80 mL water. This white solid was transferred from the glass frit into a tared 300 mL flask and placed on high vacuum to dry overnight. Note: The transfer process was rather messy, as the white solid on the frit is still wet and sticky. Yield of the dried dimethyl ester = 18.94 g (74%.) Melting point (mp) = 176°C.

²) Thionyl chloride (FW=118.97 g*mol⁻¹; d=1.631 g*cm⁻³) was obtained from Aldrich; cat.# 23,046-4.

Preparation of dimethyl bis-(*p*-nitroanilino)-maleate

The procedure mimics that reported by Jaffe and Matrick for their preparation of bis-(anilino)-maleates.

To a 100 mL pear-shaped flask was placed a magnetic stirbar, 9.90 g of dimethyl dihydroxyfumarate (56.2 mmol) and 15.3 g, 111 mmol of *p*-nitroaniline³. This was followed by 42 ml of anhydrous methanol. After mixing, 1 ml of conc. HCl was added, and a reflux condenser was attached. The reaction mixture was brought to reflux (using a heating mantle.) The mixture cleared partially after about 1.5 hour of reflux, and about that time an orange precipitate started forming. As the reflux proceeded (≈ 3 hrs. after start), the orange precipitate started forming a solid porous precipitate which was quite pronounced after 4 hours of reflux, at which time the reflux was terminated. The flask was allowed to cool slowly to room temperature and then was placed on an ice bath to cool further. The orange-brick-colored solid was collected on a medium porosity frit. The solid was washed several times with cold methanol, and placed on high vacuum to dry overnight. Yield = 14.2 g (61%.) M.P. 239-243°C.

Preparation of 2-methoxycarbonyl-3-(*p*-nitroanilino)-6-nitro-4-quinolone

Dowtherm A (150 mL) was brought to reflux in a 3-neck flask (500 mL capacity) fitted with a reflux condenser, a thermometer, and a glass stopper. The stopper was replaced with a funnel, and dimethyl bis-(*p*-nitroanilino)-maleate (14.2 g, 34.1 mmol) was added in small portions over 30 min. The addition must be slow to keep the reflux vigorous at $\approx 260^\circ\text{C}$. At the end of the 30 min. period, the addition funnel was rinsed with 15 mL of Dowtherm A, and replaced with a glass stopper. The solution was refluxed for 15 min. more (color changed gradually from red to dark-red,) and subsequently allowed to slowly cool to room temperature. The resulting brown-orange precipitate was collected on a medium porosity glass frit and washed with 400 mL of petroleum ether. Note: Previous workers in this labs used only up to 250 mL.) The crumbled filter cake was dried under high vacuum overnight. Yield = 10.03 g (77%.) M.P. 264-268°C (decomp.)

3) 4-nitroaniline (FW=138.13 g*mol⁻¹) was from Aldrich; cat. # 18,531-0

Preparation of 2-methoxycarbonyl-3-(*p*-ammonium anilino)-6-ammonium-4-quinolone dichloride

2-methoxycarbonyl-3-(*p*-nitroanilino)-6-nitro-4-quinolone (1.5 g, 3.9 mmol) was added to conc. HCl (100 mL), and the mixture was heated on a steam bath for 10 min. Tin(II) chloride dihydrate⁴ (7.5 g, 33 mmol) was added and the mixture became a red solution. About 5 min. of heating on the steam bath was needed before the mixture turned almost a clear-red solution. The solution was heated for additional 5 min. and then it was filtered (while still hot) through a glass frit. Subsequently, the filtered solution was cooled to room temperature, and evaporated on a high vacuum rotary evaporator (it bumps!) The resulting brown gum residue was dissolved in 30 mL of acetonitrile and filtered through a glass frit. Subsequently, precipitation of a pale-yellow product was induced by addition of 200 mL of diethyl ether. After settling down, the solid precipitate was collected on a glass frit, washed with additional 50 mL of diethyl ether, and *quickly* placed under high vacuum because it is very hygroscopic. Yield = 1.75 g (113%, wet?) A possible explanation for this anomalous yield value is the very hygroscopic nature of the product. This product was used in the next preparation without further preparation.

Preparation of 2,8-diamino-epindolidione

A mixture of anhydrous aluminum trichloride (17 g) and finely ground sodium chloride (1.7 g) was heated in a small (25 mL) 3-neck round-bottom flask equipped with a teflon-end mechanical stirrer, a thermometer, and a reflux condenser. The eutectic melted at about 110°C, and at that time the crude 2-methoxycarbonyl-3-(*p*-ammonium anilino)-6-ammonium-4-quinolone dichloride (1.75 g) was added to the molten mixture. A viscous purple solution resulted, and it was heated to 150°C, with constant stirring. Within one hour, the mixture assumed a dark-purple color. After one hour at 150°C, the reaction melt was poured hot over a mixture of ice (25 g) and 3 mL of conc. HCl. The flask was rinsed with a minimum amount of water (\approx 25 mL), and the combined aqueous portions were heated on a steam bath for 10 min. The suspension was transferred into four 30 mL Corex centrifuge tubes, and was subjected to centrifugation for 15 min. at about 4000 rpm. The volume was kept to about no more than 20 mL/tube. The supernatant (barley transparent) was discarded and the solid was resuspended in fresh (distilled) water. The suspension was again centrifuged, and the supernatant discarded.

4) Tin(II) chloride dihydrate (FW=225.63 g \cdot mol⁻¹) from Aldrich; cat. # 24,352-3.

The solid was suspended in water and centrifuged a third time (10 min., 4000 rpm.) In order to purify the product further, it was dissolved in a minimum volume of conc. sulfuric acid. The dissolution process was very exothermic - hence cooling in ice was helpful. Water was added subsequently until a precipitate formed (the mixture got hot.) The resulting suspension was centrifuged, the supernatant discarded, and the procedure with conc. sulfuric acid repeated one more time *in contrast to the procedure followed by the other workers in these labs.* After decantation of the sulfuric acid supernatant, the solid was suspended in fresh distilled water and centrifuged. This process was repeated once more with water, then with acetonitrile. The solid was transferred as an acetonitrile slurry, evaporated to dryness, and dried on high vacuum. Yield = 0.55 g (26%.) Note: This yield is most likely an underestimate, because the 1.75 g of the starting material is likely to contain less of the starting material due to its hygroscopic nature. Also, during centrifugation, some material was lost in the supernatant. Furthermore, the dissolution step in conc. sulfuric acid was repeated twice (to obtain a purer product) which may have contributed to the lower yield.

Preparation of 2,8-bis-(N-Boc-D-Ala-NH)-epindolidione

This derivative was synthesized followed the procedure described in the Bowen thesis with some modifications.

Part I: Preparation of N-Boc-D-Ala symmetrical anhydride (Boc-D-Ala)₂O

Dissolved 2.0 g of N-Boc-D-Ala-OH⁵ in 20 mL of methylene chloride and placed on ice bath. After 10 min. on ice, (with stirring under nitrogen atmosphere) added 1.06 (0.49 eq.) of dicyclohexylcarbodiimide (DCC)⁶ in small portions. The solution turned milky-white within 1-2 min. of DCC addition. The reaction mixture was allowed to stir on ice for 30 min. Then the reaction flask was placed in a freezer (-20°C) to let dicyclohexylurea (DCU) precipitate further. Afterwards, the milky-white contents were filtered through a glass frit (medium porosity, 10-20 μ), and the filtrate was evaporated on a high vacuum rotary evaporator. Upon drying, a white, foamy solid formed. The white solid was placed on high vacuum for about 2 hours to dry. Yield of symmetrical (Boc-D-Ala)₂O anhydride = 1.03 g (54%.) mp = 97-100°C

5) All amino acid derivatives are from Bachem unless otherwise indicated

6) DCC from Aldrich; cat. # D8,000-2.

Part II: Preparation of 2,8-bis-(N-Boc-D-Ala-NH)-epindolidione

430 mg of 2,8-diamino-epindolidione was suspended in 24 mL of vacuum-distilled DMSO under nitrogen. This gave a brick-red suspension. With stirring, 358 μ L of triethylamine (TEA) was added through a syringe. The suspension turned into a reddish, clear solution. Subsequently, 0.95 g of (Boc-D-Ala)₂O was added, and the reaction was allowed to stir for 60 min. Afterwards, the solution was centrifuged for 15 min at 4000 rpm. Note: Here *the centrifugation step replaces the filtration step through celite* used by earlier workers in this lab. This is done to avoid possible excessive loss of the product when filtering through celite. The supernatant was stripped on high vacuum rotary evaporator and placed on high vacuum for 1 hour in a 45°C water bath. The resulting red crust was suspended in MeOH and centrifuged. The centrifugation from methanol was performed two more times and the supernatant discarded each time. The final pellet was transferred as a diethyl slurry, evaporated, and placed on high vacuum to dry. Yield = 84% of brick-red powdery crust.

Deprotection of 2,8-bis-(N-Boc-D-Ala-NH)-epindolidione

154 mg of 2,8-bis-(N-Boc-D-Ala-NH)-epindolidione was slurred in 10 mL of methylene chloride under nitrogen. The slurry was placed on ice for 10 min. before 10 mL of trifluoroacetic acid (TFA) was added slowly via a syringe. The suspension turned clear. After TFA addition, the reaction solution was stirred under nitrogen on ice bath for 30 minutes. At that time TLC (85 Chloroform : 10 MeOH : 5 glacial acetic acid) showed the reaction to be complete. The solvent was evaporated in vacuo (on an ice bath) and the residue was placed on high vacuum to dry for 1 hour. The resulting residue was triturated twice with diethyl ether, and transferred to a tared flask and placed on high vacuum to dry for two hours. Yield of the TFA salt = 155 mg.

Preparation of (N-Boc-Pro)₂O

To a round bottom flask (100 mL) was placed 2.0 g of N-Boc-Pro-OH . 20 mL of methylene chloride was added and the powder dissolved with stirring under nitrogen. The solution was placed on ice for 10 min. after which 0.939 g of DCC was added in small portions. Soon afterwards, the solution turned milky-white. It was allowed to stir on ice bath for 30 min. (while periodically checking the reaction progress by TLC.) At that time, the reaction flask was placed in a freezer (-20°C) to let dicyclohexylurea (DCU) precipitate further. Afterwards, the

milky-white contents were filtered through a glass frit (medium porosity, 10-20 μ), and the filtrate was evaporated on a high vacuum rotary evaporator. In contrast to the procedure by which (N-Boc-D-Ala)₂O is prepared, oil instead of crystalline powder was obtained upon evaporation of the filtrate. This is typical for formation of proline-derived symmetrical anhydrides. The oil was placed for about one hour on high vacuum to dry further. Then, about 25 ml of hexanes was added. This was sonicated briefly (30 sec.), and the bottom of the flask was scratched with a glass rod for about 5 minutes. The hexane suspension was placed on ice and after settling down (5 min.), the hexane was removed (most of it) with a pipette. The rest of the solvent was stripped and the oil put on high vacuum for an additional hour. Afterwards, hexane was added again, and it was sonicated for 5 minutes. During sonication, a white-milky suspension in the hexane solvent formed. After settling down, most of the hexane was decanted, and upon evaporation of the residue one obtained a white solid residue. Note: The sonication was not employed by the previous workers mentioned above, but it seems helpful in the trituration process. Yield of dried anhydride = 1.25 g (65%). M.P. = 73-75°C. This product was used in the next reaction without further purification.

Preparation of 2,8-bis-(Boc-Pro-D-Ala-NH)-epindolidione

155 mg of the deprotected material was dissolved in 30 mL of freshly distilled (from ninhydrin) DMF. 75 μ L of TEA was added - precipitation resulted. 436 mg of (N-Boc-Pro)₂O was added and the mixture was allowed to stir. TLC was taken at time intervals to monitor the progress of the reaction. Note: At the start of the reaction, the color is brick-yellow suspension. However, 11 hours into the reaction, the suspension had cleared. TLC indicates one yellow spot with R_f = 0.65. Let stir one more hour and centrifuged the reaction solution for 15 min at 4000 RPM. Discarded the small reddish-green pellet, and evaporated the supernatant on high vacuum rotary evaporator. Suspended the resulting residue in methanol (with help of sonication) and centrifuged. Decanted the supernatant. The pellet was once more suspended in methanol, and centrifuged. The pellet was transferred as an ether slurry, evaporated, placed on high vacuum overnight. Yield = 145 mg.

Preparation of the isocyanate of the ethyl ester of glycine

Ethyl ester of the glycine hydrochloride (3.0 g, 1.0 eq) was added through a funnel to a 50 ml 3-neck flask fitted with a reflux condenser and a rubber septum through which a long needle connected to a nitrogen tank was pierced. Afterwards, 30 mL of toluene was added and the slurry was stirred. Next, triphosgene⁷ (5.7g, 0.89 eq.) was added with a stream of nitrogen blowing over the surface of the slurry. Subsequently, the mixture was heated on an oil bath to 110°C when reflux begun. The mixture was refluxed with stirring and occasional nitrogen flashing for 1.5 hour. TLC taken at 1 hour and 15 min into the reaction. two spots appear- one small spot at about 0.1-0.2 Rf, the other, larger one at about 1.0 Rf. The TLC was developed with ninhydrin spray. After stopping the reflux, let the reaction cool slowly to room temperature, while maintaining a steady nitrogen stream (for 1 hour) under the surface of the solution to blow-off the phosgene. Subsequently, poured the solution into a Kugelrohr flask and evaporated on high vacuum rotary evaporator to a brownish-colored oil. (Note: the evaporation should be done in a hood due to the potential evolution of phosgene.) The resulting oil was short-path distilled through a Kugelrohr apparatus. An oil with suspending particles was distilled at an oven temperature of 40-50°C. The flask contents were transferred to a small conical flask with 1-2 mL of methylene chloride, evaporated at water-aspirator pressures, and placed on high vacuum -it bumps ! Because of the bumping, placed the flask for a longer time on the water-aspirator, and then on high vacuum for 2 hours. Yield = 401 mg (22%; Note: The isocyanate is volatile, and slowly evaporates on high vacuum. The relatively low yield is likely due to the fact that it was kept too long on high vacuum (2 hrs.) This guess was confirmed by finding some of the isocyanate in the trap !)

Preparation of 2,8-bis-[(N-ureido-Gly-OEt)-Pro-D-Ala-NH]-epindolidione

I. Boc-deprotection

340 mg of 2,8-bis-(Boc-Pro-D-Ala-NH)-epindolidione was slurred in 20 mL of methylene chloride with stirring under nitrogen, and placed on ice bath. 10 min. later, 20 mL of TFA was introduced via a syringe and the slurry dissolved. The reaction was followed by TLC (85 : 10 : 5 Chloroform/MeOH/Glacial acetic acid.) Initially (t = 1 min.) there were two spots, but after 30 min. only, one spot could be observed at the origin (Rf = 0). The reaction was

⁷) Triphosgene, (CCl₃O)₂CO, (FW=286.45 g*mol⁻¹) from Aldrich; cat. # 33,075-2

stopped after 40 min. by evaporation of the solvent in vacuo still on the ice bath. The resulting residue was dried on high vacuum for an additional 15 min. and the triturated with ether, evaporated, and placed on high vacuum for two hours. Yield = 364 mg.

II. The Urea-coupling reaction

364 mg of the Boc-protected material was dissolved in 30 mL of dry DMF. The reaction flask was flashed with nitrogen, and a nitrogen-filled balloon was attached. Next, 130 μ l of TEA (2.2 eq.) was added - the solution turned pink-turbid in a matter of seconds. Subsequently, 135 μ l (2.8 eq.) of glycine ethyl ester isocyanate was added. The pink-turbid suspension cleared within \approx 5 minutes. Monitored the reaction progress by TLC (85 : 10 : 5 Chloroform/MeOH/Glacial acetic acid.) After 20 hrs., concentrated the reaction mixture to about 10 ml. Next, subjected that crude reaction mixture to purification by gel filtration chromatography on a sephadex LH-20⁸ column. Each injection on the column consisted of 2.0 mL of the above 10 mL crude, concentrated reaction mixture. Since each run takes about 4 hours, the whole purification on the LH-20 column took approximately 20 hrs. The fractions containing the desired product (fractions checked by TLC) were pooled together and evaporated on a high vacuum rotary evaporator. Yield = 314 mg (LH20-purified.)

A. General Procedure for Preparation of 2,8-bis-[(N-ureido-AA3-OR)-Pro-D-Ala-NH]-epindolidione (AA3 = Thr(OtBu), Trp, Lys(Boc), Tyr(OtBu), Asp(tBu), Glu(tBu), and Gln(DOD).)

Below are given three illustrative cases of preparation of the activated urethanes of Thr(OtBu), Tyr (OtBu), and Asp(OtBu). The other four activated urethanes that were used to prepare the tripeptide-epindolidione derivatives mentioned above were prepared by procedures very similar to those used to prepare the three derivatives described below. The main variables in the procedures seem to be due to the different solubility profiles of the activated urethanes formed (due to the difference in the structure of the respective amino acid residue side chain.) Also, one expects the reaction rates to be somewhat different, depending on the exact nature of the amino acid residue. The procedures are modifications of the procedure given for preparation of non-symmetrical ureas by Steglich et al., Chem Ber. 112, 727-733 (1979).

8) Sephadex LH-20 from Pharmacia Biotech.

B. Preparation of an activated urethane of the Methyl Ester of Thr(OtBu)

650 mg (2.88 mmol, 1.0 eq.) of methyl ester of threonine *tert*-butyl ether hydrochloride was dissolved completely in 30 mL of dry chloroform under a nitrogen atmosphere to give a clear, yellow solution. 502 μ L (2.88 mmol, 1.0 eq) of diisopropylethylamine (DIEA) was added via a syringe. TLC taken at that moment (TLC developing solvent = acetone.) Next, 0.94 g (2.88 mmol, 1.0 eq.) of 4,6-diphenylthieno[3,4-d][1,3]dioxol-2-one-5,5-dioxide (Steglich reagent)⁹ was added. This dissolved within 1-2 minutes to give a clear yellow solution. TLC taken at 1 min. after addition of the Steglich reagent. The reaction was allowed to stir under nitrogen overnight. The clear yellow reaction solution, became a milky suspension after \approx 18 hrs. into the reaction, most likely indicating product formation. This conclusion is supported by TLC analysis. 23 hrs. into the reaction, the milky suspension (of 18 hrs.) became a yellowish (off-white) cloudy suspension. The suspension was warmed for about 15 min. to 50°C, which caused complete clarification to give a clear, yellow solution. This solution remained clear even when cooled back to room temperature. The reaction was stopped after 24.5 hrs. by extracting 3 times each with saturated sodium bicarbonate, followed by 3x with 20 wt. % citric acid. After the first extraction with saturated sodium bicarbonate, the organic phase changed color from yellow to orange. The aqueous phase (discarded) is yellow. In each case 40 mL of the extracting solution was used. After the first extraction with 20 wt. % citric acid, the organic phase became pale-yellow. After the above-mentioned six extractions, the pale-yellow organic phase was dried over anhydrous magnesium sulfate for about 20 min. Then it was filtered through a medium porosity frit, and evaporated and dried under high vacuum overnight. Yield = 0.800 g. M.P. = 144-149°C.

C. Preparation of an activated urethane of the Methyl Ester of Asp(OtBu)

710 mg (2.96 mmol, 1.0 eq.) of methyl ester of aspartate *tert*-butyl ester hydrochloride (HCl • H-Asp(OtBu)-OMe) was suspended in 30 mL of chloroform under a nitrogen atmosphere. 520 μ l (2.96 mmol, 1.0 eq.) of DIEA was added via a syringe. The suspension cleared within about 5 minutes. (Note: brief (5-10 min.) warming of the solution to \approx 50°C speeds up the dissolution of all of the methyl ester of aspartate *tert*-butyl ester

⁹4,6-diphenylthieno[3,4-d][1,3]dioxol-2-one-5,5-dioxide is from Aldrich (95%, FW= 326.33); cat.#34,590-3

hydrochloride.) Took TLC #1 (acetone.) Next, with vigorous stirring, 0.97 g (2.96 mmol, 1.0 eq.) of 4,6-diphenylthieno[3,4-d][1,3]dioxol-2-one-5,5-dioxide (Steglich reagent) was added, resulting in a barely transparent yellow suspension. Flashed the addition funnel with 5 ml of chloroform, took TLC #2. After 25 hrs. put the reaction flask on warm bath ($\approx 50^{\circ}\text{C}$) for 0.5 hour. This somewhat clarified the suspension. Added 50 mL more of chloroform-suspension persisted. Increased bath temperature to $\approx 60^{\circ}\text{C}$ for about 0.5 hour (TLC #3 taken), which resulted in a clear solution. This solution remained clear even when cooled back to room temperature. The reaction was stopped after ≈ 26 hrs. by extracting 3 times each with saturated sodium bicarbonate, followed by 3x with 20 wt. % citric acid. After the first extraction with saturated sodium bicarbonate, the organic phase changed color from yellow to orange. The aqueous phase (discarded) is yellow. In each case 50 mL of the extracting solution was used. After the first extraction with 20 wt. % citric acid, the organic phase became pale-yellow. After the above-mentioned six extractions, the pale-yellow organic phase was dried over anhydrous magnesium sulfate for about 20 min. Then it was filtered through a medium porosity frit, and evaporated and dried under high vacuum overnight. TLC analysis is as follows: TLC #1 (see above) has two spots: one at the origin (very faint) the other at ≈ 0.8 Rf. Yield = 1.12 g. M.P. = $153\text{-}157^{\circ}\text{C}$. In TLC #2 the spot at the origin become even more faint, and two spots were observed away from the origin. One, brown-colored spot at $R_f \approx 1$, and another, yellow-color at $R_f \approx 0.9$. TLC #3 is similar to TLC #2, except that the very faint yellow spot at the origin of #2, became a pink-orange spot with a R_f of ≈ 0.1 .

D. Preparation of an activated urethane of the Methyl Ester of Tyr(OtBu)

0.84 g (2.91 mmol, 1.0 eq.) of the methyl ester of the *tert*-butyl ether of tyrosine hydrochloride was dissolved in 30 ml of chloroform under nitrogen with stirring. Next, 507 μl (2.91 mmol, 1.0 eq.) of DIEA was introduced via a syringe. This was followed by 0.95 g (2.91 mmol, 1.0 eq.) of the Steglich reagent. A clear, yellow solution was obtained. After about two hours, the clear, yellow solution turned cloudy (product formation.) The cloudiness increased with time. The reaction was stopped after ≈ 24 hrs. by extracting 3 times each with saturated sodium bicarbonate, followed by 3x with 20 wt. % citric acid. After the first extraction with saturated sodium bicarbonate, the organic phase changed color from yellow to orange. The aqueous phase (discarded) is yellow. In each case 50 mL of the extracting solution was used. After the first extraction with 20 wt. % citric acid, the organic phase became pale-yellow.

After the above-mentioned six extractions, the pale-yellow organic phase was dried over anhydrous magnesium sulfate for about 20 min. Then it was filtered through a medium porosity frit, and evaporated and dried under high vacuum overnight. Yield = 1.257 g. mp = 178-184°C (decomp.?)

D. Procedure for Preparation of 2,8-bis-[(N-ureido-Tyr(OtBu)-OMe)-Pro-D-Ala-NH]-epindolidione

The procedure to prepare 2,8-bis-[(N-ureido-Tyr(OtBu)-OR)-Pro-D-Ala-NH]-epindolidione will serve as an example of the general way that the tripeptide-epindolidione derivatives mentioned under (A) above were prepared. As before, the main variables between the different the procedures seem to be due to the different solubility profiles of the activated urethanes (due to the difference in the structure of the respective amino acid residue side chain.) Also, one expects the reaction rates to be somewhat different, depending on the exact nature of the amino acid residue involved.

Dissolved 6 mg (7.0 mmol, 1.0 eq.) of the TFA salt of PdA-epindolidione ammonium ion in 3.0 mL of dry DMF under nitrogen atmosphere. Added 5 μ l (\approx 3.8 eq.) DIEA, followed by \approx 71 mg (as a paste; 70 mmol, 10 eq.) of the methyl ester activated urethane of the *tert*-butyl ether of tyrosine. Followed the reaction progress by TLC (85 Chloroform : 10 MeOH : 5 glacial acetic acid.) The TLC shows that the reaction is essentially complete within 30 minutes. Nevertheless, let stir under nitrogen overnight. Stopped reaction by evaporating the solvent. Placed on high vacuum for one hour to dry. Redissolved in 0.5 ml of DMF and injected onto LH-20 column. Collected the appropriate fractions, evaporated, placed overnight on high vacuum to dry. Yield = 6.5 mg.

E. Procedure for Preparation of 2,8-bis-[(N-ureido-Tyr(OtBu)-OH)-Pro-D-Ala-NH]-epindolidione

6.5 mg (5.65 μ mol, 1.0 eq.) of 2,8-bis-[(N-ureido-Tyr(OtBu)-OMe)-Pro-D-Ala-NH]-epindolidione was dissolved in 5 mL of THF. 5 mL of distilled water was added. (TLC taken; (85 Chloroform : 10 MeOH : 5 glacial acetic acid.) Next, 28.3 μ l of 2N LiOH (10 eq.) was introduced via a syringe. TLC taken 5 min. after LiOH addition. TLC shows that the reaction has gone essentially to completion after 3 hours. To ensure reaction completion, added 60 μ l more of 2N LiOH at that point, and let stir for another hour. Stopped the reaction after a total of four

hours be evaporating the THF on a water-aspirator. Subsequently acidified the aqueous phase with 2 ml of 1N HCl. Precipitate formed. Centrifuged at 4000 RPM for \approx 10 min. discarded the supernatant. Resuspended in 5 mL of distilled water, and centrifuged again. Transferred as an acetonitrile slurry, evaporated, and placed on high vacuum to dry. Yield \approx 6 mg.

General Procedure for Preparation of 2,8-bis-[(N-ureido-AA3-AA4-N-Me₂)-Pro-D-Ala-NH]-epindolidione

To a 25 ml flask with 6 mg (5.3 μ mol, 1.0 eq.) of the diacid 2,8-bis-[(N-ureido-Tyr(OtBu)-OH)-Pro-D-Ala-NH]-epindolidione was added 12 mg (53 μ mol, 10 eq.) of the Hbr salt of Valine-N,N-dimethylamide. 3 ml of dry DMF was introduced and the mixture was stirred under nitrogen atmosphere when 10 μ l of DIEA was added via a syringe. This was followed by 9 μ l (53 μ mol, 10 eq.) of diisopropylcarbodiimide (DIC). The reaction was monitored by TLC (85 Chloroform : 10 MeOH : 5 glacial acetic acid.) Comparison of TLC taken at 5 min., 1 hour, and 14 hours into the reaction shows that the reaction is essentially complete after 14 hours. The reaction was stopped after 22 hrs. by evaporating the solvent. The residue obtained was dissolved in 1:1 v/v A:B (0.5 mL), where A = 20% acetonitrile, 0.1% TFA, and B = 100 % acetonitrile, 0.1% TFA. This solution was subjected to a preparative HPLC purification with the following conditions: 0 \rightarrow 100% B in 30 min. The product (2,8-bis-[(N-ureido-Tyr(OtBu)-Val-N-Me₂)-Pro-D-Ala-NH]-epindolidione) eluted at 21.2 min into the gradient. The product fractions were pooled, evaporated, and placed on high vacuum to dry. Yield \approx 4 mg.

tert-butyl-deprotection of 2,8-bis-[(N-ureido-Tyr(OtBu)-Val-N-Me₂)-Pro-D-Ala-NH]-epindolidione

\approx 2 mg of 2,8-bis-[(N-ureido-Tyr(OtBu)-Val-N-Me₂)-Pro-D-Ala-NH]-epindolidione was dissolved in 1 mL of methylene chloride and placed on an ice bath. Then 1 mL of TFA was added. TLC (85 Chloroform : 10 MeOH : 5 glacial acetic acid), showed that the acidolysis reaction is completed within 20 minutes. At 1 min. into the reaction there are three spots on the TLC (starting material, the "half"-product, and the fully-deprotected product.) At 20 min. into the reaction, only one spot is visible. The reaction was stopped by evaporation of the solvent. The residue was dissolved in a 1:1 mixture of A:B (0.2mL), where A = 10%

acetonitrile, 0.1% TFA, and B = acetonitrile, 0.1% TFA. The solution was subjected to preparative HPLC with the following gradient conditions: 0 → 100% B in 20 min. The product peak elutes at 13 min. The fractions corresponding to the product peak were pooled together, evaporated, and placed on high vacuum to dry. Yield < 1 mg.

Note: Analogous acidolysis conditions were employed for deprotection of the other *tert*-butyl-protected tetrapeptide-epindolidione derivatives. The only variable was the time necessary for the acidolysis to be complete.

Preparation of L-Valine diethyl amide hydrobromide

The following synthesis followed the general procedure for the preparation of amino acid dimethyl amide hydrobromides described in the Bowen and Blanchard theses with minor alterations.

Attempted distillation of dimethylamine hydrochloride salt through cannula as described in the Blanchard theses, but with limited success. The dimethylamine hydrochloride was very wet (it is a very hygroscopic material) and it was hard to get a homogenous mixture of the dimethylamine hydrochloride salt and sodium hydroxide due to the excess of moisture. Therefore, decided to distill the amine (bp = 7°C) using distillation apparatus and ice-chilled water bath. The crude mixture of the wet dimethylamine hydrochloride salt and finely ground sodium hydroxide was heated using an oil bath to about 100 °C. Several milliliters of the amine distilled through a cannula, and this was collected in an ice-bath chilled flask under nitrogen. At the same time, 2g of *p*-nitrophenyl ester of Z-protected valine was dissolved in 15 ml of methylene chloride and chilled on an ice-bath. The freshly-distilled dimethylamine was quickly poured to the methylene chloride solution and a yellow precipitate formed immediately. The reaction was allowed to stir on ice-bath for 10 minutes, and then was filtered through a medium porosity glass frit and the yellow residue washed with an additional 30-40 ml of methylene chloride. The filtrate was washed in a separatory funnel with each of 2X: 30 ml saturated sodium bicarbonate; 0.1 N HCl, and brine. This extraction procedure removed the colored compound present in the methylene chloride phase. The organic phase was dried over anhydrous magnesium sulfate for 10 min., filtered—a very slow process—and evaporated to a faintly yellow glass at water-aspirator pressure.

Z-group Deprotection

15 mL of 40% HBr in acetic acid was added to the crude product of the last reaction. A drying tube was attached and the flask was swirled until all of the material dissolved (≈ 10 min.) The solution was let stand for an additional 20 min. (small bubbles of gas evolved from the viscous solution-CO₂ ?) At that point stopped the reaction by adding ≈ 200 mL of diethyl ether. White suspension formed. Placed the flask (with the drying tube attached) in a refrigerator overnight to allow precipitation to occur. In the morning, the white ether suspension has cleared to form a white gum substance that deposited on the wall of the flask. Decanted the ether, added 200 mL fresh diethyl ether, swirled, placed in a refrigerator for 1 hour, decanted the ether, added 50 mL more ether, swirled and sonicated, let stand the suspension settled, then decanted the ether. Rotovaped the remaining ether, and placed on high vacuum in a vacuum desiccator with potassium hydroxide. Subsequently dissolved in acetonitrile, filtered through a glass frit (to get rid of rubber from a stopper) and evaporated to a foamy solid of yellowish-brown color. Triturated with diethyl ether, evaporated, placed on high vacuum to dry overnight. Yield = 955 mg.

Preparation of [Boc-D-Lys(ϵ -2-Cl-Z)]₂O Symmetrical anhydride

2.0 g (1.0 eq, 4.82 mmol) of Boc-D-Lys(ϵ -2-Cl-Z)-OH was placed into a 10 mL capacity flask equipped with a magnetic stirrer. 5.2 mL of methylene chloride was added with a syringe. The amino acid dissolved after about 2 min. of stirring under a nitrogen atmosphere. After the solid has dissolved, the solution was placed on ice-bath and kept for about 10 min. Afterwards, 0.488 g (0.49 eq., 2.36 mmol) of DCC was added to the solution in small portions. The solution turned milky white within ≈ 1 min. of DCC addition. The reaction was allowed to stir on ice-bath for 30 min., after which it was removed from the ice-bath and filtered through a fine (4-8 μ) glass frit. Few more milliliters of ice-cold methylene chloride was to wash the reaction flask, and the filtrate was evaporated and placed on high vacuum to dry. Note: The solid that forms upon evaporation foams! It is useful to use a large flask when evaporating. Yield = 1.38 g (71%).

Preparation of 2,8-bis-[Boc-D-Lys(ϵ -2-Cl-Z)-NH]-epindolidione

In 24 mL of freshly distilled dimethyl sulfoxide (DMSO), was suspended 296 mg (0.61 mmol) of 2,8-diamino-epindolidione bis-bisulfate. This suspension seems to clarify somewhat upon addition of 178 μ L of freshly distilled triethylamine (TEA.) Furthermore, addition of TEA resulted in a change of color from dark-brick-yellow suspension to deep-brown-red suspension. To this was added 1.38 g (1.70 mmol, 2.8 eq.) of [Boc-D-Lys(ϵ -2-Cl-Z)]₂O symmetrical anhydride, and the mixture was left to stir under nitrogen for 22 hrs. During the course of the reaction, one could notice the development of a greenish-brown tint. After 22 hrs., the reaction was concentrated in vacuo to a thick, dark-greenish-brown color paste, and then 5 mL of acetonitrile was added. The resultant suspension was centrifuged at 4000 RPM for 6 min. The supernatant was decanted, the residue suspended again in acetonitrile (with help of vortex mixer) and centrifuged again at 4000 RPM for 6 min. This process was repeated once more, and this time the pellet was suspended in a minimal volume of acetonitrile, evaporated, and placed on high vacuum to dry overnight. Yield = 0.62 g (94%) Note: Unlike noted in the Doctoral Theses of Blanchard and Muendel, the product that was obtained in the above reaction does not have a red-brown color, but has a rust color. It is possible that the red color is due to the presence of an impurity which may be absent in the product obtained above.

Boc-Deprotection of 2,8-bis-[Boc-D-Lys(ϵ -2-Cl-Z)-NH]-epindolidione

Slurried 500 mg of 2,8-bis-[Boc-D-Lys(ϵ -2-Cl-Z)-NH]-epindolidione in 3 mL of methylene chloride. Placed on an ice bath under nitrogen atmosphere while stirring (10 min.) Added 3 mL of trifluoroacetic acid (TFA.) Kept on ice bath for 40 min while monitoring the reaction progress with TLC: (85 Chloroform : 10 MeOH : 5 glacial acetic acid.) Subsequently, evaporated in vacuo at 0°C. Placed on high vacuum for 1 hour. Then triturated with diethyl ether, evaporated, and placed on high vacuum for 2 hours. Yield = 480 mg.

Preparation of 2,8-bis-[Boc-Pro-D-Lys(ϵ -2-Cl-Z)-NH]-epindolidione

54 mg (48.6 μ mol) of Boc-deprotected product from the last reaction above was dissolved in 5 mL of dry DMF. To this was added 16 μ L (2.3 eq.) of TEA. Separately dissolved (with difficulty) 2.1 g of (Boc-Pro)₂O symmetrical anhydride (as oil) in 5 mL of dry DMF.

Added 1.0 mL of this solution (≈ 15 eq. of the anhydride) to the above solution of TFA salt. Kept the reaction stirring under nitrogen atmosphere while monitoring periodically with TLC: (85 Chloroform : 10 MeOH : 5 glacial acetic acid.) Stopped reaction after 19 hrs. by evaporating the solvent in vacuo. Redissolved in a minimal amount of DMF (1 mL) and subjected to purification by LH-20 chromatography. Collected appropriate fractions (11-16), evaporated in vacuo, and placed on high vacuum to dry overnight. Yield = 64 mg.

Boc-Deprotection of 2,8-bis-[Boc-Pro-D-Lys(ϵ -2-Cl-Z)-NH]-epindolidione

64 mg of 2,8-bis-[Boc-Pro-D-Lys(ϵ -2-Cl-Z)-NH]-epindolidione was slurried in 5 mL of methylene chloride. Placed on an ice bath under nitrogen atmosphere while stirring (10 min.) Added 5 mL of trifluoroacetic acid (TFA.) Kept on ice bath for 30 min while monitoring the reaction progress with TLC: (85 Chloroform : 10 MeOH : 5 glacial acetic acid.) Subsequently, evaporated in vacuo at 0°C. Placed on high vacuum for 1 hour. Then triturated with diethyl ether, evaporated, and placed on high vacuum for 2 hours. Yield ≈ 51 mg.

Preparation of 2,8-bis-[(N-ureido-Lys(ϵ -Boc)-OMe)-Pro-D-Lys(ϵ -2-Cl-Z)-NH]-epindolidione

Dissolved 40 mg (1.0 eq, 26.1 μ mol) of the TFA salt obtained in the last reaction above in 5 mL of dry DMF under nitrogen. Added 140 mg (10 eq., 261 μ mol) of the activated urethane of Lys(ϵ -Boc)-OMe, followed by 9 μ L (2.3 eq.) of TEA. Monitored the reaction by TLC: (85 Chloroform : 10 MeOH : 5 glacial acetic acid.) At the beginning of the reaction (no activated urethane of Lys(ϵ -Boc)-OMe yet added) TLC shows one spot at the origin. At $t=15$ min. into the reaction, the following TLC pattern was obtained: 4 spots; one at $R_f=0$, one at $R_f=0.14$, one at $R_f=0.63$ (probably the product), and one at 0.71 (yellow, not fluorescent.) With time, this TLC pattern did not change appreciably, but apparently the third (product) spot increased in intensity. At 15 hrs. into the reaction, heated the reaction on an oil bath for 0.5 hrs. at 65 °C. However TLC showed essentially no change. Stopped the reaction at 16.5 hrs. by loading the crude reaction mixture onto LH-20 column. Collected fractions 9-13, evaporated, placed on high vacuum to dry overnight. Yield ≈ 40 mg.

HBr/AcOH Deprotection of 2,8-bis-[(N-ureido-Lys(ϵ -Boc)-OMe)-Pro-D-Lys(ϵ -2-Cl-Z)-NH]-epindolidione

\approx 40mg of the above LH-20 purified product was dissolved in 5 mL of 30 wt% HBr/AcOH. After 30 min. of swirling (deep-red solution) in a flask equipped with a drying tube, 150 mL of diethyl ether was added and the flask placed in a refrigerator for 3 hrs. At that time the ether was decanted, and the residue (red-brown powder after evaporation) was transferred as an ether slurry to a corex 30 mL capacity centrifuge tube. This was centrifuged for 5 min. at 4000 RPM. The clear supernatant was discarded, and the pellet resuspended in ether and centrifuged again. This process was repeated one more time. The pellet was transferred as an ether slurry and dried on high vacuum in preparation for preparative HPLC. Yield = 17 mg.

Preparative HPLC purification of the HBr/AcOH deprotected product from the last reaction

The prep. HPLC was performed twice. Conditions: 0 \rightarrow 100% B in 40 min. A = 10 % acetonitrile/0.1% TFA; B= pure acetonitrile. The collected fraction was evaporated, and placed on high vacuum to dry. Yield \approx 5 mg. This product was then lyophilized twice from 0.1 N HCl obtain the hydrochloride salt. Yield \approx 3.2 mg.

Preparation of 2,8-bis-[(N-ureido-Val-Val-OMe)-Pro-D-Ala-NH]-epindolidione

Dissolved 3.1 mg (1.0 eq., 3.4 μ mol) of 2,8-bis-[(N-ureido-Val-OH)-Pro-D-Ala-NH]-epindolidione in 1.0 mL of dry DMF under argon atmosphere. Added 10.0 mg (8.0 eq., 27.2 μ mol) of the methyl ester of Valine hydrochloride salt, followed by 11 μ L (8.0 eq, 27.2 μ mol) of DIEA and 8.0 mg (8.0 eq, 27.2 μ mol) of HOBt hydrate, and 10 μ L (8.0 eq, 27.2 μ mol) of diisopropylcarbodiimide (DIC). Followed reaction by TLC: (85 Chloroform : 10 MeOH : 5 glacial acetic acid.) Let stir under nitrogen overnight. Stopped reaction after 24 hrs. by evaporating the solvent. Placed on high vacuum for three hours to dry. Redissolved in 0.5 ml of DMF and injected onto LH-20 column. Collected the appropriate fractions, evaporated, placed overnight on high vacuum to dry. Yield < 1mg.

Preparation of 2,8-bis-[(N-ureido-Val-Gly-OMe)-Pro-D-Ala-NH]-epindolidione

Dissolved 3.1 mg of 2,8-bis-[(N-ureido-Val-OH)-Pro-D-Ala-NH]-epindolidione in 1.0 mL of dry DMF under argon atmosphere. Added 10.0 mg of the methyl ester of glycine hydrochloride salt, followed by 14 μ L of DIEA and 11 mg of HOBt hydrate, and 13 μ L of DIC. Followed reaction by TLC: (85 Chloroform : 10 MeOH : 5 glacial acetic acid.) Let stir under nitrogen overnight. Stopped reaction after \approx 24 hrs. by evaporating the solvent. Placed on high vacuum for three hours to dry. Redissolved in 1.0 ml of DMF and injected onto LH-20 column. Collected the appropriate fractions, evaporated, placed overnight on high vacuum to dry. Yield < 1mg.

Preparation of 2,8-bis-[(N-ureido-Val-OGly-OMe)-Pro-D-Ala-NH]-epindolidione

Dissolved 5 mg (1.0 eq., 5.5 μ mol) of 2,8-bis-[(N-ureido-Val-OH)-Pro-D-Ala-NH]-epindolidione in 3.0 mL of dry DMF under argon atmosphere. Added 2.5 μ L of methyl glycolate¹⁰ (6.0 eq., 33 μ mol) followed by 5 mg (6 eq., 33 μ mol) of HOBt and 5 μ L (6 eq., 33 μ mol) of DIC. Followed reaction by TLC: (85 Chloroform : 10 MeOH : 5 glacial acetic acid.) TLC indicated that the reaction is essentially complete at 13 hrs. Let stir under argon for a total of 18 hrs. to assure that the reaction is complete. Stopped reaction (after 18 hrs.) by evaporation of the solvent on a high vacuum rotary evaporator. Placed on high vacuum to dry for about two hours to dry (remove the excess of methyl glycolate.) At that point, redissolved the residue in 1 mL of DMF and injected on LH-20. Run the column at 40% pump speed. Collected the product fractions (as usual relying on UV-Vis inspection) and evaporated on a high vacuum rotary evaporator. Placed on high vacuum to dry overnight. Yield \approx 3 mg.

Preparation of 2,8-bis-[(N-ureido-Val-OAla-OMe)-Pro-D-Ala-NH]-epindolidione

Dissolved 5 mg (1.0 eq., 5.5 μ mol) of 2,8-bis-[(N-ureido-Val-OH)-Pro-D-Ala-NH]-epindolidione in 3.0 mL of dry DMF under argon atmosphere. Added 3 μ L

¹⁰) Methyl glycolate from Aldrich; cat. # 32,526-0; 98%; FW 90.08 g \cdot mol⁻¹

(6 eq., 33 μmol) of methyl (S)-(-)-lactate¹¹ followed by 5 mg (6 eq., 33 μmol) of HOBt and 5 μL (6 eq., 33 μmol) of DIC. Followed reaction by TLC: (85 Chloroform : 10 MeOH : 5 glacial acetic acid.) TLC indicated that the reaction is essentially complete at ≈ 15 hrs. Let stir under argon for a total of 21 hrs. Stopped reaction (after 21 hrs.) by evaporation of the solvent on a high vacuum rotary evaporator. Placed on high vacuum to dry for about two hours to dry (remove the excess of methyl (S)-(-)-lactate.) Redissolved the residue in 1 mL of DMF and injected on LH-20. Run the column at 40% pump speed. Collected the product fractions (as usual relying on UV-Vis inspection) and evaporated on a high vacuum rotary evaporator. Placed on high vacuum to dry overnight. Yield ≈ 4 mg.

Saponification (Hydrolysis) of 2,8-bis-[(N-ureido-Val-OGly-OMe)-Pro-D-Ala-NH]-epindolidione

Note: a potential source of problem in this reaction is the hydrolysis of the internal ester bond in addition to the desired terminal methyl ester. However, the latter reaction should be much faster than the former one.

Dissolved ≈ 3 mg of 2,8-bis-[(N-ureido-Val-OGly-OMe)-Pro-D-Ala-NH]-epindolidione in 5 mL/5 mL THF/water. Added 2.4 eq. of 1N lithium hydroxide. Followed reaction by TLC: (85 Chloroform : 10 MeOH : 5 glacial acetic acid.) TLC indicated that the reaction is essentially complete at ≈ 2 hrs. Let stir under argon for a total of 17 hrs. After 17 hrs., added 10 eq. of 1N HCl. A suspension formed. Evaporated THF and centrifuged. Resuspended in distilled water, centrifuged again. Suspended in acetonitrile and centrifuged. Transferred as an acetonitrile slurry and evaporated to dryness. Placed on high vacuum to dry overnight. Yield < 1 mg.

Preparation of 2,8-bis-[(N-ureido-Val-OGly-N-Me₂)-Pro-D-Ala-NH]-epindolidione

Dissolved ≈ 1 mg (1 eq., ≈ 1 μmol) of 2,8-bis-[(N-ureido-Val-OGly-OH)-Pro-D-Ala-NH]-epindolidione in 1 mL of dry DMF. Added 0.9 mg (12 eq., 12 μmol) of dimethylamine hydrochloride salt followed by 2 μL (12 eq., 12 μmol) of DIEA, 2 μL (12 eq., 12 μmol) of DIC, and 1.8 mg of HOBt. TLC: (85 Chloroform : 10 MeOH : 5 glacial acetic acid) shows two (?) spots

¹¹) Methyl (S)-(-)-lactate, 98%, from Aldrich; cat.# 23,034-0; FW 104.11 $\text{g}^*\text{mol}^{-1}$

at $R_f = 0.4$ and 0.6 throughout the reaction. Spots smear, making TLC difficult to follow due to overlap. Let stir under argon for 10 hrs. Stopped reaction by evaporating the solvent. Placed on high vacuum to dry for 3 hours. Redissolved the residue (< 1 mg) in 0.5 mL DMF and subjected to LH-20 purification. Run the column at 40% pump speed. Collected the product fractions and evaporated on a high vacuum rotary evaporator. Placed on high vacuum to dry overnight. Yield < 1 mg. NMR analysis of the LH-20 purified product indicates the presence of a minor impurity. Evaporated the DMSO- d_6 on high vacuum, placed on high vacuum to dry for 3 hrs., dissolved in 250 μ L of DMF and subjected to LH-20 purification. Run the column at 40% pump speed. Collected the product fractions and evaporated on a high vacuum rotary evaporator. Placed on high vacuum to dry overnight. NMR still shows some minor impurity, but MS indicates the presence of the sought product. Note: Preparative HPLC seems not a useful option as the derivative has a poor solubility profile in water-acetonitrile mixtures. Yield < 1 mg.

Saponification (Hydrolysis) of 2,8-bis-[(N-ureido-Val-OAla-OMe)-Pro-D-Ala-NH]-epindolidione

Dissolved ≈ 4 mg of 2,8-bis-[(N-ureido-Val-OAla-OMe)-Pro-D-Ala-NH]-epindolidione in 5 mL/ 5 mL THF/water. Added 2.4 eq. of 1 N lithium hydroxide. Followed reaction by TLC: (85 Chloroform : 10 MeOH : 5 glacial acetic acid.) TLC indicated that the reaction is essentially complete at ≈ 2 hrs. Let stir under argon for a total of 17 hrs. After 17 hrs., added 10 eq. of 1 N HCl. A suspension formed. Evaporated THF and centrifuged. Resuspended in distilled water, centrifuged again. Suspended in acetonitrile and centrifuged. Transferred as an acetonitrile slurry and evaporated to dryness. Placed on high vacuum to dry overnight. Yield ≈ 2 mg.

Preparation of 2,8-bis-[(N-ureido-Val-OAla-N-Me₂)-Pro-D-Ala-NH]-epindolidione

Dissolved ≈ 1 mg (1 eq., ≈ 1 μ mol) of 2,8-bis-[(N-ureido-Val-OAla-OH)-Pro-D-Ala-NH]-epindolidione in 1 mL of dry DMF. Added 1 mg (12 eq., 12 μ mol) of dimethylamine hydrochloride salt followed by 2 μ L (12 eq., 12 μ mol) of DIEA, 2 μ L (12 eq., 12 μ mol) of DIC, and 1.6 mg of HOBt. TLC: (85 Chloroform : 10 MeOH : 5 glacial acetic acid.) TLC spots smear, making TLC difficult to follow. Let stir under argon overnight (21 hrs.). Stopped reaction by evaporating the solvent. Placed on high vacuum to dry for 3 hours. Redissolved the residue ($<$

1 mg) in 0.5 mL DMF and subjected to LH-20 purification. Run the column at 40% pump speed. Collected the product fractions and evaporated on a high vacuum rotary evaporator. Placed on high vacuum to dry overnight. Yield < 1 mg. NMR analysis of the LH-20 purified product indicates the presence of a minor impurity. Evaporated the DMSO-d₆ on high vacuum, placed on high vacuum to dry for 3 hrs., dissolved in 250 μ L of DMF and subjected to LH-20 purification. Run the column at 40% pump speed. Collected the product fractions and evaporated on a high vacuum rotary evaporator. Placed on high vacuum to dry overnight. NMR still shows some minor impurity, but MS indicates the presence of the sought product. Note: As in the case of 2,8-bis-[(N-ureido-Val-OGly-N-Me₂)-Pro-D-Ala-NH]-epindolidione, preparative HPLC was not attempted as the derivative has a poor solubility profile in water-acetonitrile mixtures. Yield < 1 mg.

Esterification of L- α -Hydroxyisovaleric acid

L- α -Hydroxyisovaleric acid (from Bachem) was esterified by standard procedure: (Wen-ren Li et al., JACS 112, No. 21, 1990.)

1.0 g (8.47 mmol) of the acid was refluxed for 3 hours in 10 ml of anhydrous methanol with 200 μ L of conc. sulfuric acid added as an acid catalyst. Subsequently, the reaction was allowed to cool to room temperature and was concentrated in vacuo, diluted with 100 mL of ether, and washed with saturated sodium bicarbonate (10 mL) and brine (10 mL.) The organic ether phase was dried with sodium sulfate, filtered through a medium porosity glass frit, and concentrated to an oil. The crude oil was used without further purification. Yield = 0.34 g.

Preparation of 2,8-bis-[(N-ureido-Val-OVal-OMe)-Pro-D-Ala-NH]-epindolidione

Dissolved 5 mg (1.0 eq., 5.5 μ mol) of 2,8-bis-[(N-ureido-Val-OH)-Pro-D-Ala-NH]-epindolidione in 3.0 mL of dry DMF under argon atmosphere. Added 7.3 mg (oil) of (10 eq., 55 μ mol) of methyl L- α -Hydroxyisovalerate followed by 7.4 mg (10 eq., 55 μ mol) of HOBt and 9 μ L (10 eq., 55 μ mol) of DIC. Followed reaction by TLC: (85 Chloroform : 10 MeOH : 5 glacial acetic acid.) TLC indicated that the reaction is essentially complete within 6-7 hrs. Let stir under argon for a total of 22 hrs. Stopped reaction (after 22 hrs.) by evaporation of the solvent on a high vacuum rotary evaporator. Placed on high vacuum to dry for about two hours to dry (remove the excess of methyl L- α -Hydroxyisovalerate.) Redissolved the residue in 1 mL

of DMF and injected on LH-20. Run the column at 40% pump speed. Collected the product fractions (as usual relying on UV-Vis inspection) and evaporated on a high vacuum rotary evaporator. Placed on high vacuum to dry overnight. Yield \approx 2 mg.

Saponification (Hydrolysis) of 2,8-bis-[(N-ureido-Val-OVal-OMe)-Pro-D-Ala-NH]-epindolidione

Dissolved \approx 2 mg of 2,8-bis-[(N-ureido-Val-OAla-OMe)-Pro-D-Ala-NH]-epindolidione in 5 mL/5 mL THF/water. Added 2.4 eq. of 1N lithium hydroxide. Followed reaction by TLC: (85 Chloroform : 10 MeOH : 5 glacial acetic acid.) TLC indicated that the reaction is essentially complete at \approx 2-3 hrs. Let stir under argon for a total of 17 hrs. After 17 hrs., added 10 eq. of 1N HCl. A suspension formed. Evaporated THF and centrifuged. Resuspended in distilled water, centrifuged again. Suspended in acetonitrile and centrifuged. Transferred as an acetonitrile slurry and evaporated to dryness. Placed on high vacuum to dry overnight. Yield < 1 mg.

Preparation of 2,8-bis-[(N-ureido-Val-OVal-N-Me₂)-Pro-D-Ala-NH]-epindolidione

Dissolved < 1 mg (1 eq., \approx 0.9 μ mol) of 2,8-bis-[(N-ureido-Val-OVal-OH)-Pro-D-Ala-NH]-epindolidione in 1 mL of dry DMF. Added 1 mg (10 eq., 10 μ mol) of dimethylamine hydrochloride salt followed by 2 μ L (10 eq., 10 μ mol) of DIEA, 2 μ L (12 eq., 12 μ mol) of DIC, and 1.5 mg of HOBt. TLC: (85 Chloroform : 10 MeOH : 5 glacial acetic acid.) TLC spots smear, making TLC virtually useless. Let stir under argon overnight (26 hrs.). Stopped reaction by evaporating the solvent. Placed on high vacuum to dry for 3 hours. Redissolved the residue (< 1mg) in 0.5 mL DMF and subjected to LH-20 purification. Run the column at 40% pump speed. Collected the product fractions and evaporated on a high vacuum rotary evaporator. Placed on high vacuum to dry overnight. Yield < 1mg. NMR analysis of the LH-20 purified product indicates the presence of a minor impurity. Evaporated the DMSO-d₆ on high vacuum, placed on high vacuum to dry for \approx 3 hrs., dissolved in 250 μ L of DMF and subjected to LH-20 purification. Run the column at 40% pump speed. Collected the product fractions and evaporated on a high vacuum rotary evaporator. Placed on high vacuum to dry overnight. NMR shows some minor impurity, but MS indicates the presence of the sought product. Note: As in the case of 2,8-bis-[(N-ureido-Val-OGly-N-Me₂)-Pro-D-Ala-NH]-epindolidione and 2,8-bis-[(N-

ureido-Val-OAla-N-Me₂)-Pro-D-Ala-NH]-epindolidione, preparative HPLC was not attempted as the derivative has a poor solubility profile in water-acetonitrile mixtures. Yield < 1mg.

Procedure for crystallization of 2,8-bis-[(N-ureido-Gly-Val-N-Me₂)-Pro-D-Ala-NH]-epindolidione (VG:PdA)

Two conical vials (2.5 mL capacity) were cleaned with conc. nitric acid, washed repeatedly with distilled water, and boiling methanol. Subsequently, they were placed in an oven to dry for 15 min. After cooling to room temperature, the vials were coated with sigma-coat, and then left overnight to dry.

5 mL of dry acetonitrile was added to \approx 20 mg of VG:PdA that was purified 2X by preparative HPLC. A drying tube was attached, and the flask was heated on an oil bath at 100 °C. Almost all of the solid had dissolved during the heating, but some remained undissolved. After about 10 min. at 100 °C, the almost-clear solution was filtered through kimwipe - 1.5 mL each into the two 2.5 mL conical vials which were placed on a hot plate. The solution of VG:PdA in acetonitrile in each vial was allowed to boil gently for few minutes, and subsequently the vials were capped tightly and placed in a 100 mL capacity beaker that has been partially filled with water at near-boiling temperature. This beaker was placed in another beaker of 300 mL capacity with glass wool insulation. This assembly was then placed in a styrofoam container for 3 days. Inspection after 3 days indicated the presence of crystals as confirmed by Prof. D.S. Kemp and Dr. Zerkowski. The crystals have been transported (by Dr. Zerkowski) to Dr. J. Flippen-Anderson for attempt at obtaining an X-Ray structure.

Table 1a

Experimental Data for DMSO-Soluble "Antiparallel" Epindolidione Derivatives VX:PdA

AA3	Mol. Formula	Mol. Wt. (M + 1)¹
Tyr	C ₆₆ H ₈₈ N ₁₄ O ₁₄	1295.47 (1295.4)
Arg	C ₆₀ H ₉₀ N ₂₀ O ₁₂	1283.51 (1282.4)
Asn	C ₅₆ H ₇₆ N ₁₆ O ₁₄	1196.79 (1197.8)
Gln	C ₅₈ H ₈₀ N ₁₆ O ₁₄	1225.38 (1226.1)
Asp(OtBu)	C ₆₄ H ₉₀ N ₁₄ O ₁₆	1311.51 (1311.4)
Glu(OtBu)	C ₆₆ H ₉₄ N ₁₄ O ₁₂	1339.56 (1339.7)
Gly	C ₅₂ H ₇₀ N ₁₄ O ₁₂	1083.22 (1082.4)
Lys	C ₆₀ H ₉₀ N ₁₆ O ₁₂	1227.48 (1226.6)
Thr	C ₅₆ H ₇₈ N ₁₄ O ₁₄	1171.53 (1172.5)
Trp	C ₇₀ H ₈₄ N ₁₆ O ₁₂	1341.54 (1341.3)

¹Molecular weight is calculated. The number in parentheses refers to the M + 1 ion molecular weight obtained from plasma desorption mass spectroscopy (PDMS).

Table 1b

Experimental Data for DMSO-Soluble Antiparallel Epindolidione Ester Derivatives

Derivative	Mol. Formula	Mol. Wt. (M + 1)¹
MeOGV:PdA	C ₅₀ H ₆₄ N ₁₂ O ₁₄	1057.13 (1056.5)
MeOVV:PdA	C ₅₆ H ₇₆ N ₁₂ O ₁₄	1141.29 (1143.7)
GOV:PdA	C ₅₂ H ₆₈ N ₁₂ O ₁₄	1085.19 (1083.0)
AOV:PdA	C ₅₄ H ₇₂ N ₁₂ O ₁₄	1113.24 (1112.4)
VOV:PdA	C ₅₈ H ₈₀ N ₁₂ O ₁₄	1169.35 (1170.8)

¹Molecular weight is calculated. The number in parentheses refers to the M +1 ion molecular weight obtained from plasma desorption mass spectroscopy (PDMS).

Table 2

Purification Information for DMSO Derivatives VX:PdA

AA3	Mode of Purif.	Retention Time	% Yield
Tyr	HPLC(40%)	13 min. (10-100%), 20 min.	36
Tyr(OtBu)	HPLC(50%)	21.2 min. (20-100%), 30 min.	53
Arg	HPLC(10%)	17.6 min. (10-50%), 20 min.	
	HPLC(10%)	15.2 min. (10-60%), 20 min.	
Asn	HPLC(30%)	12.7 min. (10-100%), 30 min.	43
Gln	HPLC(30%)	17.5 min. (10-100%), 40 min.	17
Gln(DOD)	HPLC(50%)	18.4 min. (20-100%), 30 min.	60
Asp	HPLC(50%)	13.8 min. (10-100%), 30 min.	44
Asp(OtBu)	HPLC(40%)	12.5 min. (20-100%), 20 min.	
	HPLC(40%)	16.5 min. (20-100%), 30 min.	7
Glu	HPLC(40%)	14.6 min. (10-100%), 30 min.	
	HPLC(40%)	10.5 min. (10-100%), 30 min.	33
Glu(OtBu)	HPLC(40%)	14.5 min. (20-100%), 20 min.	
	HPLC(40%)	18.0 min. (0-100%), 30 min.	75
Gly	HPLC(40%)	8.7 min. (20-100%), 20 min.	
	HPLC(40%)	8.7 min. (20-100%), 20 min.	42
Lys	HPLC(10%)	9.8 min. (10-100%), 30 min.	44
Lys(ϵ -Boc)	HPLC(30%)	14.6 min. (10-100%), 30 min.	84
Trp	HPLC(20%)	12.7 min. (20-100%), 20 min.	
	HPLC(20%)	12.5 min. (20-100%), 20 min.	98
Thr(OtBu)	HPLC(60%)	20 min. (20-100%), 30 min.	38
	HPLC(60%)	20 min. (20-100%), 30 min.	
Thr	HPLC(20%)	10 min. (20-100%), 20 min.	37

Table 3

NMR Resonances (ppm) for DMSO derivatives VX:PdA; **s** = singlet **d** = doublet, **dd** = doublet of doublets, **t** = triplet, **m** = multiplet

AA3	H1	H3	H4
Asp	8.78 (d)	8.16 (dd)	8.09 (d)
Asp(OtBu)	8.79	8.29	8.10
Glu	8.79	8.40	8.11
Glu(OtBu)	8.79	8.46	8.10
Asn	8.78	8.14	8.08
Thr	8.78	8.52	8.14
Thr(OtBu)	8.77	8.48	8.12
Gln	8.78	8.33	8.10
Gln(DOD)	8.81	8.31	8.10
Lys	8.80	8.45	8.11
Lys(ϵ -Boc)	8.81	8.44	8.12
Tyr	8.83	8.55	8.16
Tyr(OtBu)	8.84	8.63	8.15
Trp	(overlaps)	8.61	8.11
Arg	8.81	8.41	8.10

Table 3 (continued)

AA3	PyrNH	AryINH	D-Ala NH	Val NH	AA3 NH (Urea NH)
Asp	11.91	9.79	8.54	(overlaps)	6.59
Asp(OtBu)	11.92	9.74	8.61	8.32	6.54
Glu	11.91	9.74	8.63	8.53	6.34
Glu(OtBu)	11.92	9.73	8.68	8.57	6.34
Asn	11.94	9.79	8.53	8.07	6.66
Thr	11.85	9.73	8.68(extrp.)	8.70(extrp.)	5.84
Thr(OtBu)	11.94	9.77	8.67	8.81	5.51
Gln	11.91	9.75	8.62	8.41	6.42
Gln(DOD)	11.92	9.75	8.61	8.35	6.38
Lys	-	9.70	8.73	8.67	6.30
Lys(ϵ -Boc)	11.90	9.70	8.67	8.56	6.26
Tyr	11.72	9.71	8.69	8.62	6.19
Tyr(OtBu)	11.72	9.70	8.72	8.76	6.33
Trp	11.57	9.78	8.75	(overlaps)	6.06
Arg	11.92	9.73	8.64	8.57	6.31

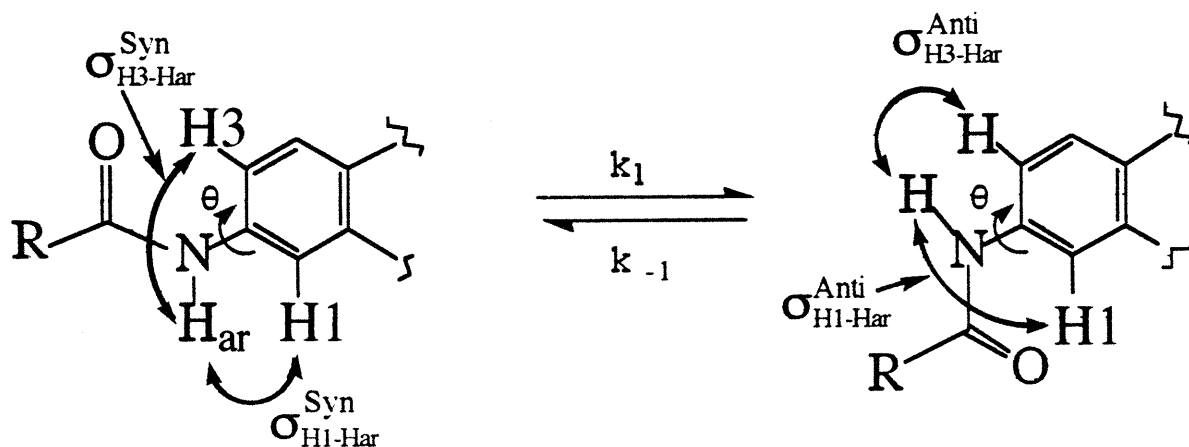
Table 3 (continued)

AA3	D-Ala C α H	Pro C α H	AA3 C α H	Val C α H	D-Ala Me
Asp	4.41	4.23	4.75	4.65	1.38d
Asp(OtBu)	4.42	4.22	4.84	4.66	1.38
Glu	4.41	4.19	4.78	4.72	1.38
Glu(OtBu)	4.39	4.21	4.77	4.75	1.39
Asn	4.41	4.22	4.70	4.59	1.38
Thr	4.40	4.22	4.94	4.80	1.39
Thr(OtBu)	4.43	4.22	4.90	4.76	1.38
Gln	4.41	4.19	overlap \longleftrightarrow	overlap	1.38
Gln(DOD)	4.42	4.19	overlap \longleftrightarrow	overlap	1.38
Lys	4.39	4.22	overlap \longleftrightarrow	overlap	1.39
Lys(ϵ -Boc)	4.43	4.20	overlap \longleftrightarrow	overlap	1.39
Tyr	4.40	4.20	4.90	4.64	1.38
Tyr(OtBu)	4.43	4.19	5.04	4.70	1.37
Trp	4.44	4.23	5.15	4.71	1.40
Arg	4.44	4.22	4.79	4.73	1.38

Table 3 (continued)

AA3	Val $-\gamma\text{CH}_3$	Side-chain of AA3 C β H's, C γ H's, etc.
Asp	0.82dd	2.68dd, 2.54dd (partial overlap with DMSO)
Asp(OtBu)	0.83	2.62dd, 2.47dd (partial overlap with DMSO)
Glu	0.83	Both C β H's & C γ H's of Glu overlap with Pro C β & C γ H's
Glu(OtBu)	0.87	1.73m(C β 2H); C γ 2H of E(OtBu) overlap with Pro C γ 2H
Asn	0.81	Asn C β 2H overlaps with DMSO
Thr	0.8(overlap)	3.88m (Thr C β 2H); 0.85d (Thr C γ 3H or Me)
Thr(OtBu)	0.8(overlap)	3.85m (Thr C β 2H); 0.87d (Thr C γ 3H or Me)
Gln	0.81	C β & C γ hydrogens of Gln not resolved
Gln(DOD)	0.79	C β & C γ hydrogens of Gln(DOD) not resolved
Lys	0.84	1.60m (Lys C β 2H); Lys CH γ , δ , and ϵ not resolved.
Lys(ϵ -Boc)	0.85	2.65(ϵ -2H); 1.57 (2H- β); δ and γ not resolved.
Tyr	0.85t	dd, dd(Thr C β 2H) ; 6.69 (arom. H3,5) & 6.24 (arom. H2,6.)
Tyr(OtBu)	0.86d	dd, dd(Thr C β 2H) ;6.76 (arom. H3,5) & 6.36 (arom. H2,6.)
Trp	0.87d	Trp C β not resolved; [Indole: H2' 6.85d; NH 10.55; H4' 6.94d; H5' 6.71t; H6' 6.50t; H7' 7.15d.]
Arg	0.83dd	Arg C β , γ and δ not assigned; δ NH, 7.30

Appendix A



Syn conformation (**1a**) ($\theta \approx 0^\circ$)

Anti conformation (**1b**) ($\theta \approx 180^\circ$)

Figure 1. The acylanilide region of the two conformations depicted in Fig. 5a & 5b of Chapter 3 of this thesis, with "R" representing the peptide. k_1 and k_{-1} represents the forward and reverse rate constants for interconversion of the *syn* and *anti* conformers. The relevant NOE interactions are indicated by the curved arrows and represent cross-relaxation rate constants, σ_{i-j} .

Let N^{Syn} = fractional population of the *Syn* conformation,

N^{Anti} = fractional population of the *Anti* conformation, (i.e., $N^{Syn} + N^{Anti} = 1$.)

Assumptions:

- 1) Let us assume that the only two conformations that are populated to any significant extent are the planar *Syn* (**1a**) and *Anti* (**1b**) conformations depicted in Fig.1. In other words, the system behaves as a two-state system.¹
- 2) Conformers **1a** and **1b** are in fast exchange on both the chemical shift and T_1 time scales, i.e., $k_1, k_{-1} \gg \delta, R_1$ [where $R_1 = (T_1)^{-1}$.]

1) Camilleri, P., Kirby, A.J., Lewis, R.J., and Sanders, J.K.M., J. Chem. Soc., Chem. Commun., 1988, p. 1537.

3) There are no magnetic spins present in the immediate region between either H1 or H3 and the aryl NH (Har) in either the *Syn* or *Anti* conformers. In other words, to a first approximation, we neglect the effect of the group R. Note: as we will see later, if condition 3) is satisfied, then indirect (spin diffusion) contributions to the NOE enhancements will be negligible.

Since we assumed under 2) above that exchange is fast relative to spin-lattice relaxation, we must use $\langle R_1 \rangle$ and $\langle \sigma_{ij} \rangle$, or the averaged spin-lattice and cross-relaxation rate constants rather than simply R_1 and σ_{ij} ². $\langle R_1 \rangle$ and $\langle \sigma_{ij} \rangle$ are defined as follows:

$$\langle R_{H_j} \rangle = \sum_i N^i R_{H_j}^i, \quad (\text{Eq. 1})$$

where N^i is the fractional population of conformer i , and $R_{H_j}^i$ is the spin-lattice relaxation rate constant of H_j in conformer i . Similarly,

$$\langle \sigma_{H_j-H_k} \rangle = \sum_i N^i \sigma_{H_j-H_k}^i, \quad (\text{Eq. 2})$$

where N^i is defined as in Eq. 1, and $\sigma_{H_j-H_k}^i$ is the cross-relaxation rate constant between protons j and k in conformer i . Applying the general equations 1 & 2 to our two-state system in Fig. 1, we can write the following expressions,

$$\langle \sigma_{H1-Har} \rangle = N^{syn} \sigma_{H1-Har}^{syn} + N^{anti} \sigma_{H1-Har}^{anti}, \quad (\text{Eq. 3})$$

and

$$\langle \sigma_{H3-Har} \rangle = N^{syn} \sigma_{H3-Har}^{syn} + N^{anti} \sigma_{H3-Har}^{anti}, \quad (\text{Eq. 4})$$

where σ_{H1-Har}^{syn} , and σ_{H1-Har}^{anti} are the cross-relaxation rate constants between protons H1 and aryl NH in the *syn* and *anti* conformations, respectively, and σ_{H3-Har}^{syn} and σ_{H3-Har}^{anti} are the cross-relaxation rate constants between protons H3 and aryl NH in the *syn* and *anti* conformation, respectively.

2) (a) Schirmer, R.E.; Davis, J.P., Noggle, J.H., Hart, P.A., J. Am. Chem. Soc. 1972, 94, 2561.

(b) Neuhaus, D., Williamson, M., "The Nuclear Overhauser Effect in Structural and Conformational Analysis", CVCH Publishers, New York, NY, 1989, pp 161-163.

In general, $\sigma_{\text{Hi-Hj}}$ is defined by Eq. 5,

$$\sigma_{\text{Hi-Hj}} = \left(\frac{\mu_o}{4\pi} \right)^2 \frac{\hbar^2 \gamma_{\text{Hi}}^2 \gamma_{\text{Hj}}^2}{10} \left[\frac{6}{1 + (\omega_{\text{Hi}} + \omega_{\text{Hj}})^2 \tau_c^2} - \frac{1}{1 + (\omega_{\text{Hi}} - \omega_{\text{Hj}})^2 \tau_c^2} \right] \tau_c r_{\text{Hi-Hj}}^{-6}$$

However, in a homonuclear system $\omega_{\text{Hi}} \approx \omega_{\text{Hj}} \approx \omega$. Thus we can simplify Eq. 5 as follows

$$\sigma_{\text{Hi-Hj}} \cong \left(\frac{\mu_o}{4\pi} \right)^2 \frac{\hbar^2 \gamma^4}{10} \left[\frac{6}{1 + 4\omega^2 \tau_c^2} - 1 \right] \tau_c r_{\text{Hi-Hj}}^{-6} \quad (\text{Eq. 6})$$

Equation 6 is an important result, because it tells us that a cross-relaxation rate constants between protons Hi and Hj is directly proportional to the rotational correlation time, τ_c , of the Hi-Hj vector, and inversely proportional to the distance between Hi and Hj raised to the sixth power. In other words,

$$\sigma_{\text{Hi-Hj}} \propto \tau_c r_{\text{Hi-Hj}}^{-6}$$

Next, we can simplify Equations 3 and 4 because as Fig. 1 shows $r_{\text{H1-Har}}^{\text{syn}} > r_{\text{H3-Har}}^{\text{syn}}$, and

$r_{\text{H3-Har}}^{\text{anti}} > r_{\text{H1-Har}}^{\text{anti}}$. Therefore, because of the r^{-6} dependence of σ on r , we can rewrite Equations 3

& 4 as follows,

$$\langle \sigma_{\text{H1-Har}} \rangle \cong N^{\text{syn}} \sigma_{\text{H1-Har}}^{\text{syn}} \quad (\text{Eq. 7})$$

$$\langle \sigma_{\text{H3-Har}} \rangle \cong N^{\text{anti}} \sigma_{\text{H3-Har}}^{\text{anti}} \quad (\text{Eq. 8})$$

Eq. 7 & 8 is an additional assumption 4). Later on we will remove this assumption to see what effect the inclusion of the additional terms (as appears in Eq. 3 & 4) may have on our analysis of the conformer populations.

To make further progress, we need expressions for $\langle R_{\text{H1}} \rangle$ and $\langle R_{\text{H3}} \rangle$.

$$\langle R_{\text{H1}} \rangle = N^{\text{syn}} \rho_{\text{H1-Har}}^{\text{syn}} + N^{\text{anti}} \rho_{\text{H1-Har}}^{\text{anti}} + \sum_x \rho_{\text{H1-Hx}} + \rho_{\text{H1-H3}} + \rho_{\text{H1}}^* \quad (\text{Eq. 9})$$

$$\langle R_{\text{H3}} \rangle = N^{\text{syn}} \rho_{\text{H3-Har}}^{\text{syn}} + N^{\text{anti}} \rho_{\text{H3-Har}}^{\text{anti}} + \sum_x \rho_{\text{H3-Hx}} + \rho_{\text{H3-H1}} + \rho_{\text{H3}}^* \quad (\text{Eq. 10})$$

where $\rho_{\text{Hi-Hj}}$ represents a two-spin dipolar longitudinal relaxation rate constant as defined in the two-spin Solomon equation³. The Solomon equation (Eq. 11 below) is central to understanding NOE theory, therefore, before we proceed, we should examine it in more detail.

$$\frac{dI_z(t)}{dt} = \rho_{\text{IS}} [I_z^\circ - I_z(t)] + \sigma_{\text{IS}} [S_z^\circ - S_z(t)]. \quad (\text{Eq. 11})$$

The derivation of Eq. 11 is rather involved and is given in 3b. The nomenclature used in Eq. 11 is that originally used by Solomon^{3a}. In this nomenclature, S represents the spin that is saturated, and I is the spin whose resonance is measured^{3b}. In relation to Fig.1, aryl NH is S, and H1 or H3 is I. $I_z(t)$ and $S_z(t)$ represent the respective longitudinal macroscopic magnetizations that exist just prior to the application of the observe pulse (usually a $\pi/2$ pulse.) I_z° and S_z° are the corresponding equilibrium values. Eq. 11 is a differential equation that tells us the magnitude of I_z as a function of time after saturation of spin S. As we will see, the Solomon equation is used to derive expressions for the steady-state as well as kinetic NOE experiments. The Solomon equation is also useful from another perspective, i.e., it gives a clear meaning to the two-spin terms σ_{ij} and ρ_{ij} . Let us examine what Eq. 11 predicts at $t = 0$ when one applies a selective $\pi/2$ pulse to the resonance I.

$$\left. \frac{dI_z(t)}{dt} \right|_{t=0, (\pi/2)_I} = \rho_{\text{IS}} [I_z^\circ - 0] + \sigma_{\text{IS}} [S_z^\circ - S_z^\circ] = \rho_{\text{IS}} I_z^\circ$$

Thus, ρ_{IS} can be thought of as the initial rate for recovery of the signal due to resonance I following selective ($\pi/2$) transmitter pulse. On the other hand, if one applies a selective $\pi/2$ pulse to the resonance S, Eq. 11 predicts at $t = 0$,

$$\left. \frac{dI_z(t)}{dt} \right|_{t=0, (\pi/2)_S} = \rho_{\text{IS}} [I_z^\circ - I_z^\circ] + \sigma_{\text{IS}} [S_z^\circ - 0] = \sigma_{\text{IS}} S_z^\circ = \sigma_{\text{IS}} I_z^\circ$$

Thus, σ_{IS} can be thought of as the initial rate of NOE observed in resonance I following a selective $\pi/2$ pulse applied to resonance S.

3) (a) Solomon, I. *Phys. Rev.* 1955, 99, 559.

(b) Neuhaus, D., Williamson, M., "The Nuclear Overhauser Effect in Structural and Conformational Analysis", CVCH Publishers, New York, NY, 1989, pp 27-30.

To proceed further with our analysis of the conformer equilibrium in Fig. 1, we need to examine Equations 12-15, which can all be derived from the Solomon equation (Eq. 11.)

$$f_{H1}\{\text{Har}\}(t) = \frac{\langle \sigma_{H1-\text{Har}} \rangle}{\langle R_{H1} \rangle} (1 - e^{-\langle R_{H1} \rangle t}) \quad (\text{Eq. 12})$$

$$f_{H3}\{\text{Har}\}(t) = \frac{\langle \sigma_{H3-\text{Har}} \rangle}{\langle R_{H3} \rangle} (1 - e^{-\langle R_{H3} \rangle t}) \quad (\text{Eq. 13})$$

$$f_{H1}^{ss}\{\text{Har}\} = \frac{\langle \sigma_{H1-\text{Har}} \rangle}{\langle R_{H1} \rangle} - \frac{\sum_x f_{HX}^{ss}\{\text{Har}\} \sigma_{\text{Har}-HX}}{\langle R_{H1} \rangle} \quad (\text{Eq. 14})$$

$$f_{H3}^{ss}\{\text{Har}\} = \frac{\langle \sigma_{H3-\text{Har}} \rangle}{\langle R_{H3} \rangle} - \frac{\sum_x f_{HX}^{ss}\{\text{Har}\} \sigma_{\text{Har}-HX}}{\langle R_{H3} \rangle} \quad (\text{Eq. 15})$$

Equations 12 & 13 are derived from the two-spin Solomon equation (Eq. 11) assuming truncated driven NOE (TOE) conditions. The TOE conditions are such that in the above nomenclature, spin S is saturated for a duration t, after which the effect on the signal corresponding to I is observed. Equations 14 & 15. Are examples of multi-spin Solomon equation with assumption of the steady-state conditions. Steady-state condition corresponds to the situation in which spin S is saturated for a time $t > 5 \times T_1$ (to assure spin equilibrium) and then the effect on spin I is observed. If we apply assumption 4) (which is represented by Eqs. 7 & 8) to Eqs. 12 & 13, we get Eqs. 16 & 17,

$$f_{H1}\{\text{Har}\}(t) \cong \frac{N^{syn} \sigma_{H1-\text{Har}}^{syn}}{\langle R_{H1} \rangle} (1 - e^{-\langle R_{H1} \rangle t}) \quad (\text{Eq. 16})$$

$$f_{H3}\{\text{Har}\}(t) \cong \frac{N^{anti} \sigma_{H3-\text{Har}}^{anti}}{\langle R_{H3} \rangle} (1 - e^{-\langle R_{H3} \rangle t}) \quad (\text{Eq. 17})$$

We can also simplify Eqs. 14 & 15 by applying assumption 3) (from page 2) as well as assumption 4). Assumption 3) allows us, if effect, to ignore the "indirect" terms $f_{HX}^{ss}\{\text{Har}\}$ in Eqs. 14 & 15. Thus, we have

$$f_{H1}^{ss} \{Har\} \cong \frac{\langle \sigma_{H1-Har} \rangle}{\langle R_{H1} \rangle} \cong \frac{N^{syn} \sigma_{H1-Har}^{syn}}{\langle R_{H1} \rangle} \quad (\text{Eq. 18})$$

$$f_{H3}^{ss} \{Har\} \cong \frac{\langle \sigma_{H3-Har} \rangle}{\langle R_{H3} \rangle} \cong \frac{N^{anti} \sigma_{H3-Har}^{anti}}{\langle R_{H3} \rangle} \quad (\text{Eq. 19})$$

With Eqs. 16-19, we are ready to compute the conformer ratio represented in Fig. 1.

CASE I: Using Steady-State Approach

Combining Eqs. 18 & 19 we can solve for the following conformer ratio:

$$\frac{N^{anti}}{N^{syn}} = \frac{f_{H3}^{ss} \{Har\}}{f_{H1}^{ss} \{Har\}} \left(\frac{\langle R_{H3} \rangle}{\langle R_{H1} \rangle} \right) \left(\frac{\sigma_{H3-Har}^{anti}}{\sigma_{H1-Har}^{syn}} \right) \quad (\text{Eq. 20})$$

now, since we know that $\sigma_{ij} \propto \tau_c \Gamma_{ij}^{-6}$, substituting this into Eq. 20, we get

$$\frac{N^{anti}}{N^{syn}} = \frac{f_{H3}^{ss} \{Har\}}{f_{H1}^{ss} \{Har\}} \left(\frac{\langle R_{H3} \rangle}{\langle R_{H1} \rangle} \right) \left(\frac{\tau_{c,H3-Har}^{anti}}{\tau_{c,H1-Har}^{syn}} \right) \left(\frac{\Gamma_{H3-Har}^{anti}}{\Gamma_{H1-Har}^{syn}} \right)^{-6} \quad (\text{Eq. 21})$$

To proceed, we need to make two further assumptions.

Assumption 5):

$$\left(\frac{\Gamma_{H3-Har}^{anti}}{\Gamma_{H1-Har}^{syn}} \right)^{-6} \approx 1$$

From examination of the two conformers **1a** and **1b** in Fig. 1, this assumption seems very reasonable. Also, we have considered this issue in chapter 3, where it was shown that even small deviations from planarity for either **1a** or **1b** will not alter the above ratio much beyond unity.

Assumption 6):

$$\left(\frac{\tau_{c,H3-Har}^{anti}}{\tau_{c,H1-Har}^{syn}} \right) \approx 1$$

This assumption is more problematic, as it suggests that the rotational correlation time of **1a** and

I b are very similar. Nevertheless, from the study of Kruse et al.⁴ it appears that correlation time ratios are often close to unity, unless the two states have very different molecular tumbling rates. With assumptions 5) and 6), we can rewrite Eq. 21 in terms of experimentally measurable quantities.

$$\frac{N^{anti}}{N^{syn}} \cong \frac{f_{H3}^{ss}\{Har\}}{f_{H1}^{ss}\{Har\}} \left(\frac{\langle R_{H3} \rangle}{\langle R_{H1} \rangle} \right) \quad (\text{Eq. 22})$$

To solve Eq. 22, we need to have $f_{H1}^{ss}\{Har\}$, $f_{H3}^{ss}\{Har\}$, $\langle R_{H1} \rangle$, and $\langle R_{H3} \rangle$

Both $f_{H1}^{ss}\{Har\}$, and $f_{H3}^{ss}\{Har\}$ can be obtained from a conventional steady-state NOE difference experiment or from its TOE equivalent. However, were to obtain the rate constants $\langle R_{H1} \rangle$ and $\langle R_{H3} \rangle$ at least initially may not seem obvious. As Eqs. 9 & 10 show, many terms contribute to the overall parameters $\langle R_{H1} \rangle$ and $\langle R_{H3} \rangle$. Using assumptions 3) and 4) we can simplify Eqs. 9 & 10 to obtain Eqs. 23 & 24

$$\langle R_{H1} \rangle \cong N^{syn} \rho_{H1-Har}^{syn} + \rho_{H1}^* \quad (\text{Eq. 23})$$

$$\langle R_{H3} \rangle \cong N^{anti} \rho_{H3-Har}^{anti} + \rho_{H3}^* \quad (\text{Eq. 24})$$

Here the terms ρ_{H1}^* and ρ_{H3}^* represent the contributions to $\langle R_{H1} \rangle$ and $\langle R_{H3} \rangle$ that are due to a variety of nondipolar relaxation mechanisms (e.g., chemical shift anisotropy, or spin-rotation), but most often these factors are due to intermolecular dipole-dipole relaxation, most commonly due to the dissolved oxygen⁵. One might use the often widely used inversion-recovery experiment in order to estimate the T_1 's for H1 and H3, and use these values [$R_1 = (T_1)^{-1}$] for the required rate constants. However the results of an inversion recovery experiment differ depending how the experiment is performed (nonselective vs selective T_1 experiment.) Furthermore, it can be shown

4) Kruse, L. I., DeBrosse, C.W., Kruse, C.H., J. Am. Chem. Soc. 1985, 107, 5435.

5) Neuhaus, D., Williamson, M., "The Nuclear Overhauser Effect in Structural and Conformational Analysis", CVCH Publishers, New York, NY, 1989, p 41.

that neither the selective or the nonselective T1 values will correspond directly to the reciprocals of the $\langle R_{H1} \rangle$ and $\langle R_{H3} \rangle$ rate constants that we seek⁶. Fortunately, both $\langle R_{H1} \rangle$ and $\langle R_{H3} \rangle$ as well as $f_{H1}^{ss}\{\text{Har}\}$, $f_{H3}^{ss}\{\text{Har}\}$ can be obtained by fitting the time dependence of Fig. 4 in chapter 3 to the equation

$$F_{Hi}(t) = f_{Hi}^{ss}\{\text{NHar}\}[1 - \exp(-R_{Hi}t)]. \quad (\text{Eq. 25})$$

This equation describes the NOE buildup of a proton Hi as a function of time, which is obtained from a truncated version of a NOE difference experiment or TOE⁷. From the fit of the data in Fig. 4 of chapter 3 to Eq. 25, we get

$$f_{H1}^{ss}\{\text{Har}\} = 0.4088 \pm 0.0015$$

$$f_{H3}^{ss}\{\text{Har}\} = 0.02300 \pm 0.0023$$

$$\langle R_{H1} \rangle = 0.2702 \pm 0.00389 \text{ (sec.)}, \text{ and}$$

$$\langle R_{H3} \rangle = 0.8107 \pm 0.03375 \text{ (sec.)}$$

Then using Eq. 22

$$\frac{N^{anti}}{N^{syn}} \cong \frac{f_{H3}^{ss}\{\text{Har}\}}{f_{H1}^{ss}\{\text{Har}\}} \left(\frac{\langle R_{H3} \rangle}{\langle R_{H1} \rangle} \right) = \left(\frac{0.2300}{0.4088} \right) \left(\frac{0.8107}{0.2702} \right) = 1.69.$$

CASE II: Using the Initial Rate Approximation

To obtain expression for the initial slopes of the NOE buildup curves in Fig. 4 of chapter 3, we take derivatives of Eqs. 16 & 17 to obtain

$$\frac{d}{dt} [f_{Hi}\{\text{Har}\}(t)]_{t=0} \cong \frac{d}{dt} \left[\frac{N^{syn} \sigma_{H1-Har}^{syn}}{\langle R_{H1} \rangle} (1 - e^{-\langle R_{H1} \rangle t}) \right]_{t=0} = N^{syn} \sigma_{H1-Har}^{syn} \equiv m_{H1}$$

$$(\text{Eq. 26})$$

6) Neuhaus, D., Williamson, M., "The Nuclear Overhauser Effect in Structural and Conformational Analysis", CVCH Publishers, New York, NY, 1989, p 436.

7) Wagner, G. and Wüthrich, K., *J. Magn. Res.* **33**, 675-680 (1979)

$$\frac{d}{dt} [f_{H3}\{Har\}(t)]_{t=0} \cong \frac{d}{dt} \left[\frac{N^{anti}\sigma_{H3-Har}^{anti}}{\langle R_{H3} \rangle} (1 - e^{-\langle R_{H3} \rangle t}) \right]_{t=0} = N^{anti}\sigma_{H3-Har}^{anti} \equiv m_{H3}$$

(Eq. 27)

Equations 26 & 27 tell us that the initial slopes for the NOE buildup curves (say in the TOE experiments of Fig.4 in chapter 3) are given simply by the populational mole fraction times the respective cross-relaxation rate constants, σ_{ij} . Since $\sigma_{ij} \propto \tau_c * (r_{ij})^{-6}$, we can write

$$\frac{N^{anti}}{N^{syn}} = \left(\frac{m_{H3}}{m_{H1}} \right) \left(\frac{\sigma_{H1-Har}^{syn}}{\sigma_{H3-Har}^{anti}} \right) = \left(\frac{m_{H3}}{m_{H1}} \right) \left(\frac{r_{H3-Har}^{-6}}{r_{H1-Har}^{-6}} \right) \left(\frac{\tau_{c, H3-Har}}{\tau_{c, H1-Har}} \right) \approx \left(\frac{m_{H1}}{m_{H3}} \right). \quad (\text{Eq. 28})$$

In Eq. 28, m_{H1} and m_{H3} represent the initial slopes. These are represented by the slopes in Fig. 5 of chapter 3. Furthermore, as before, we assume that the ratio of the respective distances (taken to the -6th power) and the ratio of the correlation times for the two states is close to unity. This leads to the simple expression

$$\frac{N^{anti}}{N^{syn}} \approx \left(\frac{m_{H3}}{m_{H1}} \right). \quad (\text{Eq. 29})$$

From the linear regression fit to the data points in Fig. 5 of chapter 3, we obtain $m_{H1} = 10.743$, and $m_{H3} = 16.7$. Since determination of the initial slopes is inherently less accurate than determination of steady-state enhancements (due to the small NOE's present during the short irradiation times), the error present in the slope estimates is at least 10%. With this values, we obtain

$$\frac{N^{anti}}{N^{syn}} \approx \left(\frac{m_{H3}}{m_{H1}} \right) = \frac{16.7}{10.74} = 1.6 \pm 0.16.$$

Thus we see that the initial rate approximation value of 1.6 ± 0.16 is within experimental error of the steady-state value obtained above as 1.69.

Next let us see what happens if we lift assumption 4) which is expressed with Eqs. 7 & 8. In other words, let us compare how different are the above calculations if we use the full

expressions represented by Eqs. 3 & 4. In this case, let us see the effect on the steady-state data. Taking the ratios of Eqs. 18 & 19, we get

$$\frac{f_{H1}^{ss}\{Har\}}{f_{H3}^{ss}\{Har\}} \cong \frac{\frac{\langle \sigma_{H1-Har} \rangle}{\langle R_{H1} \rangle}}{\frac{\langle \sigma_{H3-Har} \rangle}{\langle R_{H3} \rangle}} = \frac{N^{syn} \sigma_{H1-Har}^{syn} + N^{anti} \sigma_{H1-Har}^{anti}}{N^{syn} \sigma_{H3-Har}^{syn} + N^{anti} \sigma_{H3-Har}^{anti}} \left(\frac{\langle R_{H3} \rangle}{\langle R_{H1} \rangle} \right) \quad (\text{Eq. 30})$$

For simplicity let $\sigma_{H1-Har}^{syn} \approx \sigma_{H3-Har}^{anti} \equiv \sigma_{\text{close}} \equiv \sigma_c$, and $\sigma_{H3-Har}^{syn} \approx \sigma_{H1-Har}^{anti} \equiv \sigma_{\text{far}} \equiv \sigma_f$

Substituting into Eq. 30, we get

$$\frac{f_{H1}^{ss}\{Har\}}{f_{H3}^{ss}\{Har\}} \cong \frac{N^{syn} \sigma_c + N^{anti} \sigma_f}{N^{syn} \sigma_f + N^{anti} \sigma_c} \left(\frac{\langle R_{H3} \rangle}{\langle R_{H1} \rangle} \right), \quad (\text{Eq. 31})$$

solving Eq. 31 for the (N^{syn}/N^{anti}) ratio, we obtain

$$\frac{N^{syn}}{N^{anti}} = \frac{f_{H3}^{ss}\{Har\} \sigma_f \langle R_{H3} \rangle - f_{H1}^{ss}\{Har\} \sigma_c \langle R_{H1} \rangle}{f_{H1}^{ss}\{Har\} \sigma_f \langle R_{H1} \rangle - f_{H3}^{ss}\{Har\} \sigma_c \langle R_{H3} \rangle} \quad (\text{Eq. 32})$$

but $\sigma_c = k \tau_c r_c^{-6}$, and $\sigma_f = k \tau_f r_f^{-6}$. Therefore, substituting into Eq. 32, we get

$$\frac{N^{syn}}{N^{anti}} = \frac{f_{H3}^{ss}\{Har\} \langle R_{H3} \rangle r_f^{-6} - f_{H1}^{ss}\{Har\} \langle R_{H1} \rangle r_c^{-6}}{f_{H1}^{ss}\{Har\} \langle R_{H1} \rangle r_f^{-6} - f_{H3}^{ss}\{Har\} \langle R_{H3} \rangle r_c^{-6}}; \quad (\text{Eq. 33})$$

dividing Eq. 33 through r_c^{-6} and setting $\left(\frac{r_f}{r_c}\right)^{-6} \equiv r_{fc}^{-6}$, we get

$$\frac{N^{anti}}{N^{syn}} = \frac{(f_{H3}^{ss}\{Har\} \langle R_{H3} \rangle) r_{fc}^{-6} - (f_{H1}^{ss}\{Har\} \langle R_{H1} \rangle)}{(f_{H1}^{ss}\{Har\} \langle R_{H1} \rangle) r_{fc}^{-6} - (f_{H3}^{ss}\{Har\} \langle R_{H3} \rangle)} \equiv \frac{\kappa_1 r_{fc}^{-6} - \kappa_2}{\kappa_2 r_{fc}^{-6} - \kappa_1} \quad (\text{Eq. 34})$$

where $\kappa_1 \equiv f_{H1}^{ss}\{Har\} \langle R_{H1} \rangle$, and $\kappa_2 \equiv f_{H3}^{ss}\{Har\} \langle R_{H3} \rangle$. We can invert Eq. 34 to obtain the

familiar (N_{anti}/N_{syn}) conformer ratio (Eq. 35)

$$\frac{N_{anti}}{N_{syn}} = \frac{(f_{H3}^{ss}\{\text{Har}\} \langle R_{H3} \rangle) r_{fc}^{-6} - (f_{H1}^{ss}\{\text{Har}\} \langle R_{H1} \rangle)}{(f_{H1}^{ss}\{\text{Har}\} \langle R_{H1} \rangle) r_{fc}^{-6} - (f_{H3}^{ss}\{\text{Har}\} \langle R_{H3} \rangle)} \equiv \frac{\kappa_1 r_{fc}^{-6} - \kappa_2 \left(\frac{r_{fc}^6}{r_{fc}^6} \right)}{\kappa_2 r_{fc}^{-6} - \kappa_1 \left(\frac{r_{fc}^6}{r_{fc}^6} \right)} = \frac{\kappa_1 - \kappa_2 r_{fc}^6}{\kappa_2 - \kappa_1 r_{fc}^6}$$

Now we are ready to test what happens when we relax assumption 4)

First,

$$\kappa_1 \equiv f_{H1}^{ss}\{\text{Har}\} \langle R_{H1} \rangle = (0.4088)(0.2702) = 0.1104; \text{ and}$$

$$\kappa_2 \equiv f_{H3}^{ss}\{\text{Har}\} \langle R_{H3} \rangle = (0.2300)(0.8107) = 0.1865.$$

Assumption 4) states that $r_f \gg r_c \Rightarrow r_{fc} = (r_f/r_c) \gg 1 \Rightarrow (r_{fc})^6 = (r_f/r_c)^6 \gg \gg 1$. It is

easy to see that in this case Eq. 35 reduces to the ratio $-(\kappa_2/\kappa_1) = (0.1865)/(0.1104) = 1.69$ as

expected. Now let us see what happens when r_f becomes comparable to r_c .

$$\text{For } r_f = 1.5 r_c \Rightarrow (r_{fc})^6 = (r_f/r_c)^6 = (1.5 r_c/r_c)^6 = 11.39$$

$$\frac{N_{anti}}{N_{syn}} = \frac{\kappa_1 - \kappa_2 r_{fc}^6}{\kappa_2 - \kappa_1 r_{fc}^6} = \frac{0.1104 - (0.1865)(11.39)}{0.1865 - (0.1104)(11.39)} = 1.88$$

Now let us compute the same ratio for $r_f = 1.4 r_c$, $r_f = 1.3 r_c$, $r_f = 1.2 r_c$, and $r_f = 1.1 r_c$.

$$\left(\frac{N_{anti}}{N_{syn}} \right)_{r_f=1.4 r_c} = \frac{\kappa_1 - \kappa_2 r_{fc}^6}{\kappa_2 - \kappa_1 r_{fc}^6} = \frac{0.1104 - (0.1865)(7.53)}{0.1865 - (0.1104)(7.53)} = 2.01$$

$$\left(\frac{N_{anti}}{N_{syn}} \right)_{r_f=1.3 r_c} = \frac{\kappa_1 - \kappa_2 r_{fc}^6}{\kappa_2 - \kappa_1 r_{fc}^6} = \frac{0.1104 - (0.1865)(4.83)}{0.1865 - (0.1104)(4.83)} = 2.28$$

$$\left(\frac{N_{anti}}{N_{syn}} \right)_{r_f=1.2 r_c} = \frac{\kappa_1 - \kappa_2 r_{fc}^6}{\kappa_2 - \kappa_1 r_{fc}^6} = \frac{0.1104 - (0.1865)(2.99)}{0.1865 - (0.1104)(2.99)} = 3.11$$

$$\left(\frac{N_{anti}}{N_{syn}} \right)_{r_f=1.1 r_c} = \frac{\kappa_1 - \kappa_2 r_{fc}^6}{\kappa_2 - \kappa_1 r_{fc}^6} = \frac{0.1104 - (0.1865)(1.77)}{0.1865 - (0.1104)(1.77)} = 24.7.$$

Thus, from the above calculations, it is obvious that if we use assumption **4**) the value of the $(N^{\text{anti}}/N^{\text{syn}})$ conformer ratio that we obtain (1.69) represents the *lower limit* of the ratio.

Table A-1.

Chemical shift data used to generate Figures 3-7 & 3-8 in Chapter 3.

TOE time (sec)	- f_{H1} {Har} (%)	- f_{H3} {Har} (%)
0	0.0	0.0
0.200	2.2	3.7
0.300	3.2	5.2
0.400	4.3	6.7
1.000	9.7	12.7
4.00	26.8	21.2
12.00	39.7	23.0
20.00	40.4	23.4
30.00	40.8	23.3

Table A-2.

Chemical shift data used to generate Figures 3-9 & 3-10 in Chapter 3.

TOE time (sec)	- f_{H_1} {Har} (%)	- f_{H_3} {Har} (%)
0	0.0	0.0
0.100	0.93	2.4
0.200	2.3	5.1
0.300	2.8	7.0
1.000	9.5	16.7
4.00	28.2	20.0
8.00	35.3	27.7
20.00	39.8	28.1
30.00	39.6	28.0

Table A-3.

Chemical shift data used to generate Figures 3-11 & 3-12 in Chapter 3.

TOE time (sec)	- $f_{H1}\{\text{Har}\}$ (%)	- $f_{H3}\{\text{Har}\}$ (%)
0	0.0	0.0
0.200	6.8	3.6
0.300	9.1	5.1
1.000	23.2	12.5
5.00	34.2	20.5
15.00	37.2	23.5
30.00	37.6	22.9

Table A-4

Chemical shift data used to generate Figures 3-13 & 3-14 in Chapter 3.

Derivative (XY:PX)	-fH3{Har}	- fH1{Har}	H3/H1 NOE ratio	δ_{H3} (ppm)	Method of NOE estimation	Estimated NOE ratio error (%)
VN:PdA	1.42	1.53	0.928	8.14	NOESY Integration	6
FG:PdA ¹	34.0	49.0	0.694	8.19	NOESY Integration	8
VG:PdA	1.20	1.66	0.723	8.21	NOESY Integration	5
FL:PG ¹	32.0	54.0	0.593	8.30	NOESY Integration	9
VK(Boc):PdA	17.1	30.9	0.553	8.44	TOE analysis	5
FV:PG ¹	30.0	68.0	0.441	8.50	NOESY Integration	7
VT:PdA	1.29	4.27	0.302	8.52	NOESY Integration	9
VY:PdA	0.833	2.29	0.364	8.55	NOESY Integration	5
FV:PdA ¹	34.0	123	0.276	8.60	NOESY Integration	4
VW:PdA	0.297	1.02	0.291	8.61	NOESY Integration	6

¹Data adopted from Giallourakis, "¹H NMR and ¹H NOESY Analysis of β -Turn Formation in Epindolidione Template Initiated Antiparallel β -Sheets." B.S. Thesis, MIT, 1992.

Table A-5

Chemical shift data used to generate Figure 3-15 in Chapter 3.

Derivative (non-aromatic) (XY:PdA)	H3 Chemical Shift (ppm)	AA4 (X) Chemical Shift (ppm)
1. VV:PdA ¹	8.67	8.93
2. AV:PdA ¹	8.57	8.86
3. LV:PdA ¹	8.56	8.78
4. VT:PdA	8.52	8.69
5. GV:PdA ¹	8.47	8.54
6. VL:PdA ¹	8.46	8.57
7. VE(OtBu):PdA	8.46	8.57
8. VK:PdA	8.45	8.67
9. VK(Boc):PdA	8.44	8.56
10. VR:PdA	8.41	8.57
11. VE:PdA	8.40	8.53
12. VA:PdA ¹	8.39	8.42
13. LL:PdA ¹	8.33	8.37
14. VQ:PdA	8.33	8.41
15. AL:PdA ¹	8.32	8.46
16. VQ(DOD):PdA	8.31	8.35
17. AA:PdA ¹	8.29	8.37
18. VD(OtBu):PdA	8.29	8.32
19. LA:PdA ¹	8.28	8.25

20. GA:PdA ¹	8.26	8.16
21. VG:PdA	8.21	8.16
22. LG:PdA ¹	8.17	8.01
23. VD:PdA	8.16	8.09
24. VN:PdA	8.14	8.07

¹Data adopted from Blanchard, D.E., Ph.D. Thesis, Massachusetts Institute of Technology, 1992.

Appendix B

As was mentioned in Chapters one and two of this thesis, Blanchard attempted to evaluate the actual numerical values of the equilibrium constants K_1 , K_2 , and K_3 . However, to do so, he had to assume that at least for two of the amino acids used in the data base, their respective intrinsic propensities are independent of the actual position in the peptide-epindolidione model **1 a** (Fig 2-1). In other words, Blanchard had to assume that for at least two amino acid residues, which he chose to be Gly and Val, $K_{2G} = K_{3G}$, and $K_{2V} = K_{3V}$ (Blanchard, 1992). In order for this assumption to hold, it is necessary that in the peptide-epindolidione model **1 a** (Fig. 2-1, Chapter 2), the first and second strand hydrogen bonds are equal in strength, and that there is no structural bias in either position. However, the experimental work to be described in the rest of this Appendix provides evidence that Blanchard's assumption that $K_{2G} = K_{3G}$, and $K_{2V} = K_{3V}$ is not true.

One way to test if Blanchard's assumption that $K_{2G} = K_{3G}$, and $K_{2V} = K_{3V}$ holds for a pair of amino acid residues G and V is to synthesize peptide-epindolidione "control" derivatives in which select amide bonds are replaced by ester bonds. Figures B-1a and B-1b show the five amide-to-ester peptide-epindolidione derivatives prepared by this researcher. Figure B-1a shows the structure of two peptide-epindolidione derivatives in which the terminal N,N-dimethylamide functionality of **1** (Fig 4-1) has been replaced by a methyl ester. Since the carbonyl oxygen of an ester is much less basic than that of the amide, the derivatives in B-1a cannot form the second strand hydrogen bond. This is equivalent to saying that $K_3 \approx 0$ for both derivatives MeO-GV:PdA, and MeO-VV:PdA of Fig. B-1a. In an analogous fashion, the three derivatives of Fig. B-1b cannot form the first strand hydrogen bond. Thus for the derivatives GOV:PdA, AOV:PdA, and VOV:PdA in Fig. B-1b, $K_2 \approx 0$. The δ_{H3} values for the three derivatives GOV:PdA, AOV:PdA, and VOV:PdA in Fig. B-1b are 8.00 ppm, 8.02 ppm, and 8.00 ppm, respectively, which is almost the same as $\delta_o = 7.97$ ppm for a derivative with no strand structure. From this we can conclude that the three derivatives in Fig. B-1b are not structured. This is an expected result, and confirms the hypothesis that the first strand hydrogen bond is necessary for the formation of the second one.

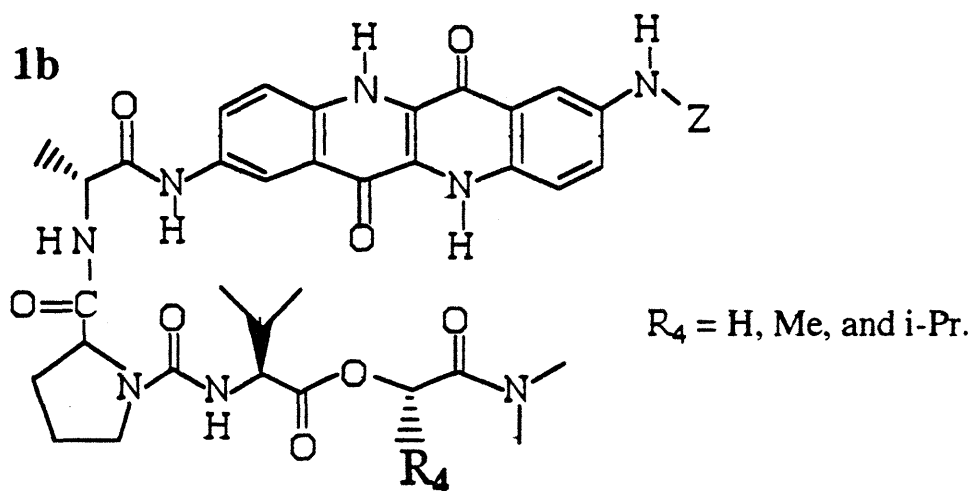
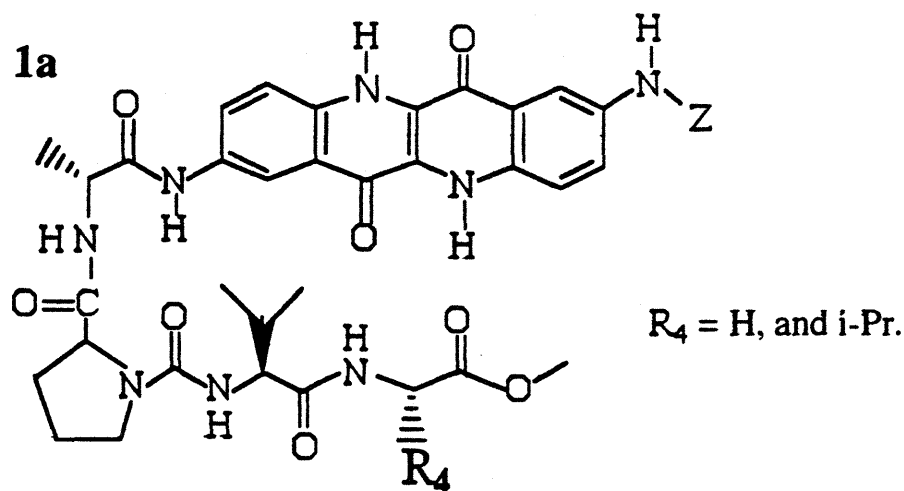


Figure B-1a) Peptide-epindolidione derivatives in which the terminal N,N-dimethylamide functionality of **1a** (Fig 2-1) has been replaced by a methyl ester. We name the two derivatives in which $R_4 = \text{H}$, or $R_4 = \text{i-Propyl (i-Pr)}$ as MeO-GV:PdA and MeO-VV:PdA, respectively.

B-1b) Peptide-epindolidione derivatives in which the amide nitrogen of the fourth amino acid residue in **1a** (Fig. 2-1) has been replaced by an ester oxygen. We name the three derivatives in which $R_4 = \text{H}$, Me, or i-Propyl (i-Pr) as GOV:PdA, AOV:PdA, and VOV:PdA respectively.

We can obtain a quantitative estimate for several K_{3X} constants from the appropriate χ values. Thus,

$$\chi(\text{MeO-GV:PdA}) = \frac{\delta_{\text{H}\beta} - \delta_0}{\delta_{\beta} - \delta_{\text{H}\beta}} = \frac{K_1}{1 + K_1} K_{2V} (1 + K_{3G}) = \frac{K_1}{1 + K_1} K_{2V}, \text{ since } K_{3G} = 0.$$

in a similar fashion,

$$\chi(\text{MeO-VV:PdA}) = \frac{\delta_{\text{H3}} - \delta_{\text{O}}}{\delta_{\beta} - \delta_{\text{H3}}} = \frac{K_1}{1 + K_1} K_{2V} (1 + K_{3V}) = \frac{K_1}{1 + K_1} K_{2V}, \text{ since } K_{3V} = 0.$$

From the chemical shifts of the H3 proton (δ_{H3}) of MeO-GV:PdA and MeO-VV:PdA we can calculate the respective χ values as follows,

$$\chi(\text{MeO-GV:PdA}) = \frac{\delta_{\text{H3}} - \delta_{\text{O}}}{\delta_{\beta} - \delta_{\text{H3}}} = \frac{8.11 - 7.97}{8.91 - 8.11} = \frac{K_1}{1 + K_1} K_{2V} = 0.175, \text{ and}$$

$$\chi(\text{MeO-VV:PdA}) = \frac{\delta_{\text{H3}} - \delta_{\text{O}}}{\delta_{\beta} - \delta_{\text{H3}}} = \frac{8.14 - 7.97}{8.91 - 8.14} = \frac{K_1}{1 + K_1} K_{2V} = 0.221.$$

The average of both values is 0.20 with a standard deviation of 0.032 (or 0.20 ± 0.03).

Furthermore, since

$$\chi(\text{XV:PdA}) = \frac{K_1}{1 + K_1} K_{2V} (1 + K_{3X}),$$

substituting 0.20 for $\frac{K_1}{1 + K_1} K_{2V}$ in the above Equation, and using the appropriate values of

$\chi(\text{XV:PdA})$ that can be calculated using Eq.2-1 & data in Table 2-1, we can directly solve for K_{3G} ,

K_{3A} , K_{3L} , K_{3F} , and K_{3V} .

These values are listed in Table B-1 which also lists the corresponding K_3 values as reported by Blanchard in his thesis (Blanchard, 1992).

Table B-1.

Equilibrium Constants K_3 for the peptide-epindolidione model **1a** (Fig. 2-1).

Amino Acid Residue (X)	K_3	K_3 (Blanchard, 1992).
Gly	4.6	0.19
Ala	7.7	0.48
Leu	7.4	0.53
Phe	9.1	0.98
Val	13.4	1.54

From Table B-1 it is clear that Blanchard's K_3 values that he estimated using the assumption that $K_{2V} = K_{3V}$ and $K_{2G} = K_{3G}$ (Blanchard, 1992) are much smaller than the values calculated here using the test derivatives MeO-GV:PdA and MeO-VV:PdA.

The large difference between the K_3 values estimated by Blanchard and in this thesis suggests that Blanchard's assumption that $K_{2V} = K_{3V}$ and $K_{2G} = K_{3G}$ does not hold. In terms of the peptide-epindolidione model **1a** (Fig. 2-1), this implies that the two strand positions X and Y in XY:PdA (**1a** in Fig. 2-1) are not equivalent as Blanchard assumed. This in turn suggests that the first and second strand hydrogen bonds in the peptide-epindolidione model **1a** are not equal in strength and/or there is a structural bias in either of the strand positions. In his assumption that $K_{2X} = K_{3X}$ and $K_{2Y} = K_{3Y}$ for at least one pair of residues, X and Y, Blanchard used Val and Gly. He chose Val and Gly in order to minimize the effect of any structural bias that may exist in either position X or Y. In Blanchard's words "One case in which the assumption would be false is where the third position residue is stabilized (or destabilized) by an interaction of its side chains with either the functional groups involved in the hydrogen bonds or with the epindolidione core. A way to avoid such a bias is to use amino acids, such as valine, alanine, or glycine which are compact and will have minimal opportunity to interact." (Blanchard, 1992, p. 125). The fact that the K_3 values reported in this thesis are so different from those of Blanchard (Table B-1) even though he chose amino acids that are likely to exhibit minimal structural bias (i.e. Val and Gly) suggests that the two strand positions differ due to a difference in the strength of the first and second strand hydrogen bonds rather than to any other structural bias. This conclusion is further supported by similar ranking of the relative propensities for most amino acid residues determined from either position X or Y (Blanchard, 1992). It is clear that if the first and second strand hydrogen bonds are different in strength, this will reflect itself in the difference of the absolute strand propensities (i.e. K_2 and K_3) but not the relative ones, since the latter ones are reported as ratios of equilibrium constants. Furthermore, the experimental and theoretical data that will be described next, strongly suggests that it is the difference in the strand 1 and strand 2 hydrogen bond strengths of the peptide-epindolidione model **1a** (Fig. 2-1) that is most likely the cause of the large difference in the K_3 values reported here and by Blanchard (Table B-1).

It is possible to obtain additional insights as to why the K_3 values obtained in this thesis are so much larger than expected from Blanchard's calculations by synthesis and conformational analysis of model systems that unlike the epindolidione template cannot form the second strand

hydrogen bond. Figure B-2 gives a general structure of such a system. It is clear from Fig. B-2 that the model derivative designated as EtNH-X:PdA-*m*Phe-NHEt can form the turn and the first strand hydrogen bonds which are structurally analogous to those of the peptide-epindolidione system **1a** (Fig. 2-1). However, this system does not allow formation of the second strand hydrogen bond.

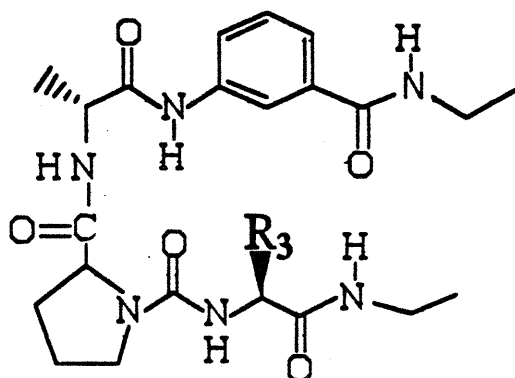


Figure B-2. Structure of a tripeptide conjugated to a 3-amino-N-ethylbenzamide functionality. This model system has the short-hand designation EtNH-X:PdA-*m*Phe-NHEt where X denotes the variable third amino acid residue, followed by the chain-reversing urea functionality and the β -turn-promoting l-Pro-d-Ala dipeptide which is covalently attached to the *m*-aminobenzamide functionality which is designated as "*m*Phe."

Before we analyze the data from derivatives of the general structure of Fig. B-2, it is may be helpful to discuss the rational for the design of this model system. Development of the new model system of Fig. B-2 was guided by the primary aim that the structure-reporting and initiating features that have proven useful in the peptide-epindolidione model **1a**(Fig. 2-1) should be retained in the new model system. To see this in more detail, let us examine Figure B-3 which shows a peptide-epindolidione conjugate **3** with the reporting region of the epindolidione template shown enclosed in the box. This structural motif appears to the right of the arrow in its simplest structural form. The equilibrium depicted by the double arrow between structures (conformers) **3a** and **3b** focuses attention on the N-acylanilide function which is the crucial reporting feature present in the epindolidione template. It is expected that the chemical shifts of proton H_b will vary linearly with the abundance-weighted populations of **3a** and **3b**, which precisely mirrors the properties of the epindolidione proton H₃. We also expect the system **3ab** to have analogous NOE behavior to that of the epindolidione. In other words, as was demonstrated in Chapter three of this thesis, we expect that the ratio of the NOE's between the aryl NH and the protons H_a and H_b should correlate

with the chemical shift changes observed for proton Hb. In order for the system **3ab** to be a useful reporter function, the structured conformation must show a preference for one of the conformers shown (either **3a** or **3b**) and the random coil conformation must prefer the other one, or preferably show no bias for either conformer.

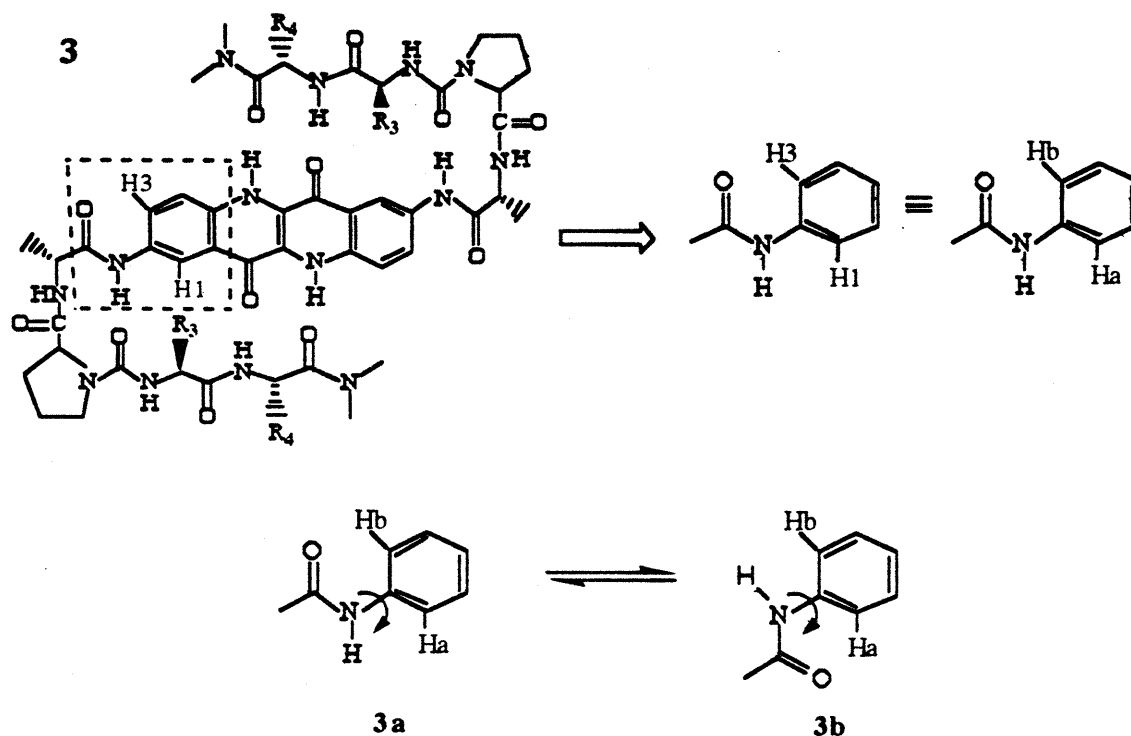


Figure B-3. Schematic diagram showing the structure-reporting N-acylanilide functionality of the peptide-epindolidione template enclosed in the box in **3**. The N-acylanilide represented by **3ab** can be incorporated into simpler systems such as that shown in Fig. B-2, with the hope of retaining the reporting properties of **3**.

Besides the N-acylanilide reporting functionality depicted in Figure B-3, Figure B-4 shows a peptide-epindolidione conjugate with the 4-quinolone region of the epindolidione template shown enclosed in the box. This structural region appears to the right of the arrow in its simple bicyclic 4-quinolone form followed by the monocyclic benzamide structure shown to the right of the second arrow. It is important to emphasize that the 4-quinolone structural motif in the epindolidione template is a vinologous amide, the benzamide in Figure B-4, on the other hand, is a normal amide, and it is the simplest possible structure that resembles the 4-quinolone structure. As further shown in Figure B-4, because of the loss of cyclization, unlike in the 4-quinolone, there is a free rotation possible around the C1-CO bond of the benzamide as indicated by the curved arrow.

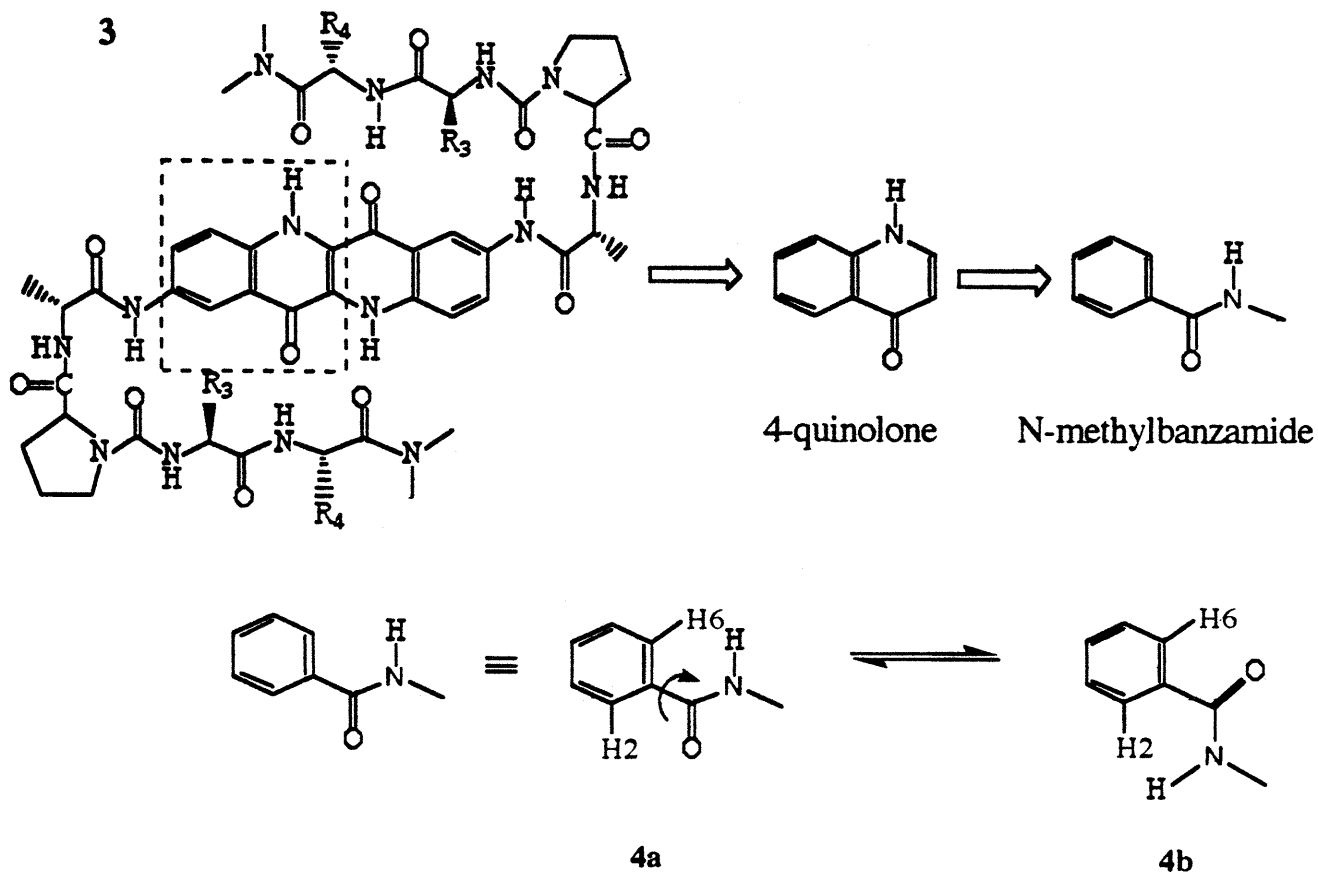


Figure B-4. Schematic diagram showing the potential structure-reporting N-alkylbenzamide functionality derived from the 4-quinolone moiety of the epindolidione template (shown enclosed in the box).

This new degree of freedom, that is not present in the epindolidione nor the 4-quinolone structures, leads to a possible new NMR reporter function in the benzamide structure. This new potential reporter feature of the benzamide is expected to be qualitatively similar to the reporter feature of the N-acylanilide function represented by **3ab** in Figure B-3 with the important difference that the NOE characteristics of the benzamide are expected to be more pronounced in comparison to the N-acylanilide, and the anisotropy effect at either H2 or H6 in **4ab** of Figure B-4 is expected to be less pronounced than that at Ha or Hb in **3ab** due to a difference in the geometry of the two systems.

We can combine the separate reporter properties of systems **3ab** and **4ab** into one structure, the Acetyl-*meta*-Phenylene-NHMe reporter (Acetyl-*m*-Phe-NHMe) depicted in Figure B-5. The *m*-phenylene functionality can be considered as the simplest possible and most versatile reporter function that still contains the unique **3ab** N-acylanilide reporter feature of the

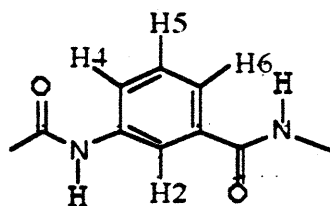


Figure B-5. The Acetyl-*m*-phenylene-NHMe functionality: the results from a combination of the separate reporter properties of systems **3ab** (Fig. B-6) and **4ab** (Fig. B-4) into one structure.

epindolidione template. The *m*-phenylene owes its unusual simplicity not only to its simple structure, but also because of its very simple synthesis which is only two steps away from the starting material, 3-aminobenzoic acid.

Having justified the rationale for the use of the *m*-Phe functionality in the model system of Fig. B-2, we are ready to examine experimental NMR results obtained with the *m*-phenylene and its peptide conjugates. Figure B-6 presents the structures of three *m*-phenylene-peptide conjugates and also select proton chemical shifts in DMSO-*d*₆ at 25 °C. Also shown in the Figure is the structure of the *m*-phenylene template itself including its proton chemical shifts. In naming these derivatives we use single letter amino acid codes. Thus the name EtNH-G:PdA-*m*Phe-NHEt implies the structure starting with an N-ethylamide followed by the amino acid glycine. The colon (as before) designates the direction-reversing urea function followed by the amino acids proline and d-alanine and the *m*-phenylene function ending with the ethyl amide. Both the structures MeO-V:PdA-*m*Phe-NHEt and Acetyl-*m*Phe-NHEt serve the purpose of control derivatives. Acetyl-*m*Phe-NHEt gives the chemical shifts of the relevant protons for the derivative with no structure, i.e., it models the chemical shift values of a hypothetical peptide-*m*Phe template conjugate in which the peptide is in a structureless or random-coil conformation. The derivative MeO-V:PdA-*m*Phe-NHEt is able to form the first (but not the second) hydrogen bond between the urea carbonyl oxygen and the aryl NH of the template. This is reflected in the substantial change in the chemical shift of the aryl NH, from 10.06 ppm in the non-hydrogen bonded state to 9.60 ppm in the state where the above-mentioned hydrogen bond can form. The same trend is observed in the case of peptide-epindolidione derivatives (Blanchard, 1992). However, comparison of the chemical shifts of the other relevant protons tells us that besides the formation of the first hydrogen bond, there is no other structuring effect that may cause alteration in those chemical shifts. Thus if we compare the chemical shifts for H4, H5, and H6 of derivatives Acetyl-*m*Phe-NHEt and

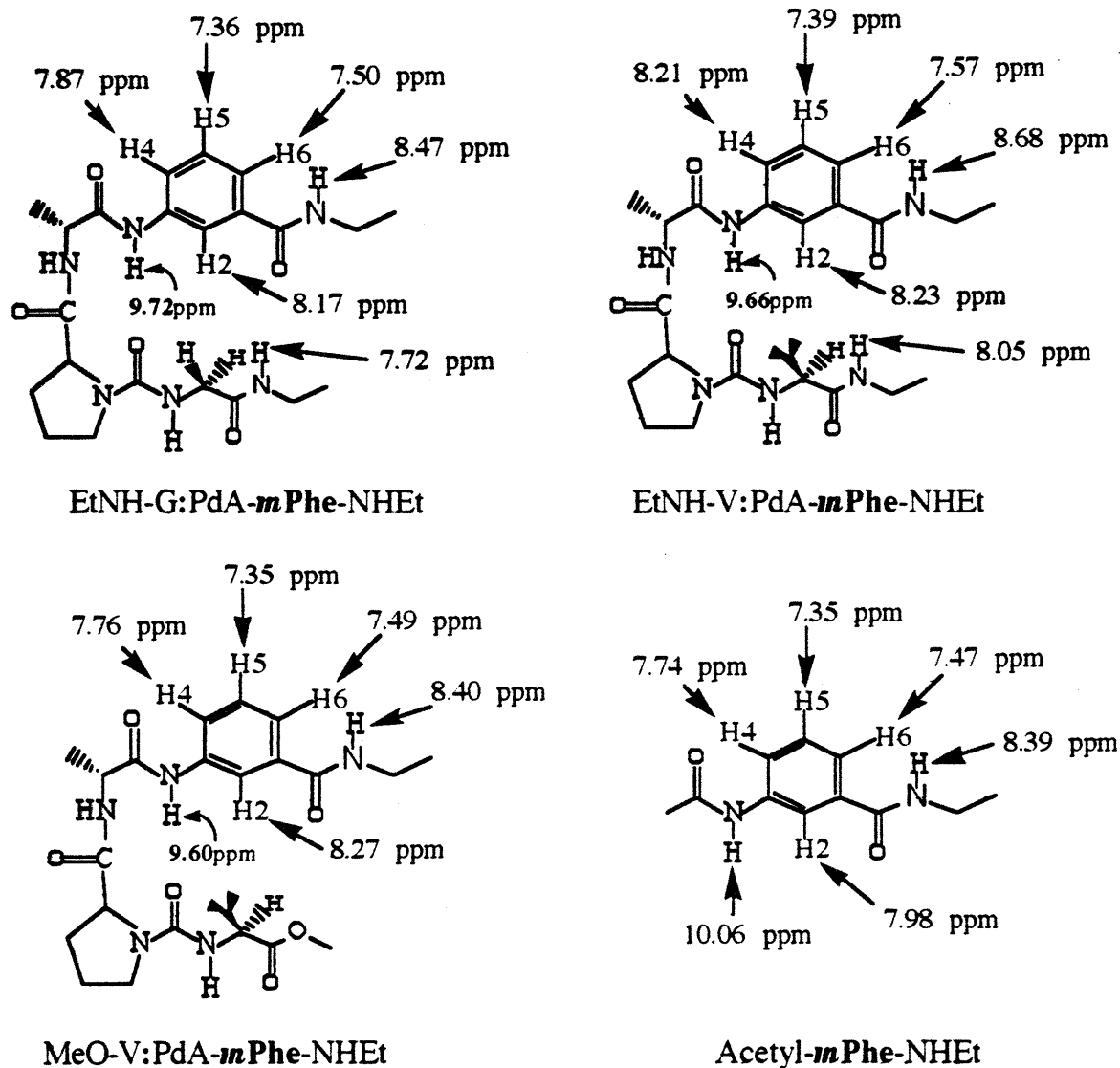


Figure B-6. Structures of three *m*-phenylene-peptide conjugates together with select proton chemical shifts obtained in DMSO- d_6 at 25 °C. The fourth derivative, acetyl-*m*Phe-NHEt plays the role of a control derivative that is not able to form any structure.

MeO-V: PdA-*m*Phe-NHEt, we see that the changes are very small or not existent. H2 chemical shift, however, experiences a change of 0.29 ppm. The H2 is more deshielded in the MeO-V: PdA-*m*Phe-NHEt derivative in contrast to the simple Acetyl-*m*Phe-NHEt derivative. This deshielding is most likely due to the close proximity of the peptide in the former. The most striking difference in certain proton chemical shifts is seen when we compare the derivative EtNH-V: PdA-*m*Phe-NHEt with Acetyl-*m*Phe-NHEt. H4 shows a large (0.47 ppm) downfield shift. This observation is crucial because in the *m*Phe template, the H4 proton is analogous to the H3 proton in the epindolidione template.

With the availability of this data we can make a direct comparison between the *m*-phenylene derivative EtNH-V:PdA-*mPhe*-NHEt of Fig. B-6 and the peptide-epindolidione terminal ester derivatives MeO-GV:PdA and MeO-VV:PdA of Fig. B-1a. Both derivatives MeO-GV:PdA and MeO-VV:PdA can only form the turn and the first strand hydrogen bonds. The same is true for the derivative EtNH-V:PdA-*mPhe*-NHEt. However, comparison of the chemical shifts of the reporter protons for the respective derivatives gives an unexpected and striking result as clearly shown by Equations B-1 and B-2,

$$\frac{\delta_{\text{H4, Val}}^{\text{mPhe}} - \delta_{\text{H4, 0}}^{\text{mPhe}}}{\delta_{\text{H3, Val}}^{\text{MeO-GV:PdA}} - \delta_{\text{O}}^{\text{mPhe}}} = \frac{8.21 \text{ ppm} - 7.74 \text{ ppm}}{8.11 \text{ ppm} - 7.97 \text{ ppm}} = 3.36, \text{ and} \quad (\text{Eq. B-1})$$

$$\frac{\delta_{\text{H4, Val}}^{\text{mPhe}} - \delta_{\text{H4, 0}}^{\text{mPhe}}}{\delta_{\text{H3, Val}}^{\text{MeO-VV:PdA}} - \delta_{\text{O}}^{\text{mPhe}}} = \frac{8.21 \text{ ppm} - 7.74 \text{ ppm}}{8.14 \text{ ppm} - 7.97 \text{ ppm}} = 2.76. \quad (\text{Eq. B-2})$$

The numerator of both Eqs. B-1 & B-2 is the downfield shift (0.47 ppm) of the H4 reporter proton of the derivative EtNH-V:PdA-*mPhe*-NHEt relative to the control derivative Acetyl-*mPhe*-NHEt. The denominators of Eqs. B-1 & B-2 represent the analogous downfield shifts (0.14 & 0.17 ppm) of the H3 reporter proton of the derivatives MeO-GV:PdA and MeO-VV:PdA relative to $\delta_{\text{O}} = 7.97$ ppm. The equations tell us that the relative shifts of the reporter proton of the *m*-phenylene derivative EtNH-V:PdA-*mPhe*-NHEt is three times that of the averaged shift of the derivatives MeO-GV:PdA and MeO-VV:PdA. This suggests that the derivative EtNH-V:PdA-*mPhe*-NHEt is much more structured than either derivative MeO-GV:PdA or MeO-VV:PdA. This is an unexpected result because one would expect the epindolidione template to be a better nucleator than the *m*-phenylene template, because the latter has less bond fixation as discussed above. One way to explain this result is to propose that the second hydrogen bond of the derivative EtNH-V:PdA-*mPhe*-NHEt is much stronger than the analogous first strand hydrogen bond in either derivative MeO-GV:PdA or MeO-VV:PdA. This in turn implies that the first strand hydrogen bond in the peptide-epindolidione derivatives **1a** (Fig. 2-1) is weak. A weak first strand hydrogen bond in **1** will lead to a small value of K_2 for **1a**. We have seen from Table B-1 that the K_3 values for the available residues in the data base of **1a** are unexpectedly large. The likely conclusion is that the two first and second strand hydrogen bonds in the epindolidione model **1a** are not equal in strength. Clearly the first strand hydrogen bond being inherently weaker than the second one. It is important to emphasize that this effect cannot be detected from the magnitude of

the χ values. Since χ is defined in terms of product of the equilibrium constants [i.e., $\chi = K_1 K_2 (1 + K_3) / (1 + K_1)$, see Eq. 2-1], a large value of K_3 will be dwarfed by a small value of K_2 . It is clear, therefore, that Blanchard could not predict this result without the data from the derivatives in Fig. B-1a and B-6.

It is possible to obtain additional insights about the systems MeO-GV:PdA, MeO-VV:PdA of Fig. B-1a and the model system of Fig. B-6 by considering the electrostatic interactions depicted in Figure B-7a and B-7b. As discussed before, the derivatives MeO-GV:PdA and MeO-VV:PdA of 7a can form only the first strand hydrogen bond. The double-headed arrow in 7a shows the repulsive electrostatic interaction between the dipoles of the pyridone NH proton and the NH proton of the fourth amino ester residue. On the other hand, this repulsive interaction does not exist in 7b. Based on this qualitative theoretical consideration, it is possible to justify why the hydrogen bond in 7a is seen to be much weaker in comparison to the one in system 7b. Examination of the derivative shown in 7c (which is XV:PdA of Fig. 2-1) shows that formation of the second strand hydrogen bond in 7c, which is expected to be strong based on the calculated values of K_3 (Table B-1), is likely to compensate for the repulsive interaction present in both 7a and 7c, as well as the additional one indicated by the second double-headed arrow in 7c.

The electrostatic interactions shown in Fig. B-7 suggest that there is a fundamental difference between systems such as B-7ab and B-7c due to the presence of quadrupolar interactions in B-7c.

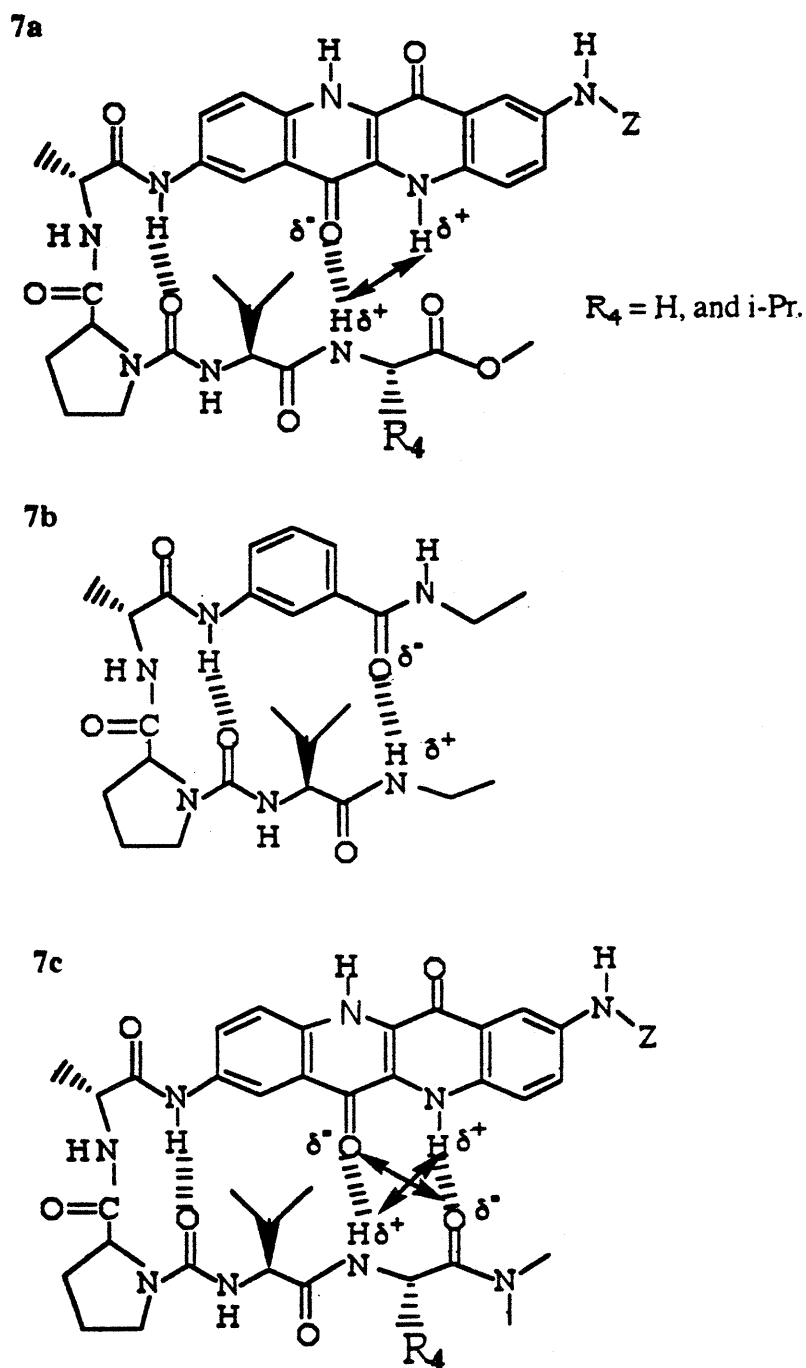


Figure B-7. Schematic diagram showing possible electrostatic interactions in the respective derivatives. **7a)** MeO-XV: PdA derivative has only one hydrogen bond in the strand region, and the repulsive interaction indicated by the double arrow. **7b)** EtNH-V: PdA-*m*Phe-NHEt has a hydrogen bond, but no repulsive interactions like in **7a**. **7c)** XV: PdA has two hydrogen bonds in the β -strand region in addition to the two repulsive interactions indicated by the double-headed arrows.

Appendix C

As we have seen in the previous chapters, the study of peptides conjugated with the epindolidione template developed in our laboratories enables us to study formation of beta-strands in a variety of solvents, including water, without many of the problems inherent to strand formation. Furthermore, peptide-epindolidione systems offer a number of important advantages when studying protein folding that are not present in simple peptides alone. Formation of a hairpin beta-strand is likely to be thermodynamically unfavorable, however, if one of the beta strands of the hairpin is replaced with a rigid organic template molecule like the epindolidione which provides the same hydrogen bonding donor and acceptor groups, this will result in a more stable structure because the entropic loss to constrain one of the two strands of the beta-sheet hairpin into an extended conformation is avoided. Furthermore, the aromatic, planar nature of the epindolidione template ensures minimal van der Waals steric interactions with the adjacent extended peptide strand. As we have seen, this allows the study of the role of rigidly oriented hydrogen bond donors and acceptors in nucleation of beta-strand structure. However, despite the fact that the epindolidione template proved to be an excellent first model system for studying the intrinsic propensity of individual amino acid residues to form a beta-strand, it has several disadvantages:

- 1) it has a relatively lengthy and difficult synthesis,
- 2) it has poor solubility properties, especially in aqueous solvents; furthermore, because of its C2 symmetry, its structure cannot be easily modified, for example in order to increase its water solubility or to functionalize it with two different peptides, which should allow investigation of interchain interaction across the hydrogen bonding network of a beta-strand hairpin model.
- 3) it has only one useful NMR reporting probe (the H3 chemical shift).

In view of the above arguments, our paradigm for the design of new reporting templates for strand structure is guided by the following aims:

- 1) design of templates with the simplest possible structure as well as synthesis, which nevertheless retain the nucleating and reporting features of the epindolidione system that has proved especially useful in the past.

- 2) design of templates that can be easily structurally modified for a variety of purposes some of which may be
- a) to increase water solubility for aqueous studies,
 - b) to introduce either hydrophobic or hydrophilic character in order to test its effect on either nucleation and/or energetics of strand structures,
 - c) to incorporate additional NMR reporting probes in addition to those present in the epindolidione template.
- 3) design of templates that can be functionalized with two different peptides which should allow investigation of interchain interaction across the hydrogen bonding network of a beta-strand hairpin model.
- 4) design of templates with special symmetry features that either simplify NMR analysis or provide unique features that can be used to further probe the structural and energetic state of the attached peptide.

In order to carry out these aims, it is useful to separately analyze the reporting and initiating features of the epindolidione template that we hope to transfer to these simpler systems.

Figure 1 A shows a peptide-epindolidione conjugate with the reporting region of the epindolidione shown enclosed in the box. This structural motif appears to the right of the arrow in its simplest structural form (**B**). The equilibrium depicted by the double arrow between structures (conformers) **1 a** and **1 b** in 1 C focuses attention on the N-acylanilino function which is the crucial reporting feature present in the epindolidione template. It is expected that the chemical shifts of protons Ha and Hb will vary linearly with the abundance-weighted populations of **1 a** and **1 b**, which precisely mirrors the properties of the epindolidione proton H3. We also expect the system **1 a b** to have analogous NOE behavior to that of the epindolidione. In other words, as was demonstrated in chapter 3 of this thesis, we expect that the ratio of the NOE's between the aryl NH and the protons Ha and Hb should correlate with the chemical shift changes observed for protons Ha and Hb. In

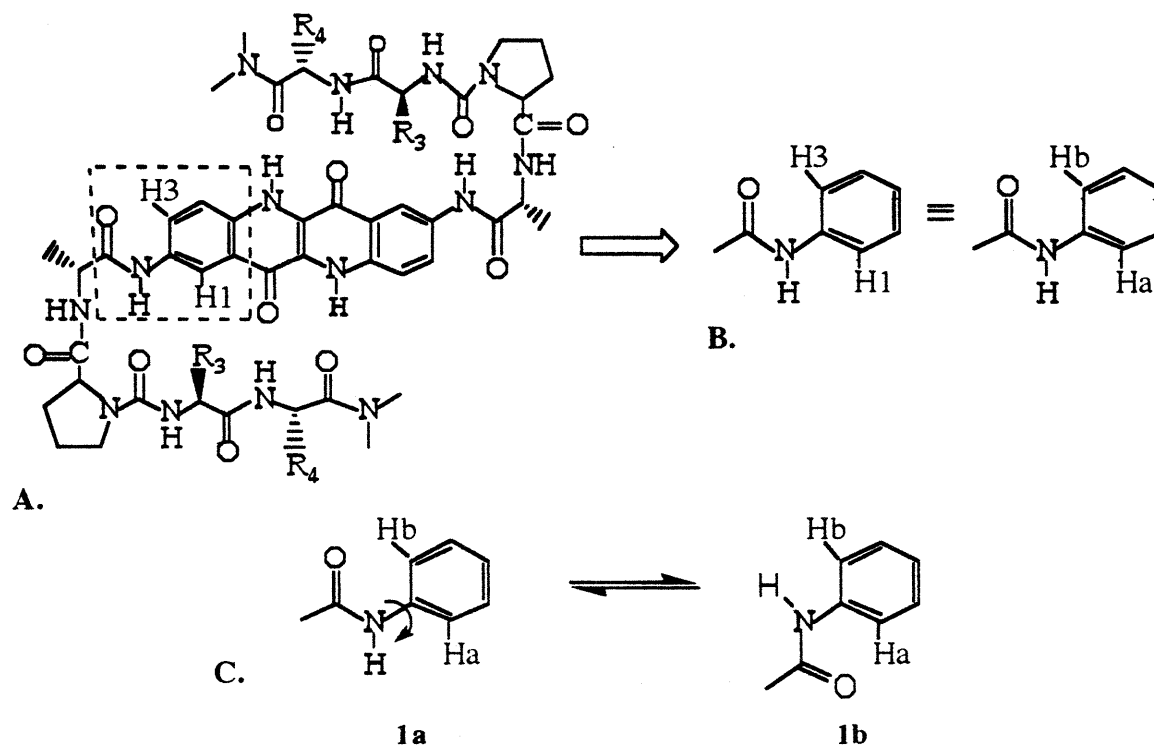


Figure 1

- A. Peptide-epindolidione conjugate with the reporting region of the epindolidione shown enclosed in the box.
 B. N-acylaniline reporting structural motif.
 C. Two conformers (1a and 1b) of the N-acylaniline reporting structural motif depicted in B.

order for the system **1ab** to be a useful reporter function, the structured conformation must show a preference for one of the conformers shown (either **1a** or **1b**) and the random coil conformation must prefer the other one, or otherwise show no bias for either conformer.

In contrast to the system **1ab** shown in Figure 1C, the proton Ha, shown in Figure 2 is unlikely to display equally useful reporter properties because this system is most likely locked in the conformation **2a** by the local interaction between the dipoles of the acyl N-H and the adjacent pyridone carbonyl. Furthermore, the steric repulsion of the carbonyl oxygens shown in **2b** should even further destabilize conformer **2b**, thus pushing the equilibrium towards conformer **2a**. Having shown that the N-acylanilide function of the epindolidione is the crucial reporting function, let us pose the following question: How can we simplify the structure of the epindolidione template

and yet maintain the reporting feature of the system **1ab** as well as the strand-initiating property of the epindolidione template.

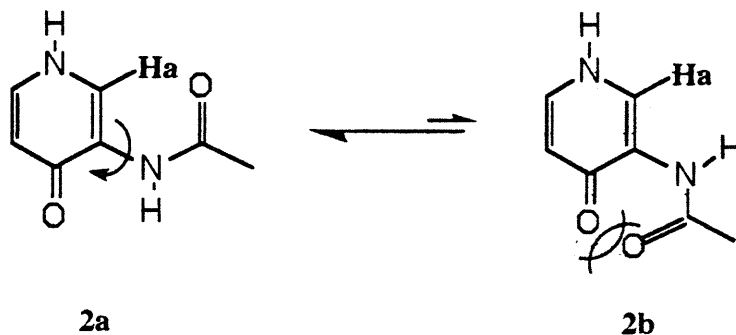


Figure 2.

3-acetamidopyridone, showing the equilibrium between the two conformers shown. **2a** is the more abundant conformer due to the favorable dipole-dipole interaction. **2b** is much less populated due to the steric repulsion of the carbonyl oxygens.

Figure **3a** shows a peptide-epindolidione conjugate with the structural region of the epindolidione template crucial for strand initiation and reporting functions enclosed in the box. This structural region appears to the right of the arrow in its simplest tricyclic form **3b**. The tricyclic structure can be further simplified by converting the cyclic pyridone (at the right side of **3b**) which is a vinologous amide, to an acyclic N-acylamino function, which is much closer in structure to a normal amide. This gives us the 3,6-diacylamino-4-quinolone, **3c**. We can see from Figure **3**, that the 3,6-diacylamino-4-quinolone, **3c** template embodies the initiating and reporting features of the epindolidione template and yet it is a simpler and potentially more versatile template.

If we look at Figures **1a** and **2a**, it is clear that **3c** contains both features of **1ab** and **2a**. This is clearly depicted in Figure **4**. From this direct comparison, it is clear that proton H7 in **3c** or **4b** is analogous to proton H3 of the epindolidione (Figure 1A), and therefore is expected to exhibit similar NMR reporting properties. As we discussed above, proton H2 of **4c** or **2a** is not very likely to be useful as a reporter proton because **4c** (or **2a**) is locked into the conformation shown for reasons mentioned above. Nevertheless, there may be some local, limited rotation possible

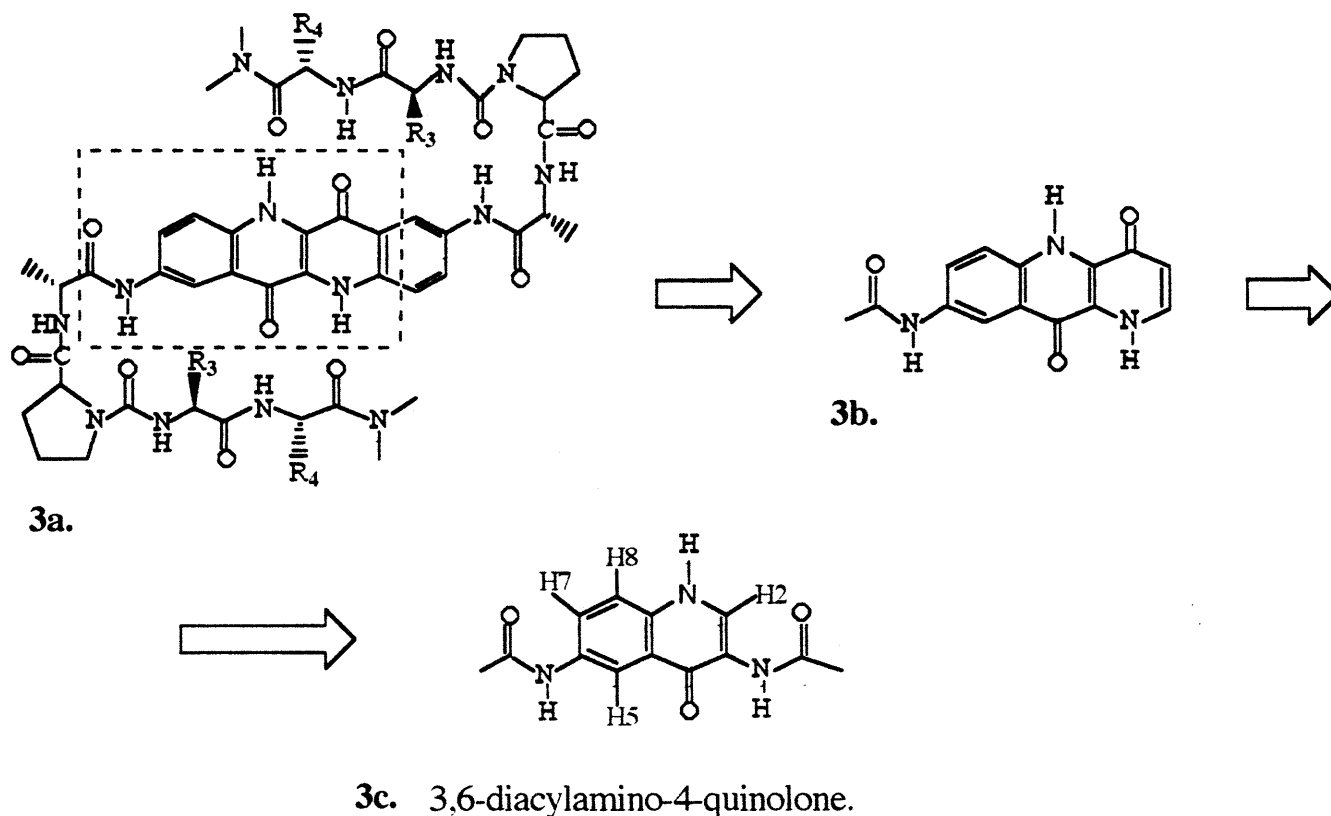


Figure 3.

3a. Peptide-epindolidione conjugate with the reporting and initiating region of the epindolidione shown enclosed in the box.

3b. The reporting and initiating region of the epindolidione shown enclosed in the box of **3a**.

3c. 3,6-diacylamino-4-quinolone template. This template embodies the initiating and reporting features of the epindolidione template, yet it is a simpler and potentially more versatile one.

around the exocyclic C3-N bond in **4c** which would lead to a potential reporting feature. If such a reporting feature would indeed be found, it could prove very valuable because it is structurally uncoupled from the H7 reporter of **4b**. This point merits further consideration which is given below.

As outlined in the previous chapter, the variation of chemical shift of the H3 proton of the epindolidione template in DMSO was most useful and allowed quantitative estimates of the propensity of various amino acid residues to be in a strand structure. From Figures **3** and **4** we can see that the quinolone template system offers at least one (and potentially two) proton(s) that can

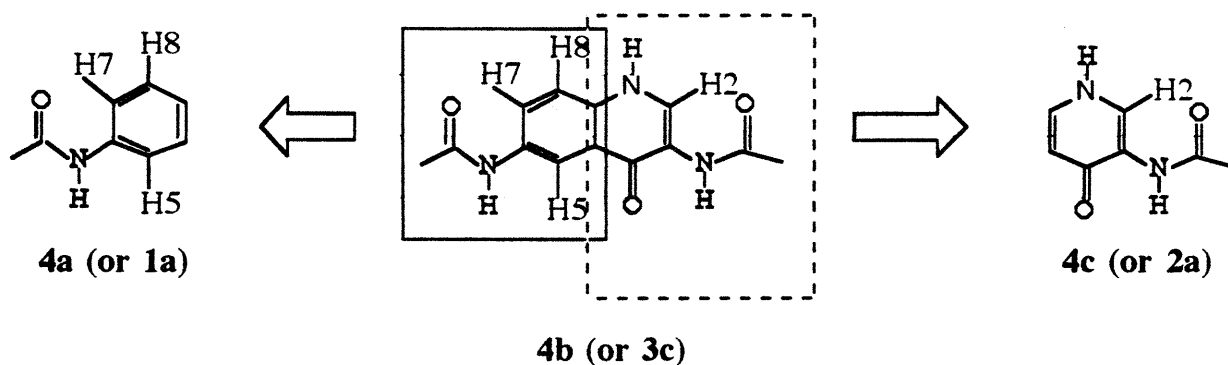


Figure 4.

4a. N-acetylaniline reporter function as appearing in 4b.

4b. 3,6-diacetylamino-4-quinolone template (same as shown in Figure 3c.)

4c. 3-acetmidopyridone structure as appearing in 4b, (same as shown in Figure 2a.)

act as structure reporters. From the structural similarity between the epindolidione and quinolone templates, it is clear that H7 in the latter template is analogous to H3 in the former. Thus, in the quinolone system, δ_{H7} will most likely be a sensitive reporter of the population of the first (P_{S1}) and second (P_{S2}) hydrogen bonded strand states. δ_{H2} , on the other hand, is expected to report exclusively on P_{S2} , the population of the state with the second strand hydrogen bond. Clearly, if the exocyclic C3-N bond in Figure 2a is allowed some free rotation (within any steric limitation) in the absence of the second strand hydrogen bond, but is even more restricted when the second strand hydrogen bond is present, this will force the acyl group carbonyl oxygen to be in close proximity to H2. The presence of the second (H2) potential reporter group should facilitate quantitative investigation of amino acid propensities as we will now demonstrate.

Let $P_{rc/t} = P_{rc} + P_t =$ the combined population fraction of the turn and random coil population fractions. $P_{S1} =$ population fraction of the state with first strand hydrogen bond,

P_{S2} = population fraction of the state with the second strand hydrogen bond.

Thus, according to this definition $P_{rc/t} + P_{s1} + P_{s2} = 1$. Further, let us define

$\delta_{o,H7}$ = the weighted average chemical shift of the H7 hydrogen for the random coil/turn states

$\delta_{o,H2}$ = the weighted average chemical shift of the H2 hydrogen for random coil, turn and first strand hydrogen bond states,

$\delta_{\beta,H7}$ = the chemical shift of the H7 proton for the fully structured strand state, and

$\delta_{\beta,H2}$ = the chemical shift of the H2 proton for the fully structured strand state. With these

definitions, we can write the following equations

$$\delta_{H7} = \delta_{o,H7} P_{rc/t} + \delta_{\beta,H7} (P_{s1} + P_{s2})$$

$$\delta_{H2} = \delta_{o,H2} (P_{rc/t} + P_{s1}) + \delta_{\beta,H2} P_{s2}$$

$$P_{rc/t} + P_{rc} + P_t = 1$$

These are three equations in three unknowns, $P_{rc/t}$, P_{s1} and P_{s2} . Solving these equations

simultaneously gives the following:

$$P_{s2} = (\delta_{H2} - \delta_{o,H2}) / (\delta_{\beta,H2} - \delta_{o,H2})$$

$$P_{s1} = [(\delta_{H7} - \delta_{o,H7})(\delta_{\beta,H2} - \delta_{o,H2}) - (\delta_{H2} - \delta_{o,H2})(\delta_{\beta,H7} - \delta_{o,H7})] / [(\delta_{\beta,H7} - \delta_{o,H7})(\delta_{\beta,H2} - \delta_{o,H2})]$$

$$P_{rc1} = (\delta_{\beta,H2} - \delta_{0,H2}) / (\delta_{\beta,H2} - \delta_{0,H2}) - P_{s1}$$

Previously (chapter 2), we defined K_1 , K_2 , and K_3 , the equilibrium constants for the formation of the first, second, and third hydrogen bond as

$$K_1 = P_t/P_{rc}, \quad K_2 = P_{s1}/P_t, \quad \text{and} \quad K_3 = P_{s2}/P_{s1}. \quad \text{Thus, we can immediately solve for } K_3$$

$$K_3 = (\delta_{H2} - \delta_{0,H2}) / [\delta_{H7}(\delta_{\beta,H2} - \delta_{0,H2}) + \delta_{0,H7}(\delta_{H2} - \delta_{\beta,H2}) + \delta_{\beta,H7}(\delta_{0,H2} - \delta_{H2})]$$

This is a very important result. It tells us that if $\delta_{H2} \neq \delta_{0,H2}$, we can solve directly for K_3 in terms of experimentally derivable quantities. This is not possible for the epindolidione system without making the assumption that for at least two amino acid residues $K_2 = K_3$. However, as was demonstrated in this thesis and in [ref. 1], there is actual evidence that $K_2 \neq K_3$ for some amino acids, which casts some doubts about the validity of such an assumption.

K_3 represents the equilibrium constant for formation of the second strand hydrogen bond.

Since $\Delta G^0 = -RT \ln(K_3)$, the value of K_3 gives an estimate of the free energy for formation of this hydrogen bond. In a simplistic fashion we can split ΔG^0 into two terms [ref. 2], the first one corresponds to fixing two rotors (ϕ , and ψ angles of the fourth residue) and is energetically unfavorable ($\Delta S^0 < 0$, $\Delta G^0 > 0$); the second, which corresponds to formation of the third

hydrogen bond must be favorable ($\Delta G^0 < 0$) if K_3 is to be greater than unity. Thus, the value of K_3 should represent a quantitative measure of the propensity of the amino acid in the fourth position to be in a β -strand.

Besides the potential additional reporter function in the form of H2 chemical shift, the 3,4-diacetylamino-4-quinolone (quinolone) template has several other advantages in comparison to the epindolidione template:

- 1) the quinolone template can be structurally modified, for example to increase its solubility for study in aqueous solutions.
- 2) the quinolone template, because it lacks C2 symmetry, can be functionalized with two different peptides which should allow investigation of interchain interaction across the hydrogen bonding network of a beta-strand hairpin model.
- 3) the quinolone template-peptide system can be cyclized, thus providing the spectroscopic signature for fully structured states which are absolutely essential for quantitative determination of conformational behavior of these systems.

Because of the potentially valuable features of the quinolone template **4b**, we set out to synthesize it. Figure **5abc** shows three possible retrosynthetic pathways from 3,6-diacetylamino-4-quinolone (1, or **4b**) to either anthranilic acid hydrochloride (**5a c**), or 5-nitroanthranilic acid hydrochloride, (**5b**). In Figure **5a** we start with the 3,6-diacetylamino-4-quinolone (1) and proceed to the 3,6-diamino-4-quinolone (2), followed by the 3,6-dinitro-4-quinolone (3), and finally the starting material anthranilic acid. Figure **5b** retrosynthetic analysis differs from the one in Figure **5a** in the final part, where the 3,6-dinitro-4-quinolone (3) is simplified to 5-nitroanthranilic acid instead of anthranilic acid as in Figure **5a**. In Figure **5c** we see a retrosynthetic

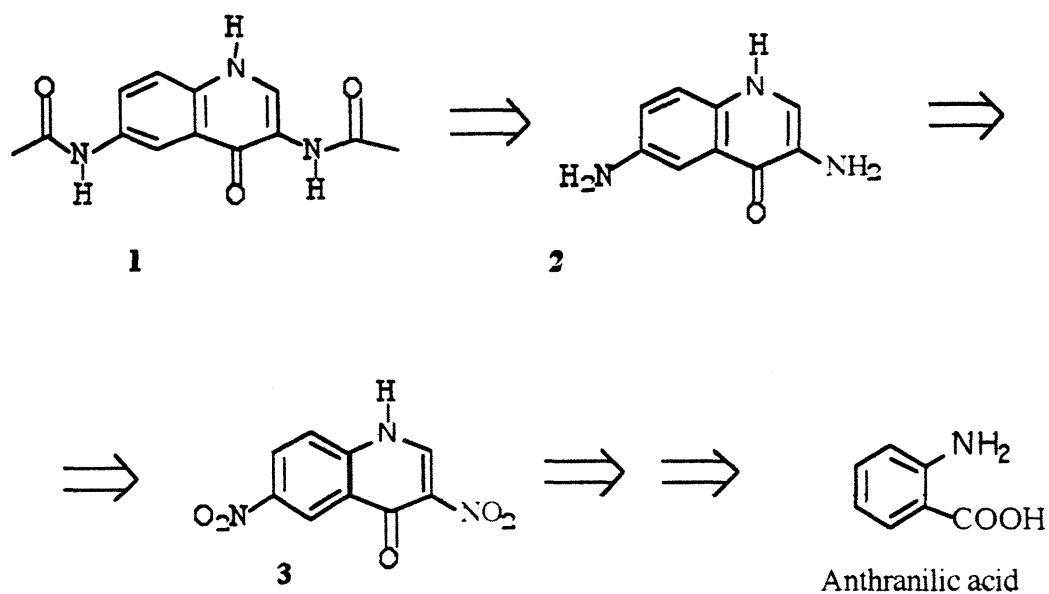


Figure 5a.
One possible retrosynthetic analysis leading from 3,6-diacetylaminopyridin-4(1H)-one template **1** (4b) to anthranilic acid.

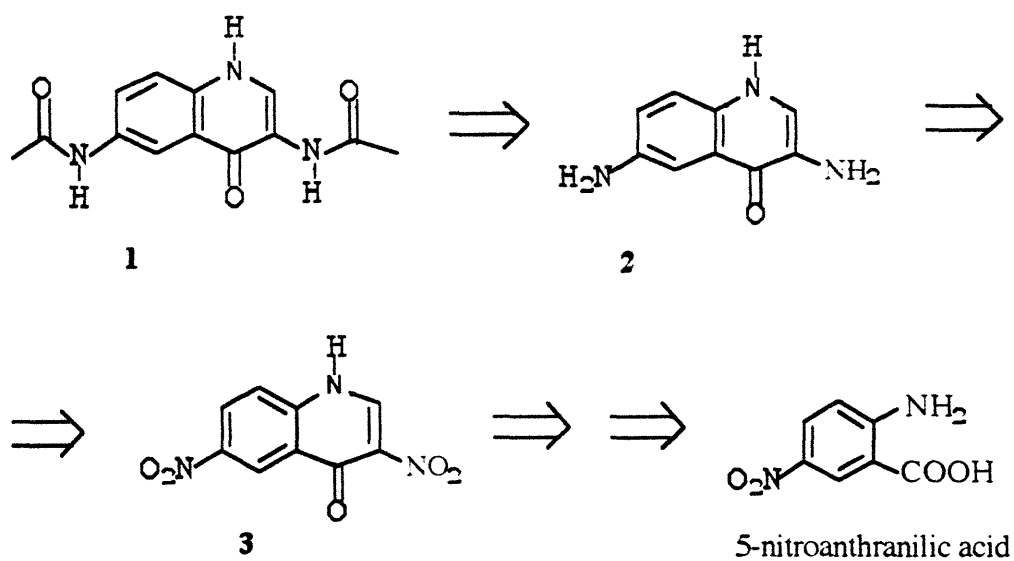


Figure 5b.
One possible retrosynthetic analysis leading from 3,6-diacetylaminopyridin-4(1H)-one template **1** (4b) to 5-nitroanthranilic acid.

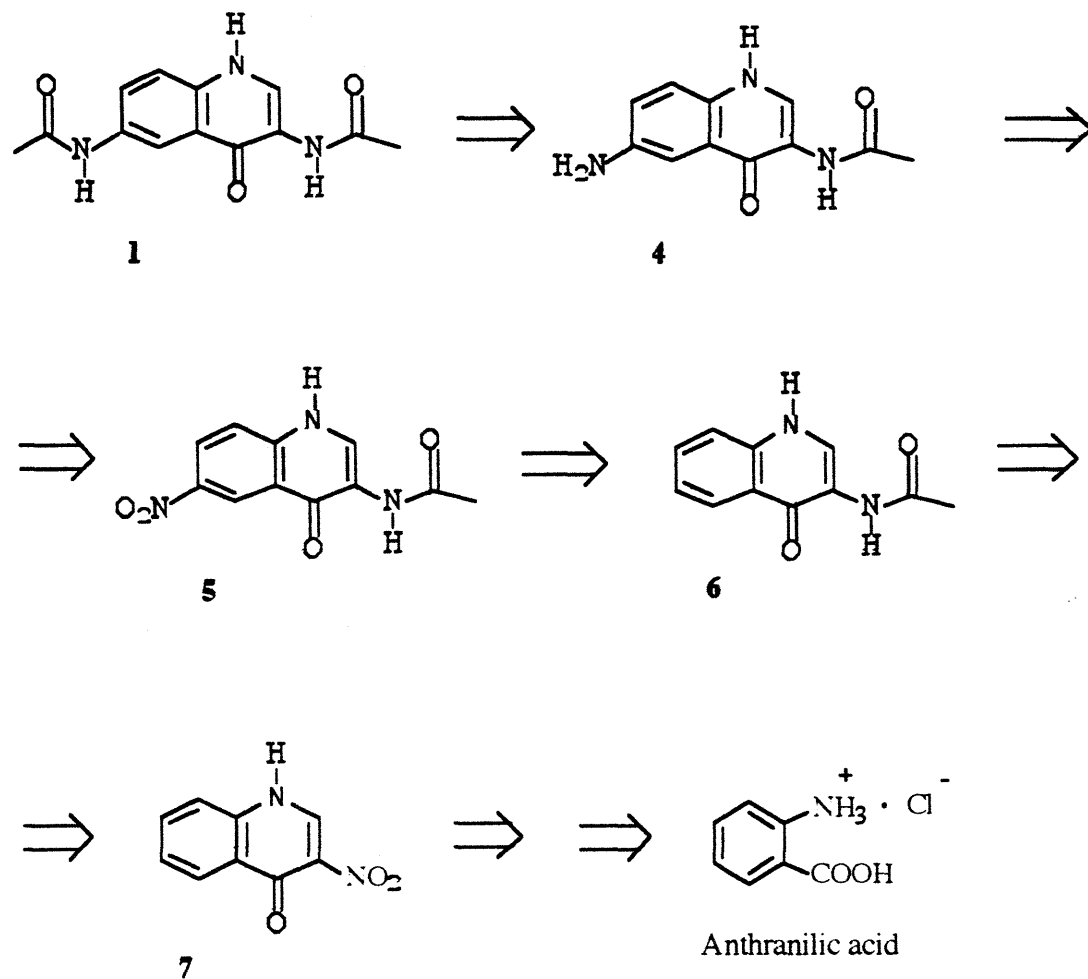


Figure 5c.

Another possible retrosynthetic analysis leading from 3,6-diacetylaminopyridin-4(1H)-one template 1 (4b) to anthranilic acid. This retrosynthetic analysis differs from those in Figures 5a & 5b in that (1) is disconnected to (4) instead of (2). This difference leads to a somewhat more complex retrosynthesis in comparison to the ones depicted in Figures 5a & 5b. Nevertheless, as indicated in the text, this scheme has important advantages over the other retrosynthetic analyses.

analysis that is conceptually different from retrosyntheses in both Figures 5a and 5b. The first step simplifies the structure (1) to the 6-amino-3-acetylaminopyridin-4(1H)-one (4), followed by 6-nitro-3-acetylaminopyridin-4(1H)-one (5), 3-acetylaminopyridin-4(1H)-one (6), 3-nitropyridin-4(1H)-one (7), and finally the starting material anthranilic acid. Next we will examine the practical syntheses that have been modeled based on the retrosyntheses of Figures 5abc.

In 1947 Bachman et al. [ref. 3] gave a procedure for the preparation of 3-nitro-4-quinolone from anthranilic acid. Figure 6a shows the general outline of this synthetic procedure as employed in this work.

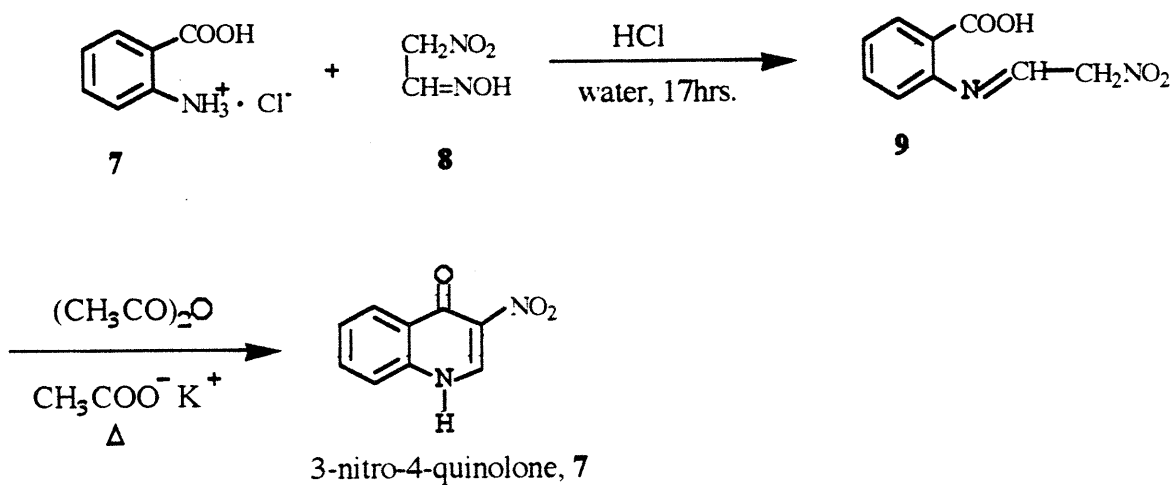


Figure 6a.

Preparation of 3-nitro-4-quinolone (7) from anthranilic acid hydrochloride (7)

Anthranilic acid hydrochloride (7) is condensed with methazonic acid (8) to give the 2-β-nitroethylidenaminobenzoic acid (9) which is then dehydrated to the 3-nitro-4-quinolone (7) by refluxing in acetic anhydride in the presence of anhydrous potassium acetate salt. The first reaction proceeds in good yield. Bachman et al. report a yield of 80-90% for (9). In this work, the same reaction was run three times on a large scale (> 10g), and gave a consistent yield of ≈ 83%. Figure 6b shows one potential way how (7) can be converted to the desired 3,6-diacetylamino-4-quinolone (1). In practice, (7) could be prepared in yields of only ≈ 44% from the 2-β-nitroethylidenaminobenzoic acid (9), following the procedure of Bachman et al. Bachman et al. studied this dehydration-cyclization reaction extensively, but could not improve the reported yields above 43-45%. Furthermore, the authors found that the use of the anhydrous alkali metal

catalyst (either sodium or potassium acetate) in refluxing acetic anhydride is essential for the reaction to proceed.

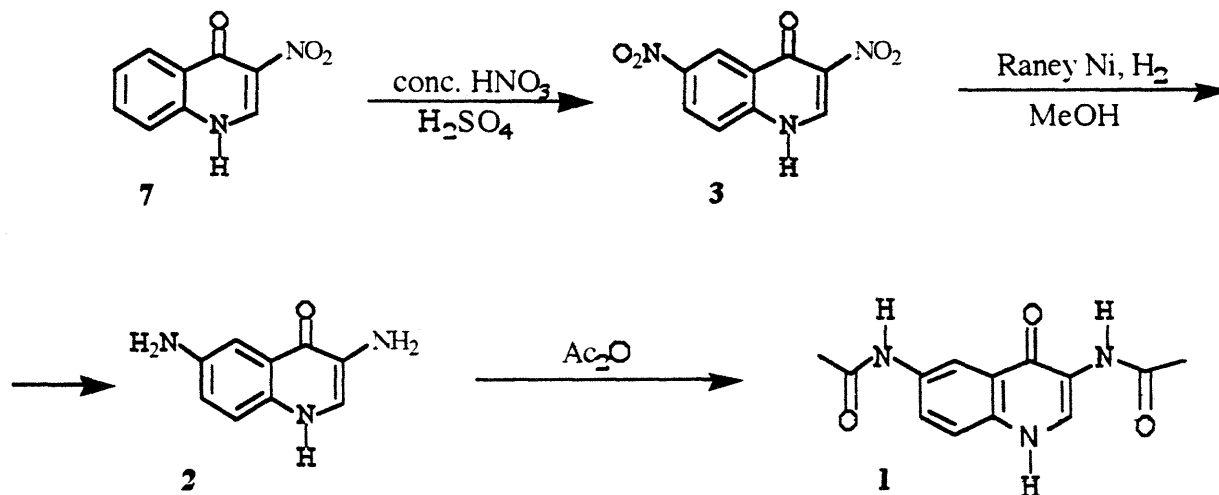


Figure 6b.
Preparation of 3,6-diacetylamino-4-quinolone (1) from 3-nitro-4-quinolone (7).

Attempts to prepare (3) as shown in Figure 6b, failed to give the desired product. Instead we consistently obtained a yellow product that was judged heterogenous by NMR. Attempts at recrystallization from glacial acetic acid did not improve NMR -judged purity of the product. Flash chromatographic attempts at purification of the heterogenous yellow product proved of little use, as the product solubility is rather low in such common solvents as chloroform, acetone, or ethyl acetate. Furthermore, when attempting flush chromatography, extensive smearing was observed, thus making purification virtually hopeless. NMR spectrum of the crude yellow product proved impossible to interpret, implying that the reaction from (7) to (3) shown in Figure 6b must be giving a complex product mixture that is very difficult to purify. From the crude NMR spectrum of the yellow product and the knowledge of the likely mechanism of the reaction under the given condition, one can offer a possible explanation for the failure to obtain (3) in Figure 6b. Figure 7a shows the proposed major products of the attempted second nitration reaction. (9) and (10) are the

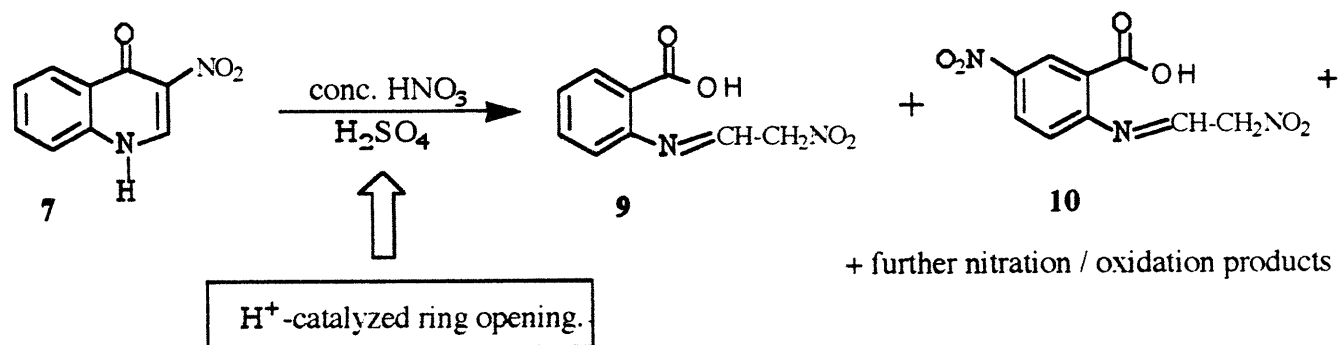
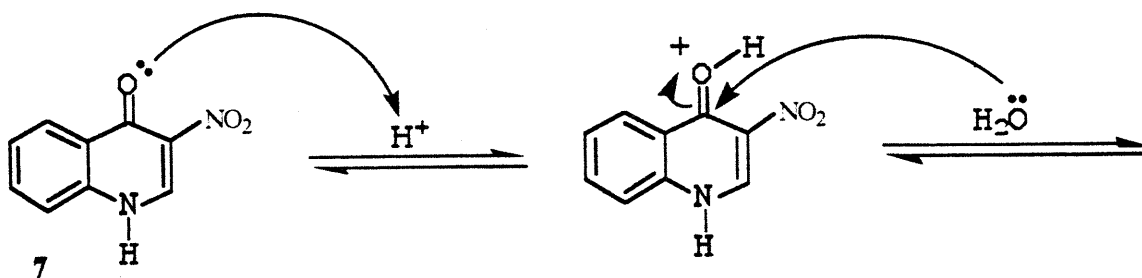


Figure 7a.

Proposed reaction scheme that (7) undergoes under the strongly acidic condition of the nitration reaction. (9) is the product of a H^+ -catalyzed ring opening. (10) is the result of simple nitration of (9) once it is formed. Under the strong oxidizing environment of the nitration reaction, both (9) and (10) can undergo further, nitration/oxidation reactions, thus giving a complex product mixture.

proposed products of a H^+ -catalyzed ring opening mechanism. This proposed mechanism is shown in Figure 7b, which shows how (9) is produced from (7) under the strongly acidic and oxidizing conditions of the reaction. The mechanism, as shown in Figure 7b, constitutes essentially the reverse of the dehydration-cyclization reaction. (10) is produced by simple nitration of (9), once it is produced.

Possible Mechanism for formation of 9 :



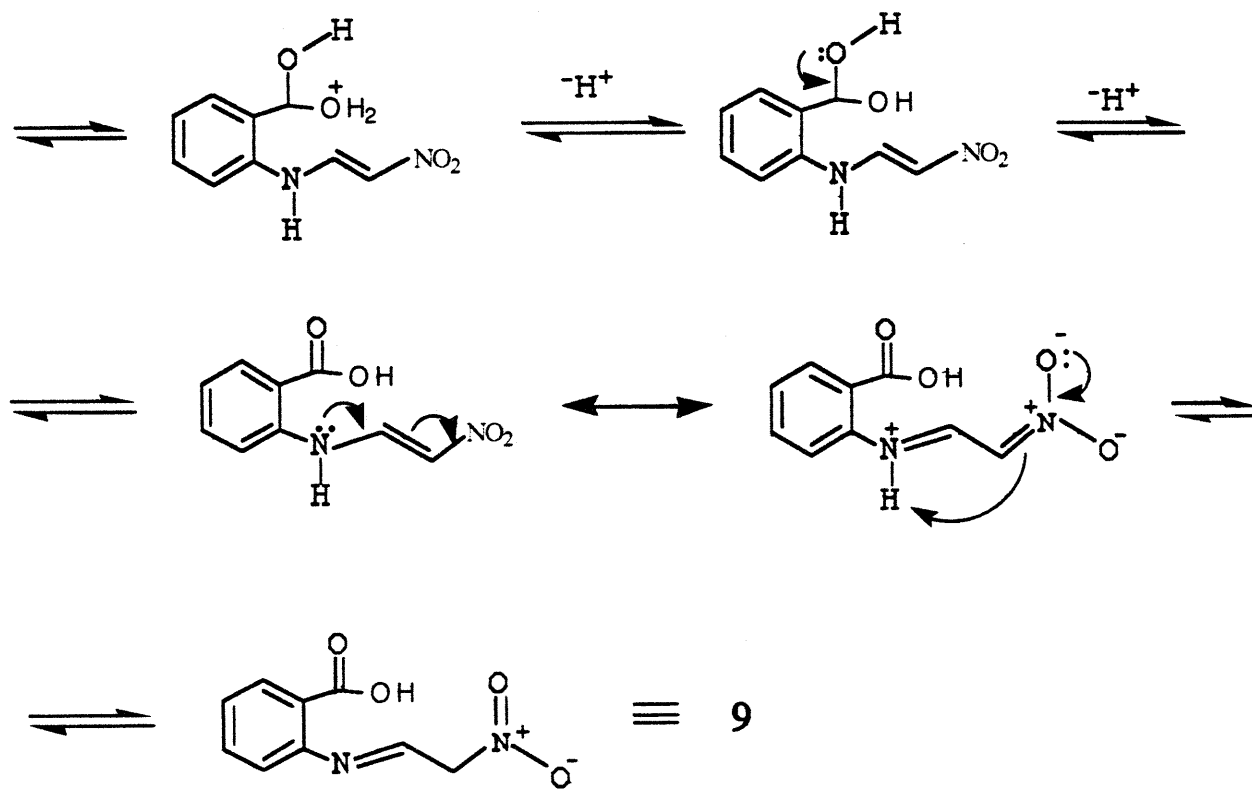


Figure 7b.

A possible reaction mechanism explaining the conversion of (7) to (9) under the strongly acidic conditions of the nitration reaction.

From the above arguments and the likely mechanism outlined in Figure 7ab, it is clear that we can not use acid-catalyzed nitration of (7) as a means of synthesizing (3). The synthetic scheme resulting from the retrosynthetic analysis of Figure 5a, and outlined in Figure 6b was therefore abandoned.

An alternative synthetic pathway to 3,6-diacetylamino-4-quinolone (1) based on the retrosynthetic analysis of Figure 5b is outlined in Figure 8. However, in practice, it proved impossible to carry out the first reaction shown in Figure 8. Obviously this reaction is analogous to the reaction shown in Figure 6a. The only difference is that the starting material is

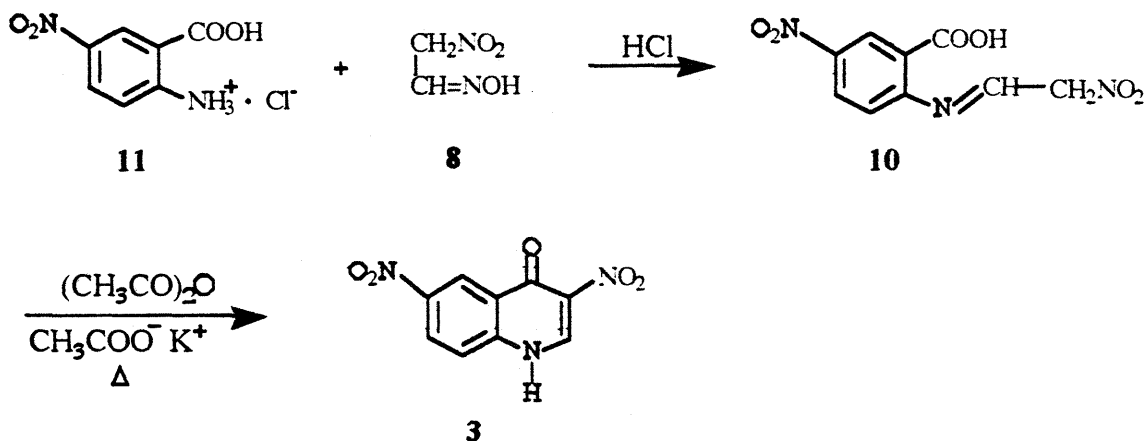


Figure 8.

An alternative synthetic pathway to 3,6-diacetylamino-4-quinolone (1) based on the retrosynthetic analysis of Figure 5b. As explained in the text, (10) does not form under the general reaction conditions that were applied in the reaction in Figure 6a to form (9). The possible reason for this failure to form (10) under the above conditions is given in the text.

5-nitroanthranilic acid hydrochloride instead of anthranilic acid hydrochloride. Application of the procedure of Bachman et al. to the reaction in Figure 8 proved inadequate. In that procedure one prepares anthranilic acid hydrochloride from anthranilic acid by acidification with HCL in water. Anthranilic acid which is only sparingly soluble in room temperature water, dissolves immediately upon addition of HCL due to formation of the hydrochloride salt. However, in the case of 5-nitroanthranilic acid, the same procedure fails to dissolve the acid, most likely because the strongly electron-withdrawing nitro group makes the amino group much less basic. Therefore, in attempts to remedy this situation, much more HCL had to be added to dissolve the 5-nitroanthranilic acid in the case of the reaction in Figure 8, in contrast to that in Figure 6a. Nevertheless, the reaction to obtain (10) under such strong acid conditions failed as no (10) was ever formed. As described in the experimental section at the end of this chapter, addition of anthranilic acid hydrochloride to the freshly prepared methazonic acid results in formation of a bright yellow precipitate within 1-2 minutes. This never happened in the case of 5-nitroanthranilic acid. We can try to rationalize this failure to react by suggesting that the amino group of the

5-nitroanthranilic acid is much less nucleophilic (due to the presence of the electron-withdrawing nitro group) than the amino group of anthranilic acid. This can be seen more clearly if one examines the possible mechanism of condensation of anthranilic acid with methazonic acid as shown in Figure 9. Figure 9 first shows the conversion of methazonic acid (8, which is an oxime) to the aldehyde which then reacts with the aromatic amino group of anthranilic acid to give the enamine (9). It is easy to rationalize why this reaction may fail (or be very slow) from the structure of 5-nitroanthranilic acid. The nitro group in the 1,4- position relative to the amino group acts as a powerful electron withdrawing group. This makes the amino group of 5-nitroanthranilic acid much less nucleophilic in contrast to the amino group of anthranilic acid. This argument clearly shows that it is not possible to prepare 3,6-dinitro-4-quinolone (3) starting from 5-nitroanthranilic acid. This further implies that the retrosynthetic scheme shown in Figure 5b cannot be utilized, at least through the application of the known synthetic methodology. This turns our attention to the retrosynthetic analysis presented in Figure 5c. This retrosynthesis is more complicated than the previous ones, but in another way it simplifies the problem one would face if one tried to functionalize 3,6-diamino-4-quinolone (an intermediate in both 5a & b) with different acyl groups. Clearly one can not expect the two amino groups of 3,6-diamino-4-quinolone to possess equal basicity or nucleophilicity. Hence, if faced with reacting 3,6-diamino-4-quinolone with two different acyl groups (e.g., a peptide and acetic acid) one will run into reactions that may produce a complex mixture of products which are difficult to separate. This problem is avoided if one considers the retrosynthesis of Figure 5c. In the last step one can react the 6-amino-3-acetylamino-4-quinolone with either acetic anhydride (as shown) or with a symmetrical anhydride of an amino acid if one wants to functionalize the template with a peptide. Figure 10 shows the reactions that were used to prepare 3,6-diacetylamino-4-quinolone (1) which is a *model system* for more complex peptide-template derivatives, an aspect that will be discussed later in this chapter. The first two reactions in Figure 10 were already discussed in detail above. The next reaction, starting with 3-nitro-4-quinolone, (7) to give 3-nitro-N-methylacetate-4-quinolone (11) serves the purpose of

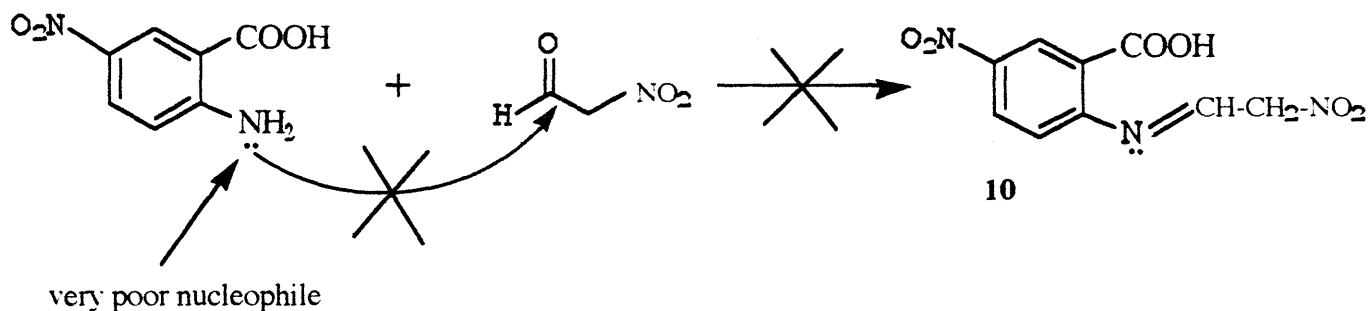
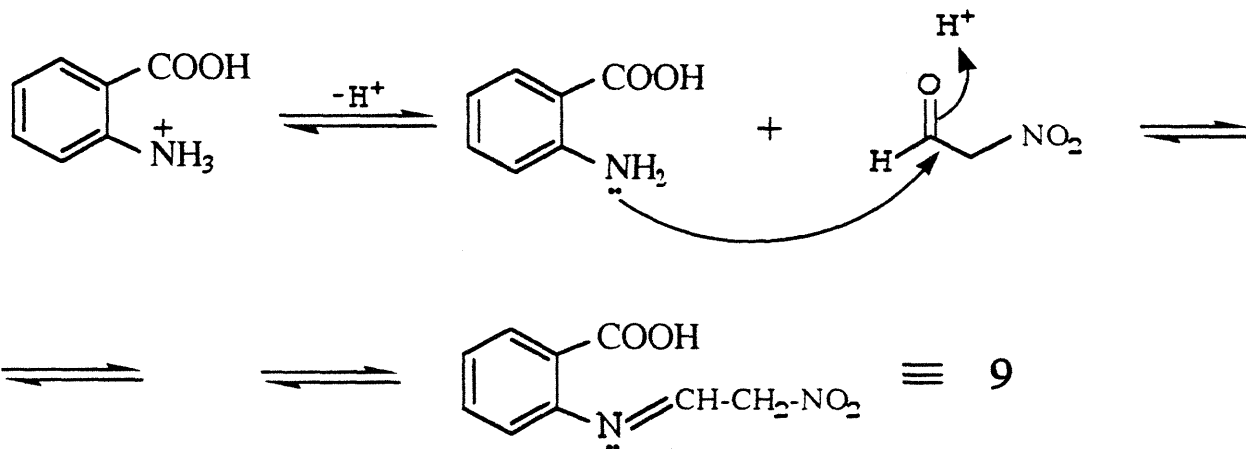
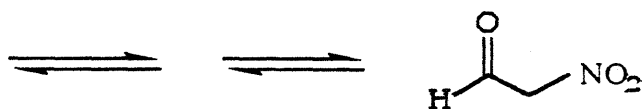
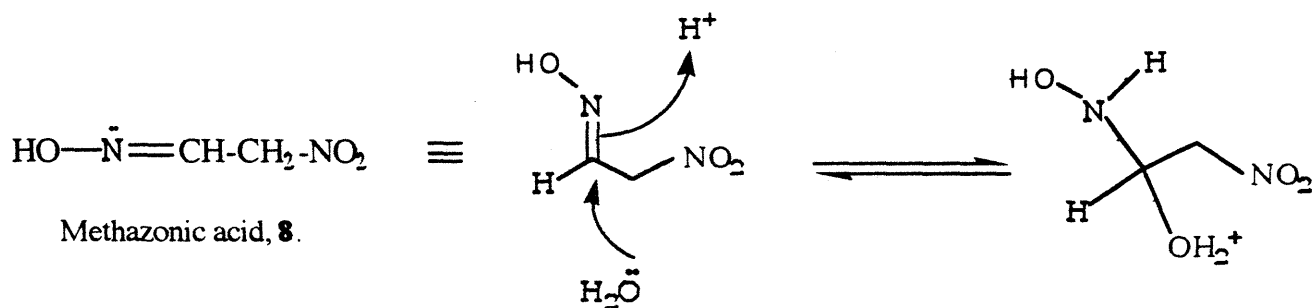
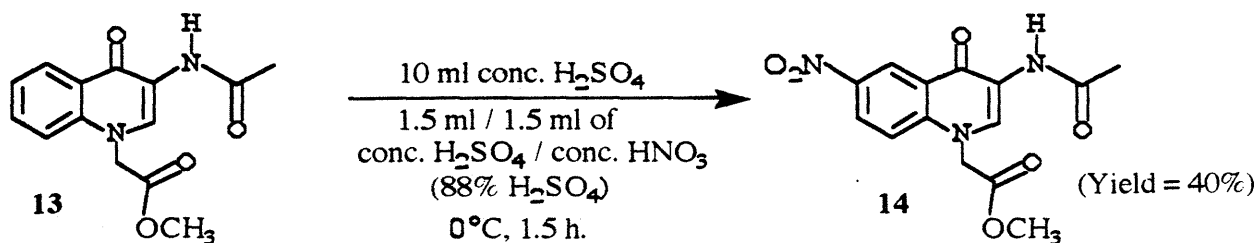
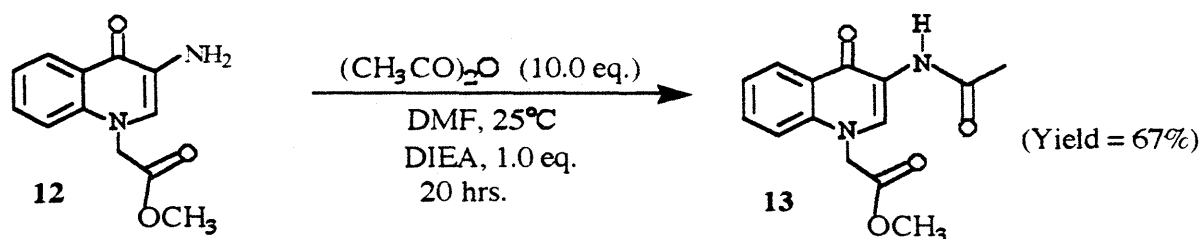
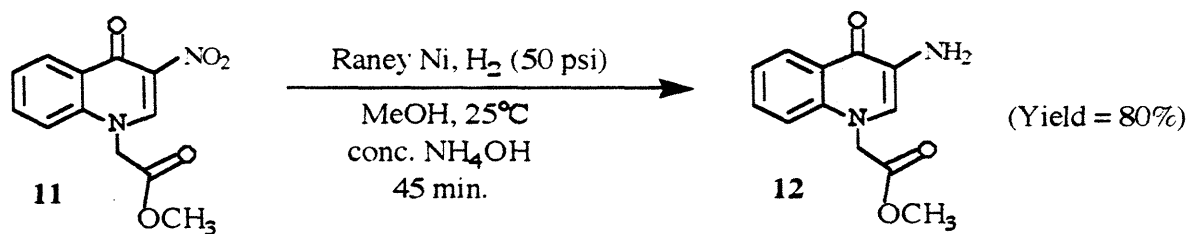
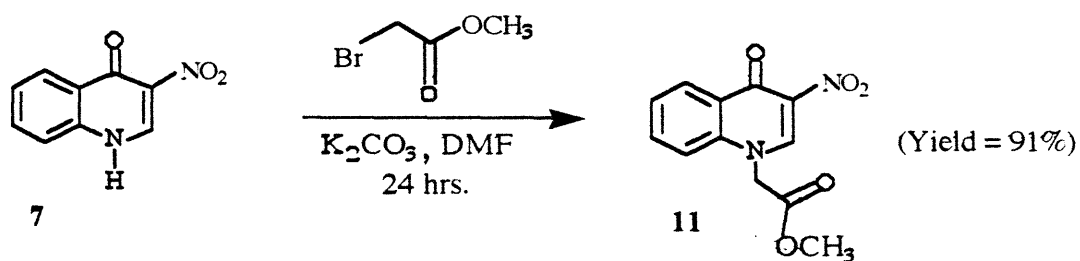
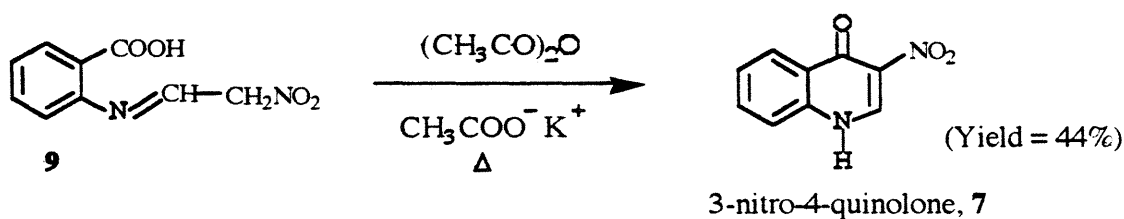
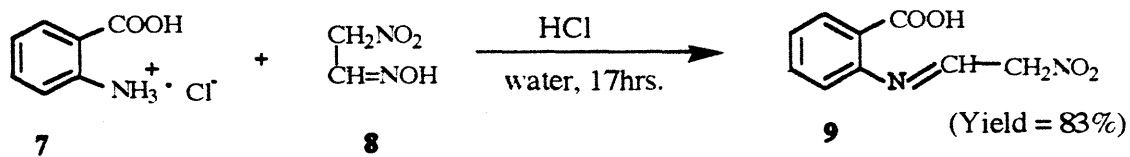


Figure 9. A possible mechanism of the condensation of anthranilic acid with methazonic acid (actually the nitro-aldehyde formed from methazonic acid.) Also shown is the likely reason why 5-nitroanthranilic acid fails to react in the same way as anthranilic acid does.



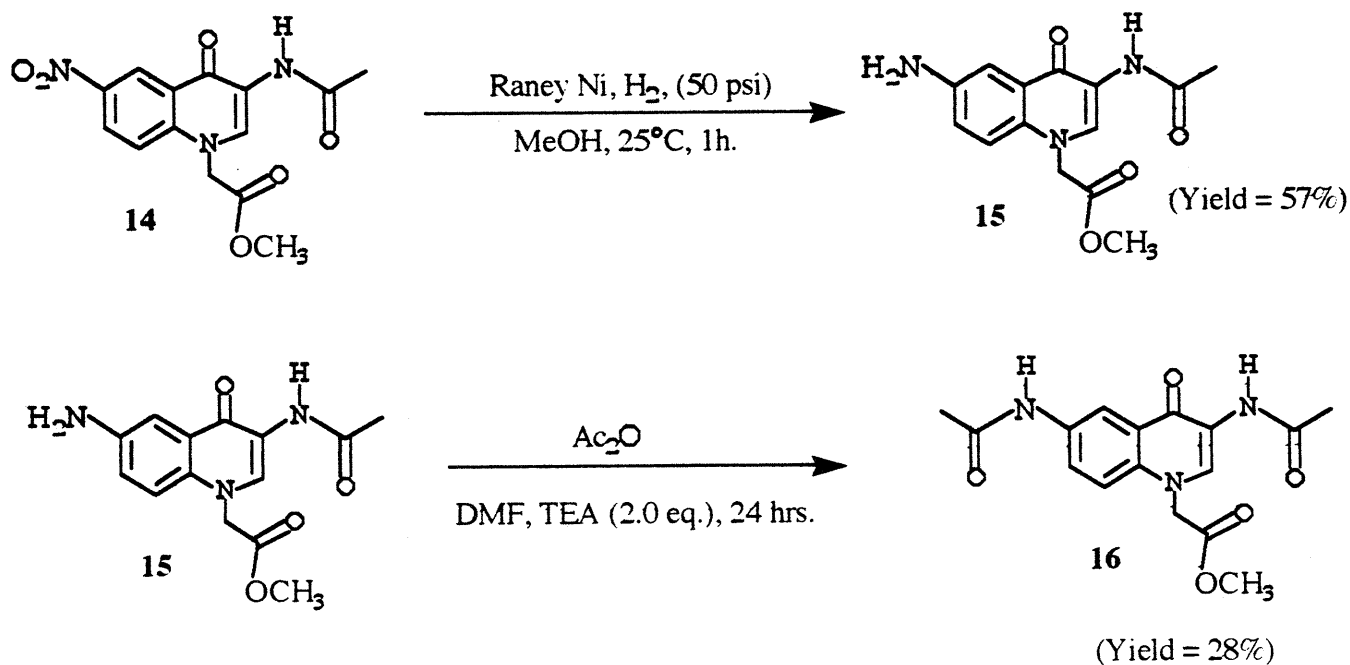


Figure 10.

The reaction employed in this work to prepare the final synthetic target 3,6-diacetyl-amino-4-quinolone (1).

replacing the acidic hydrogen of (7) with a neutral methylacetate group. This group is also intended to function as a potential “handle” for modifying the solubility properties of the quinolone template. Furthermore, as we will see below, it proves useful in NOE assignment of the 6-nitro-3-acetyl-amino-N-methylacetate-4-quinolone, (14). The reaction that gives (11) proceeds in high yield of 91%. Here, the salt K₂CO₃ is used as a base that deprotonates the acidic hydrogen of (7) to give the corresponding anion which then acts as a nucleophile in an S_N2 reaction with methyl bromoacetate to give (11). (11) is easily isolated, as it precipitates from the solvent, DMF during the course of the reaction. Simple filtration, and washing with water provides (11) in essentially pure form. The next reaction is a simple reduction of the 3-amino group with basic Raney Nickel in methanol. 50 psi of H₂ is applied in the hydrogenation apparatus for 45 minutes to give (12).

1.0 ml of concentrated ammonium hydroxide is added as a catalyst [ref. 3] It is interesting to note

that (11) has a relatively poor solubility in methanol, thus it is initially in the form of a suspension. This presents no problem, as (12) is soluble in methanol. (12) is very easily oxidized by molecular oxygen, thus once (12) is formed, it should be handled under an inert atmosphere and acetylated as soon as possible. When (12) is left exposed to air, it turns to a black tar with time. The reaction from (12) to (13) is a standard amine acylation reaction. The next reaction, the nitration of (13) to give (14) deserves a special consideration. Hutt and MacKellar [ref. 4] carried out the nitration of N-methylacetate-4-quinolone to 6-nitro-N-methylacetate-4-quinolone as a part of a study aimed at identification of the nitration products of quinoline by NOE. Reasoning that structure (13) of Figure 10 differs from N-methylacetate-4-quinolone only by the presence of the 3-acetamido group which is far removed from the "6" position where one intends to put the nitro group, we have used the same reaction conditions as Hutt and MacKellar did for the conversion of (13) to (14) in Figure 10. The reaction is regiospecific since only the 6-nitro regioisomer (14) is produced. This is clearly demonstrated in Figure 11. In the Figure we can see that the nitration reaction of (13) can potentially lead to four different nitration products, (14), (17), (18), and (19). However, J-coupling analysis combined with NOE data proves conclusively that the only (detectable) regioisomer produced is the regioisomer (14). Figure 12a shows the ^1H NMR spectrum of 6-nitro-3-acetamido-N-methylacetate-4-quinolone (14) together with the ppm and integral values of relevant resonances. Figure 12b shows the NOE difference spectrum of the same derivative (14), resulting from continuous, low power irradiation of the methylene protons of (14). From this Figure it is clear that the irradiation of the methylene protons of (14) leads to a significant positive NOE of proton resonances corresponding to hydrogens H2 and H8 of (14). This is schematically illustrated in the bottom part of Figure 11. The J-coupling analysis of the NOE difference spectrum, together with the spectrum of Figure 12a implies that the structure of the regioisomer is (14). The next reaction which converts (14) to (15) in Figure 10 is a straightforward Raney Nickel reduction. The 6-amino product (15) that is produced can then be

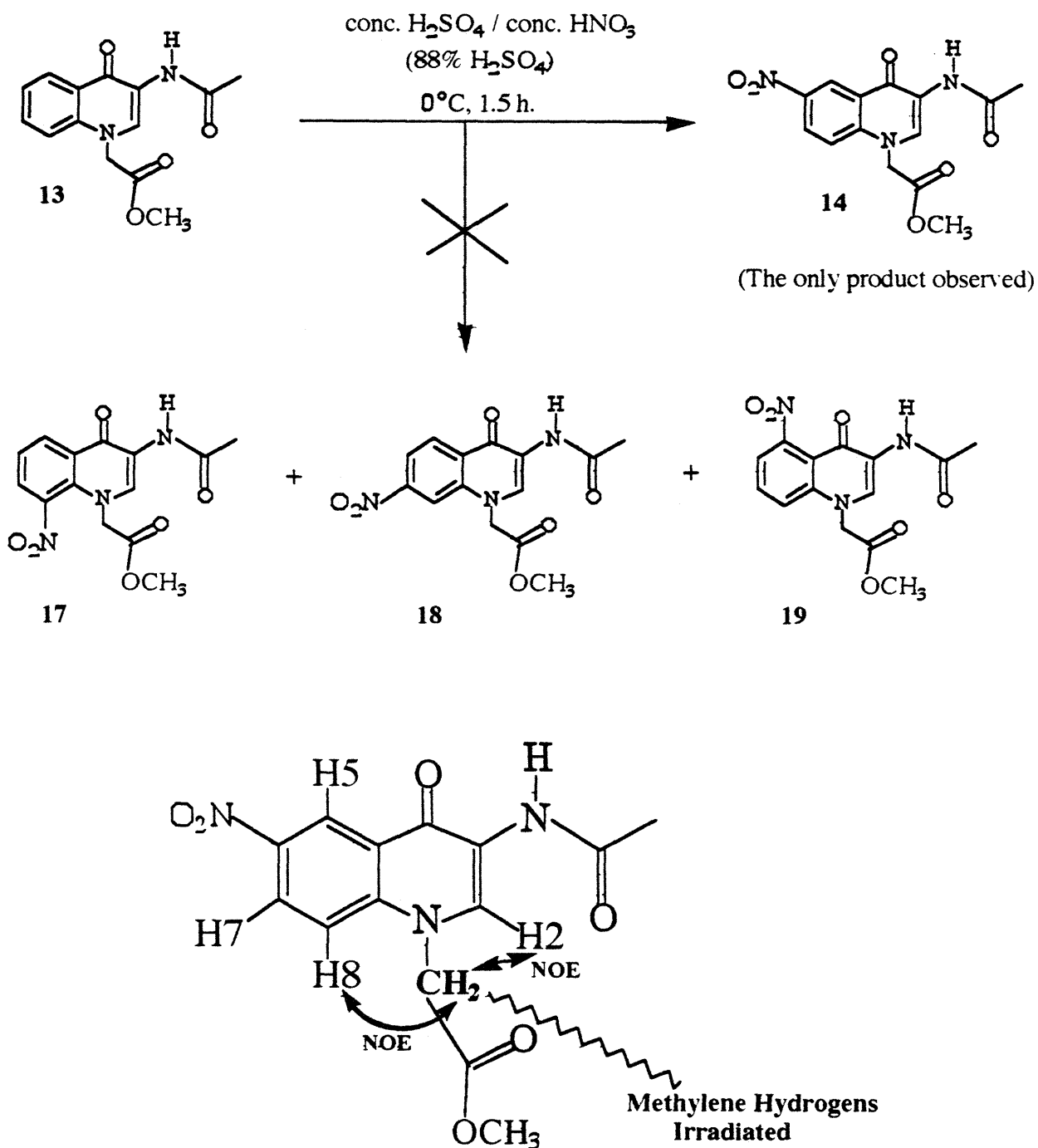


Figure 11. Demonstration of the highly regioselective nature of the nitration reaction that gives 14 as the only detectable regioisomer out of the possible four regioisomers. At the bottom, we see the schematic diagram of the NOE experiment that (in conjunction with J-coupling analysis) proves that the (14) is indeed the only detectable regioisomer that is produced.

acetylated to give the final product (16) in Figure 10. The relatively low yield of the last acylation reaction (28%) is likely due to two factors. First, HPLC and NMR analysis of product (16) suggest that in addition to the methyl ester derivative, there is present an acid contaminant. In other words, the crude product mixture corresponding to (16) contains a significant amount of the free carboxylic acid. This byproduct is likely to form in the Raney Nickel reduction, which occurs under basic conditions. Second, in obtaining the crude (16), we used centrifugation from water to purify (1). This purification step serves its purpose by preferentially removing the acid contaminant obtained from the Raney Nickel reduction as well as the unreacted amine component, however, it lowers the overall yield of the crude (16). Figure 13 shows the downfield region of the NMR spectrum of (16) purified by preparative HPLC. As before, the assignment of the resonances was obtained by a combination of J-coupling data with NOE analysis.

The NMR spectrum of 3,6-diacetylamino-N-methylacetate-4-quinolone (16) serves as an important control derivative. The chemical shifts of the protons of (16) give a reference shifts for any template-peptide derivative that is in the random coil state. In other words, each of the resonance chemical shifts in Figure 13 represent a δ_{O} reference shift for the given proton. To give a specific example, we can see in Figure 13 that the $\delta_{\text{H7}} = 7.91$ ppm. This chemical shift has the same meaning as the δ_{H3} of peptide-epindolidione derivative that is in the random coil superstate. We have seen in the previous chapter that δ_{H3} for such a derivative was taken to be 7.96 ppm, and it was denoted as $\delta_{\text{O, H3}}$. By the same token, we define δ_{H7} of (12) as $\delta_{\text{O, H7}}$. Furthermore, it is interesting to note the proximity of the two chemical shifts. In other words, $\delta_{\text{O, H3}} - \delta_{\text{O, H7}} = 7.96 - 7.91$ ppm = 0.05 ppm. This small difference may be a coincidence. However, we should

notice that structure (16) and the 2,8-diacylamino-epindolidione have very similar structure. This structural similarity is especially close if one considers only the local magnetic environment of either proton H7 of (16) or proton H3 of 2,8-diacylamino-epindolidione in its random coil superstate.

Another point that may be of significance, is the “non-overlapping” nature of the spectrum in Figure 13. The resonance corresponding to H2 is a sharp singlet. As we have seen above, the chemical shift of H2 may serve as a potential independent NMR reporter function. Since its span is likely to be small (due to the structural arguments presented above), the sharp and well defined resonance of H2 ($\delta_{\text{O, H2}}$) may prove useful in this respect.

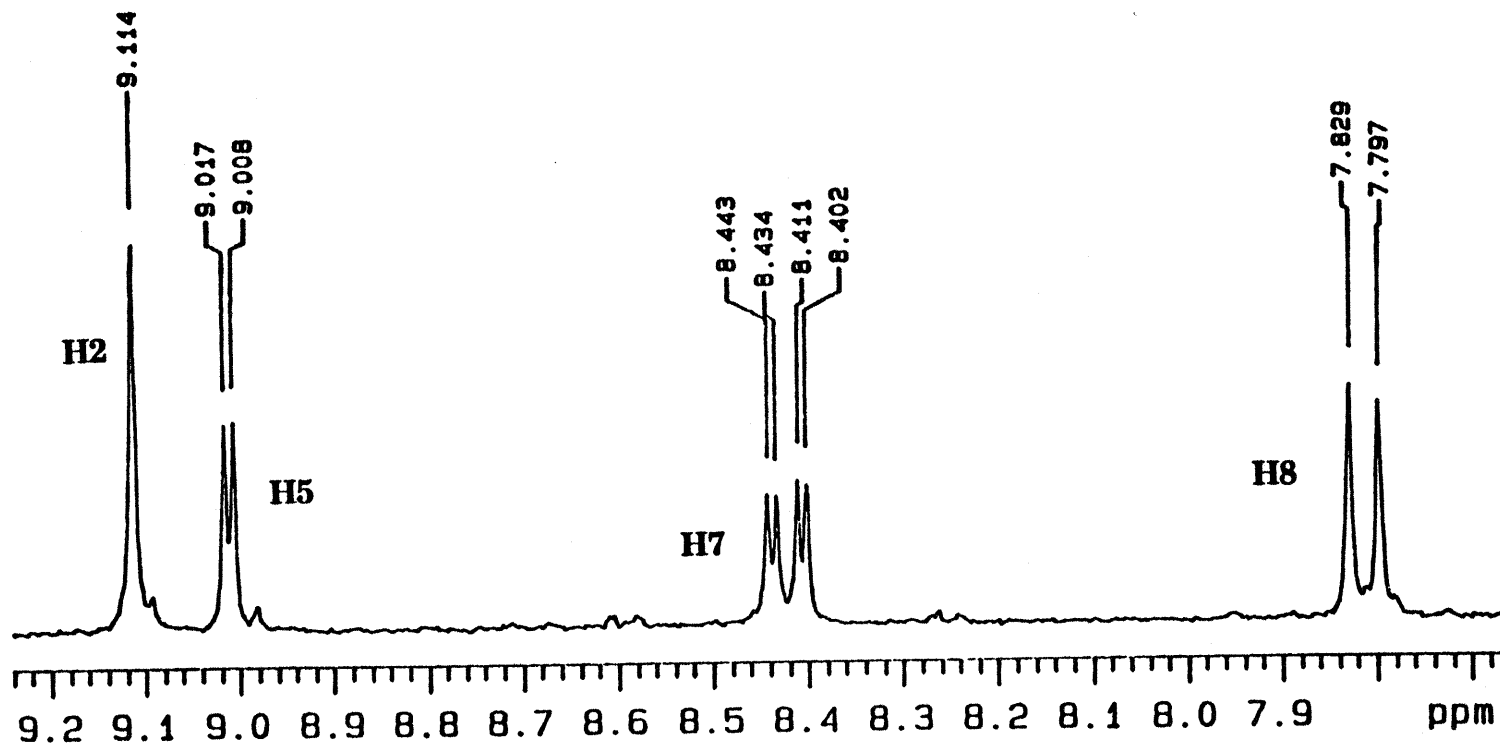


Figure 12a. ¹H NMR spectrum of (14) in DMSO-d₆ at 25 °C, together with select chemical shifts (ppm).

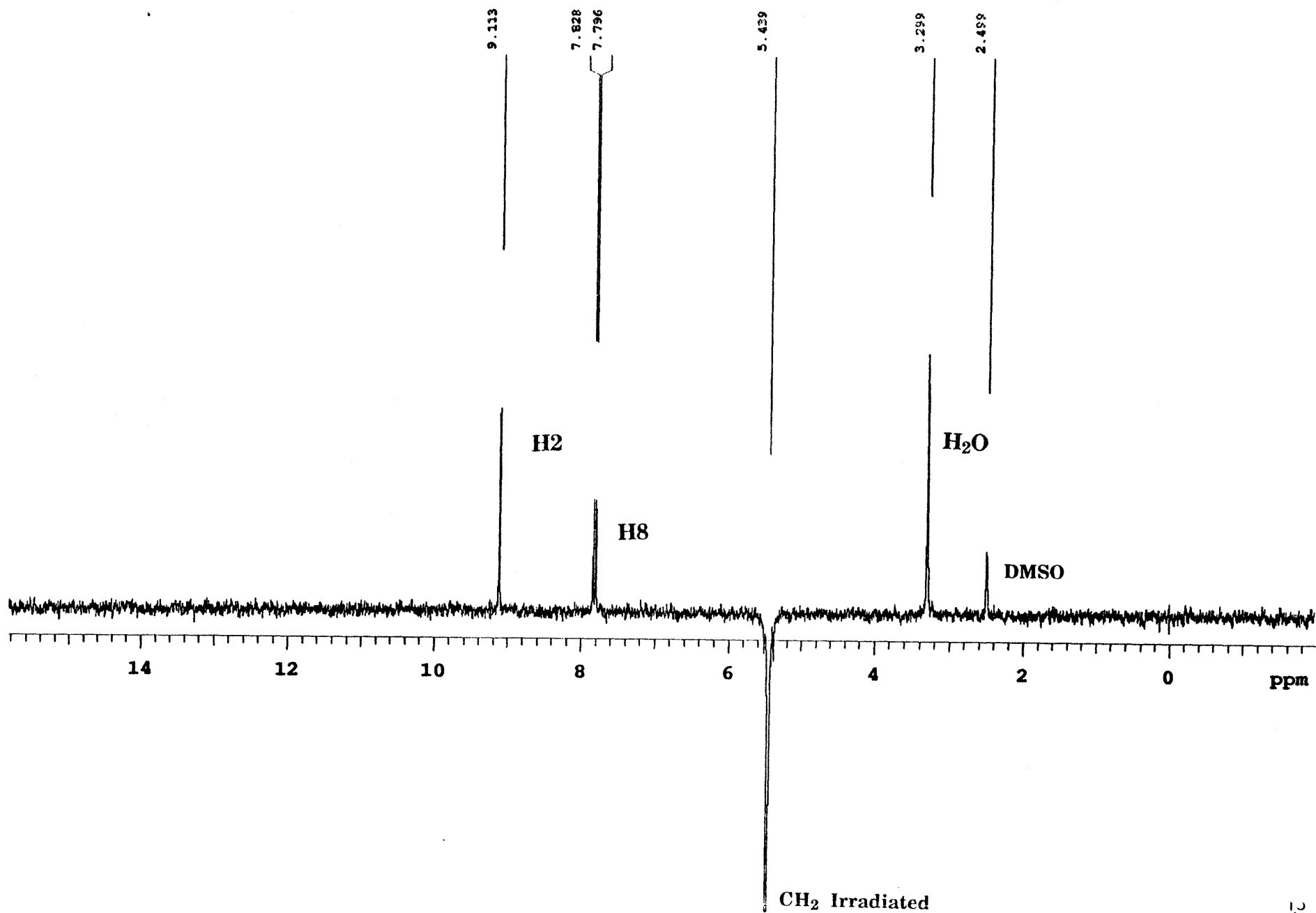


Figure 12b. The NOE difference spectrum of derivative (14) resulting from a continuous, low-power irradiation of the methylene protons of (14) as indicated in Fig. 11.

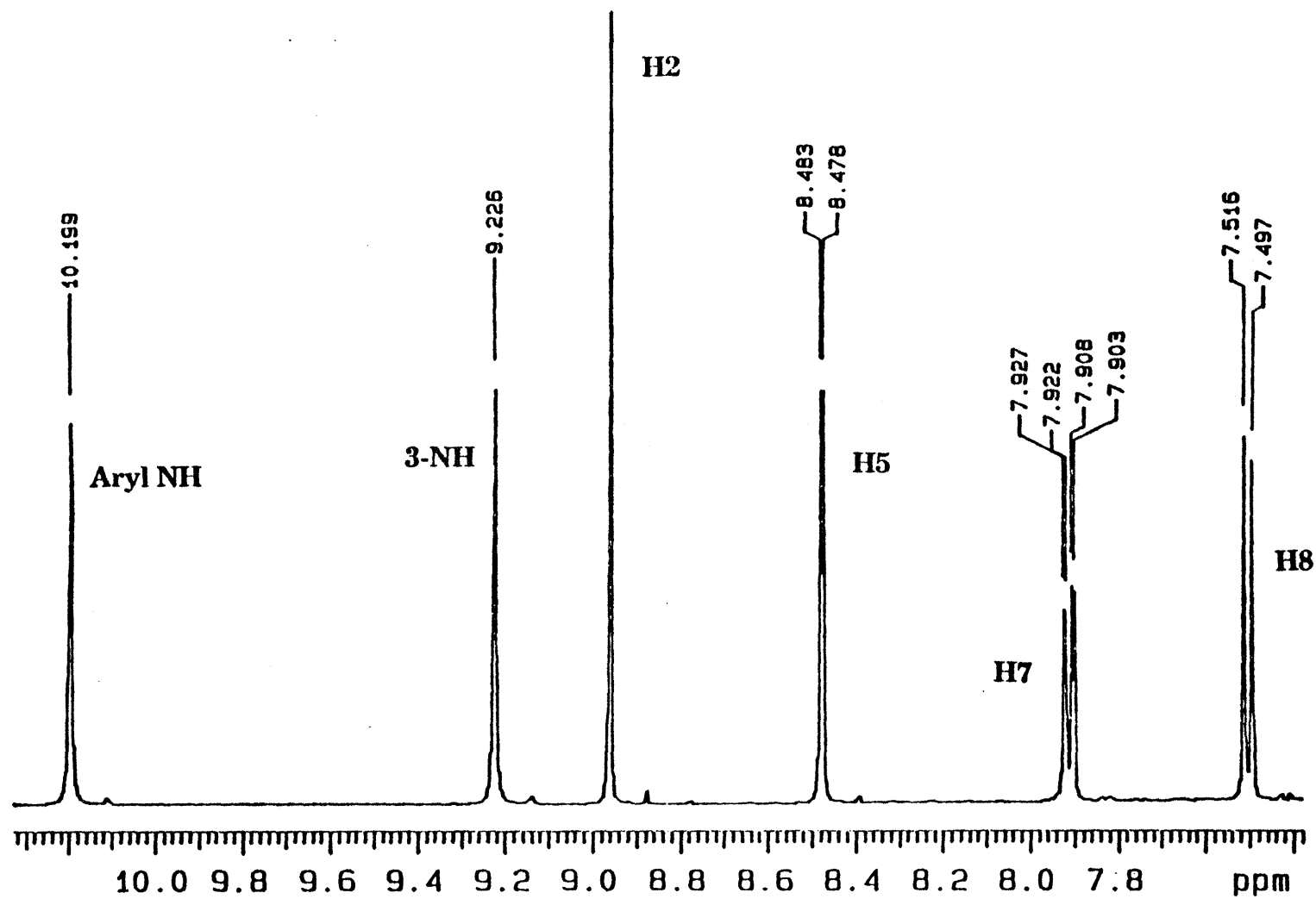


Figure 13. The downfield region of the ^1H NMR spectrum of 3,6-diacetylamino-N-methylacetate-4-quinolone template (16), purified by preparative HPLC.

Experimental

High resolution ^1H Nuclear Magnetic Resonance (NMR) spectroscopy was carried out on the Varian Spectrometers located at the MIT Chemistry Department Spectroscopy Laboratory. 1D nuclear Overhauser effect (1D NOE) experiments were run on either the Varian VXR-500S ("Bullwinkle"), or VXR-501S ("Rocky") 500 MHz spectrometers at the MIT Chemistry Department Spectroscopy Laboratory. At the MIT Chemistry Department Spectroscopy Laboratory, the FIDs (Free Induction Decays) after being saved to either the 3M DC 6150 Data Cartridge tape (150 Mbytes) or the HEWLETT[®] PACKARD 90 meters DDS-1 Data Cartridge (2 Gbytes) tape, were processed on either the Sun Microsystems Sparc 2 workstation using the Varian Instruments 3.1 VNMR software version, or on the Silicon Graphics Personal Indigo IRIS[®] workstation using the Varian Instruments revised 4.3 VNMR software version. Chemical shifts are reported in parts per million (ppm, δ) relative to tetramethylsilane (TMS) for organic solvents. Splitting patterns are abbreviated as: s, singlet; d, doublet; t, triplet, q, quartet; dd, doublet of doublets; m, unresolved multiplet; b, broad.

1D NOE experiments were performed exclusively on either the Varian VXR-500S ("Bullwinkle"), or VXR-501S ("Rocky") 500 MHz spectrometers according to the general procedure of Hall and Sanders (Hall & Sanders, 1980.) Pure DMSO- d_6 samples were degassed by at least five freeze-thaw cycles using a dry ice-isopropanol cold bath while under nitrogen or high vacuum. After the final freeze-thaw cycle, nitrogen was introduced into the NMR tube, and the tube was capped.

Preparation of 2- β -Nitroethylidenaminobenzoic acid (9)

The following synthetic procedure has been based on the procedure of Bachman et al.[ref. 3.]

Here it has been scaled down 20 times.

13.4 g. of 98.6% NaOH (from Mallinckrod, as pellets) was placed in a 100 ml 3-neck round bottom flask equipped with pressure-equalizing addition funnel, a thermometer, and a mechanical stirrer. 27 ml of distilled water was introduced with a syringe. Temperature rose to 70-80°C. The NaOH suspension was placed on a water-ice cold bath. When temperature rose to 25-30°C, the ice bath was replaced with just a water bath kept at 25-30°C. All NaOH had dissolved at this point. While the solution was stirred mechanically, 6.7g (0.11 mol, 5.95 ml) of nitromethane was added slowly (dropwise) keeping the temperature at about 28°C. During nitromethane addition, a yellow suspension formed gradually. When the first portion of nitromethane was added, the temperature was raised to 40°C. This clarified the suspension to give a red-brownish clear solution. At 40°C a second portion, 6.7g (0.11 mol, 5.95 ml), of nitromethane was added dropwise (1 drop per 5-10 sec.) During the second addition, some precipitate was present (white particles) which clarified (dissolved) after the addition of nitromethane was complete. About 5 min. after the addition of nitromethane was complete (at 42°C), the temperature of the clear deep-red-brownish solution was raised to 52°C for 5 min. Then the solution was cooled to 30°C; precipitate formed. This precipitate was poured onto 30 g. of chipped ice and acidified with 30 ml of conc. HCl. The HCl addition resulted in a clear reddish-brown solution. This solution of methazonic acid was immediately added to a previously filtered solution of 13.7 g of anthranilic acid (0.1 mol, recrystallized from water) and 9.2 ml of conc. HCl in 200 ml of distilled water. (**Note:** When the anthranilic acid (0.1 mol, recrystallized from water) is added to 200 ml of distilled water at room temperature, a suspension results. Addition of 9.2 ml of conc. HCl results in a brownish solution, with some undissolved particles in it. These particles were removed by subsequent filtration with a medium porosity glass frit, resulting in a clear brownish solution of anthranilic acid hydrochloride.) The

resulting solution (in a 500 ml capacity beaker) became a yellow thick suspension within 2-5 minutes of methazonic acid addition. This increasingly thick yellow suspension was allowed to stand for 17 hours (without stirring.) Afterwards, the thick, yellow suspension was filtered (with the help of dilution with distilled water) through a medium porosity glass frit. The first washings were red-brownish in color. The yellow product was repeatedly washed with distilled water until the washing were yellow. The filter cake was crumbled and placed in an oven preset to 100°C for about 25 min. Afterward, it was placed under a bell jar under high vacuum to further dry overnight. Yield is 17.3g of yellow powder (83%), m.p. 194-196°C (Bachman et. al., m.p. 196-197°C.)

Preparation of 3-nitro-4-quinolone (7)

10.4 g of 2-β-Nitroethylidenaminobenzoic acid (0.05 mol) was placed in a 100 ml 3-neck flask equipped with a thermometer, mechanical stirrer, a reflux condenser, and a heating mantle. 50 ml of acetic anhydride was introduced with a syringe. A yellow suspension resulted. The suspension was stirred and heated. At $\approx 87^{\circ}\text{C}$ the yellow suspension became a clear, brownish solution. This was further heated to $\approx 96^{\circ}\text{C}$, then 5g of anhydrous (oven and high-vacuum-dried) potassium acetate was added. **Note:** Unlike in the experimental procedure of Bachman et al. [ref. 3], the temperature did not rise spontaneously to $\approx 138^{\circ}\text{C}$, (i.e., to the boiling point of acetic anhydride) but remained at $\approx 96^{\circ}\text{C} - 98^{\circ}\text{C}$. Therefore, the reaction was heated to reflux (138°C) for 15 min. After addition of the potassium acetate salt, when the temperature reached 100°C , the clear brownish solution became a dark-brownish suspension which became even darker upon further heating to reflux.

After 15 min. of reflux, allowed the reaction mixture to cool slowly to room temperature. After about 1 hour, the precipitated crude product was filtered through a medium porosity glass frit and washed with glacial acetic acid until the washing were colorless, (the first washing are dark, tar-

like in color.) Then suspended (in the frit) in 50 ml distilled water, filtered, washed repeatedly with distilled water. Dried at 100°C (30 min.) and subsequently under high vacuum (overnight.) The dried product is a tan-colored powder. Yield = 4.14 g (44%), m.p. above 300°C (Bachman et. al., m.p. above 325°C.)

¹H NMR (DMSO-d₆, 500 MHz, 25°C): 13.004 (1H, b), 9.196 (1H, s), 8.264 (1H, dd, J = 1.04 Hz, J = 8.05 Hz), 7.805 (1H, t, J = 1.3 Hz, J = 7.66 Hz), 7.731 (1H, d, J = 8.05 Hz), 7.528 (1H, t, J = 0.78 Hz, J = 7.66 Hz),

Preparation of 3-nitro-N-methylacetate-4-quinolone (11)

To 1.0 g of 3-nitro-4-quinolone (5.3 mmol) was added 20 ml of DMF. Tan-colored suspension resulted. Then 1.1 g of anhydrous potassium acetate was added. Within 5 min. the tan-colored suspension became a dark, greenish-yellow solution. Subsequently, 4.1 g (2.5 ml) of methyl bromoacetate (from Aldrich) was introduced. No (immediate) color change can be observed. Within about 1 hour, the solution became a thick (hard to stir) tan-colored suspension. TLC analysis (developing solution: 85% chloroform : 14% MeOH : 1% glacial AcOH) showed that the reaction (product RF ~ 0.6, reactant at the origin, smearing) was essentially complete within 1.5 hour. Let stir overnight. Worked-up by evaporating the solvent. Suspended the residue in 0.1N HCl. Filtered through a medium porosity glass frit. Washed with ~200 ml 0.1 N HCl, followed by ~200 ml distilled water (pinkish color washing.) Dried under high vacuum to obtain a tan-colored powder product. Yield = 1.27g (91%), m.p. above 260°C, decomposes.

¹H NMR (DMSO-d₆, 500 MHz, 25°C): 9.43 (1H, s), 8.37, 8.35 (1H, d), 7.89, 7.86, & 7.84 (1H, t), 7.74, 7.71, (1H, d), 7.63, 7.60, & 7.58 (1H, t), 5.49 (2H, s), 3.74 (3H, s).

Preparation of 3-amino-N-methylacetate-4-quinolone (12)

300 mg of 3-amino-N-methylacetate-4-quinolone (12) was suspended in 10 ml of anhydrous

methanol in a hydrogenation vessel. The suspension was flashed with $N_2(g)$ stream.

Subsequently, 100 μ l of conc. ammonium hydroxide was introduced via a syringe followed by

~ 0.5 g of activated Raney Nickel[®] (from Aldrich.) The suspension was hydrogenated under initial pressure of 50 p.s.i. of $H_2(g)$ in a hydrogenation apparatus for 45 min. Then, the reaction mixture was filtered through celite, additional ~50 ml of methanol was used to wash the celite. The filtrate was evaporated on a high vacuum rotary evaporator and dried on high vacuum to obtain a thick, yellow oil. (Yield = 80%.) **Note:** This amine product (12) apparently is very sensitive to oxidation by molecular oxygen when exposed to air for more than a few minutes, (it turns into a tar after more than ~0.5 hour of air exposure.)

Preparation of 3-acetylamino-N-methylacetate-4-quinolone (13)

0.688 g (2.97 mmol, 1.0 eq.) of amine was dissolved in 10 ml of degassed DMF under nitrogen atmosphere. This resulted in a brownish-orange solution, (TLC taken at this point.) Next, 2.75 ml (10.0 eq.) of acetic anhydride was added with stirring. Within 1-2 min. the clear solution became a tan-colored opaque suspension. Then 517 μ l (1.0 eq.) of DIEA was introduced, (no color change observed.) Followed reaction by TLC. Let stir for ~20 hrs. at room temperature. Next, evaporated the solvent under high vacuum. Placed on high vacuum for ~1 hour. Subsequently added dist. water; sonicated, filtered, washed repeatedly with dist. water. Dried on high vacuum (after azeotroping with acetonitrile.) Yield = 0.551g (67%, m.p. above 300°C.)

1H NMR (DMSO- d_6 , 300 MHz, 25°C): 9.248 (1H, s), 9.009 (1H, s), 8.282 (1H, dd, J = 1.47 Hz, J = 8.15 Hz), 7.707 (1H, t, J = 1.63 Hz, J = 7.83 Hz), 7.524 (1H, d, J = 7.8 Hz), 7.389 (1H, t, J = 8.15), 5.333 (2H, s), 3.320 (3H, s), 2.134 (3H, s).

Preparation of 6-nitro-3-acetylamino-N-methylacetate-4-quinolone (14)

(Procedure adapted from J. Heterocyclic Chem., **21**, 349 (1984).)

500mg of 3-acetylamino-N-methylacetate-4-quinolone (13) was dissolved with stirring in 10 ml of conc. sulfuric acid. This thick solution was placed on ice bath. To this thick solution was added dropwise (~1 drop per 5 sec.) a 1: 1 nitrating mixture of 1.5 ml conc. nitric acid and 1.5 ml of conc. sulfuric acid using a pressure-equalizing addition funnel. The brownish solution was stirred under a nitrogen atmosphere for 1.5 hour at 0°C (ice bath.) Subsequently, it was poured into a beaker containing 50 ml of ice-cold water and 50 g of chipped ice. Yellow precipitate formed immediately. After letting stand for about 5 min., this yellow suspension was collected through filtration (**Note:** use larger than 60 ml funnel, because filtration through a 60 ml, medium porosity funnel takes a long time.) The yellow filter cake was crumbled and dried under high vacuum overnight. Yield = 157 mg (40%; m.p. above 300°C.)

¹H NMR (DMSO-d₆, 300 MHz, 25°C): 9.486 (1H, s), 9.114 (1H, s), 9.013 (1H, d, J = 2.93 Hz), 8.423 (1H, dd, J = 2.94 Hz, J = 9.62 Hz), 7.814 (1H, d, J = 9.78 Hz), 5.440 (2H, s), 3.723 (3H, s), 2.156 (3H, s).

Preparation of 6-amino-3-acetylamino-N-methylacetate-4-quinolone (15)

154 mg (492 μmol) of 6-nitro-3-acetylamino-N-methylacetate-4-quinolone (14) was suspended in 21 ml of anhydrous methanol in a hydrogenation vessel. This gave a yellow suspension. The hydrogenation vessel was flashed with a stream of nitrogen (1 min.) Then, 200 μl conc. ammonium hydroxide was added and the mixture was hydrogenated under ~50 psi of H₂(g) in a hydrogenation apparatus for 1 hour. Then, the reaction mixture was filtered through celite, additional ~50 ml of methanol was used to wash the celite. The filtrate was evaporated on a high vacuum rotary evaporator and dried on high vacuum to obtain a thick, yellow oil.

(Yield = 63.8 mg, \approx 46 %.)

Preparation of 3,6-diacetylamino-N-methylacetate-4-quinolone (16)

63.8 mg (0.221 mmol, 1.0 eq.) of the amine was dissolved in 10 ml of DMF under nitrogen. 39 μ l (1.0 eq.) of DIEA was introduced, (TLC taken.) Then 410 μ l (20 eq.) of Ac₂O was added via a syringe, (TLC taken within one min.) (**Note:** The amine is not well-soluble in 10 ml DMF - a yellow suspension forms. Added 1.0 ml more Ac₂O.) At 15 hrs. into the reaction added 2 ml more Ac₂O and placed on 55-60°C water bath for 0.5 hour. Added 120 μ l (3 eq. more) DIEA. Let stir at room temp. two more hours, for a total of \sim 17 hour. Carrot-like color (impurity?) Evaporated the solvent. Placed on high vacuum for about 1 hour. Subjected the crude reaction mixture to prep. HPLC purification. (TLC analysis inconclusive.) **Note:** There are always only two major spots on the TLC whose position is essentially not changing with the time of the reaction. However, the two spots (at t = 0, and t = 2 min.) develop visible color after several hours on the TLC plate; but the ones taken at t = 15 h. or 17 h. remain only UV-visible. Furthermore, the UV-color of the t = 0 spot is different from that of the t = 15-17 h., which is more bluish. Possible interpretation: From prep-HPLC and NMR analysis of the fractions, besides some color impurities, there are two major fractions. These are most likely the sought methyl ester (16), and its carboxylic acid analog. The acid is likely a by-product of the basic Raney Nickel reduction reaction. Yield of crude (16) is about 28 %. After prep HPLC, obtained 19.7 mg of the pure (16) as shown by NMR analysis. The prep-HPLC conditions are as follows: 0 to 100% B in 30 min. A = 10% acetonitrile, 0.1% TFA. B = 30 % acetonitrile, 0.1% TFA. $\lambda=280 \text{ \AA}$. The sought product (16) elutes at 6.6 min., (m.p. above 290°C, decomposes.) While the acid elutes at 5.2 min., (the colored impurity elutes much later in the gradient.)

¹H NMR (DMSO-d₆, 500 MHz, 25°C): 10.199 (1H, s), 9.226 (1H, s), 8.963 (1H, s), 8.481 (1H, d, J = 2.47 Hz), 7.915 (1H, dd, J = 2.59 Hz, J = 9.35 Hz), 7.506 (1H, d, J = 9.35 Hz), 5.301 (2H, s), 3.707 (3H, s), 2.130 (3H, s), 2.077 (3H, s).

Appendix C References

- 1) Blanchard, D.E. Template Initiation of Antiparallel β -Sheet. Ph.D. Thesis, MIT, 1992.
- 2) Williams, D.H. The molecular Basis of Biological Order. *Aldrichimica Acta* **24**: 71-80, 1991.
- 3) Bachman, G. B., Welton, D.E., Jenkins, G.L., and Christian J.E. Quinolone Derivatives from 3-Nitro-4-hydroxyquinoline. *J. Amer. Chem. Soc.* **69**:365-371, 1947.
- 4) M. P. Hutt and F. A. MacKellar. Identification of Quinoline Nitration Products by NOE. *J. Heterocyclic Chem.*, **21**, 349 (1984).

Bibliography

- Amodeo, P., Motta, A., Picone, D., Saviano, G., Tancredi, T., and Temussi, P.A., *J. Magn. Reson.* (1991), 95, 201-207.
- Arico-Muendel, C.C., Ph.D. Thesis, Massachusetts Institute of Technology, 1992.
- Aue, W.P., Bartholdi, E., & Ernst, R.R., *J. Chem. Phys.* 64, 2229 (1976).
- Bax, A., & Davis, D.G., *J. Magn. Reson.* (1985), 63, 207-213.
- Bax, A., & Davis, D.G., *J. Magn. Reson.* (1985), 65, 355-360.
- Bax, A., & Freeman, R., *J. Magn. Reson.*, (1981), 44, 542-561.
- Blanchard, D. Ph.D. Thesis, Massachusetts Institute of Technology, 1992.
- Bowen, B., Ph.D. Thesis, Massachusetts Institute of Technology, 1988.
- Brown, S.C., Weber, P.L., and Mueller, L., *J. Magn. Reson.* (1988), 77, 166-169.
- Braunschweiler, L. & Ernst, R.R. *J. Magn. Reson.* (1983), 53, 521-528.
- Bundi, A., Grathwohl, C., Hochmann, J., Keller, R.M., Wagner, G., & Wüthrich, K. *J. Magn. Res.* 1975, 18, 191-198.
- Camilleri, P., Kirby, A.J., Lewis, R.J., and Sanders, J.K.M., *J. Chem. Soc., Chem. Commun.*, 1988, p. 1537.
- Cowie, J.M.G., & Toporowski, P.M., *Can. J. Chem.* 39, 1961, 2240.
- Creighton, T.E., "PROTEINS: Structures and Molecular Properties" Second Ed., W.H. Freeman and Company, New York, 1993.
- Davies, P.L., & Hew, C.L., 1990, *FASEB (Fed. Am. Soc. Exp. Biol.) J.* 4:2460-2468.
- DeVries, A.L., & Wohlschlag, D.E., (1969) *Science*, 163, 1073-1075.
- Douzou, P. (1977) *Cryobiochemistry, An introduction.* Academic Press, New York.
- Douzou, P., & Petsko, G.A., *Adv. Protein Chem.* 1984, 36, 245-261.
- Fahy, G.M., Levy, D.I., & Ali, S.E., *Cryobiology* 24, 196-213, 1987.

- Fink, A.L., *Cryobiology* 23, 28-37, 1986.
- Giallourakis, C.C., B.S. Thesis, Massachusetts Institute of Technology, 1992.
- Gordalla, B.C. & Zeidler, M.D., *Molecular Physics*, 1991, v. 74, 5, p. 975
- Hall, D.L., & Sanders, J.K.M., *J. Am. Chem. Soc.* 1980, 102, 5703.
- Jaffe, E.E., & Matrick, H. (1968) *J. Org. Chem.* 33, 4004.
- Karlsson, J.O.M., Cravalho, E.G., Borel Rinkes, H.M., Tompkins, R.G., Yarmush, M.L., & Toner, M. *Biophys. Journal* 65, 2524-2536, 1993.
- Karlsson, J.O.M., Cravalho, E.G., & Toner, M. *Cryo-Letters* 14, 323-334 (1993).
- Karlsson, J.O.M., & Toner, M. *Biomaterials* 17, No.3, 1996.
- Kautz, R., unpublished results (Kautz, R., Blanchard, D.E., Flippen-Anderson, J.L., & Kemp, D.S., submitted for publication to *Science*, but rejected).
- Kemp, D.S., & Bowen, B.R., *Tetrahedron Lett.* 1988, 29, 5077.
- Kessler, H., *Angew. Chem. Int. Ed. Engl.* 21 (1982) 512-523.
- Kruse, L. I., DeBrosse, C.W., Kruse, C.H., *J. Am. Chem. Soc.* 1985, 107, 5435.
- Link, M.J.L., Master's Thesis, Massachusetts Institute of Technology, 1983.
- Luzar, A. & Chandler, D., *J. Chem. Phys.* 98 (10), 1993, 8160-8173.
- Mersh, J.D. & Sanders, J.K.M. *Tetrahedron Lett.* 1981, 22, 4029.
- Motta, A., Tancredi, T. & Temussi, A. (1987) *FEBS Lett.* 215, 215-218.
- Neuhaus, D., Williamson, M., "The Nuclear Overhauser Effect in Structural and Conformational Analysis", CVCH Publishers, New York, NY, 1989.
- Polge, C., Smith, A.U., Parkes, A.S., *Nature* 1949; 164:666
- Pollard, E.C., in "The Aqueous Cytoplasm" (A.D. Keith, Ed.), pp. 1-22, Dekker, New York, 1976.

- Rucker, S.P. & Shaka, A.J., *Mol. Phys.* 1989,68, No. 2, 509-517.
- Schaal, W. Master's Thesis, Massachusetts Institute of Technology, 1991.
- Schichman, S.A., & Amey, R.L., *J. Phys. Chem.*, 75, No.1, 1971, 98.
- Schmidt, H., Hollitzer, O., Seewald, A., und Steglich, W., *Chem. Ber.* 112, 727-733 (1979).
- Soper, A.K., & Luzar, A., *J. Chem. Phys.*,97, 1992, 1320-1331.
- States, D.J., Haberkorn, R.A., & Ruben, D.J. *J. Magn. Reson.*(1982),48, 286-292.
- Templeton G, E.F., & Kenney-Wallace, G.A. *J. Chem. Phys.*,90, 1986, 2896-2900.
- Temussi, P.A., Picone, D., Saviano, G., Amodeo, P., Motta, A., Tancredi, T., Salvadori, S., & Tomatis, R., *Biopolymers* 1992, 32, 367-372.
- Tobias, B., & Markley, J.L., *J. Magn. Reson.* (1986), 69, 381.
- Turner, C.J., (1993) "*RNMR & U A Customer Handbook*" Francis Bitter National Magnet Laboratory, Massachusetts Institute of Technology
- Van der Maarel, J.R.C., Lankhorst, D., DeBleijser, J., & Leyte, J.C., *Chem. Phys. Lett.*,1985, 122, 541.
- Verheyden, P., Franco, W., Pepermans, H., & Van Binst, G., *Biopolymers*, 30, 855-860 (1990)
- Wagner, G., & Wüthrich, K. *J. Magn. Reson.* (1979), 33, 675-680.
- Wen, D., & Laursen, R.A., *Biophys. Journal*, 63, 1992, 1659-1662.
- Wüthrich, K., Billeter, M., & Braun, W., *J. Mol. Biol.* 1984, 180, p.715